Functional Characterization of Homeodomain Transcription Factors and Retinoic Acid Signaling in Hematopoiesis

by

Laura Melinda Pillay

A thesis submitted in partial fulfillment of the requirements for the degree of

Doctor of Philosophy

in

Molecular Biology and Genetics

Department of Biological Sciences
University of Alberta

Abstract

Improper regulation of hematopoiesis generates a spectrum of defects that range from anemia and embryonic lethality to leukemia. Identifying the molecular pathways that regulate hematopoiesis is therefore a major goal of both basic and clinical biology. Vertebrate hematopoiesis occurs in two embryonic waves. The first wave, primitive hematopoiesis, influences the morphology of the developing embryonic circulatory system and produces circulating erythrocytes that facilitate tissue oxygenation during periods of rapid embryonic growth. The second, definitive wave of hematopoiesis produces multipotent hematopoietic stem cells (HSCs) that are able to differentiate into all mature blood cell lineages, self-renew, and maintain adult hematopoiesis for life. A major challenge in developmental hematopoiesis is to determine the molecular cues that regulate each phase of hematopoiesis.

Previous analyses using vertebrate models have identified molecular pathways that govern both primitive and definitive hematopoiesis. These pathways are conserved among vertebrates, and the critical mammalian hematopoietic genes have clear orthologues in zebrafish. Using zebrafish as a model organism, we have identified essential regulators of both primitive and definitive hematopoiesis. We have defined a critical role for the homeodomain transcription factors Meis1 and Pbx in regulating primitive erythropoiesis. Inhibiting zebrafish Meis1 and Pbx protein synthesis cripples the production of circulating erythrocytes, and generates defects in erythropoietic gene expression. Our data place Meis1 and Pbx upstream of *gata1* in the erythropoietic transcription factor hierarchy.

We have also elucidated a novel role for retinoic acid (RA) signaling in definitive hematopoiesis, as RA-depleted embryos fail to produce HSCs. Previous studies have

implicated RA as a critical regulator of murine Notch1 signaling, and suggest that endothelial cells require RA in order to adopt a hemogenic fate. However, our research suggests that RA is required for HSC formation prior to the formation of dorsal aorta hemogenic endothelium and that, unlike in mice, zebrafish RA does not regulate HSC formation through the Notch1-signaling pathway.

Previous research by our lab has implicated the homeodomain transcription factor Hmx4 as a critical regulator of zebrafish forebrain and ocular development, and has shown that Hmx4 modulates RA signaling. However, prior to this work, the contribution of Hmx4 to embryonic hematopoiesis was unknown. We have identified putative RA-independent and dependent roles for Hmx4 in regulating primitive and definitive hematopoiesis, respectively.

Preface

This thesis is an original work by Laura M. Pillay. The study, of which this thesis is a part, has received research ethics approval from the University of Alberta Animal Policy and Welfare Committee. The author has met the Canadian Council on Animal Care (CCAC) mandatory training requirements for animal users on the Care and Use of Animals in Research, Teaching, and Testing.

A version of Chapter 3 was published:

Laura M. Pillay, A. Michael Forrester, Timothy Erickson, Jason N. Berman, and Andrew J. Waskiewicz (2010). The Hox cofactors Meis1 and Pbx act upstream of *gata1* to regulate primitive hematopoiesis. *Developmental Biology*, 340(2):306-317.

Laura M. Pillay performed experiments, analyzed data, and wrote the manuscript. Timothy Erickson performed the Meis1 immunohistochemical analysis and Cdx *in situ* hybridization demonstrated in Figure 3.18, helped to analyze data, and edited the manuscript. A. Michael Forrester replicated the *lyz* and *lcp1 in situ* hybridization data demonstrated in Figure 3.11. Jason N. Berman analyzed data and edited the manuscript. Andrew J. Waskiewicz was the supervisory author, analyzed data and edited the manuscript.

A portion of Chapter 5 was contributed by the author to the following publication:

Patricia A. Gongal, Lindsey D. March, Vanessa L. Holly, Laura M. Pillay, Karyn M. Berry-Wynne, Hiroyuki Kagechika, and Andrew J. Waskiewicz (2011). Hmx4 regulates Sonic hedgehog signaling through control of retinoic acid synthesis during forebrain patterning. *Developmental Biology*, 355(1): 55-64.

This includes Figure 5.1C, C' and Figure 5.2G. Laura M. Pillay also analyzed data and edited the manuscript.

A version of Chapter 6 was published:

Laura M. Pillay, Lyndsay G. Selland, Valerie C. Fleisch, Patricia L. A. Leighton, Caroline S. Cheng, Jakub K. Famulski, R. Gary Ritzel, Lindsey D. March, Hao Wang, W. Ted Allison, and Andrew J. Waskiewicz (2013). Evaluating the mutagenic activity of

targeted endonucleases containing a *Sharkey* FokI cleavage domain variant in zebrafish. *Zebrafish*, 10(3): 353-364.

Laura M. Pillay performed experiments, analyzed data, and wrote the manuscript. Valerie C. Fleisch generated the *prp2* ZFNs. R. Gary Ritzel generated the *crx* ZFNs. Lyndsay G. Selland is responsible for the construction of *hoxb1b* and *wwtr1* TALENS, and for performing zebrafish mutagenesis using TALENs. Figure 1 appears courtesy of Caroline S. Cheng. Figure 2C appears courtesy of Jakub K. Famulski. The data presented in Table 1 results from experiments performed in collaboration with Valerie C. Fleisch and Lindsey D. March. The data presented in Figure 3C results from experiments performed in collaboration with Caroline S. Cheng. The data presented in Figure 4A results from experiments performed in collaboration with Lyndsay G. Selland. The data presented in Table 2 is courtesy of Lyndsay G. Selland. Lyndsay G. Selland, Valerie C. Fleisch, Patricia L. A. Leighton, Caroline S. Cheng, and Jakub K. Famulski helped to analyze data, and edited the manuscript. Andrew J. Waskiewicz and W. Ted Allison were co-supervisory authors, analyzed data and edited the manuscript.

Unless otherwise specified, data presented in this thesis is the author's original work.

Acknowledgements

I would like to express deep appreciation to my supervisor Dr. Andrew Waskiewicz for having faith that my unorthodox projects would bear fruit, and for encouraging me to write more concisely. Your mentorship and criticism have made me a better scientist, writer, and presenter. Thank you also to all the past and present members of the lab for making my graduate experience so enjoyable. Your selfless time, friendship and advice were greatly appreciated. Thanks especially to Timothy Erickson for teaching me molecular biology and zebrafish husbandry techniques when I was a lowly undergraduate student with stars in my eyes. Finally, thank you to my husband: Your emotional support throughout my graduate degree was sometimes all that kept me going.

Table of Contents

List of Tables

List of Figures

List of Common Abbreviations

°C	Degrees celsius
aa	Amino acid
AGM	Aorta-gonad-mesonephros
ALL	Acute lymphoblastic leukemia
ALPM	Anterior lateral-plate mesoderm
AML	Acute myeloid leukemia
BCIP	5-bromo-4-chloro-3-indolyl-phosphate, toluidine-salt solution
bp	Base pair
BSA	Bovine serum albumin
cDNA	Complementary deoxyribonucleic acid
CHIP-seq	Chromatin immunoprecipitation and massively parallel sequencing
CLP	Common lymphoid progenitor
CRISPR	Clustered regularly interspaced short palindromic repeats
Ct	Cycle threshold
DAPT	N-[N-(3,5-Difluorophenacetyl)-L-alanyl]-S-phenylglycine t-butyl ester
DEAB	Diethylaminobenzaldehyde
DEPC	Diethylpyrocarbonate
DIG	Digoxigenin
DMSO	Dimethyl sulfoxide
DNA	Deoxyribonucleic acid
DNAse	Deoxyribonuclease
dNTP	Deoxyribonucleotide triphosphate
dpf	Days post fertilization
DTT	Dithiothreitol
ECL	Enhanced chemiluminescence
EDTA	Ethylenediaminetetraacetic acid
EM	Embryo media
h	Hours
hpf	Hours post fertilization
HRMA	High resolution melt curve analysis
HRP	Horseradish peroxidase

HSC	Hematopoietic stem cell
ICM	Intermediate cell mass
INT	2-(4-iodophenyl)-5-(4-nitrophenyl)-3-phenyltetrazolium chloride solution
kb	Kilobase
M	Molar
mg	Milligram
min	Minutes
ml	Millilitre
mM	Millimolar
MO	Morpholino antisense oligonucleotide
mRNA	Messenger ribonucleic acid
NAD	Nicotinamide adenine dinucleotide
NBT	4-nitro blue tetrazolium chloride solution
ng	Nanogram
NICD	Notch intracellular domain
PBS	Phosphate-buffered saline
PBSDTT	PBST + 1% DMSO + 0.1% Triton X-100
PBST	PBS + 0.1% Tween-20
PCR	Polymerase chain reaction
PFA	Paraformaldehyde
PID	Pbx-Interaction Domain
PLM	Posterior lateral-plate mesoderm
PTU	1-phenyl 2-thiourea
PVDF	Polyvinylidene difluoride
qPCR	Real-time quantitative PCR
RA	Retinoic acid
RARE	Retinoic acid response element
RBI	Rostral blood islands
RNA-seq	RNA-sequencing
RNAse	Ribonuclease
rpm	Revolutions per minute
RT	Room temperature
s	Seconds
SDS	Sodium dodecyl sulfate

SSC	Sodium saline citrate
TALE	Three amino acid loop extension
TALEN	Transcription activator-like effector nuclease
TBST	Tris-buffered saline + 0.1% Tween-20
Tm	Melting temperature
µl	Microlitres
ZFN	Zinc finger nuclease

List of Gene Abbreviations

Aldh1a, Raldh	Aldehyde dehydrogenase 1 family, member A
APC	Adenomatous polyposis coli complex
Axin	Axis inhibition protein
Bcdo2	β,β-carotene-9′,10′-dioxygenase
Bcmo1	β,β-carotene-15,15′-monooxygenase
CAMKII	Calmodulin-dependent protein kinase C
Cas9	CRISPR-associated 9
CBP	CREB binding protein
CD41, Itga2b	Integrin alpha 2b
CD45, Ptprc	Protein tyrosine phosphatase, receptor type, C
Cdx	Caudal type homeobox
Cmyb	V-myb avian myeloblastosis viral oncogene homolog
Crx	Cone-rod homeobox
Cyp1b1	Cytochrome P450, family 1, subfamily B, polypepetide 1
Cyp26	Cytochrome P450 subfamily 26
Dkk	Dickkopf
Dlc	DeltaC
Dld	DeltaD
Ef1a	Eukaryotic translation elongation factor 1 alpha 1a
Efn	Ephrin
Egr2b, Krox20	Early growth response 2b
Eng2a	Engrailed homeobox 2a
Epha3	Eph receptor A3
Fli1a	Fli-1 proto-oncogene
Foxn1	Forkhead box N1
Gata	GATA binding protein
Gli	GLI family zinc finger
GSK3β	Serine/threonine glycogen synthase kinase 3β
Hbae3	Hemoglobin alpha embryonic-3
HDAC	Histone deacetylase
Her	Hairy-related

Hes	Hairy and enhancer of split
Hh	Hedgehog
Hmx, Nk5	H6 Homeobox
Hmx4, Soho1	H6 Homeobox 4
Hox	Homeobox
Ihh	Indian hedgehog
Ikaros, Ikzf1	IKAROS family zinc finger 1
IP3	Inositol 1,4,5,-triphosphate
Jam	Junctional adhesion molecule
Jnk	Jun-kinase
Kdrl, Flk1a	Kinase insert domain receptor like
Lcp1	L-plastin
Lef	Lymphoid enhancer binding factor
Lmo2	LIM domain only 2
Lrp	Low density lipoprotein receptor-related protein
Lyz	Lysozyme C
Meis1	Myeloid ecotropic integration site 1
Mib	Mindbomb
Ncor	Nuclear receptor corepressor 1
NFAT	Nuclear factor of activated T-cells
NFkB	Nuclear factor kappa B
Nkx2.2a	NK2 homeobox 2a
p53, Tp53	Tumor protein p53
Pbx	Pre-B-cell leukemia homeobox
PCP	Planar cell polarity
Prep, PKnox	Pbx knotted homeobox
Prp2, Prnprs3	Prion protein 2
Ptc	Patched
Pu.1, Spi1b	Spi-1 proto-oncogene b
Rag1	Recombination activating gene 1
RAR	Retinoic acid receptor
RARE	Retinoic acid receptor element
RBPjκ	Recombination signal binding protein for immunoglobulin kappa J region

Rdh10	Retinol dehydrogenase 10
Ror	Receptor tyrosine kinase-like orphan receptor
Runx1	Runt-related transcription factor 1
RXR	Retinoid X receptor
Scl, Tal1	Stem cell leukemia
Shh	Sonic Hedgehog
Smo	Smoothened
SMRT, Ncor2	Nuclear receptor corepressor 2
Tcf	T-cell factor
Wnt	Wingless-type MMTV integration site family
Wwtr1, Taz	WW domain containing transcription regulator 1

Chapter 1

Introduction

1.1 Zebrafish as a model to study embryonic hematopoiesis

Zebrafish have recently become one of the most powerful model organisms with which to study embryonic hematopoieisis. They are highly amenable to genetic manipulation, and forward genetic screens have yielded mutants with a variety of hematopoietic defects. Analyses of these mutants have resulted in the identification of molecular pathways and hematopoietic transcription factors that are critical for the development of various hematopoietic lineages. These molecular pathways are conserved among vertebrates, and the critical mammalian (including human) hematopoietic genes have clear orthologues in zebrafish (reviewed by Davidson and Zon, 2004). Studies of zebrafish hematopoiesis may therefore be of clinical relevance.

Zebrafish embryos develop externally, and are optically transparent. These traits permit easy visualization of embryogenesis, and facilitate the use of immunohistochemical and *in situ* hybridization staining techniques to analyze protein and gene expression in whole embryos, at single-cell resolution. Using transgenic strains, researchers are also able to visualize hematopoietic cell formation *in vivo*, in real-time. Owing to their small size, zebrafish embryos can survive up to five days post fertilization (dpf) without active oxygen uptake. This permits researchers to analyze embryos lacking erythrocytes, or a functional circulatory system, without worrying about embryonic viability. Furthermore, zebrafish erythrocytes develop within the first 25 hours post fertilization (hpf), and hematopoietic stem cell emergence occurs by 30 hpf (Figure 1.1A, B). Consequently, the functional examination of genes that regulate the formation of both of these cell types can be conducted in a short time frame when using zebrafish as a model organism.

1.2 Biology of zebrafish primitive hematopoiesis

Primitive hematopoiesis influences morphology of the developing embryonic circulatory system (Baumann and Dragon, 2005; Hove et al., 2003) and produces circulating erythrocytes that facilitate tissue oxygenation during periods of rapid embryonic growth (Orkin and Zon, 2008). Zebrafish primitive hematopoiesis occurs primarily in the intermediate cell mass (ICM), which forms from bilateral stripes of posterior lateral-plate mesoderm (PLM) (Figure 1.1A, B). The intra-embryonic ICM is equivalent to the extra-

embryonic yolk sac blood islands of mammals and birds, and is responsible for generating the majority of embryonic hematopoietic cells (Figure 1.1C). Primitive hematopoiesis occurs within a short transitory period, and is subject to precise molecular regulation.

The earliest molecular marker of zebrafish hematopoiesis, the basic helix-loop-helix transcription factor *scl* is expressed as early as 10.5 hpf in the PLM (Figure 1.1B; Davidson et al., 2003; Gering et al., 1998). Domains of gene expression become more refined at 11 hpf, as mesoderm cell fate is progressively restricted to endothelial and erythroid lineages (Figure 1.1A, B). At this stage, cells of the PLM demonstrate overlapping expression patterns of *scl*, and other hematopoietic transcription factors such as the LIM domain protein *lmo2,* and the ETS family member *fli1a* (Figure 1.1B; Davidson and Zon, 2004). By 12 hpf, cell fate is irreversibly determined, and ICM precursors adopt one of two fates: (i) erythroid cell fate, characterized by *gata1* expression (Detrich et al., 1995); or (ii) angioblast (presumptive vascular) fate, which is characterized by the expression of the vascular endothelial growth factor receptor *kdrl* (Figure 1.1A, B; Davidson et al., 2003; Liao et al., 1997; Sumoy et al., 1997).

In addition to the PLM, zebrafish also possess a second, more anterior hematopoietic site. Known as the rostral blood islands (RBI), this site originates from anterior lateral-plate mesoderm, and is responsible for generating primitive macrophages and granulocytes (Figure 1.1B; Bennett et al., 2001; Herbomel et al., 1999; Lieschke et al., 2002). At 10 hpf, RBI cells express *scl* in an overlapping domain with the myeloid marker and ETS family transcription factor *pu.1* (Figure 1.1B; Bennett et al., 2001; Liao et al., 1998; Lieschke et al., 2002). By 24 hpf, these cells adopt more specific myeloid fates, expressing either the macrophage-specific marker *l-plastin* (*lcp1*) or the granulocyte marker *lysozyme C* (*lyz*) (Bennett et al., 2001; Herbomel et al., 1999; Lieschke et al., 2002; Liu and Wen, 2002).

Analyses in vertebrate models have identified a cascade of transcription factors that are critical for the specification of primitive erythrocytes. However, the upstream mechanisms by which these factors are regulated remain largely unclear. Previous research has shown that overexpressing posteriorly expressed *hox* genes partially rescues erythropoietic gene expression in mutants with defects in primitive blood cell differentiation (Davidson et al.,

2003; Davidson and Zon, 2006). These data support a model whereby Hox proteins serve to regulate primitive hematopoiesis.

1.3 Hox proteins in hematopoiesis and leukemia

Hox proteins are homeodomain-containing transcription factors with collinear temporal and spatial genomic organization. The DNA-binding homeodomain consists of a tri-alpha-helical structure spanning a minimum of 60 amino acids. Zebrafish possess 7-8 clusters of *hox* genes (Wagner et al., 2003), and 13 Hox paralogue groups. The Hox paralogue groups 5-13 are expressed in overlapping domains within the PLM (reviewed in Mallo et al., 2010), and several lines of evidence suggest that Hox proteins act as master regulators of hematopoietic cell fate decisions (Abramovich and Humphries, 2005). For example, mice bearing deletions in *Hoxb3*, *Hoxb4*, *Hoxb6*, *Hoxa7*, *Hoxc8,* or *Hoxa9* possess defects in the development of multiple hematopoietic lineages (Brun et al., 2004; Izon et al., 1998; Kappen, 2000; Ko et al., 2007; Lawrence et al., 1997; Magnusson et al., 2007; Shimamoto et al., 1999; So et al., 2004). In zebrafish, Caudal homeobox (Cdx) depletion results in diminished PLM *hox* gene expression, and a concomitant loss of erythroid gene expression (Davidson et al., 2003; Davidson and Zon, 2006). Overexpressing *hoxb6b*, *hoxb7a*, and *hoxa9a* partially rescues erythroid gene expression in *cdx1a*/*cdx4*-depleted embryos (Davidson et al., 2003; Davidson and Zon, 2006), placing Hox downstream of Cdx in the hematopoietic transcription factor hierarchy.

Hox genes are also implicated as proto-oncogenes in hematological malignancies (Kroon et al., 2001; Nakamura et al., 1996b; Pineault et al., 2003; Slape and Aplan, 2004), as dysregulated HOX expression is associated with poor prognosis in a variety of acute myeloid leukemias (AML) and acute lymphoblastic leukemias (ALL) (Argiropoulos and Humphries, 2007; Armstrong et al., 2002; Golub et al., 1999). Furthermore, gene fusions of *HOXA9* (Borrow et al., 1996; Nakamura et al., 1996a), *HOXA13* and HOXA11 (Taketani et al., 2002), *HOXC11* and *HOXC13,* (Taketani et al., 2002) or *HOXD13* (Raza-Egilmez et al., 1998) to the nuclear pore complex component gene *NUP98* are implicated in human AML, and their overexpression generates an AML-like phenotype in murine models (Dash et al., 2002; Pineault et al., 2003). Individual overexpression of *HOXB3* (Sauvageau et al., 1997;

Thorsteinsdottir et al., 2001), *HOXB6* (Fischbach et al., 2005), *HOXB8* (Perkins et al., 1990), *HOXA9* (Kroon et al., 1998) or *HOXA10* (Thorsteinsdottir et al., 1997) in mice also produces an AML-like phenotype. Combined, these data suggest that Hox proteins participate in both normal and malignant hematopoiesis.

1.4 Hox cofactors Pbx and Meis

The Hox homeodomain binds a 5'-TAAT-3' core motif (reviewed in Affolter et al., 2008; Berger et al., 2008; Noyes et al., 2008). The specificity of Hox proteins is therefore achieved through their interaction with other DNA-binding cofactors (Mann, 1995; Mann and Affolter, 1998; Mann and Chan, 1996). Such cofactors include the Three Amino acid Loop Extension (TALE)-class homeodomain transcription factors Meis (Myeloid Ecotropic Integration Site), Pbx (Pre-B-Cell Leukemia Homeobox), and Prep/PKnox (Pbx Knotted Homeobox) (reviewed in Mann et al., 2009; Moens and Selleri, 2006). The TALE occurs between the first and second alpha helix of the homeodomain (Burglin, 1997). Meis/Prep and Pbx coordinately bind DNA with Hox proteins, typically increasing their DNA-binding affinity as well as specificity (Berthelsen et al., 1998a; Chan and Mann, 1996; Chan et al., 1996; Chang et al., 1997; Ebner et al., 2005; Knoepfler et al., 1996; LaRonde-LeBlanc and Wolberger, 2003; Mann, 1995; Mann and Chan, 1996). Notably, interactions between Hoxc6, Hoxb7, or Hoxb8 and Pbx/Meis proteins increase Hox DNA binding affinity but not specificity (Neuteboom and Murre, 1997), while the reverse is true for the interaction between Hoxa9 and Pbx1 (LaRonde-LeBlanc and Wolberger, 2003). Pbx binds Hox paralogue groups 1-4 through both its TALE motif and a tryptophan-containing hexapeptide motif termed the Pbx-Interaction Domain (PID) (Chang et al., 1995; Knoepfler and Kamps, 1995; Mann, 1995; Mann and Chan, 1996; Neuteboom et al., 1995; Peltenburg and Murre, 1996). This PID is not present in Hox paralogue groups 11-13. Notably, Meis is able to directly bind Hox paralogue groups 9-13 through a C-terminal domain (Shen et al., 1997; Williams et al., 2005).

All paralogue group 1 Hox proteins require Pbx and Meis/Prep proteins to activate transcription (Uhl et al., 2010). Subsequently, embryos lacking Meis and Pbx display phenotypes that are consistent with a total lack of Hox function. For example, loss of both

Pbx2 and Pbx4 in the zebrafish hindbrain generates an anteriorizing homeotic transformation of the neural tube, in which rhombomeres 2-6 take on the molecular and neuronal identity of rhombomere 1 (Popperl et al., 2000; Waskiewicz et al., 2002). A nearly identical phenotype results from the knockdown of *Hoxa1, Hoxb1,* and *Hoxd1* gene products in *Xenopus* (McNulty et al., 2005). In zebrafish, overexpressing *meis3* in combination with *pbx4* and *hoxb1b* posteriorizes the neural tube, transforming the presumptive forebrain and midbrain regions into a hindbrain fate (Vlachakis et al., 2001). Combined, these data illustrate the significant role that TALE-class proteins play as Hox cofactors *in vivo*.

Previous studies have contributed to our knowledge of the mechanisms by which TALE-class homeodomain transcription factors modulate transcription (reviewed by Ladam and Sagerstrom, 2014). Consistent with their role as transcriptional activators, Pbx and Meis bind the histone acetyltransferase CBP (Chariot et al., 1999; Choe et al., 2009; Goh et al., 2009; Huang et al., 2005; Saleh et al., 2000; Wang et al., 2010). Pbx also functions as transcriptional repressor, interacting with histone deacetylases (HDACs) and SMRT/NCoR transcriptional co-repressors on its own, or when in a complex with Hox (Asahara et al., 1999; Saleh et al., 2000). Addition of Meis to the Hox-Pbx complex generates a conformational change in Pbx that displaces HDACs and permits the recruitment of transcriptional activators (Choe et al., 2009). Recently, Choe et al. (2014) demonstrated that zebrafish Pbx and Meis/Prep proteins occupy the *hoxb1a* promoter in the absence of Hox. This facilitates the recruitment of histone acetylating enzymes (such as CBP), and RNA Polymerase II, thereby activating transcription (Choe et al., 2014). Notably, this association also increases trimethylation of histone H3 on lysine 27 (H3K27me3), which is associated with transcriptional repression. The addition of Hoxb1b to the TALE complex enhances transcription by reducing H3K27me3 levels and increasing RNA Polymerase II activity (Choe et al., 2014).

It should be noted that Pbx and Meis/Prep1 proteins also form stable heterodimeric complexes in the absence of Hox proteins (Berthelsen et al., 1998b; Chang et al., 1997; Rieckhof et al., 1997), and are regulated both pre- and post-transcriptionally. For example, Meis1 is normally sequestered in the cytoplasm, but Pbx-Meis complexes are actively transported into the nucleus (Abu-Shaar et al., 1999; Berthelsen et al., 1999; Jaw et al., 2000;

Mercader et al., 1999; Rieckhof et al., 1997; Vlachakis et al., 2001). Meis and Pbx proteins also bidirectionally stabilize each other. This stabilization is dependent upon domains that mediate Meis-Pbx complex formation (Jaw et al., 2000; Longobardi and Blasi, 2003; Waskiewicz et al., 2001).

1.5 Role of Pbx and Meis in hematopoiesis and leukemia

In addition to their role in hindbrain patterning, there is evidence that TALE-class proteins play an important role in regulating embryonic hematopoiesis. *Pbx1*-knockout mice display a lethal reduction in definitive multipotent blood progenitors, leading to reduced hematocrit and severe embryonic anemia (DiMartino et al., 2001). *Meis1*-deficient mice display a severe reduction in myeloerythroid progenitors (Azcoitia et al., 2005; Hisa et al., 2004), and *Prep1*-deficient mice exhibit profound anemia (Di Rosa et al., 2007; Ferretti et al., 2006; Penkov et al., 2005).

Further support for the function of Pbx and Meis as hematopoietic regulators lies in their role as oncogenes. Pbx was initially identified as part of the E2A-Pbx1 fusion protein, which is found in 25% of pediatric pre-B cell acute lymphoblastic leukemias (Carroll et al., 1984), as well as in a fraction of acute myeloid and T-lymphoid leukemias (Troussard et al., 1995). E2A-Pbx1 is a product of the t(1,19) chromosomal translocation, and contains the transcriptional activation domains of the immunoglobulin enhancer-binding protein E2A fused to the Pbx1 homeodomain (Kamps and Baltimore, 1993; Nourse et al., 1990). E2A-Pbx1 generates AML in mice (Dedera et al., 1993; Kamps et al., 1991).

As with Pbx, Meis1 has also been implicated in leukemia. Retroviral integration and concomitant upregulation of Meis1 expression is found in 15% of BXH2 myeloid leukemias (Moskow et al., 1995; Nakamura et al., 1996b), and most leukemias with Meis1 retroviral integration also exhibit retroviral integration upstream of *Hoxa7* and *Hoxa9*, leading to their increased expression (Nakamura et al., 1996a). Furthermore overexpressing Meis1 along with *Hoxa9* in murine models reduces the period of latency required to generate AML (Kroon et al., 1998; Thorsteinsdottir et al., 2001). Combined, these findings suggest that Meis1 acts in concert with *Hoxa7*/*Hoxa9* to induce leukemia.

1.6 Biology of definitive hematopoiesis

All adult vertebrate hematopoietic lineages arise from a common multipotent progenitor, the hematopoietic stem cell (HSC). This definitive hematopoietic cell type is able to self renew, differentiate into all major blood lineages, and maintain adult hematopoiesis for life. The HSC arises intraembryonically, in an anatomically distinct site from primitive hematopoietic cells (reviewed in Davidson and Zon, 2004; Palis and Yoder, 2001). HSCs emerge from mesoderm-derived hemogenic endothelium, in close association with the dorsal aorta (Figure 1.1; Dzierzak, 2005; Palis and Yoder, 2001). In mice, this region is termed the aorta-gonad-mesonephros (AGM). Analogous structures in other vertebrates include the para-aortic splanchnopleura of humans (Tavian et al., 1996) and chick (reviewed in Dieterlen-Lievre, 2001), and the dorsolateral plate of Xenopus (Chen and Turpen, 1995). Following their emergence, mammalian HSCs then migrate to the fetal liver and spleen before becoming established in the bone marrow (Figure 1.1C; reviewed by Cumano and Godin, 2007; Moore and Metcalf, 1970).

Like in mammals, the zebrafish site of definitive hematopoiesis shifts throughout development (Figure 1.1B). Zebrafish HSCs first emerge from dorsal aorta hemogenic endothelium (in a region analogous to the mammalian AGM) at 30 hpf (Figure 1.1A, B; Burns et al., 2002; Kalev-Zylinska et al., 2002; Thompson et al., 1998). These cells express *runx1* and *cmyb* (Burns et al., 2002; Kalev-Zylinska et al., 2002), transcription factors essential for HSC formation (Figure 1.1B; Burns et al., 2002; Burns et al., 2005; Gering and Patient, 2005; Kalev-Zylinska et al., 2002; Okuda et al., 1996; Thompson et al., 1998; Wang et al., 1996a), and emergence (Zhang et al., 2011), respectively. Following their emergence, these cells migrate posteriorly to the caudal hematopoietic tissues (CHT; analogous to the mammalian liver) by 48 hpf, before becoming established in the thymus by 3 days post fertilization (dpf) and pronephros by 4 dpf (Figure 1.1B; Jin et al., 2007; Murayama et al., 2006). The kidney (equivalent to mammalian bone marrow) is the major site of adult teleost hematopoiesis (Figure 1.1B; reviewed by Cumano and Godin, 2007; Paik and Zon, 2010).

Although much is known about the cellular and functional properties of vertebrate HSCs, little information exists about the genetic pathways that govern HSC induction, expansion, and homeostasis. However, loss and gain of function analyses in mouse and

zebrafish have implicated the Notch, Wnt, Hedgehog and retinoic acid developmental signaling pathways in vertebrate HSC formation.

1.7 Notch signaling

Notch signaling plays a critical role in several developmental processes, by allowing for direct cell-to-cell communication that regulates proliferation, differentiation and apoptosis (reviewed in Bray, 2006; Guruharsha et al., 2012; Kopan and Ilagan, 2009). Figure 1.2 provides a schematic overview of the Notch signal transduction pathway. Notch is a transmembrane surface receptor. Binding of the Notch receptor to its Delta or Jagged transmembrane ligand on a neighboring cell induces a conformational change in the Notch receptor that renders it susceptible to cleavage by γ-secretase. This cleavage event releases the Notch intracellular domain (NICD). The NICD then enters the nucleus, where it acts as a transcriptional activator in a complex with Recombination signal binding protein for immunoglobulin kappa J region (RBPjκ) (Kopan and Ilagan, 2009; Lai, 2002). The basic helix-loop-helix transcription factors hairy and enhancer of split (Hes) are transcriptional targets of the Notch signaling pathway. These proteins act as Notch-dependent transcriptional regulators, and serve to mediate the majority of Notch function (Iso et al., 2003; Iso et al., 2001). Zebrafish possess four Notch receptors: *notch1a*, *notch1b*, *notch2*, and *notch3*. Of these *notch1b*, and *notch3* are expressed in both the dorsal aorta and HSCs (Bertrand et al., 2010). So is *her6*, the zebrafish orthologue of *hes1* (Bertrand et al., 2010; Chen et al., 2007).

1.8 Notch signaling in definitive hematopoiesis

The Mindbomb (Mib) protein is critical for Delta and Jagged ligand maturation (Appel et al., 1999; Itoh et al., 2003; Jiang et al., 1996; Riley et al., 1999; Schier et al., 1996; Wang et al., 1996a). Studies of zebrafish *mib* mutants have revealed an integral role for Notch signaling in arterial fate specification (reviewed in Rossant and Hirashima, 2003; Weinstein and Lawson, 2002). *mib* mutants exhibit absent arterial gene expression, and ectopic venous gene expression within the dorsal aorta (Gering and Patient, 2005; Lawson et al., 2001). Treating embryos with the γ-secretase inhibitor N-[N-(3,5-Difluorophenacetyl)-L-alanyl]-S-

phenylglycine t-butyl ester (DAPT) elicits a similar phenotype (Bertrand et al., 2010; Burns et al., 2005; Gering and Patient, 2005). Given the relationship between arterial fate specification and HSC formation, it is therefore not surprising that both *mib* mutants, and DAPT-treated zebrafish embryos also fail to produce HSCs (Bertrand et al., 2010; Burns et al., 2005; Gering and Patient, 2005).

Notably, *Jagged1*-mutant mice and zebrafish also fail to produce HSCs, but do not exhibit defects in specifying arterial cell fate (Robert-Moreno et al., 2008). Furthermore, activation of Notch signaling in *hsp70:gal4*;*UAS:NICD* zebrafish embryos is sufficient to drive ectopic HSC gene expression, but does not induce ectopic arterial gene expression (Burns et al., 2005). Combined, these data support an angiogenesis-independent function for Notch signaling in definitive hematopoiesis.

Further support for the angiogenesis-independent function of Notch signaling in specifying HSCs comes from analyses of individual components of the Notch signaling pathway. *Notch1* is expressed in endothelial cells of the murine AGM (Kumano et al., 2003; Villa et al., 2001), while *Notch1* and *Notch2* are both expressed in hemogenic progenitors and HSCs (Bigas et al., 1998; Kumano et al., 2003; Milner et al., 1994). However, only NOTCH1 is required for the initiation of definitive hematopoiesis, as explant cultures derived from the para-aortic splanchnopleura (a mesodermal precursor of the AGM) of *Notch1*, but not *Notch2*-mutant mice exhibit defects in HSC formation (Kumano et al., 2003; Robert-Moreno et al., 2005). Notably, although *Notch1*-mutant embryos also exhibit defects in angiogenesis (Krebs et al., 2000), they exhibit wild type numbers of hemogenic endothelial cells (Kumano et al., 2003), suggesting that NOTCH1 is required for rendering hemogenic endothelial cells competent to produce HSCs. As only a small subset of HSC progeny are affected in conditional *Notch1*-mutant mice when NOTCH1 is disrupted after birth (Radtke et al., 1999), these combined data suggest that NOTCH1 is required to initiate, but not maintain HSC formation. Notably, *Notch1*-mutant embryonic stem cells fail to contribute to the wild type adult hematopoietic system in mouse chimeras, indicating that NOTCH1 acts in a cell-autonomous fashion to specify HSCs (Hadland et al., 2004).

RBPjκ acts in a nuclear complex with the NICD, and is essential to Notch signaling (Han et al., 2002; Pear and Radtke, 2003; Pui et al., 1999; Radtke et al., 1999). In addition to

defects in HSC formation, both *Notch1*- and *RBPjκ*-mutant mice exhibit reduced para-aortic splanchnopleura expression of *Runx1*, *Scl*, and *Gata2* (Kumano et al., 2003; Robert-Moreno et al., 2005), transcription factors essential for definitive hematopoiesis (Okuda et al., 1996; Porcher et al., 1996; Tsai et al., 1994). Notably, retroviral transfection of *Runx1*, but not *Scl* or *Gata2* is able to rescue HSC formation in para-aortic splanchnopleura explants derived from *Notch1*-mutant embryos (Nakagawa et al., 2006). Combined, these data place RBPjκ and Notch1 upstream of *Runx1* in definitive hematopoiesis.

1.9 Hedgehog signaling

Previous research has led to the identification of Hedgehog (Hh) signaling components, and to a general understanding of the basic mechanism behind Hh signal transduction (Figure 1.3; reviewed by Hooper and Scott, 2005). Following a series of post-translational modifications (Farzan et al., 2008), the mature Hh ligand is exported from the cell. It then binds to the Patched (Ptc) receptor. This interaction results in de-repression of the membrane-associated Smoothened (Smo) protein. Smo is then free to initiate a signal transduction cascade that results in the cleavage and/or activation of GLI family zinc finger (Gli) transcription factors. Gli transcription factors act as both transcriptional activators and repressors in response to Hh signaling. Notably, *ptc* is itself a transcriptional target of Hh signaling (Hooper and Scott, 2005; Ingham and McMahon, 2001).

Drosophila have only a single member of each Hh pathway component. Conversely, a series of evolutionary duplication events have allowed vertebrates to possess multiple copies of certain components. There are three Hh proteins in mammals: Sonic hedgehog (SHH), Desert hedgehog (DHH), and Indian hedgehog (IHH). Zebrafish possess two paralogues each of *ihh* (*ihha*, *ihhb*) and *shh* (*shha*, *shhb*). Both mice and zebrafish possess two Ptc proteins (Ptc1, and Ptc2).

Gli protein functions have diverged throughout vertebrate evolution. There are three Gli proteins in vertebrates (Gli1, Gli2 and Gli3). Zebrafish possess two *gli2* paralogues (*gli2*a, *gli2b*) In mice, GLI2 is the predominant activating Gli in response to Hh signaling, and exhibits partial functional redundancy with GLI1. Conversely, murine GLI3 acts as a repressor. In zebrafish, Gli1 is the predominant activating Gli. Depending on the

developmental stage and tissue examined, zebrafish Gli2a, Gli2b and Gli3 may act as both transcriptional repressors and activators (Karlstrom et al., 2003; Tyurina et al., 2005).

1.10 Hedgehog signaling in definitive hematopoiesis

In vitro studies have implicated Hh signaling in definitive hematopoiesis. For example, treating mouse anterior epiblast explant cultures with IHH induces them to form blood and endothelial cells (Dyer et al., 2001). Conversely, embryonic stem cells that lack *Ihh* or *Smo*, or have been treated with Hh signaling inhibitors, fail to produce hematopoietic cells in culture (Byrd et al., 2002; Maye et al., 2000). More recently, Geon Kim et al. (2012) demonstrated that overexpressing *Ihh* in vascular endothelial cells derived from a mouse embryonic stem cell line generates an increase in the number of cells that express the hemogenic endothelial marker CD45, and a subsequent increase in the number of CD41-positive definitive hematopoietic cells. Notably, IHH treatment of CD41-positive cells did not promote their expansion (Kim et al., 2013), suggesting that vascular endothelial cells, but not their hematopoietic progeny, are responsive to IHH. Combined, these *in vitro* data implicate Hh signaling in the specification of hemogenic endothelium.

In vivo evidence for the role of Hh signaling in definitive hematopoiesis has been provided by analyzing zebrafish Hh signaling pathway component mutants, as well as embryos treated with the Smo antagonist cyclopamine (Barresi et al., 2001; Chen et al., 2002a; Chen et al., 2002b). Zebrafish *smo* (*slow-muscle-ommited*/*smu*) mutants, and embryos treated with cyclopamine during gastrulation display incomplete migration of dorsal aorta progenitors to the embryonic midline (Gering and Patient, 2005; Wilkinson et al., 2012; Williams et al., 2010). These embryos also fail to produce a dorsal aorta (Wilkinson et al., 2012; Williams et al., 2010), and display a corresponding severe reduction in HSCs (Gering and Patient, 2005). Owing to the continued presence and partial redundancy of other hedgehog proteins (Shha and Ihhb) (Schauerte et al., 1998), the *shha* mutant (*sonic-you*/*syu*) displays complete migration of dorsal aorta progenitors to the midline (Gering and Patient, 2005; Lawson et al., 2002). However, *shha* mutants, and embryos treated with cyclopamine after gastrulation, or from 14 hpf onwards fail to specify arterial cell fate (Gering and Patient, 2005; Lawson et al., 2002). These embryos do not produce a dorsal aorta (Brown et al., 2000),

and fail to produce HSCs (Gering and Patient, 2005). Notably, zebrafish embryos treated with cyclopamine from 16.5 hpf onwards exhibit proper expression of arterial cell fate markers, form a dorsal aorta, and are able to produce HSCs (Gering and Patient, 2005). These data suggest that Hh signaling is not required at the time when HSCs first emerge from dorsal aorta hemogenic endothelium (30 hpf; Burns et al., 2005; Kalev-Zylinska et al., 2002; Thompson et al., 1998). This is somewhat surprising, given that Hh proteins continue to be secreted from the notochord at this time (Krauss et al., 1993; Lewis et al., 1999; Roy et al., 2001), and the Hh target genes *ptc1* and *ptc2* are expressed in the dorsal aorta (Lewis et al., 1999). Combined, these data suggest that Hh signaling participates in definitive hematopoiesis at two distinct developmental time points prior to HSC emergence: first, by facilitating the migration of dorsal aorta progenitors towards the embryonic midline, and then by specifying arterial cell fate.

Studies suggest that in addition to Hh signaling, Notch signaling is also essential for arterial fate specification (reviewed by Rossant and Hirashima, 2003; Weinstein and Lawson, 2002). Activation of Notch signaling rescues HSC formation in cyclopamine-treated zebrafish embryos (Kim et al., 2013). Furthermore, *notch5* dorsal aorta gene expression is lost in both *shha*-mutants and cyclopamine-treated zebrafish embryos (Lawson et al., 2002). Taken together, these data suggest that Hh signaling act upstream of Notch to regulate arterial specification and definitive hematopoiesis.

1.11 Wnt signaling

Wnt (Wingless-type MMV integration site family) ligands are secreted glycoproteins that bind to members of the Frizzled and LRP (low density lipoprotein receptor-related protein) family of transmembrane co-receptors (Huang and He, 2008; Mikels and Nusse, 2006). The secreted protein Dickkopf (Dkk) competitively inhibits the interaction between Wnt and its receptors by acting as a ligand for LRP (Bafico et al., 2001; MacDonald et al., 2009; Mao et al., 2001a; Semenov et al., 2001).

Figure 1.4 provides a schematic overview of the canonical Wnt signaling pathway. Canonical Wnt signaling occurs through the stabilization of β-catenin (reviewed by Grigoryan et al., 2008). In the absence of Wnt, β-catenin is phosphorylated and ubiquitinated

by a destruction complex containing Serine/threonine glycogen synthase kinase 3β (GSK3β), Axis inhibition protein (Axin), and Adenomatous polyposis coli complex (APC). This leads to its proteosomal degradation (Aberle et al., 1994; Behrens et al., 1998; Liu et al., 2002; Marikawa and Elinson, 1998; Salomon et al., 1997; Yanagawa et al., 2002). In the presence of the Wnt, LRP is phosphorylated, allowing it to bind and sequester Axin. This prevents assembly of the β-catenin destruction complex (Bilic et al., 2007; Mao et al., 2001b; Schwarz-Romond et al., 2007a; Schwarz-Romond et al., 2007b). β-catenin then enters the nucleus, binding the T-cell factor (Tcf) and lymphoid enhancer binding factor (Lef) family of transcription factors, and activating the transcription of Wnt target genes (reviewed by Clevers, 2006; Nelson and Nusse, 2004; Willert and Jones, 2006).

The non-canonical Wnt signaling pathways are less understood compared to canonical Wnt signaling. Both pathways may include Frizzled receptors. However, the non-canonical Wnt signaling pathways may not make use of LRP co-receptors, and do not require β-catenin (reviewed by Semenov et al., 2007). Multiple non-canonical signaling pathways have been described. Of these, the Wnt/Jun-kinase (JNK)/planar cell polarity/(PCP), and the Wnt-Ca^{2+} pathways have been implicated in definitive hematopoiesis (reviewed in Staal et al., 2008). The Wnt/JNK/PCP pathway uses the receptor tyrosine kinase-like orphan receptor (ROR) family of co-receptors. This pathway acts through the Dishevelled protein to activate RhoA/Rac signaling, and JNK. This leads to the transcription of Wnt/JNK/PCP target genes, and the regulation of cytoskeleton organization and cell polarity.

The Wnt-Ca^{2+} pathway may also use ROR family of co-receptors. Activation of this pathway results in the phospholipase C-mediated cleavage of phosphatidylinositol and the production of diacylglycerol (DAG) and inositol 1,4,5,-triphosphate (IP3). IP3 then binds to gated calcium channels, leading to the release of internal Ca^{2+} stores and the activation of Calmodulin-dependent protein kinase C (CaMKII). DAG activates protein kinase C (Kuhl et al., 2000a; Kuhl et al., 2000b; Sheldahl et al., 1999; Slusarski et al., 1997). This allows for the downstream activation of the transcriptional co-activators Nuclear factor of activated T-cells (NFAT) and Nuclear factor kappa B (NFκB) to enter the nucleus and initiate the transcription of non-canonical Wnt target genes.

1.12 Wnt signaling in definitive hematopoiesis

Given the widespread tissue expression of the *wnt* gene family, it is no surprise that Wnt proteins have been implicated in a multitude of developmental processes, including hematopoiesis. Canonical Wnt signaling is essential for patterning the anterior-posterior axis, and for mesoderm formation (Haegel et al., 1995; Huelsken et al., 2000; Morkel et al., 2003). Consequently, abrogation of Wnt signaling often generates severe, gross morphological defects. This has made it difficult to determine if canonical Wnt signaling possesses a specific role in regulating definitive hematopoiesis, or if perturbations in HSC formation are a secondary consequence of alterations in mesoderm patterning. For example, although *Wnt3a*-mutant mice exhibit reduced numbers of HSCs (Luis et al., 2009), these embryos also lack caudal tissues, and fail to form a dorsal aorta (Takada et al., 1994). Researchers have therefore relied primarily on gain-of-function experiments to elucidate the role of canonical Wnt signaling in definitive hematopoiesis (reviewed in Staal and Luis, 2010). Studies using Tcf-GFP reporters have indicated that the canonical Wnt signaling pathway is active in HSCs (Rattis et al., 2004; Reya and Clevers, 2005). Furthermore, constitutive activation of β-catenin in HSCs increases their numbers, whereas expressing the Wnt signaling antagonist Axin in HSCs reduces their capacity to reconstitute lethally irradiated mice (Reya, 2003; Willert et al., 2003). Combined, these data suggest that canonical Wnt signaling is likely involved in expanding and maintaining HSC populations. Further evidence that canonical Wnt signaling may play a role in definitive hematopoiesis comes from examining transgenic zebrafish embryos expressing inducible forms of Wnt signaling antagonists. Transient induction of *Dkk*, *Axin*, or dominant-negative *Tcf* at 14 hpf generates a strong reduction in embryonic HSC gene expression (Goessling et al., 2009), suggesting that canonical Wnt signaling may be required for HSC formation.

As with canonical Wnt signaling, studies elucidating the role of non-canonical Wnt signaling in definitive hematopoiesis have been based primarily on overexpression assays and *in vitro* cell-culture assays (reviewed in Kokolus and Nemeth, 2010). Consequently, the precise *in vivo* requirement for non-canonical Wnt signaling components in definitive

hematopoiesis has remained elusive until recently, when Clements et al. (2011) demonstrated a requirement for Wnt16 in zebrafish hematopoiesis.

The human *WNT16* orthologue was initially identified as a gene misexpressed in pre-B-cell acute lymphoblastic leukemia cells generated by the E2A-PBX1 (t1:19) chromosomal translocation (McWhirter et al., 1999), implicating it in definitive hematopoiesis. In zebrafish, *wnt16* is expressed in paraxial mesoderm between 10 hpf and 24 hpf (Clements et al., 2011). Although *wnt16*-morphant zebrafish embryos exhibit normal arterial gene expression within the dorsal aorta, these embryos exhibit a severe reduction in HSC and common lymphoid progenitor gene expression (Clements et al., 2011). These data suggest that Wnt16 is required for HSC formation. Wnt16 participates in a non-canonical Wnt signaling pathway, as its depletion has no effect on the expression of β-catenin/Tcf-dependent reporter transgene expression (Clements et al., 2011).

Notably, in addition to hematopoietic defects, *wnt16*-depleted zebrafish embryos also exhibit reduced expression of the Notch ligands *dlc* and *dld* (Clements et al., 2011). Furthermore, HSC gene expression is lost in dlc mutants injected with *dld* morpholino, and *dlc* and *dld* overexpression rescues HSC gene expression in *wnt16*-morphants (Clements et al., 2011). Combined, these data suggest that Wnt16 acts upstream of the Notch signaling pathway to regulate definitive hematopoiesis.

Artificial activation of Notch signaling prior to dorsal aorta formation (15-17 hpf) in *wnt16*-morphant zebrafish embryos rescues their HSC gene expression defects (Clements et al., 2011). As Wnt16 is not required for arterial specification, and is not expressed within the dorsal aorta, these combined data suggest that it acts in a non-cell-autonomous fashion to regulate HSC formation. These data also suggest that Wnt16 (as well as *dlc*/*dld*) acts in parallel to the Shh/Notch pathway that regulates arterial specification. Notably, *wnt16* expression is abrogated in *ptc1/2*-mutant zebrafish, suggesting that it is negatively regulated by Shh signaling (Wilkinson et al., 2012).

1.13 RA signaling

The vitamin A (retinol) derivative retinoic acid (RA) is an extremely potent diffusible morphogen. Consequently, levels of RA are tightly regulated within the developing embryo.

Figure 1.5 provides a schematic overview of RA metabolism and signaling. Catalysis from cellular retinol occurs through a series of enzymatic reactions. First, Retinol dehydrogenase 10 (Rdh10) converts retinol into retinaldehyde (Sandell et al., 2007). Then, Aldehyde dehydrogenase 1a (Aldh1a; also known as Retinaldehyde dehydrogenase 1a, Raldh1a) proteins convert retinaldehyde into RA (reviewed in Duester, 2000; Kam et al., 2012). The *aldh1a* genes encode the rate-limiting enzymes in RA synthesis, and high levels of RA occur in tissues that express them (Begemann et al., 2001; Niederreither et al., 1999; Niederreither et al., 2000). Mammals posses three *aldh1a* genes: *aldh1a1*, *aldh1a2*, and *aldh1a3*. Zebrafish possess only *aldh1a2* and *aldh1a3*. Of the known *aldh1a* genes expressed in early zebrafish development, only *aldh1a2* is expressed in the paraxial mesoderm and somites (Begemann et al., 2001; Grandel et al., 2002). It is also expressed within the dorsal retina (Begemann et al., 2001; Grandel et al., 2002). *aldh1a3* expression is limited to the ventral retina (Pittlik et al., 2008). Mouse *Aldh1a2* mutants strongly recapitulate phenotypes associated with Vitamin A deficiency, suggesting that Aldh1a2 is the main source of RA in the vertebrate embryo (Niederreither et al., 1999; Niederreither et al., 2000).

Cyp1b1 (Cytochrome P450, family 1, subfamily B, polypepetide 1) is another protein that has been shown to catalyze RA synthesis in multiple tissues throughout chick development (Chambers et al., 2007). Zebrafish *cyp1b1* expression is limited to the retina, midbrain-hindbrain boundary and diencepalon (Yin et al., 2008). It is therefore unlikely to participate in zebrafish hematopoiesis.

Levels of RA are also modulated through the actions of Cytochrome P450 subfamily 26 (Cyp26) proteins. Cyp26 proteins hydroxylate RA, targeting it for degradation (reviewed in White and Schilling, 2008). Zebrafish possess three *cyp26* genes: *cyp26a1*, *cyp26b1*, and *cyp26c1*. *cyp26a1* is expressed within the anterior neurectoderm and tail bud (Kudoh et al., 2002). *cyp26b1* and *cyp26c1* are expressed within the developing diencephalon, telencephalon, and hindbrain (Gu et al., 2005; Hernandez et al., 2007; White and Schilling, 2008; Zhao et al., 2005). The combined action of the Aldh1a and Cyp26 proteins generate a dynamic gradient of RA as development proceeds (Shimozono et al., 2013).

Previous research has also implicated the Bcdo2 (β,β-carotene-9′,10′-dioxygenase), and Bcmo1 (β,β-carotene-15,15′-monooxygenase) enzymes in RA metabolism, although their

contributions to vertebrate RA signaling are not well established. Bcmo1 catalyzes the conversion of retinol to retinal (von Lintig and Vogt, 2000). Zebrafish *bcmo1* is expressed in the head, ventral optic primordia, pectoral fin buds, and within mesoderm along the anteroposterior axis of the yolk boundary (Lampert et al., 2003). Bcmo1-depletion in zebrafish produces phenotypes that are reminiscent of a mild RA-deficiency (Lampert et al., 2003). These include diminished *hoxb4a* expression, and misshapen pectoral fins.

Bcdo2 has been shown to participate in retinol metabolism in both mouse and *Drosophila* (Kiefer et al., 2001; von Lintig and Vogt, 2000; von Lintig and Vogt, 2004) and catalyzes the assymetric cleavage of beta-carotene into beta-apocarotenoic acid, which can be metabolized to form RA in an Aldh1a-independent fashion (Wang et al., 1996b). During zebrafish development, *bcdo2* is expressed in the neural crest, heart, and in ventral cells along the anteroposterior axis of the yolk boundary (Lobo et al., 2012). Following organogenesis, zebrafish *bcdo2* expression becomes restricted to the liver, intestine, and ovary (Levi et al., 2012; Lobo et al., 2012). Bcdo2-depleted zebrafish embryos display no obvious morphological defects, but demonstrate blood cell apoptosis leading to anemia (Lobo et al., 2012). It is not clear whether or not this phenotype is the result of altered RA signaling.

Once synthesized, RA binds to retinoic acid receptor (RAR) and retinoid X receptor (RXR) heterodimers on the retinoic acid receptor elements (RAREs) of genes. These RAREs consist of two direct repeats separated by a 5 base pair spacer (reviewed by Germain et al., 2006; Mangelsdorf and Evans, 1995). In the absence of RA, RAR-RXR heterodimers repress transcription by binding to NCor and SMRT-type corepressors. Upon binding RA, RAR undergoes a conformational change that permits the release of these corepressors. The subsequent recruitment of p300 and NCoA coactivator proteins then activate transcription (reviewed by Belandia and Parker, 2003; Glass and Rosenfeld, 2000). Zebrafish possess four *rar* genes (*rarαa*, *rarαb*, *rarγa*, *rarγb*) and six *rxr* genes (*rxrαa*, *rxrαb*, *rxrβa*, *rxrβb*, *rxrγa*, *rxrγb*). Each *rar* and *rxr* exhibits a distinct developmental expression pattern (Hale et al., 2006; Tallafuss et al., 2006; Waxman and Yelon, 2007), allowing for further spatial and temporal regulation of RA signaling within the developing embryo.

1.14 RA signaling in primitive hematopoiesis

Evidence for the role of RA signaling in primitive hematopoiesis has emerged from analyses of Vitamin-A deficiency models, as well as yolk sac explants and embryos treated with RA agonists or antagonists. Treating murine yolk sac explants with exogenous RA reduces their ability to differentiate into the erythroid lineage (de Jong et al., 2010). Conversely, cells and explants treated with the Alhdehyde dehydrogenase inhibitor diethylaminobenzaldehyde (DEAB), or the Retinoic acid receptor antagonist AGN193109, exhibit increased erythroid potential (de Jong et al., 2010). These *in vitro* studies suggest that RA may serve to limit the formation of primitive erythroid progenitors. *In vivo* support for this role comes from examining Zebrafish and *Xenopus* embryos, which when treated with exogenous RA exhibit reduced primitive erythroid gene expression (de Jong et al., 2010; Sive and Cheng, 1991). Conversely, embryos treated with DEAB exhibit strongly upregulated primitive erythroid gene expression (Ma et al., 2010). These data therefore provide evidence to suggest that RA plays an inhibitory role in vertebrate erythropoiesis. Notably, RA signaling appears to play an activating role in avian primitive erythropoiesis, as Vitamin A-deficient quail exhibit reduced numbers of primitive erythrocytes (Ghatpande et al., 2002). The close association between endothelial cell development and primitive hematopoiesis may explain these apparently contradictory results, as Vitamin A-deficient quail possess gross defects in vascular development (Ghatpande et al., 2002), whereas RA-deficient zebrafish and mice do not exhibit decreased endothelial gene expression (de Jong et al., 2010; Goldie et al., 2008; Ma et al., 2010).

In addition to its function in primitive erythropoiesis, studies in mouse and zebrafish have also elucidated a role for RA signaling in primitive myelopoiesis. Zebrafish treated with exogenous RA exhibit reduced numbers of primitive myeloid cells in the anterior lateral-plate mesoderm (Liang et al., 2012). As these embryos also exhibit reduced expression of anterior hemangioblast markers (Liang et al., 2012), the myelopoietic defects observed in RA-treated embryos may be the indirect result of losing anterior hemangioblast cell fate. Notably, DEAB-treated zebrafish embryos exhibit increased numbers of primitive myeloid cells (Liang et al., 2012; Ma et al., 2010). Combined, these data suggest that, as with primitive erythropoiesis, RA serves to limit primitive myelopoieisis.

1.15 RA signaling in definitive myelopoiesis and leukemia

In addition to its role in primitive hematopoiesis, multiple studies have implicated RA signaling in definitive myeloid cell differentiation (reviewed by Collins, 2008; Drumea et al., 2008). Treatment of bone marrow cells or hematopoietic progenitor cells with exogenous RA drives the terminal differentiation of granulocytes from committed myeloid progenitors, and generates an expansion in granulocyte cell fate (Collins, 2002; Gratas et al., 1993; Labbaye et al., 1994; Van Bockstaele et al., 1994). This expansion appears to occur at the expense of erythroid cell fate (Labbaye et al., 1994). Markedly, RA signaling does not appear to be required for granulocyte specification *in vivo*: In mice, both *RARα* and *RARγ* are expressed within the granulocyte lineage. However, *RARα*/*RARγ* double-mutant mice exhibit wild type levels of granulocytes (Kastner et al., 2001; Labrecque et al., 1998). Furthermore, vitamin A-deficient mice, and mice treated with the RAR antagonist BMS493 do not exhibit reduced numbers of bone marrow-derived myeloid cells and granulocytes (Kastner et al., 2001; Kuwata et al., 2000) As exogenous RA treatment fails to enhance granulocyte differentiation in *RARα*-mutant mice (Kastner et al., 2001), and vitamin A-deficient, and BMS493-treated mice exhibit increased numbers of immature granulocytes, these combined data suggest that although RA signaling is not required for specification of the myeloid lineage, it may serve to promote the terminal differentiation of granulocytes. Support for this hypothesis comes from analyses of the leukemic oncogene PML-RARα, which is derived from the t(15:17) translocation, and is the major cause of acute promyelocytic leukemia (APL) (Borrow et al., 1990; de The et al., 1990; Di Croce, 2005).

The PML-RARα chimeric protein contains the DNA- and ligand-binding domains of RARα, and is able to interact with the same transcriptional targets as RARα (Puccetti and Ruthardt, 2004). However, PML-RARα is less responsive to RA than RARα and predominantly functions as a transcriptional repressor (Di Croce et al., 2002; Minucci et al., 2000). Patients with PML-RARα-induced APL possess increased numbers of undifferentiated promyelocytic myeloid cells. All-*trans* RA is used to treat these patients, whereby it stimulates cell-cycle arrest and promotes the terminal differentiation of malignant promyelocytes (Breitman et al., 1980; Huang et al., 1988; Warrell et al., 1993). Notably, RA has also been

shown to contribute to the proteosome-mediated, and caspase-mediated degradation of the PML-RARα moiety (Nervi et al., 1998; Zhu et al., 1999).

1.16 RA signaling in definitive hematopoiesis

Multiple studies have implicated RA signaling in HSC maintenance. RA has been shown to enhance the short and long-term repopulating activity of HSCs in suspension culture and serial transplantation assays (Purton et al., 1999; Purton et al., 2000). Conversely, treatment of HSCs with the RAR antagonist AGN 193109 reduces HSC repopulating activity (Purton et al., 2000). Furthermore, *RARγ*-mutant mice exhibit a reduction in bone marrow HSC number, but display increased numbers of hematopoietic progenitors (Purton et al., 2006). These data suggest that RA signaling, through RARγ, contributes to HSC maintenance and/or self-renewal.

Evidence for the role of RA signaling in HCS formation has emerged from analyses of *Aldh1a2*-mutant mice. These mice exhibit decreased numbers of yolk sac hemogenic endothelial cells, and a corresponding loss in the formation of multipotent blood progenitors that give rise to myeloid and erythroid lineages (Goldie et al., 2008). At embryonic day 8.0, *Aldh1a2*-mutants exhibit normal endothelial cell-specific gene expression, and normal circulation (Goldie et al., 2008; Lai et al., 2003). These data suggest that RA signaling is not required for general endothelial cell formation, but rather for yolk sac vascular endothelial cells to adopt a hemogenic fate. Support for this hypothesis comes from recent analyses of mice with a conditional deletion of *Aldh1a2* in VE-cadherin-positive endothelial cells (Chanda et al., 2013), as yolk sac vascular endothelial cells isolated from these mice fail to reconstitute lethally irradiated recipients. Notably, *Aldh1a2*-mutant mice die of severe vascular defects by embryonic day 10.5 (Niederreither et al., 1999), prior to HSC emergence. This early embryonic lethality makes mice a challenging model in which to examine the native developmental functions of RA in definitive hematopoiesis. Consequently, although existing studies suggest that RA signaling is required to regulate hemogenic endothelial cell formation, they fail to elucidate other potential functions of RA signaling in specifying HSCs *in vivo*.

1.17 Hmx transcription factors

Hmx (H6 homeobox; Nk5) proteins are an ancient, evolutionarily conserved family of homeodomain transcription factors. Members of the Hmx family are present in sea urchin (*TgHbox5*; (Wang et al., 1990), *C. elegans* (Abdus-Saboor et al., 2012; Hawkins and McGhee, 1990), *Drosophila* (Wang et al., 2000), cricket, (Wang et al., 2000), amphioxus (Kozmik et al., 1999), ascidians (Wada et al., 1998), and all vertebrates examined (Adamska et al., 2000; Stadler et al., 1995; Wang et al., 2000). Hmx proteins are not found in yeast, trypanosomes, or hydra (Wang et al., 2000). There are three *Hmx* family members (*Hmx1*/*Nkx5-3*/*GH6)*, *Hmx2*/*Nkx5-2*, and *Hmx3*/*Nkx5-1*) present in frog, mouse, and human. An additional *Hmx* gene (*Hmx4*/*Soho1*) is present in zebrafish, while medaka boasts five *Hmx* genes (*Hmx1-4* and *OlNkx5-1.2*) (Adamska et al., 2000). Three *Hmx* family members (*Hmx1*, *Hmx2*, and *Hmx4*) are present in chick (Adamska et al., 2000).

Hmx proteins display limited homology with other homeodomain proteins, sharing only ~60% homeodomain amino acid sequence identity with their closest relatives, the NK-family of transcription factors (Amendt et al., 1999; Stadler et al., 1995), and less than 55% identity with *Dlx* and *Hox* genes (Wang et al., 2000). It is therefore hypothesized that Hmx proteins diverged from other homeodomain proteins early in evolution (Wang et al., 2000). Most *Hmx* (*Hmx1-3*) family members exhibit strong (~90%) amino acid sequence conservation within the homeodomain (Wang et al., 2000), but conservation outside of the homeodomain is limited to two small carboxy-terminal domains of unknown function, termed SD1 and SD2 (Yoshiura et al., 1998). *Hmx4* shares a high level of conservation (85-90%) with other *Hmx* family members (*Hmx1-3*) within the homeodomain (Wang et al., 2000). However, *Hmx4* lacks the conserved SD1 and SD2 amino acid domains present immediately C-terminal to the homeodomain of all other (*Hmx1-3*) Hmx family members (Wang et al., 2000; Yoshiura et al., 1998). Unlike most homeodomain proteins, which bind a core 5'-TAAT-3' sequence motif (Dessain et al., 1992; Gehring et al., 1994; Kornberg, 1993; Lin and McGinnis, 1992; Scott et al., 1989; Wilson et al., 1996), Hmx family members preferentially bind a 5'-CAAGTG-3' motif (*Hmx1*) (Amendt et al., 1999), or a 5'-CTTAAG-3' motif (*Hmx2*/*Hmx3*) (Mennerich et al., 1999). Given that *Hmx1* has been shown to repress the transcription of a luciferase reporter gene containing the aforementioned 5'-CAAGTG-3'

motif (Amendt et al., 1999), it is hypothesized that *Hmx* proteins may act as transcriptional repressors.

Hmx2 is found immediately downstream of *Hmx3* on the same chromosome (mouse Chromosome 7, human chromosome 37, zebrafish chromosome 13) (Bober et al., 1994; Wang and Lufkin, 1997), and shares the same transcriptional orientation (Adamska et al., 2000; Wang et al., 2000). *Hmx1* and *Hmx4* are also found immediately adjacent to one another on the same chromosome (zebrafish chromosome 1) and share the same transcriptional orientation (Rinkwitz-Brandt et al., 1996). *Hmx4* is downstream of *Hmx1*. Based on their chromosomal locations, and the high degree of amino acid sequence conservation present within their homeodomains, it is hypothesized that all *Hmx* genes (*Hmx1-4*) arose from a common ancestor by tandem duplication, followed by chromosomal duplication (Adamska et al., 2000), and that mammals lost *HMX4* (Adamska et al., 2000; Wang et al., 2000), while birds lost *HMX2* (Adamska et al., 2000).

Drosophila *Hmx* is expressed within the developing central nervous system (Wang et al., 2000), possibly hinting at the ancestral function of the *Hmx* gene family. *Hmx* expression is expanded in vertebrates, as mammalian *HMX* genes exhibit both distinct and overlapping expression patterns within the central and peripheral nervous system, brachial arches, and the uterus (reviewed in Adamska et al., 2001; Bober et al., 1994; Rinkwitz-Brandt et al., 1996; Rinkwitz-Brandt et al., 1995; Stadler and Solursh, 1994; Wang et al., 2000; Yoshiura et al., 1998). Notably, all vertebrate *Hmx* family members are expressed in developing sensory-organ related structures such as the eye and otic vesicle (Bober et al., 1994; Rinkwitz-Brandt et al., 1996; Rinkwitz-Brandt et al., 1995; Stadler and Solursh, 1994; Wang et al., 1998; Yoshiura et al., 1998). Although *Hmx3* is expressed slightly earlier in development than *Hmx2*, the two exhibit nearly identical expression patterns within the developing ear and CNS (Wang et al., 2001). In addition to the CNS, *Hmx1* is also expressed in PNS tissues derived from neural crest, such as cranial mesenchyme and nerve ganglia (Yoshiura et al., 1998). In zebrafish, *hmx4* transcript is detected from the onset of development, and is ubiquitously expressed throughout gastrulation (Gongal et al., 2011), whereas *hmx1* expression is not detected until 5 hpf (Gongal et al., 2011). Later in development, *hmx1* and *hmx4* display nearly identical expression patterns, with expression becoming restricted to the

lens and retina, brachial arches, and otic vesicle (Boisset and Schorderet, 2012; Deitcher et al., 1994; Gongal et al., 2011; Yoshiura et al., 1998). Based on their chromosomal location, and their similar, overlapping temporal and spatial expression patterns, it is likely that *Hmx1/4* and *Hmx2/3* possess common regulatory elements (Adamska et al., 2000; Wang et al., 2000).

Consistent with their overlapping expression patterns, *Hmx* proteins also demonstrate partially redundant, overlapping developmental functions. For example, *Hmx2* and *Hmx3* are required for proper development of the ear and hypothalamus; Loss of *Hmx2* or *Hmx3* produces ear vestibular defects that are compounded by the absence of both genes (Feng and Xu, 2010; Hadrys et al., 1998; Wang et al., 2001; Wang et al., 2004; Wang et al., 1998). In concert with its expression in the uterus, *Hmx3*-null mice exhibit reduced fertility (Hadrys et al., 1998; Wang et al., 1998).

Human patients with mutations in *HMX1* exhibit a rare congenital syndrome that is characterized by opthalamic anomalies such as micropthalmia, and ear-lobule defects (Schorderet et al., 2008; Vaclavik et al., 2011). Notably, one out of three HMX1-deficient patients has spina bifida, as well as severe craniofacial and and dental anomalies (Schorderet et al., 2008). In addition to microphthalmia and ear-defects, *Hmx1*-null mice also exhibit craniofacial and cranial nerve defects (Munroe et al., 2009; Quina et al., 2012; Wang and Lufkin, 2005).

To date, only morpholino-based protein knockdown approaches have been used to analyze the functions of zebrafish Hmx1 and Hmx4 in development. On its own, Hmx1-depletion in zebrafish produces an extremely mild microphthalmic phenotype (Boisset and Schorderet, 2012). Conversely, *hmx4*-morphants display a host of defects, which include microphthalmia, narrowed eye-field, loss of pectoral fins, open neural tube, small ear, and reduced numbers of vagal motor neurons (Gongal et al., 2011). The severity of these defects increases slightly in *hmx1*/*hmx4* double-morphant embryos (K. Berry-Wynne, unpublished), suggesting that zebrafish Hmx1 and Hmx4 possess partially redundant developmental functions. The nature and severity of phenotypes observed in Hmx4-depleted zebrafish closely resemble those obtained through loss of HMX1 function in murine models and human patients, suggesting that zebrafish Hmx4 is the functional orthologue of mammalian *Hmx1*.

1.18 Hmx4

Hmx4 (*Soho1*) was initially identified in a screen to isolate homeodomain-containing genes with ocular expression (Deitcher et al., 1994). In chick, *HMX4* is initially expressed throughout the retina and within regions of the developing anterior CNS, otic vesicle, second brachial arch, and spinal cord dorsal root ganglia (Deitcher et al., 1994). Within the chick retina, its expression eventually becomes restricted to the nasal retina (Deitcher et al., 1994). The expression of zebrafish *hmx4* is quite similar. Expression of zebrafish *hmx4* is apparent from the one-cell stage (Gongal et al., 2011). *hmx4* continues to be broadly expressed until after gastrulation, at which point it becomes enriched in the presumptive eyefield (Gongal et al., 2011). By 14 hpf, *hmx4* displays a strong level of expression throughout the retina (Gongal et al., 2011). This domain of expression becomes restricted to the nasal-dorsal retina by 18 hpf (K. Berry-Wynne, unpublished). At 20 hpf, *hmx4* displays robust expression within the lens, and is expressed outside of the eye in the brachial arches, and otic vesicle (K. Berry-Wynne, unpublished). This late pattern of expression is maintained at 40 hpf (Feng and Xu, 2010).

Hmx4 has previously been shown to play a role in patterning the chick and zebrafish retina (K. Berry-Wynne, unpublished; Schulte and Cepko, 2000). Depletion of zebrafish Hmx4 leads to the downregulation of temporal retina *epha3*, dorsal retina *efnB2a*, and nasal retina *efna5a* expression in the eye (K. Berry-Wynne, unpublished). Using a retroviral overexpression system, Schulte and Cepko (2000) demonstrated that misexpressing *HMX4* in the chick temporal retina leads to a loss of temporal retina *EPHA3* expression. This loss results in the improper projection of some temporal retinal ganglion cell axons to the posterior tectum (Schulte and Cepko, 2000). Support for the hypothesis that Hmx4 acts as a repressor comes from an analysis of HMX4 fusion proteins in chick; fusion of the HMX4 homeodomain to the *Drosophila* Engrailed repressor domain produces a protein that produces similar phenotypes to those obtained from wild type HMX4 when misexpressed in the eye (Schulte and Cepko, 2000).

In addition to ocular defects, *hmx4*-morphant zebrafish embryos exhibit narrowing of the eyefield (Gongal et al., 2011), a phenotype that is consistent with defects in the Shh signaling pathway (Gongal et al., 2011). It is therefore not surprising that these embryos also

display a marked reduction in the forebrain expression domains of the Shh pathway targets *ptc1* and *nkx2.2a* (Gongal et al., 2011). Furthemore, *hmx4*-morphants also exhibit reduced forebrain expression of the Shh transcriptional effector *gli3,* providing a possible mechanism for the observed changes in Shh target gene expression. Notably, loss of Gil3 in murine and zebrafish models is not sufficient to produce a severe eyefield narrowing phenotype (Furimsky and Wallace, 2006; Tyurina et al., 2005), suggesting that Hmx4 may also regulate additional members of the Shh signaling pathway. Shh signaling is required for HSC formation. However, despite regulating the expression of Shh pathway components, it is not known if Hmx4 regulates definitive hematopoiesis.

1.19 Summary

All adult vertebrate hematopoietic lineages arise from a common multipotent progenitor, the hematopoietic stem cell (HSC). This definitive hematopoietic cell type is able to self renew, differentiate into all major blood lineages, and maintain adult hematopoiesis for life. HSC transplants are used to treat a spectrum of disease that ranges from anemia and other congenital blood disorders, to acute leukemia. Unfortunately, these cells are present in restrictive quantities, and recent *ex vivo* methods for expanding human HSCs for clinical therapies have achieved limited success. This is primarily due an incomplete understanding of their molecular programming; although much is known about the cellular and functional properties of vertebrate HSCs, little information exists about the genetic pathways that govern HSC induction, expansion, and homeostasis. Identifying the molecular signals that regulate HSC formation is therefore a major goal of both basic and clinical biology.

Vertebrate hematopoiesis occurs in two embryonic waves. The first wave, primitive hematopoiesis, influences the morphology of the developing embryonic circulatory system and produces circulating erythrocytes that facilitate tissue oxygenation during periods of rapid embryonic growth. Primitive hematopoiesis is also essential for HSC formation, which is dependent upon intact blood flow (North et al., 2009). The second, definitive wave of hematopoiesis produces HSCs. A major challenge in developmental hematopoiesis is therefore to determine the molecular cues that regulate each phase of hematopoiesis.

Consequently, the overall goal of this work is to contribute to our understanding of the transcriptional regulation of embryonic hematopoiesis.

Previous analyses using vertebrate models have identified molecular pathways and transcription factors that govern both primitive and definitive hematopoiesis. However, the precise molecular function of many hematopoietic regulators is not known. For example, the Hox cofactors Meis1 and Pbx are required for embryonic hematopoiesis; *Pbx1*-knockout and *Meis1*-deficient mice exhibit profound embryonic anemia (Azcoitia et al., 2005; DiMartino et al., 2001; Hisa et al., 2004). However, prior to this work, it was not known how Meis1 and Pbx regulate primitive erythropoiesis, or where Meis1 and Pbx participate in the hematopoietic transcription factor cascade. We address these questions in Chapter 3, by ablating Meis1 and Pbx proteins in Zebrafish, and characterizing their molecular effects on known markers of primitive hematopoiesis. We demonstrate that Meis1 and Pbx function downstream of Cdx, and upstream of *gata1* in the erythropoietic transcription factor hierarchy. We also describe a novel role for Meis1 and Pbx in negatively regulating primitive myelopoiesis.

The RA signaling pathway has also been implicated in vertebrate definitive hematopoiesis. RA treatment of hematovascular precursors increases their ability to generate definitive hematopoietic precursors (Chanda et al., 2013; Yu et al., 2010), suggesting that RA signaling plays an instructive role in definitive hematopoiesis. This data is in line with analyses of RA function in mice, as loss of the predominant retinoic acid synthesis gene, *Aldh1a2* in VE-cadherin-positive endothelial cells is sufficient to abrogate HSC formation (Chanda et al., 2013). *Aldh1a2*-mutant mice die of severe vascular defects prior to HSC emergence (Niederreither et al., 1999), precluding global analyses of *Aldh1a2*-function in murine definitive hematopoiesis. Consequently, although existing studies suggest that endothelial cells require ALDH1A2 in order to adopt a hemogenic fate, they fail to elucidate other potential molecular functions of RA signaling in specifying HSCs *in vivo*. The most severe zebrafish models of RA-depletion survive well after HSC emergence. We therefore used zebrafish as a model to study the role of RA signaling in definitive hematopoiesis.

Hemogenic endothelial cell formation represents one of the final stages of HSC formation. To generate HSCs for clinical therapies, it is also important to understand earlier

events that contribute to specifying HSC progenitors. *Aldh1a2* displays broad expression in the somites prior to hemogenic endothelial cell formation, and RA is a diffusible morphogen. We therefore hypothesized that RA may also function outside of pre-hemogenic endothelium to regulate HSC formation. In Chapter 4, we test this hypothesis by examining HSC gene expression in RA-deficient embryos and elucidating the temporal requirement for RA signaling in zebrafish definitive hematopoiesis. We demonstrate that RA is required for HSC formation prior to the formation of dorsal aorta hemogenic endothelium.

Research in both mouse and zebrafish has established a cell-autonomous function for Notch signaling in HSC specification, whereby Notch1-expressing cells within the dorsal aorta are instructed by adjacent cells to form HSCs (Gering and Patient, 2010; Hadland et al., 2004; Kumano et al., 2003; Robert-Moreno et al., 2005; Robert-Moreno et al., 2008). The yolk sac endothelial cells of *Aldh1a2*-mutant mice exhibit downregulated *Notch1* and Notch-target gene expression (Marcelo et al., 2013), implicating RA as a potential modulator of Notch signaling. We hypothesized that zebrafish RA regulates HSC formation through the Notch signaling pathway. We test this hypothesis in Chapter 4, by examining the expression of Notch signaling components and their transcriptional targets in RA-deficient zebrafish embryos. Our results suggest that, unlike in mice, zebrafish RA does not regulate HSC formation through the Notch1-signaling pathway.

Previous research by our lab has implicated the homeodomain transcription factor Hmx4 in RA signaling (Gongal et al., 2011). Given that RA is an essential regulator of both primitive and definitive hematopoiesis, we hypothesized that Hmx4 acts upstream of the RA signaling pathway to regulate embryonic hematopoiesis. We test this hypothesis in Chapter 5, by analyzing hematopoietic marker gene expression in Hmx4-depleted zebrafish embryos, and determining whether or not treatment with a biologically relevant dose of RA rescues their hematopoietic defects. Our work identifies a putative role for Hmx4 as a modulator of RA signaling, and as a regulator of both primitive and definitive hematopoiesis. Notably, we use two methods to analyze Hmx4 function within the developing zebrafish embryo. The first is a morpholino-based protein knockdown approach. The second is an analysis of *hmx4*-mutant embryos generated using zinc finger nuclease (ZFN) technology.

Synthetic targeted endonucleases such as ZFNs and transcription activator-like effector nucleases (TALENs) have recently emerged as powerful tools for targeted mutagenesis, especially in organisms that are not amenable to embryonic stem cell manipulation. However, the somatic mutation rate obtained by using these technologies is still quite variable (0 – 100%). Both ZFNs and TALENs consist of DNA-binding arrays fused to the non-specific FokI nuclease domain. In Chapter 6, we describe methodology used in an attempt to improve the efficiency of ZFN and TALEN synthetic targeted endonucleases for use in zebrafish mutagenesis. Towards this aim, we examine the activity of both ZFNs and TALENs containing a FokI nuclease variant termed *Sharkey*. We demonstrate that *Sharkey* ZFNs exhibit greater *in vitro* cleavage of target-site DNA than controls, and have the capacity to produce a higher frequency of insertion/deletion mutations in zebrafish. Conversely, we demonstrate that all *Sharkey* TALENs examined fail to produce any insertion/deletion mutations in zebrafish, displaying absent or significantly reduced *in vivo* mutagenic activity in comparison to control TALENs.

1.20 Figures

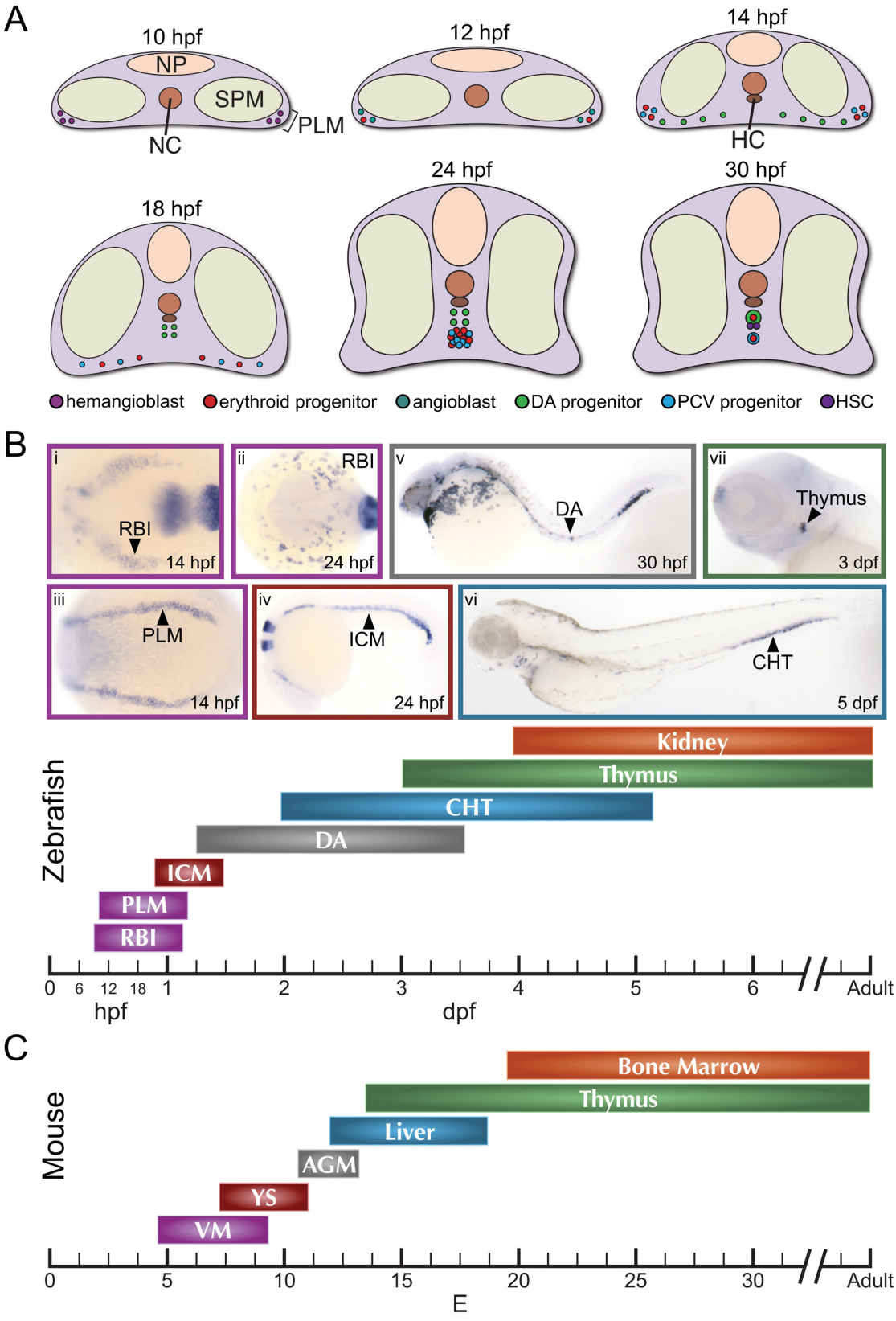
A
10 hpf
NP
SPM
NC
PLM
12 hpf
14 hpf
HC
18 hpf
24 hpf
30 hpf
hemangioblast
erythroid progenitor
angioblast
DA progenitor
PCV progenitor
HSC
B
i
RBI
14 hpf
ii
RBI
24 hpf
v
DA
30 hpf
vii
Thymus
3 dpf
iii
PLM
14 hpf
iv
ICM
24 hpf
vi
CHT
5 dpf
Zebrafish
Kidney
Thymus
CHT
DA
ICM
PLM
RBI
0 6 12 18 1 2 3 4 5 6 Adult
hpf
dpf
C
Mouse
Bone Marrow
Thymus
Liver
AGM
YS
VM
0 5 10 15 20 25 30 Adult
E

Figure 1.1. Primitive and definitive hematopoiesis. (A) Schematic illustrating zebrafish early blood and endothelial development. Diagrammatical representations of transverse sections through the embryonic trunk. The first hematopoietic cells, hemangioblasts, originate from bilateral stripes of posterior lateral-plate mesoderm (PLM) at approximately 10 hours post fertilization (hpf). By 12 hpf, these cells adopt erythroid or angioblast (presumptive vascular) fate. From 14-18 hpf, erythroid and vascular progenitors migrate towards the embryonic midline. Dorsal aorta (DA) progenitors migrate first, aggregating under the notochord (NC) and hypochord (HC). Erythrocytes and posterior cardinal vein (PCV) progenitors migrate shortly thereafter, aggregating to form the intermediate cell mass (ICM) at 24 hpf. By 25 hpf, primitive erythrocytes enter circulation, leaving behind a fully luminized PCV. By 30 hpf, hematopoietic stem cells (HSCs) emerge from DA hemogenic endothelium. NP, neural plate; SPM, somitic paraxial mesoderm. (B) Schematic illustrating shifting site of zebrafish hematopoiesis, and corresponding hematopoietic marker gene expression shown through whole-mount *in situ* hybridization. (i, ii) Dorsal view of rostral blood island (RBI) *pu.1* expression, anterior to left. *eng2a* expression in the midbrain hindbrain boundary, and *egr2b* expression in hindbrain rhombomere 3 also shown. (iii) Dorsal view of PLM *scl* expression, anterior to left. (iv) *lmo2* ICM and RBI expression shown in lateral view, anterior to left. *egr2b* expression in hindbrain rhombomeres 3 and 5 also shown. (v) Lateral view of *runx1* expression, anterior to left. (vi) Lateral view of *hbae3* expression in the caudal hematopoietic tissue (CHT), anterior to left. (vii) Lateral view of *rag1* expression, anterior to left. Stage of development is indicated in hpf or days post fertilization (dpf). (C) Schematic illustrating shifting site of murine hematopoiesis. Stage of development is indicated in embryonic days (E). VM, ventral mesoderm; YS, yolk sac; AGM, aorta-gonad mesonephros.

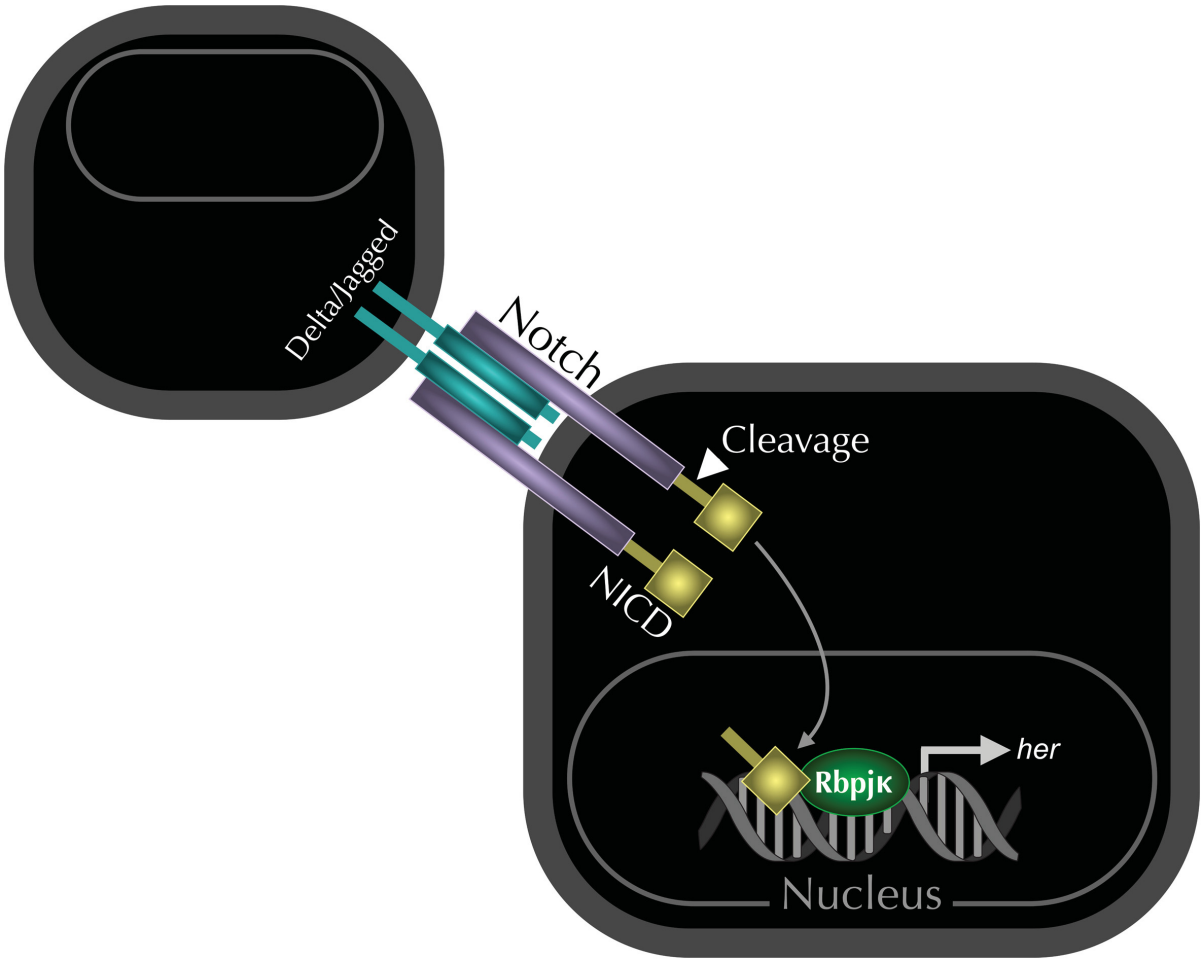

Figure 1.2. Schematic overview of Notch signal transduction. Binding of the Notch transmembrane surface receptor to a Delta or Jagged transmembrane ligand on a neighboring cell induces a conformational change in the Notch receptor that renders it susceptible to cleavage by γ-secretase. This cleavage event releases the Notch intracellular domain (NICD). The NICD enters the nucleus, acting as a transcriptional activator in a complex with RBPjκ. Hairy and enhancer of split (Hes) proteins are transcriptional targets of the Notch signaling pathway. These proteins act as Notch-dependent transcriptional regulators, and mediate the majority of Notch function.

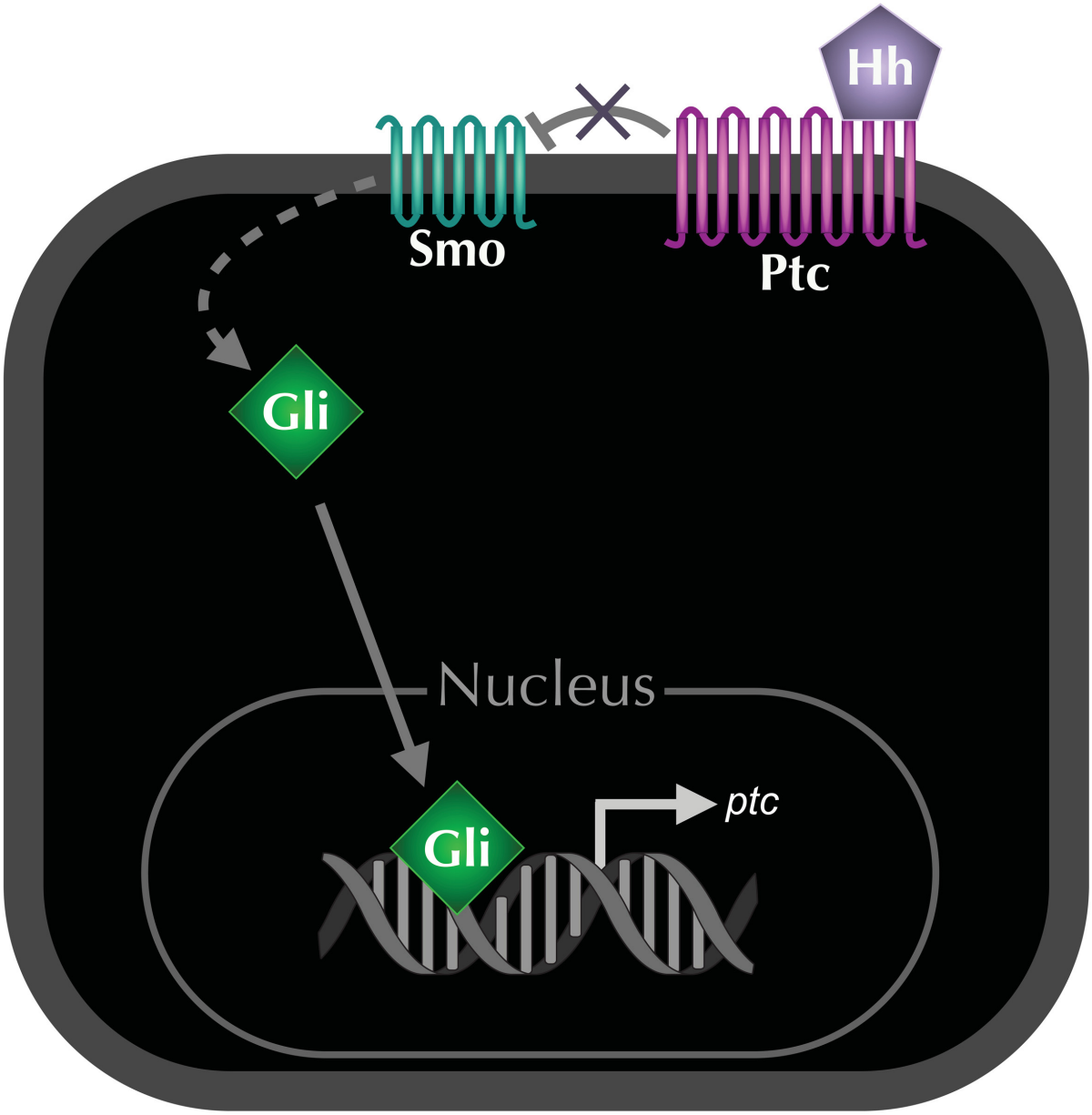

Figure 1.3. Schematic overview of the Hedgehog signaling pathway. Hedgehog (Hh) ligand binds to the Patched (Ptc) receptor. This interaction leads to de-repression of Smoothened (Smo), which initiates a signal transduction cascade that results in the cleavage and/or activation of GLI family zinc finger (Gli) transcription factors. *ptc* is itself a transcriptional target of Hh signaling.

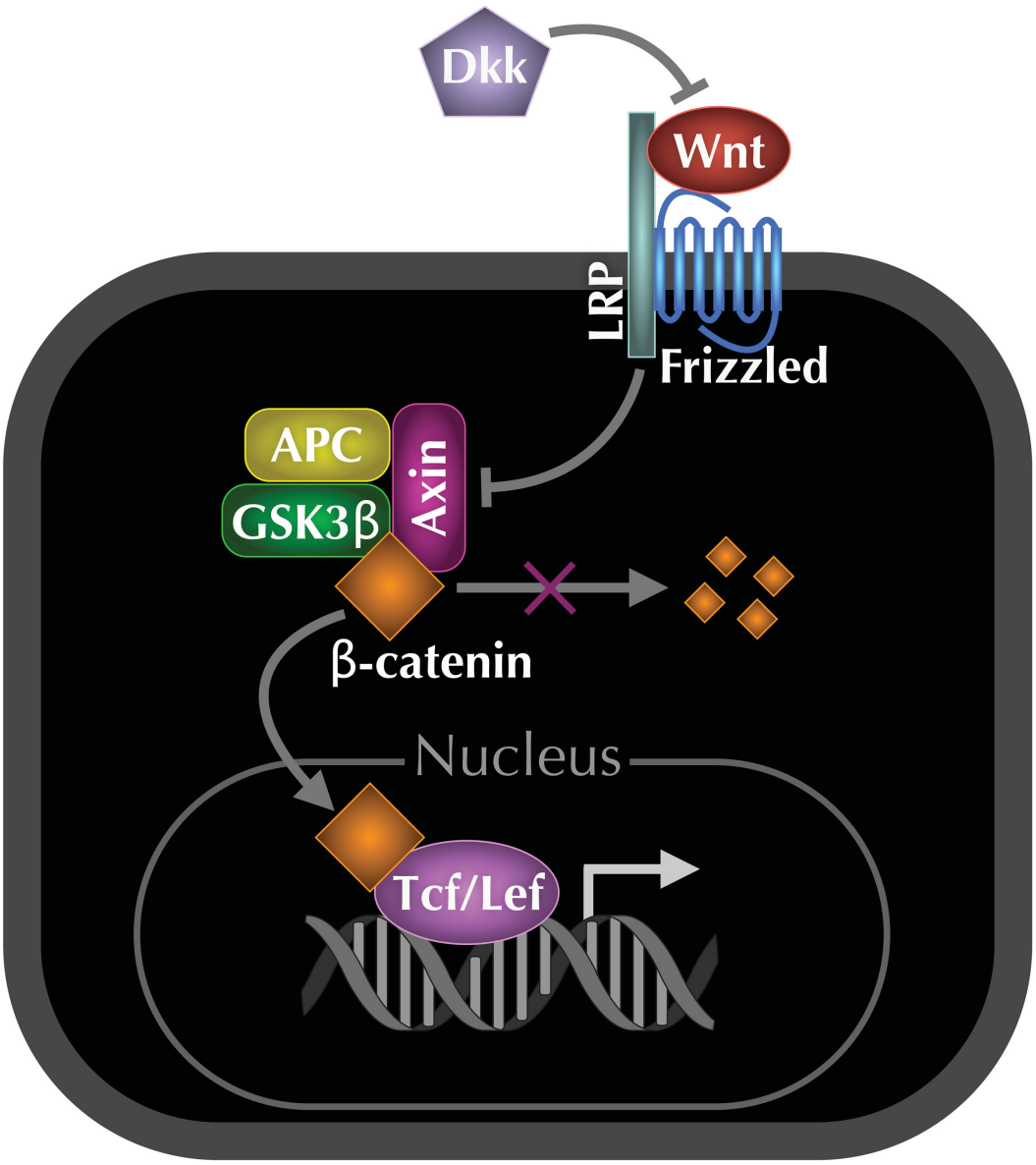

Figure 1.4. Schematic overview of the canonical Wnt signaling pathway. Wingless-type MMV integration site family (Wnt) ligands bind to members of the Frizzled and Low density lipoprotein receptor-related protein (LRP) family of co-receptors. The secreted protein Dickkopf (Dkk) competitively inhibits the interaction between Wnt and its receptors. In the presence of the Wnt, LRP prevents assembly of the β-catenin destruction complex, which contains Serine/threonine glycogen synthase kinase 3β (GSK3β), Axis inhibition protein (Axin), and Adenomatous polyposis coli complex (APC). β-catenin then enters the nucleus, binding the T-cell factor (Tcf) and Lymphoid enhancer binding factor (Lef) family of transcription factors, and activating the transcription of Wnt target genes.

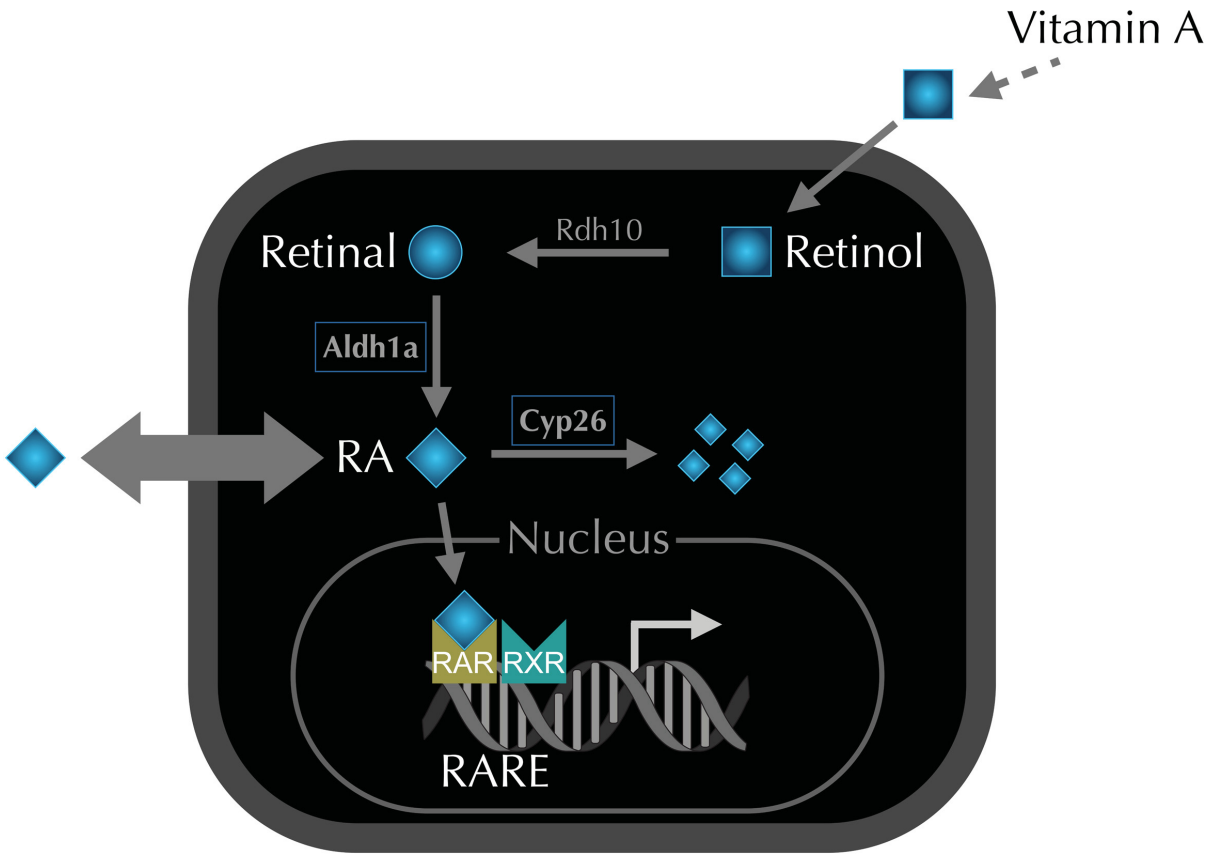

Figure 1.5. Schematic overview of retinoic acid metabolism and signaling. Cellular retinol is converted into retinal (retinaldehyde) by Retinol dehydrogenase 10 (Rdh10). Aldehyde dehydrogenase 1a (Aldh1a) proteins convert retinal into retinoic acid (RA). Once synthesized, RA enters the nucleus where it binds to retinoic acid receptor (RAR) and retinoid X receptor (RXR) heterodimers on the retinoic acid response elements (RAREs) of genes to activate their transcription. Cytochrome P450 subfamily 26 (Cyp26) proteins hydroxylate RA, targeting it for degradation. RA is a diffusible morphogen and can act non cell-autonomously, signaling to adjacent cells or tissues (double-headed arrow).

1.21 References

Abdus-Saboor, I., C.E. Stone, J.I. Murray, and M.V. Sundaram. 2012. The Nkx5/HMX homeodomain protein MLS-2 is required for proper tube cell shape in the C. elegans excretory system. *Dev Biol*. 366:298-307.

Aberle, H., S. Butz, J. Stappert, H. Weissig, R. Kemler, and H. Hoschuetzky. 1994. Assembly of the cadherin-catenin complex in vitro with recombinant proteins. *Journal of cell science*. 107 (Pt 12):3655-3663.

Abramovich, C., and R.K. Humphries. 2005. Hox regulation of normal and leukemic hematopoietic stem cells. *Curr Opin Hematol*. 12:210-216.

Abu-Shaar, M., H.D. Ryoo, and R.S. Mann. 1999. Control of the nuclear localization of Extradenticle by competing nuclear import and export signals. *Genes Dev*. 13:935-945.

Adamska, M., S. Leger, M. Brand, T. Hadrys, T. Braun, and E. Bober. 2000. Inner ear and lateral line expression of a zebrafish Nkx5-1 gene and its downregulation in the ears of FGF8 mutant, ace. *Mech Dev*. 97:161-165.

Adamska, M., A. Wolff, M. Kreusler, J. Wittbrodt, T. Braun, and E. Bober. 2001. Five Nkx5 genes show differential expression patterns in anlagen of sensory organs in medaka: insight into the evolution of the gene family. *Dev Genes Evol*. 211:338-349.

Affolter, M., M. Slattery, and R.S. Mann. 2008. A lexicon for homeodomain-DNA recognition. *Cell*. 133:1133-1135.

Amendt, B.A., L.B. Sutherland, and A.F. Russo. 1999. Transcriptional antagonism between Hmx1 and Nkx2.5 for a shared DNA-binding site. *J Biol Chem*. 274:11635-11642.

Appel, B., A. Fritz, M. Westerfield, D.J. Grunwald, J.S. Eisen, and B.B. Riley. 1999. Delta-mediated specification of midline cell fates in zebrafish embryos. *Current biology : CB*. 9:247-256.

Argiropoulos, B., and R.K. Humphries. 2007. Hox genes in hematopoiesis and leukemogenesis. *Oncogene*. 26:6766-6776.

Armstrong, S.A., J.E. Staunton, L.B. Silverman, R. Pieters, M.L. den Boer, M.D. Minden, S.E. Sallan, E.S. Lander, T.R. Golub, and S.J. Korsmeyer. 2002. MLL translocations specify a distinct gene expression profile that distinguishes a unique leukemia. *Nat Genet*. 30:41-47.

Asahara, H., S. Dutta, H.Y. Kao, R.M. Evans, and M. Montminy. 1999. Pbx-Hox heterodimers recruit coactivator-corepressor complexes in an isoform-specific manner. *Mol Cell Biol*. 19:8219-8225.

Azcoitia, V., M. Aracil, A.C. Martinez, and M. Torres. 2005. The homeodomain protein Meis1 is essential for definitive hematopoiesis and vascular patterning in the mouse embryo. *Dev Biol*. 280:307-320.

Bafico, A., G. Liu, A. Yaniv, A. Gazit, and S.A. Aaronson. 2001. Novel mechanism of Wnt signalling inhibition mediated by Dickkopf-1 interaction with LRP6/Arrow. *Nature cell biology*. 3:683-686.

Barresi, M.J., J.A. D'Angelo, L.P. Hernandez, and S.H. Devoto. 2001. Distinct mechanisms regulate slow-muscle development. *Current biology : CB*. 11:1432-1438.

Baumann, R., and S. Dragon. 2005. Erythropoiesis and red cell function in vertebrate embryos. *Eur J Clin Invest*. 35 Suppl 3:2-12.

Begemann, G., T.F. Schilling, G.J. Rauch, R. Geisler, and P.W. Ingham. 2001. The zebrafish neckless mutation reveals a requirement for raldh2 in mesodermal signals that pattern the hindbrain. *Development*. 128:3081-3094.

Behrens, J., B.A. Jerchow, M. Wurtele, J. Grimm, C. Asbrand, R. Wirtz, M. Kuhl, D. Wedlich, and W. Birchmeier. 1998. Functional interaction of an axin homolog, conductin, with beta-catenin, APC, and GSK3beta. *Science*. 280:596-599.

Belandia, B., and M.G. Parker. 2003. Nuclear receptors: a rendezvous for chromatin remodeling factors. *Cell*. 114:277-280.

Bennett, C.M., J.P. Kanki, J. Rhodes, T.X. Liu, B.H. Paw, M.W. Kieran, D.M. Langenau, A. Delahaye-Brown, L.I. Zon, M.D. Fleming, and A.T. Look. 2001. Myelopoiesis in the zebrafish, Danio rerio. *Blood*. 98:643-651.

Berger, M.F., G. Badis, A.R. Gehrke, S. Talukder, A.A. Philippakis, L. Pena-Castillo, T.M. Alleyne, S. Mnaimneh, O.B. Botvinnik, E.T. Chan, F. Khalid, W. Zhang, D. Newburger, S.A. Jaeger, Q.D. Morris, M.L. Bulyk, and T.R. Hughes. 2008. Variation in homeodomain DNA binding revealed by high-resolution analysis of sequence preferences. *Cell*. 133:1266-1276.

Berthelsen, J., C. Kilstrup-Nielsen, F. Blasi, F. Mavilio, and V. Zappavigna. 1999. The subcellular localization of PBX1 and EXD proteins depends on nuclear import and export signals and is modulated by association with PREP1 and HTH. *Genes Dev*. 13:946-953.

Berthelsen, J., V. Zappavigna, E. Ferretti, F. Mavilio, and F. Blasi. 1998a. The novel homeoprotein Prep1 modulates Pbx-Hox protein cooperativity. *EMBO J*. 17:1434-1445.

Berthelsen, J., V. Zappavigna, F. Mavilio, and F. Blasi. 1998b. Prep1, a novel functional partner of Pbx proteins. *EMBO J*. 17:1423-1433.

Bertrand, J.Y., J.L. Cisson, D.L. Stachura, and D. Traver. 2010. Notch signaling distinguishes 2 waves of definitive hematopoiesis in the zebrafish embryo. *Blood*. 115:2777-2783.

Bigas, A., D.I. Martin, and L.A. Milner. 1998. Notch1 and Notch2 inhibit myeloid differentiation in response to different cytokines. *Mol Cell Biol*. 18:2324-2333.

Bilic, J., Y.L. Huang, G. Davidson, T. Zimmermann, C.M. Cruciat, M. Bienz, and C. Niehrs. 2007. Wnt induces LRP6 signalosomes and promotes dishevelled-dependent LRP6 phosphorylation. *Science*. 316:1619-1622.

Bober, E., C. Baum, T. Braun, and H.H. Arnold. 1994. A novel NK-related mouse homeobox gene: expression in central and peripheral nervous structures during embryonic development. *Dev Biol*. 162:288-303.

Boisset, G., and D.F. Schorderet. 2012. Zebrafish hmx1 promotes retinogenesis. *Experimental eye research*. 105:34-42.

Borrow, J., A.D. Goddard, D. Sheer, and E. Solomon. 1990. Molecular analysis of acute promyelocytic leukemia breakpoint cluster region on chromosome 17. *Science*. 249:1577-1580.

Borrow, J., A.M. Shearman, V.P. Stanton, Jr., R. Becher, T. Collins, A.J. Williams, I. Dube, F. Katz, Y.L. Kwong, C. Morris, K. Ohyashiki, K. Toyama, J. Rowley, and D.E. Housman. 1996. The t(7;11)(p15;p15) translocation in acute myeloid leukaemia fuses the genes for nucleoporin NUP98 and class I homeoprotein HOXA9. *Nat Genet*. 12:159-167.

Bray, S.J. 2006. Notch signalling: a simple pathway becomes complex. *Nature reviews. Molecular cell biology*. 7:678-689.

Breitman, T.R., S.E. Selonick, and S.J. Collins. 1980. Induction of differentiation of the human promyelocytic leukemia cell line (HL-60) by retinoic acid. *Proc Natl Acad Sci U S A*. 77:2936-2940.

Brown, L.A., A.R. Rodaway, T.F. Schilling, T. Jowett, P.W. Ingham, R.K. Patient, and A.D. Sharrocks. 2000. Insights into early vasculogenesis revealed by expression of the ETS-domain transcription factor Fli-1 in wild-type and mutant zebrafish embryos. *Mech Dev*. 90:237-252.

Brun, A.C., J.M. Bjornsson, M. Magnusson, N. Larsson, P. Leveen, M. Ehinger, E. Nilsson, and S. Karlsson. 2004. Hoxb4-deficient mice undergo normal hematopoietic development but exhibit a mild proliferation defect in hematopoietic stem cells. *Blood*. 103:4126-4133.

Burglin, T.R. 1997. Analysis of TALE superclass homeobox genes (MEIS, PBC, KNOX, Iroquois, TGIF) reveals a novel domain conserved between plants and animals. *Nucleic Acids Res*. 25:4173-4180.

Burns, C.E., T. DeBlasio, Y. Zhou, J. Zhang, L. Zon, and S.D. Nimer. 2002. Isolation and characterization of runxa and runxb, zebrafish members of the runt family of transcriptional regulators. *Exp Hematol*. 30:1381-1389.

Burns, C.E., D. Traver, E. Mayhall, J.L. Shepard, and L.I. Zon. 2005. Hematopoietic stem cell fate is established by the Notch-Runx pathway. *Genes Dev*. 19:2331-2342.

Byrd, N., S. Becker, P. Maye, R. Narasimhaiah, B. St-Jacques, X. Zhang, J. McMahon, A. McMahon, and L. Grabel. 2002. Hedgehog is required for murine yolk sac angiogenesis. *Development*. 129:361-372.

Carroll, A.J., W.M. Crist, R.T. Parmley, M. Roper, M.D. Cooper, and W.H. Finley. 1984. Pre-B cell leukemia associated with chromosome translocation 1;19. *Blood*. 63:721-724.

Chambers, D., L. Wilson, M. Maden, and A. Lumsden. 2007. RALDH-independent generation of retinoic acid during vertebrate embryogenesis by CYP1B1. *Development*. 134:1369-1383.

Chan, S.K., and R.S. Mann. 1996. A structural model for a homeotic protein-extradenticle-DNA complex accounts for the choice of HOX protein in the heterodimer. *Proc Natl Acad Sci U S A*. 93:5223-5228.

Chan, S.K., H. Popperl, R. Krumlauf, and R.S. Mann. 1996. An extradenticle-induced conformational change in a HOX protein overcomes an inhibitory function of the conserved hexapeptide motif. *EMBO J*. 15:2476-2487.

Chanda, B., A. Ditadi, N.N. Iscove, and G. Keller. 2013. Retinoic acid signaling is essential for embryonic hematopoietic stem cell development. *Cell*. 155:215-227.

Chang, C.P., Y. Jacobs, T. Nakamura, N.A. Jenkins, N.G. Copeland, and M.L. Cleary. 1997. Meis proteins are major in vivo DNA binding partners for wild-type but not chimeric Pbx proteins. *Mol Cell Biol*. 17:5679-5687.

Chang, C.P., W.F. Shen, S. Rozenfeld, H.J. Lawrence, C. Largman, and M.L. Cleary. 1995. Pbx proteins display hexapeptide-dependent cooperative DNA binding with a subset of Hox proteins. *Genes Dev*. 9:663-674.

Chariot, A., C. van Lint, M. Chapelier, J. Gielen, M.P. Merville, and V. Bours. 1999. CBP and histone deacetylase inhibition enhance the transactivation potential of the HOXB7 homeodomain-containing protein. *Oncogene*. 18:4007-4014.

Chen, J., C. Jette, J.P. Kanki, J.C. Aster, A.T. Look, and J.D. Griffin. 2007. NOTCH1-induced T-cell leukemia in transgenic zebrafish. *Leukemia*. 21:462-471.

Chen, J.K., J. Taipale, M.K. Cooper, and P.A. Beachy. 2002a. Inhibition of Hedgehog signaling by direct binding of cyclopamine to Smoothened. *Genes Dev*. 16:2743-2748.

Chen, J.K., J. Taipale, K.E. Young, T. Maiti, and P.A. Beachy. 2002b. Small molecule modulation of Smoothened activity. *Proc Natl Acad Sci U S A*. 99:14071-14076.

Chen, X.D., and J.B. Turpen. 1995. Intraembryonic origin of hepatic hematopoiesis in Xenopus laevis. *Journal of immunology*. 154:2557-2567.

Choe, S.K., F. Ladam, and C.G. Sagerstrom. 2014. TALE factors poise promoters for activation by Hox proteins. *Dev Cell*. 28:203-211.

Choe, S.K., P. Lu, M. Nakamura, J. Lee, and C.G. Sagerstrom. 2009. Meis cofactors control HDAC and CBP accessibility at Hox-regulated promoters during zebrafish embryogenesis. *Dev Cell*. 17:561-567.

Clements, W.K., A.D. Kim, K.G. Ong, J.C. Moore, N.D. Lawson, and D. Traver. 2011. A somitic Wnt16/Notch pathway specifies haematopoietic stem cells. *Nature*. 474:220-224.

Clevers, H. 2006. Wnt/beta-catenin signaling in development and disease. *Cell*. 127:469-480.

Collins, S.J. 2002. The role of retinoids and retinoic acid receptors in normal hematopoiesis. *Leukemia*. 16:1896-1905.

Collins, S.J. 2008. Retinoic acid receptors, hematopoiesis and leukemogenesis. *Curr Opin Hematol*. 15:346-351.

Cumano, A., and I. Godin. 2007. Ontogeny of the hematopoietic system. *Annu Rev Immunol*. 25:745-785.

Dash, A.B., I.R. Williams, J.L. Kutok, M.H. Tomasson, E. Anastasiadou, K. Lindahl, S. Li, R.A. Van Etten, J. Borrow, D. Housman, B. Druker, and D.G. Gilliland. 2002. A murine model of CML blast crisis induced by cooperation between BCR/ABL and NUP98/HOXA9. *Proc Natl Acad Sci U S A*. 99:7622-7627.

Davidson, A.J., P. Ernst, Y. Wang, M.P. Dekens, P.D. Kingsley, J. Palis, S.J. Korsmeyer, G.Q. Daley, and L.I. Zon. 2003. cdx4 mutants fail to specify blood progenitors and can be rescued by multiple hox genes. *Nature*. 425:300-306.

Davidson, A.J., and L.I. Zon. 2004. The 'definitive' (and 'primitive') guide to zebrafish hematopoiesis. *Oncogene*. 23:7233-7246.

Davidson, A.J., and L.I. Zon. 2006. The caudal-related homeobox genes cdx1a and cdx4 act redundantly to regulate hox gene expression and the formation of putative hematopoietic stem cells during zebrafish embryogenesis. *Dev Biol*. 292:506-518.

de Jong, J.L., A.J. Davidson, Y. Wang, J. Palis, P. Opara, E. Pugach, G.Q. Daley, and L.I. Zon. 2010. Interaction of retinoic acid and scl controls primitive blood development. *Blood*.

de The, H., C. Chomienne, M. Lanotte, L. Degos, and A. Dejean. 1990. The t(15;17) translocation of acute promyelocytic leukaemia fuses the retinoic acid receptor alpha gene to a novel transcribed locus. *Nature*. 347:558-561.

Dedera, D.A., E.K. Waller, D.P. LeBrun, A. Sen-Majumdar, M.E. Stevens, G.S. Barsh, and M.L. Cleary. 1993. Chimeric homeobox gene E2A-PBX1 induces proliferation, apoptosis, and malignant lymphomas in transgenic mice. *Cell*. 74:833-843.

Deitcher, D.L., D.M. Fekete, and C.L. Cepko. 1994. Asymmetric expression of a novel homeobox gene in vertebrate sensory organs. *The Journal of neuroscience : the official journal of the Society for Neuroscience*. 14:486-498.

Dessain, S., C.T. Gross, M.A. Kuziora, and W. McGinnis. 1992. Antp-type homeodomains have distinct DNA binding specificities that correlate with their different regulatory functions in embryos. *EMBO J*. 11:991-1002.

Detrich, H.W., 3rd, M.W. Kieran, F.Y. Chan, L.M. Barone, K. Yee, J.A. Rundstadler, S. Pratt, D. Ransom, and L.I. Zon. 1995. Intraembryonic hematopoietic cell migration during vertebrate development. *Proc Natl Acad Sci U S A*. 92:10713-10717.

Di Croce, L. 2005. Chromatin modifying activity of leukaemia associated fusion proteins. *Hum Mol Genet*. 14 Spec No 1:R77-84.

Di Croce, L., V.A. Raker, M. Corsaro, F. Fazi, M. Fanelli, M. Faretta, F. Fuks, F. Lo Coco, T. Kouzarides, C. Nervi, S. Minucci, and P.G. Pelicci. 2002. Methyltransferase recruitment and DNA hypermethylation of target promoters by an oncogenic transcription factor. *Science*. 295:1079-1082.

Di Rosa, P., J.C. Villaescusa, E. Longobardi, G. Iotti, E. Ferretti, V.M. Diaz, A. Miccio, G. Ferrari, and F. Blasi. 2007. The homeodomain transcription factor Prep1 (pKnox1) is required for hematopoietic stem and progenitor cell activity. *Dev Biol*. 311:324-334.

Dieterlen-Lievre, F. 2001. [Embryogenesis of the blood system]. *Therapie*. 56:377-378.

DiMartino, J.F., L. Selleri, D. Traver, M.T. Firpo, J. Rhee, R. Warnke, S. O'Gorman, I.L. Weissman, and M.L. Cleary. 2001. The Hox cofactor and proto-oncogene Pbx1 is required for maintenance of definitive hematopoiesis in the fetal liver. *Blood*. 98:618-626.

Drumea, K., Z.F. Yang, and A. Rosmarin. 2008. Retinoic acid signaling in myelopoiesis. *Curr Opin Hematol*. 15:37-41.

Duester, G. 2000. Families of retinoid dehydrogenases regulating vitamin A function: production of visual pigment and retinoic acid. *European journal of biochemistry / FEBS*. 267:4315-4324.

Dyer, M.A., S.M. Farrington, D. Mohn, J.R. Munday, and M.H. Baron. 2001. Indian hedgehog activates hematopoiesis and vasculogenesis and can respecify prospective neurectodermal cell fate in the mouse embryo. *Development*. 128:1717-1730.

Dzierzak, E. 2005. The emergence of definitive hematopoietic stem cells in the mammal. *Curr Opin Hematol*. 12:197-202.

Ebner, A., C. Cabernard, M. Affolter, and S. Merabet. 2005. Recognition of distinct target sites by a unique Labial/Extradenticle/Homothorax complex. *Development*. 132:1591-1600.

Farzan, S.F., S. Singh, N.S. Schilling, and D.J. Robbins. 2008. The adventures of sonic hedgehog in development and repair. III. Hedgehog processing and biological activity. *American journal of physiology. Gastrointestinal and liver physiology*. 294:G844-849.

Feng, Y., and Q. Xu. 2010. Pivotal role of hmx2 and hmx3 in zebrafish inner ear and lateral line development. *Dev Biol*. 339:507-518.

Ferretti, E., J.C. Villaescusa, P. Di Rosa, L.C. Fernandez-Diaz, E. Longobardi, R. Mazzieri, A. Miccio, N. Micali, L. Selleri, G. Ferrari, and F. Blasi. 2006. Hypomorphic mutation of the TALE gene Prep1 (pKnox1) causes a major reduction of Pbx and Meis proteins and a pleiotropic embryonic phenotype. *Mol Cell Biol*. 26:5650-5662.

Fischbach, N.A., S. Rozenfeld, W. Shen, S. Fong, D. Chrobak, D. Ginzinger, S.C. Kogan, A. Radhakrishnan, M.M. Le Beau, C. Largman, and H.J. Lawrence. 2005. HOXB6 overexpression in murine bone marrow immortalizes a myelomonocytic precursor in vitro and causes hematopoietic stem cell expansion and acute myeloid leukemia in vivo. *Blood*. 105:1456-1466.

Furimsky, M., and V.A. Wallace. 2006. Complementary Gli activity mediates early patterning of the mouse visual system. *Dev Dyn*. 235:594-605.

Gehring, W.J., Y.Q. Qian, M. Billeter, K. Furukubo-Tokunaga, A.F. Schier, D. Resendez-Perez, M. Affolter, G. Otting, and K. Wuthrich. 1994. Homeodomain-DNA recognition. *Cell*. 78:211-223.

Gering, M., and R. Patient. 2005. Hedgehog signaling is required for adult blood stem cell formation in zebrafish embryos. *Dev Cell*. 8:389-400.

Gering, M., and R. Patient. 2010. Notch signalling and haematopoietic stem cell formation during embryogenesis. *Journal of cellular physiology*. 222:11-16.

Gering, M., A.R. Rodaway, B. Gottgens, R.K. Patient, and A.R. Green. 1998. The SCL gene specifies haemangioblast development from early mesoderm. *EMBO J*. 17:4029-4045.

Germain, P., P. Chambon, G. Eichele, R.M. Evans, M.A. Lazar, M. Leid, A.R. De Lera, R. Lotan, D.J. Mangelsdorf, and H. Gronemeyer. 2006. International Union of Pharmacology. LXIII. Retinoid X receptors. *Pharmacological reviews*. 58:760-772.

Ghatpande, S., A. Ghatpande, J. Sher, M.H. Zile, and T. Evans. 2002. Retinoid signaling regulates primitive (yolk sac) hematopoiesis. *Blood*. 99:2379-2386.

Glass, C.K., and M.G. Rosenfeld. 2000. The coregulator exchange in transcriptional functions of nuclear receptors. *Genes Dev*. 14:121-141.

Goessling, W., T.E. North, S. Loewer, A.M. Lord, S. Lee, C.L. Stoick-Cooper, G. Weidinger, M. Puder, G.Q. Daley, R.T. Moon, and L.I. Zon. 2009. Genetic interaction of PGE2 and Wnt signaling regulates developmental specification of stem cells and regeneration. *Cell*. 136:1136-1147.

Goh, S.L., Y. Looi, H. Shen, J. Fang, C. Bodner, M. Houle, A.C. Ng, R.A. Screaton, and M. Featherstone. 2009. Transcriptional activation by MEIS1A in response to protein kinase A signaling requires the transducers of regulated CREB family of CREB co-activators. *J Biol Chem*. 284:18904-18912.

Goldie, L.C., J.L. Lucitti, M.E. Dickinson, and K.K. Hirschi. 2008. Cell signaling directing the formation and function of hemogenic endothelium during murine embryogenesis. *Blood*. 112:3194-3204.

Golub, T.R., D.K. Slonim, P. Tamayo, C. Huard, M. Gaasenbeek, J.P. Mesirov, H. Coller, M.L. Loh, J.R. Downing, M.A. Caligiuri, C.D. Bloomfield, and E.S. Lander. 1999. Molecular classification of cancer: class discovery and class prediction by gene expression monitoring. *Science*. 286:531-537.

Gongal, P.A., L.D. March, V.L. Holly, L.M. Pillay, K.M. Berry-Wynne, H. Kagechika, and A.J. Waskiewicz. 2011. Hmx4 regulates Sonic hedgehog signaling through control of retinoic acid synthesis during forebrain patterning. *Dev Biol*. 355:55-64.

Grandel, H., K. Lun, G.J. Rauch, M. Rhinn, T. Piotrowski, C. Houart, P. Sordino, A.M. Kuchler, S. Schulte-Merker, R. Geisler, N. Holder, S.W. Wilson, and M. Brand. 2002. Retinoic acid signalling in the zebrafish embryo is necessary during pre-segmentation stages to pattern the anterior-posterior axis of the CNS and to induce a pectoral fin bud. *Development*. 129:2851-2865.

Gratas, C., M.L. Menot, C. Dresch, and C. Chomienne. 1993. Retinoid acid supports granulocytic but not erythroid differentiation of myeloid progenitors in normal bone marrow cells. *Leukemia*. 7:1156-1162.

Grigoryan, T., P. Wend, A. Klaus, and W. Birchmeier. 2008. Deciphering the function of canonical Wnt signals in development and disease: conditional loss- and gain-of-function mutations of beta-catenin in mice. *Genes Dev*. 22:2308-2341.

Gu, X., F. Xu, X. Wang, X. Gao, and Q. Zhao. 2005. Molecular cloning and expression of a novel CYP26 gene (cyp26d1) during zebrafish early development. *Gene expression patterns : GEP*. 5:733-739.

Guruharsha, K.G., M.W. Kankel, and S. Artavanis-Tsakonas. 2012. The Notch signalling system: recent insights into the complexity of a conserved pathway. *Nature reviews. Genetics*. 13:654-666.

Hadland, B.K., S.S. Huppert, J. Kanungo, Y. Xue, R. Jiang, T. Gridley, R.A. Conlon, A.M. Cheng, R. Kopan, and G.D. Longmore. 2004. A requirement for Notch1 distinguishes 2 phases of definitive hematopoiesis during development. *Blood*. 104:3097-3105.

Hadrys, T., T. Braun, S. Rinkwitz-Brandt, H.H. Arnold, and E. Bober. 1998. Nkx5-1 controls semicircular canal formation in the mouse inner ear. *Development*. 125:33-39.

Haegel, H., L. Larue, M. Ohsugi, L. Fedorov, K. Herrenknecht, and R. Kemler. 1995. Lack of beta-catenin affects mouse development at gastrulation. *Development*. 121:3529-3537.

Hale, L.A., A. Tallafuss, Y.L. Yan, L. Dudley, J.S. Eisen, and J.H. Postlethwait. 2006. Characterization of the retinoic acid receptor genes raraa, rarab and rarg during zebrafish development. *Gene expression patterns : GEP*. 6:546-555.

Han, H., K. Tanigaki, N. Yamamoto, K. Kuroda, M. Yoshimoto, T. Nakahata, K. Ikuta, and T. Honjo. 2002. Inducible gene knockout of transcription factor recombination signal binding protein-J reveals its essential role in T versus B lineage decision. *International immunology*. 14:637-645.

Hawkins, N.C., and J.D. McGhee. 1990. Homeobox containing genes in the nematode Caenorhabditis elegans. *Nucleic Acids Res*. 18:6101-6106.

Herbomel, P., B. Thisse, and C. Thisse. 1999. Ontogeny and behaviour of early macrophages in the zebrafish embryo. *Development*. 126:3735-3745.

Hernandez, R.E., A.P. Putzke, J.P. Myers, L. Margaretha, and C.B. Moens. 2007. Cyp26 enzymes generate the retinoic acid response pattern necessary for hindbrain development. *Development*. 134:177-187.

Hisa, T., S.E. Spence, R.A. Rachel, M. Fujita, T. Nakamura, J.M. Ward, D.E. Devor-Henneman, Y. Saiki, H. Kutsuna, L. Tessarollo, N.A. Jenkins, and N.G. Copeland. 2004. Hematopoietic, angiogenic and eye defects in Meis1 mutant animals. *EMBO J*. 23:450-459.

Hooper, J.E., and M.P. Scott. 2005. Communicating with Hedgehogs. *Nature reviews. Molecular cell biology*. 6:306-317.

Hove, J.R., R.W. Koster, A.S. Forouhar, G. Acevedo-Bolton, S.E. Fraser, and M. Gharib. 2003. Intracardiac fluid forces are an essential epigenetic factor for embryonic cardiogenesis. *Nature*. 421:172-177.

Huang, H., and X. He. 2008. Wnt/beta-catenin signaling: new (and old) players and new insights. *Current opinion in cell biology*. 20:119-125.

Huang, H., M. Rastegar, C. Bodner, S.L. Goh, I. Rambaldi, and M. Featherstone. 2005. MEIS C termini harbor transcriptional activation domains that respond to cell signaling. *J Biol Chem*. 280:10119-10127.

Huang, M.E., Y.C. Ye, S.R. Chen, J.R. Chai, J.X. Lu, L. Zhoa, L.J. Gu, and Z.Y. Wang. 1988. Use of all-trans retinoic acid in the treatment of acute promyelocytic leukemia. *Blood*. 72:567-572.

Huelsken, J., R. Vogel, V. Brinkmann, B. Erdmann, C. Birchmeier, and W. Birchmeier. 2000. Requirement for beta-catenin in anterior-posterior axis formation in mice. *The Journal of cell biology*. 148:567-578.

Ingham, P.W., and A.P. McMahon. 2001. Hedgehog signaling in animal development: paradigms and principles. *Genes Dev*. 15:3059-3087.

Iso, T., L. Kedes, and Y. Hamamori. 2003. HES and HERP families: multiple effectors of the Notch signaling pathway. *Journal of cellular physiology*. 194:237-255.

Iso, T., V. Sartorelli, G. Chung, T. Shichinohe, L. Kedes, and Y. Hamamori. 2001. HERP, a new primary target of Notch regulated by ligand binding. *Mol Cell Biol*. 21:6071-6079.

Itoh, M., C.H. Kim, G. Palardy, T. Oda, Y.J. Jiang, D. Maust, S.Y. Yeo, K. Lorick, G.J. Wright, L. Ariza-McNaughton, A.M. Weissman, J. Lewis, S.C. Chandrasekharappa, and A.B. Chitnis. 2003. Mind bomb is a ubiquitin ligase that is essential for efficient activation of Notch signaling by Delta. *Dev Cell*. 4:67-82.

Izon, D.J., S. Rozenfeld, S.T. Fong, L. Komuves, C. Largman, and H.J. Lawrence. 1998. Loss of function of the homeobox gene Hoxa-9 perturbs early T-cell development and induces apoptosis in primitive thymocytes. *Blood*. 92:383-393.

Jaw, T.J., L.R. You, P.S. Knoepfler, L.C. Yao, C.Y. Pai, C.Y. Tang, L.P. Chang, J. Berthelsen, F. Blasi, M.P. Kamps, and Y.H. Sun. 2000. Direct interaction of two homeoproteins, homothorax and extradenticle, is essential for EXD nuclear localization and function. *Mech Dev*. 91:279-291.

Jiang, Y.J., M. Brand, C.P. Heisenberg, D. Beuchle, M. Furutani-Seiki, R.N. Kelsh, R.M. Warga, M. Granato, P. Haffter, M. Hammerschmidt, D.A. Kane, M.C. Mullins, J. Odenthal, F.J. van Eeden, and C. Nusslein-Volhard. 1996. Mutations affecting neurogenesis and brain morphology in the zebrafish, Danio rerio. *Development*. 123:205-216.

Jin, S.W., W. Herzog, M.M. Santoro, T.S. Mitchell, J. Frantsve, B. Jungblut, D. Beis, I.C. Scott, L.A. D'Amico, E.A. Ober, H. Verkade, H.A. Field, N.C. Chi, A.M. Wehman, H. Baier, and D.Y. Stainier. 2007. A transgene-assisted genetic screen identifies essential regulators of vascular development in vertebrate embryos. *Dev Biol*. 307:29-42.

Kalev-Zylinska, M.L., J.A. Horsfield, M.V. Flores, J.H. Postlethwait, M.R. Vitas, A.M. Baas, P.S. Crosier, and K.E. Crosier. 2002. Runx1 is required for zebrafish blood and vessel development and expression of a human RUNX1-CBF2T1 transgene advances a model for studies of leukemogenesis. *Development*. 129:2015-2030.

Kam, R.K., Y. Deng, Y. Chen, and H. Zhao. 2012. Retinoic acid synthesis and functions in early embryonic development. *Cell & bioscience*. 2:11.

Kamps, M.P., and D. Baltimore. 1993. E2A-Pbx1, the t(1;19) translocation protein of human pre-B-cell acute lymphocytic leukemia, causes acute myeloid leukemia in mice. *Mol Cell Biol*. 13:351-357.

Kamps, M.P., A.T. Look, and D. Baltimore. 1991. The human t(1;19) translocation in pre-B ALL produces multiple nuclear E2A-Pbx1 fusion proteins with differing transforming potentials. *Genes Dev*. 5:358-368.

Kappen, C. 2000. Disruption of the homeobox gene Hoxb-6 in mice results in increased numbers of early erythrocyte progenitors. *Am J Hematol*. 65:111-118.

Karlstrom, R.O., O.V. Tyurina, A. Kawakami, N. Nishioka, W.S. Talbot, H. Sasaki, and A.F. Schier. 2003. Genetic analysis of zebrafish gli1 and gli2 reveals divergent requirements for gli genes in vertebrate development. *Development*. 130:1549-1564.

Kastner, P., H.J. Lawrence, C. Waltzinger, N.B. Ghyselinck, P. Chambon, and S. Chan. 2001. Positive and negative regulation of granulopoiesis by endogenous RARalpha. *Blood*. 97:1314-1320.

Kiefer, C., S. Hessel, J.M. Lampert, K. Vogt, M.O. Lederer, D.E. Breithaupt, and J. von Lintig. 2001. Identification and characterization of a mammalian enzyme catalyzing the asymmetric oxidative cleavage of provitamin A. *J Biol Chem*. 276:14110-14116.

Kim, P.G., C.E. Albacker, Y.F. Lu, I.H. Jang, Y. Lim, G.C. Heffner, N. Arora, T.V. Bowman, M.I. Lin, M.W. Lensch, A. De Los Angeles, L.I. Zon, S. Loewer, and G.Q. Daley. 2013. Signaling axis involving Hedgehog, Notch, and Scl promotes the embryonic endothelial-to-hematopoietic transition. *Proc Natl Acad Sci U S A*. 110:E141-150.

Knoepfler, P.S., and M.P. Kamps. 1995. The pentapeptide motif of Hox proteins is required for cooperative DNA binding with Pbx1, physically contacts Pbx1, and enhances DNA binding by Pbx1. *Mol Cell Biol*. 15:5811-5819.

Knoepfler, P.S., Q. Lu, and M.P. Kamps. 1996. Pbx-1 Hox heterodimers bind DNA on inseparable half-sites that permit intrinsic DNA binding specificity of the Hox partner at nucleotides 3' to a TAAT motif. *Nucleic Acids Res*. 24:2288-2294.

Ko, K.H., Q.L. Lam, M. Zhang, C.K. Wong, C.K. Lo, M. Kahmeyer-Gabbe, W.H. Tsang, S.L. Tsang, L.C. Chan, M.H. Sham, and L. Lu. 2007. Hoxb3 deficiency impairs B lymphopoiesis in mouse bone marrow. *Exp Hematol*. 35:465-475.

Kokolus, K., and M.J. Nemeth. 2010. Non-canonical Wnt signaling pathways in hematopoiesis. *Immunologic research*. 46:155-164.

Kopan, R., and M.X. Ilagan. 2009. The canonical Notch signaling pathway: unfolding the activation mechanism. *Cell*. 137:216-233.

Kornberg, T.B. 1993. Understanding the homeodomain. *J Biol Chem*. 268:26813-26816.

Kozmik, Z., N.D. Holland, A. Kalousova, J. Paces, M. Schubert, and L.Z. Holland. 1999. Characterization of an amphioxus paired box gene, AmphiPax2/5/8: developmental expression patterns in optic support cells, nephridium, thyroid-like structures and pharyngeal gill slits, but not in the midbrain-hindbrain boundary region. *Development*. 126:1295-1304.

Krauss, S., J.P. Concordet, and P.W. Ingham. 1993. A functionally conserved homolog of the Drosophila segment polarity gene hh is expressed in tissues with polarizing activity in zebrafish embryos. *Cell*. 75:1431-1444.

Krebs, L.T., Y. Xue, C.R. Norton, J.R. Shutter, M. Maguire, J.P. Sundberg, D. Gallahan, V. Closson, J. Kitajewski, R. Callahan, G.H. Smith, K.L. Stark, and T. Gridley. 2000. Notch signaling is essential for vascular morphogenesis in mice. *Genes Dev*. 14:1343-1352.

Kroon, E., J. Krosl, U. Thorsteinsdottir, S. Baban, A.M. Buchberg, and G. Sauvageau. 1998. Hoxa9 transforms primary bone marrow cells through specific collaboration with Meis1a but not Pbx1b. *EMBO J*. 17:3714-3725.

Kroon, E., U. Thorsteinsdottir, N. Mayotte, T. Nakamura, and G. Sauvageau. 2001. NUP98-HOXA9 expression in hemopoietic stem cells induces chronic and acute myeloid leukemias in mice. *EMBO J*. 20:350-361.

Kudoh, T., S.W. Wilson, and I.B. Dawid. 2002. Distinct roles for Fgf, Wnt and retinoic acid in posteriorizing the neural ectoderm. *Development*. 129:4335-4346.

Kuhl, M., L.C. Sheldahl, C.C. Malbon, and R.T. Moon. 2000a. Ca(2+)/calmodulin-dependent protein kinase II is stimulated by Wnt and Frizzled homologs and promotes ventral cell fates in Xenopus. *J Biol Chem*. 275:12701-12711.

Kuhl, M., L.C. Sheldahl, M. Park, J.R. Miller, and R.T. Moon. 2000b. The Wnt/Ca2+ pathway: a new vertebrate Wnt signaling pathway takes shape. *Trends Genet*. 16:279-283.

Kumano, K., S. Chiba, A. Kunisato, M. Sata, T. Saito, E. Nakagami-Yamaguchi, T. Yamaguchi, S. Masuda, K. Shimizu, T. Takahashi, S. Ogawa, Y. Hamada, and H. Hirai. 2003. Notch1 but not Notch2 is essential for generating hematopoietic stem cells from endothelial cells. *Immunity*. 18:699-711.

Kuwata, T., I.M. Wang, T. Tamura, R.M. Ponnamperuma, R. Levine, K.L. Holmes, H.C. Morse, L.M. De Luca, and K. Ozato. 2000. Vitamin A deficiency in mice causes a systemic expansion of myeloid cells. *Blood*. 95:3349-3356.

Labbaye, C., M. Valtieri, U. Testa, A. Giampaolo, E. Meccia, P. Sterpetti, I. Parolini, E. Pelosi, D. Bulgarini, Y.E. Cayre, and et al. 1994. Retinoic acid downmodulates erythroid differentiation and GATA1 expression in purified adult-progenitor culture. *Blood*. 83:651-656.

Labrecque, J., D. Allan, P. Chambon, N.N. Iscove, D. Lohnes, and T. Hoang. 1998. Impaired granulocytic differentiation in vitro in hematopoietic cells lacking retinoic acid receptors alpha1 and gamma. *Blood*. 92:607-615.

Ladam, F., and C.G. Sagerstrom. 2014. Hox regulation of transcription: more complex(es). *Dev Dyn*. 243:4-15.

Lai, E.C. 2002. Notch cleavage: Nicastrin helps Presenilin make the final cut. *Current biology : CB*. 12:R200-202.

Lai, L., B.L. Bohnsack, K. Niederreither, and K.K. Hirschi. 2003. Retinoic acid regulates endothelial cell proliferation during vasculogenesis. *Development*. 130:6465-6474.

Lampert, J.M., J. Holzschuh, S. Hessel, W. Driever, K. Vogt, and J. von Lintig. 2003. Provitamin A conversion to retinal via the beta,beta-carotene-15,15'-oxygenase (bcox) is essential for pattern formation and differentiation during zebrafish embryogenesis. *Development*. 130:2173-2186.

LaRonde-LeBlanc, N.A., and C. Wolberger. 2003. Structure of HoxA9 and Pbx1 bound to DNA: Hox hexapeptide and DNA recognition anterior to posterior. *Genes Dev*. 17:2060-2072.

Lawrence, H.J., C.D. Helgason, G. Sauvageau, S. Fong, D.J. Izon, R.K. Humphries, and C. Largman. 1997. Mice bearing a targeted interruption of the homeobox gene HOXA9 have defects in myeloid, erythroid, and lymphoid hematopoiesis. *Blood*. 89:1922-1930.

Lawson, N.D., N. Scheer, V.N. Pham, C.H. Kim, A.B. Chitnis, J.A. Campos-Ortega, and B.M. Weinstein. 2001. Notch signaling is required for arterial-venous differentiation during embryonic vascular development. *Development*. 128:3675-3683.

Lawson, N.D., A.M. Vogel, and B.M. Weinstein. 2002. sonic hedgehog and vascular endothelial growth factor act upstream of the Notch pathway during arterial endothelial differentiation. *Dev Cell*. 3:127-136.

Levi, L., T. Ziv, A. Admon, B. Levavi-Sivan, and E. Lubzens. 2012. Insight into molecular pathways of retinal metabolism, associated with vitellogenesis in zebrafish. *American journal of physiology. Endocrinology and metabolism*. 302:E626-644.

Lewis, K.E., J.P. Concordet, and P.W. Ingham. 1999. Characterisation of a second patched gene in the zebrafish Danio rerio and the differential response of patched genes to Hedgehog signalling. *Dev Biol*. 208:14-29.

Liang, D., W. Jia, J. Li, K. Li, and Q. Zhao. 2012. Retinoic acid signaling plays a restrictive role in zebrafish primitive myelopoiesis. *PloS one*. 7:e30865.

Liao, E.C., B.H. Paw, A.C. Oates, S.J. Pratt, J.H. Postlethwait, and L.I. Zon. 1998. SCL/Tal-1 transcription factor acts downstream of cloche to specify hematopoietic and vascular progenitors in zebrafish. *Genes Dev*. 12:621-626.

Liao, W., B.W. Bisgrove, H. Sawyer, B. Hug, B. Bell, K. Peters, D.J. Grunwald, and D.Y. Stainier. 1997. The zebrafish gene cloche acts upstream of a flk-1 homologue to regulate endothelial cell differentiation. *Development*. 124:381-389.

Lieschke, G.J., A.C. Oates, B.H. Paw, M.A. Thompson, N.E. Hall, A.C. Ward, R.K. Ho, L.I. Zon, and J.E. Layton. 2002. Zebrafish SPI-1 (PU.1) marks a site of myeloid development independent of primitive erythropoiesis: implications for axial patterning. *Dev Biol*. 246:274-295.

Lin, L., and W. McGinnis. 1992. Mapping functional specificity in the Dfd and Ubx homeo domains. *Genes Dev*. 6:1071-1081.

Liu, C., Y. Li, M. Semenov, C. Han, G.H. Baeg, Y. Tan, Z. Zhang, X. Lin, and X. He. 2002. Control of beta-catenin phosphorylation/degradation by a dual-kinase mechanism. *Cell*. 108:837-847.

Liu, F., and Z. Wen. 2002. Cloning and expression pattern of the lysozyme C gene in zebrafish. *Mech Dev*. 113:69-72.

Lobo, G.P., A. Isken, S. Hoff, D. Babino, and J. von Lintig. 2012. BCDO2 acts as a carotenoid scavenger and gatekeeper for the mitochondrial apoptotic pathway. *Development*. 139:2966-2977.

Longobardi, E., and F. Blasi. 2003. Overexpression of PREP-1 in F9 teratocarcinoma cells leads to a functionally relevant increase of PBX-2 by preventing its degradation. *J Biol Chem*. 278:39235-39241.

Luis, T.C., F. Weerkamp, B.A. Naber, M.R. Baert, E.F. de Haas, T. Nikolic, S. Heuvelmans, R.R. De Krijger, J.J. van Dongen, and F.J. Staal. 2009. Wnt3a deficiency irreversibly impairs hematopoietic stem cell self-renewal and leads to defects in progenitor cell differentiation. *Blood*. 113:546-554.

Ma, A.C., M.I. Chung, R. Liang, and A.Y. Leung. 2010. A DEAB-sensitive aldehyde dehydrogenase regulates hematopoietic stem and progenitor cells development during primitive hematopoiesis in zebrafish embryos. *Leukemia*. 24:2090-2099.

MacDonald, B.T., K. Tamai, and X. He. 2009. Wnt/beta-catenin signaling: components, mechanisms, and diseases. *Dev Cell*. 17:9-26.

Magnusson, M., A.C. Brun, H.J. Lawrence, and S. Karlsson. 2007. Hoxa9/hoxb3/hoxb4 compound null mice display severe hematopoietic defects. *Exp Hematol*. 35:1421-1428.

Mallo, M., D.M. Wellik, and J. Deschamps. 2010. Hox genes and regional patterning of the vertebrate body plan. *Dev Biol*. 344:7-15.

Mangelsdorf, D.J., and R.M. Evans. 1995. The RXR heterodimers and orphan receptors. *Cell*. 83:841-850.

Mann, R.S. 1995. The specificity of homeotic gene function. *Bioessays*. 17:855-863.

Mann, R.S., and M. Affolter. 1998. Hox proteins meet more partners. *Curr Opin Genet Dev*. 8:423-429.

Mann, R.S., and S.K. Chan. 1996. Extra specificity from extradenticle: the partnership between HOX and PBX/EXD homeodomain proteins. *Trends Genet*. 12:258-262.

Mann, R.S., K.M. Lelli, and R. Joshi. 2009. Hox specificity unique roles for cofactors and collaborators. *Current topics in developmental biology*. 88:63-101.

Mao, B., W. Wu, Y. Li, D. Hoppe, P. Stannek, A. Glinka, and C. Niehrs. 2001a. LDL-receptor-related protein 6 is a receptor for Dickkopf proteins. *Nature*. 411:321-325.

Mao, J., J. Wang, B. Liu, W. Pan, G.H. Farr, 3rd, C. Flynn, H. Yuan, S. Takada, D. Kimelman, L. Li, and D. Wu. 2001b. Low-density lipoprotein receptor-related protein-5 binds to Axin and regulates the canonical Wnt signaling pathway. *Mol Cell*. 7:801-809.

Marcelo, K.L., T.M. Sills, S. Coskun, H. Vasavada, S. Sanglikar, L.C. Goldie, and K.K. Hirschi. 2013. Hemogenic endothelial cell specification requires c-Kit, Notch signaling, and p27-mediated cell-cycle control. *Dev Cell*. 27:504-515.

Marikawa, Y., and R.P. Elinson. 1998. beta-TrCP is a negative regulator of Wnt/beta-catenin signaling pathway and dorsal axis formation in Xenopus embryos. *Mech Dev*. 77:75-80.

Maye, P., S. Becker, E. Kasameyer, N. Byrd, and L. Grabel. 2000. Indian hedgehog signaling in extraembryonic endoderm and ectoderm differentiation in ES embryoid bodies. *Mech Dev*. 94:117-132.

McNulty, C.L., J.N. Peres, N. Bardine, W.M. van den Akker, and A.J. Durston. 2005. Knockdown of the complete Hox paralogous group 1 leads to dramatic hindbrain and neural crest defects. *Development*. 132:2861-2871.

McWhirter, J.R., S.T. Neuteboom, E.V. Wancewicz, B.P. Monia, J.R. Downing, and C. Murre. 1999. Oncogenic homeodomain transcription factor E2A-Pbx1 activates a novel WNT gene in pre-B acute lymphoblastoid leukemia. *Proc Natl Acad Sci U S A*. 96:11464-11469.

Mennerich, D., S. Hoffmann, T. Hadrys, H.H. Arnold, and E. Bober. 1999. Two highly related homeodomain proteins, Nkx5-1 and Nkx5-2, display different DNA binding specificities. *Biological chemistry*. 380:1041-1048.

Mercader, N., E. Leonardo, N. Azpiazu, A. Serrano, G. Morata, C. Martinez, and M. Torres. 1999. Conserved regulation of proximodistal limb axis development by Meis1/Hth. *Nature*. 402:425-429.

Mikels, A.J., and R. Nusse. 2006. Wnts as ligands: processing, secretion and reception. *Oncogene*. 25:7461-7468.

Milner, L.A., R. Kopan, D.I. Martin, and I.D. Bernstein. 1994. A human homologue of the Drosophila developmental gene, Notch, is expressed in CD34+ hematopoietic precursors. *Blood*. 83:2057-2062.

Minucci, S., M. Maccarana, M. Cioce, P. De Luca, V. Gelmetti, S. Segalla, L. Di Croce, S. Giavara, C. Matteucci, A. Gobbi, A. Bianchini, E. Colombo, I. Schiavoni, G. Badaracco, X. Hu, M.A. Lazar, N. Landsberger, C. Nervi, and P.G. Pelicci. 2000. Oligomerization of RAR and AML1 transcription factors as a novel mechanism of oncogenic activation. *Mol Cell*. 5:811-820.

Moens, C.B., and L. Selleri. 2006. Hox cofactors in vertebrate development. *Dev Biol*. 291:193-206.

Moore, M.A., and D. Metcalf. 1970. Ontogeny of the haemopoietic system: yolk sac origin of in vivo and in vitro colony forming cells in the developing mouse embryo. *Br J Haematol*. 18:279-296.

Morkel, M., J. Huelsken, M. Wakamiya, J. Ding, M. van de Wetering, H. Clevers, M.M. Taketo, R.R. Behringer, M.M. Shen, and W. Birchmeier. 2003. Beta-catenin regulates Cripto- and Wnt3-dependent gene expression programs in mouse axis and mesoderm formation. *Development*. 130:6283-6294.

Moskow, J.J., F. Bullrich, K. Huebner, I.O. Daar, and A.M. Buchberg. 1995. Meis1, a PBX1-related homeobox gene involved in myeloid leukemia in BXH-2 mice. *Mol Cell Biol*. 15:5434-5443.

Munroe, R.J., V. Prabhu, G.M. Acland, K.R. Johnson, B.S. Harris, T.P. O'Brien, I.C. Welsh, D.M. Noden, and J.C. Schimenti. 2009. Mouse H6 Homeobox 1 (Hmx1) mutations cause cranial abnormalities and reduced body mass. *BMC Dev Biol*. 9:27.

Murayama, E., K. Kissa, A. Zapata, E. Mordelet, V. Briolat, H.F. Lin, R.I. Handin, and P. Herbomel. 2006. Tracing hematopoietic precursor migration to successive hematopoietic organs during zebrafish development. *Immunity*. 25:963-975.

Nakagawa, M., M. Ichikawa, K. Kumano, S. Goyama, M. Kawazu, T. Asai, S. Ogawa, M. Kurokawa, and S. Chiba. 2006. AML1/Runx1 rescues Notch1-null mutation-induced deficiency of para-aortic splanchnopleural hematopoiesis. *Blood*. 108:3329-3334.

Nakamura, T., D.A. Largaespada, M.P. Lee, L.A. Johnson, K. Ohyashiki, K. Toyama, S.J. Chen, C.L. Willman, I.M. Chen, A.P. Feinberg, N.A. Jenkins, N.G. Copeland, and J.D. Shaughnessy, Jr. 1996a. Fusion of the nucleoporin gene NUP98 to HOXA9 by the chromosome translocation t(7;11)(p15;p15) in human myeloid leukaemia. *Nat Genet*. 12:154-158.

Nakamura, T., D.A. Largaespada, J.D. Shaughnessy, Jr., N.A. Jenkins, and N.G. Copeland. 1996b. Cooperative activation of Hoxa and Pbx1-related genes in murine myeloid leukaemias. *Nat Genet*. 12:149-153.

Nelson, W.J., and R. Nusse. 2004. Convergence of Wnt, beta-catenin, and cadherin pathways. *Science*. 303:1483-1487.

Nervi, C., F.F. Ferrara, M. Fanelli, M.R. Rippo, B. Tomassini, P.F. Ferrucci, M. Ruthardt, V. Gelmetti, C. Gambacorti-Passerini, D. Diverio, F. Grignani, P.G. Pelicci, and R. Testi. 1998. Caspases mediate retinoic acid-induced degradation of the acute promyelocytic leukemia PML/RARalpha fusion protein. *Blood*. 92:2244-2251.

Neuteboom, S.T., and C. Murre. 1997. Pbx raises the DNA binding specificity but not the selectivity of antennapedia Hox proteins. *Mol Cell Biol*. 17:4696-4706.

Neuteboom, S.T., L.T. Peltenburg, M.A. van Dijk, and C. Murre. 1995. The hexapeptide LFPWMR in Hoxb-8 is required for cooperative DNA binding with Pbx1 and Pbx2 proteins. *Proc Natl Acad Sci U S A*. 92:9166-9170.

Niederreither, K., V. Subbarayan, P. Dolle, and P. Chambon. 1999. Embryonic retinoic acid synthesis is essential for early mouse post-implantation development. *Nat Genet*. 21:444-448.

Niederreither, K., J. Vermot, B. Schuhbaur, P. Chambon, and P. Dolle. 2000. Retinoic acid synthesis and hindbrain patterning in the mouse embryo. *Development*. 127:75-85.

North, T.E., W. Goessling, M. Peeters, P. Li, C. Ceol, A.M. Lord, G.J. Weber, J. Harris, C.C. Cutting, P. Huang, E. Dzierzak, and L.I. Zon. 2009. Hematopoietic stem cell development is dependent on blood flow. *Cell*. 137:736-748.

Nourse, J., J.D. Mellentin, N. Galili, J. Wilkinson, E. Stanbridge, S.D. Smith, and M.L. Cleary. 1990. Chromosomal translocation t(1;19) results in synthesis of a homeobox fusion mRNA that codes for a potential chimeric transcription factor. *Cell*. 60:535-545.

Noyes, M.B., R.G. Christensen, A. Wakabayashi, G.D. Stormo, M.H. Brodsky, and S.A. Wolfe. 2008. Analysis of homeodomain specificities allows the family-wide prediction of preferred recognition sites. *Cell*. 133:1277-1289.

Okuda, T., J. van Deursen, S.W. Hiebert, G. Grosveld, and J.R. Downing. 1996. AML1, the target of multiple chromosomal translocations in human leukemia, is essential for normal fetal liver hematopoiesis. *Cell*. 84:321-330.

Orkin, S.H., and L.I. Zon. 2008. Hematopoiesis: an evolving paradigm for stem cell biology. *Cell*. 132:631-644.

Paik, E.J., and L.I. Zon. 2010. Hematopoietic development in the zebrafish. *The International journal of developmental biology*. 54:1127-1137.

Palis, J., and M.C. Yoder. 2001. Yolk-sac hematopoiesis: the first blood cells of mouse and man. *Exp Hematol*. 29:927-936.

Pear, W.S., and F. Radtke. 2003. Notch signaling in lymphopoiesis. *Seminars in immunology*. 15:69-79.

Peltenburg, L.T., and C. Murre. 1996. Engrailed and Hox homeodomain proteins contain a related Pbx interaction motif that recognizes a common structure present in Pbx. *EMBO J*. 15:3385-3393.

Penkov, D., P. Di Rosa, L. Fernandez Diaz, V. Basso, E. Ferretti, F. Grassi, A. Mondino, and F. Blasi. 2005. Involvement of Prep1 in the alphabeta T-cell receptor T-lymphocytic potential of hematopoietic precursors. *Mol Cell Biol*. 25:10768-10781.

Perkins, A., K. Kongsuwan, J. Visvader, J.M. Adams, and S. Cory. 1990. Homeobox gene expression plus autocrine growth factor production elicits myeloid leukemia. *Proc Natl Acad Sci U S A*. 87:8398-8402.

Pineault, N., C. Buske, M. Feuring-Buske, C. Abramovich, P. Rosten, D.E. Hogge, P.D. Aplan, and R.K. Humphries. 2003. Induction of acute myeloid leukemia in mice by the

human leukemia-specific fusion gene NUP98-HOXD13 in concert with Meis1. *Blood*. 101:4529-4538.

Pittlik, S., S. Domingues, A. Meyer, and G. Begemann. 2008. Expression of zebrafish aldh1a3 (raldh3) and absence of aldh1a1 in teleosts. *Gene expression patterns : GEP*. 8:141-147.

Popperl, H., H. Rikhof, H. Chang, P. Haffter, C.B. Kimmel, and C.B. Moens. 2000. lazarus is a novel pbx gene that globally mediates hox gene function in zebrafish. *Mol Cell*. 6:255-267.

Porcher, C., W. Swat, K. Rockwell, Y. Fujiwara, F.W. Alt, and S.H. Orkin. 1996. The T cell leukemia oncoprotein SCL/tal-1 is essential for development of all hematopoietic lineages. *Cell*. 86:47-57.

Puccetti, E., and M. Ruthardt. 2004. Acute promyelocytic leukemia: PML/RARalpha and the leukemic stem cell. *Leukemia*. 18:1169-1175.

Pui, J.C., D. Allman, L. Xu, S. DeRocco, F.G. Karnell, S. Bakkour, J.Y. Lee, T. Kadesch, R.R. Hardy, J.C. Aster, and W.S. Pear. 1999. Notch1 expression in early lymphopoiesis influences B versus T lineage determination. *Immunity*. 11:299-308.

Purton, L.E., I.D. Bernstein, and S.J. Collins. 1999. All-trans retinoic acid delays the differentiation of primitive hematopoietic precursors (lin-c-kit+Sca-1(+)) while enhancing the terminal maturation of committed granulocyte/monocyte progenitors. *Blood*. 94:483-495.

Purton, L.E., I.D. Bernstein, and S.J. Collins. 2000. All-trans retinoic acid enhances the long-term repopulating activity of cultured hematopoietic stem cells. *Blood*. 95:470-477.

Purton, L.E., S. Dworkin, G.H. Olsen, C.R. Walkley, S.A. Fabb, S.J. Collins, and P. Chambon. 2006. RARgamma is critical for maintaining a balance between hematopoietic stem cell self-renewal and differentiation. *J Exp Med*. 203:1283-1293.

Quina, L.A., T. Kuramoto, D.V. Luquetti, T.C. Cox, T. Serikawa, and E.E. Turner. 2012. Deletion of a conserved regulatory element required for Hmx1 expression in craniofacial mesenchyme in the dumbo rat: a newly identified cause of congenital ear malformation. *Disease models & mechanisms*. 5:812-822.

Radtke, F., A. Wilson, G. Stark, M. Bauer, J. van Meerwijk, H.R. MacDonald, and M. Aguet. 1999. Deficient T cell fate specification in mice with an induced inactivation of Notch1. *Immunity*. 10:547-558.

Rattis, F.M., C. Voermans, and T. Reya. 2004. Wnt signaling in the stem cell niche. *Curr Opin Hematol*. 11:88-94.

Raza-Egilmez, S.Z., S.N. Jani-Sait, M. Grossi, M.J. Higgins, T.B. Shows, and P.D. Aplan. 1998. NUP98-HOXD13 gene fusion in therapy-related acute myelogenous leukemia. *Cancer research*. 58:4269-4273.

Reya, T. 2003. Regulation of hematopoietic stem cell self-renewal. *Recent progress in hormone research*. 58:283-295.

Reya, T., and H. Clevers. 2005. Wnt signalling in stem cells and cancer. *Nature*. 434:843-850.

Rieckhof, G.E., F. Casares, H.D. Ryoo, M. Abu-Shaar, and R.S. Mann. 1997. Nuclear translocation of extradenticle requires homothorax, which encodes an extradenticle-related homeodomain protein. *Cell*. 91:171-183.

Riley, B.B., M. Chiang, L. Farmer, and R. Heck. 1999. The deltaA gene of zebrafish mediates lateral inhibition of hair cells in the inner ear and is regulated by pax2.1. *Development*. 126:5669-5678.

Rinkwitz-Brandt, S., H.H. Arnold, and E. Bober. 1996. Regionalized expression of Nkx5-1, Nkx5-2, Pax2 and sek genes during mouse inner ear development. *Hearing research*. 99:129-138.

Rinkwitz-Brandt, S., M. Justus, I. Oldenettel, H.H. Arnold, and E. Bober. 1995. Distinct temporal expression of mouse Nkx-5.1 and Nkx-5.2 homeobox genes during brain and ear development. *Mech Dev*. 52:371-381.

Robert-Moreno, A., L. Espinosa, J.L. de la Pompa, and A. Bigas. 2005. RBPjkappa-dependent Notch function regulates Gata2 and is essential for the formation of intra-embryonic hematopoietic cells. *Development*. 132:1117-1126.

Robert-Moreno, A., J. Guiu, C. Ruiz-Herguido, M.E. Lopez, J. Ingles-Esteve, L. Riera, A. Tipping, T. Enver, E. Dzierzak, T. Gridley, L. Espinosa, and A. Bigas. 2008. Impaired embryonic haematopoiesis yet normal arterial development in the absence of the Notch ligand Jagged1. *EMBO J*. 27:1886-1895.

Rossant, J., and M. Hirashima. 2003. Vascular development and patterning: making the right choices. *Curr Opin Genet Dev*. 13:408-412.

Roy, S., T. Qiao, C. Wolff, and P.W. Ingham. 2001. Hedgehog signaling pathway is essential for pancreas specification in the zebrafish embryo. *Current biology : CB*. 11:1358-1363.

Saleh, M., I. Rambaldi, X.J. Yang, and M.S. Featherstone. 2000. Cell signaling switches HOX-PBX complexes from repressors to activators of transcription mediated by histone deacetylases and histone acetyltransferases. *Mol Cell Biol*. 20:8623-8633.

Salomon, D., P.A. Sacco, S.G. Roy, I. Simcha, K.R. Johnson, M.J. Wheelock, and A. Ben-Ze'ev. 1997. Regulation of beta-catenin levels and localization by overexpression of plakoglobin and inhibition of the ubiquitin-proteasome system. *The Journal of cell biology*. 139:1325-1335.

Sandell, L.L., B.W. Sanderson, G. Moiseyev, T. Johnson, A. Mushegian, K. Young, J.P. Rey, J.X. Ma, K. Staehling-Hampton, and P.A. Trainor. 2007. RDH10 is essential for synthesis of embryonic retinoic acid and is required for limb, craniofacial, and organ development. *Genes Dev*. 21:1113-1124.

Sauvageau, G., U. Thorsteinsdottir, M.R. Hough, P. Hugo, H.J. Lawrence, C. Largman, and R.K. Humphries. 1997. Overexpression of HOXB3 in hematopoietic cells causes defective lymphoid development and progressive myeloproliferation. *Immunity*. 6:13-22.

Schauerte, H.E., F.J. van Eeden, C. Fricke, J. Odenthal, U. Strahle, and P. Haffter. 1998. Sonic hedgehog is not required for the induction of medial floor plate cells in the zebrafish. *Development*. 125:2983-2993.

Schier, A.F., S.C. Neuhauss, M. Harvey, J. Malicki, L. Solnica-Krezel, D.Y. Stainier, F. Zwartkruis, S. Abdelilah, D.L. Stemple, Z. Rangini, H. Yang, and W. Driever. 1996. Mutations affecting the development of the embryonic zebrafish brain. *Development*. 123:165-178.

Schorderet, D.F., O. Nichini, G. Boisset, B. Polok, L. Tiab, H. Mayeur, B. Raji, G. de la Houssaye, M.M. Abitbol, and F.L. Munier. 2008. Mutation in the human homeobox gene NKX5-3 causes an oculo-auricular syndrome. *American journal of human genetics*. 82:1178-1184.

Schulte, D., and C.L. Cepko. 2000. Two homeobox genes define the domain of EphA3 expression in the developing chick retina. *Development*. 127:5033-5045.

Schwarz-Romond, T., M. Fiedler, N. Shibata, P.J. Butler, A. Kikuchi, Y. Higuchi, and M. Bienz. 2007a. The DIX domain of Dishevelled confers Wnt signaling by dynamic polymerization. *Nature structural & molecular biology*. 14:484-492.

Schwarz-Romond, T., C. Metcalfe, and M. Bienz. 2007b. Dynamic recruitment of axin by Dishevelled protein assemblies. *Journal of cell science*. 120:2402-2412.

Scott, M.P., J.W. Tamkun, and G.W. Hartzell, 3rd. 1989. The structure and function of the homeodomain. *Biochimica et biophysica acta*. 989:25-48.

Semenov, M.V., R. Habas, B.T. Macdonald, and X. He. 2007. SnapShot: Noncanonical Wnt Signaling Pathways. *Cell*. 131:1378.

Semenov, M.V., K. Tamai, B.K. Brott, M. Kuhl, S. Sokol, and X. He. 2001. Head inducer Dickkopf-1 is a ligand for Wnt coreceptor LRP6. *Current biology : CB*. 11:951-961.

Sheldahl, L.C., M. Park, C.C. Malbon, and R.T. Moon. 1999. Protein kinase C is differentially stimulated by Wnt and Frizzled homologs in a G-protein-dependent manner. *Current biology : CB*. 9:695-698.

Shen, W.F., J.C. Montgomery, S. Rozenfeld, J.J. Moskow, H.J. Lawrence, A.M. Buchberg, and C. Largman. 1997. AbdB-like Hox proteins stabilize DNA binding by the Meis1 homeodomain proteins. *Mol Cell Biol*. 17:6448-6458.

Shimamoto, T., Y. Tang, Y. Naot, M. Nardi, P. Brulet, C.J. Bieberich, and K. Takeshita. 1999. Hematopoietic progenitor cell abnormalities in Hoxc-8 null mutant mice. *J Exp Zool*. 283:186-193.

Shimozono, S., T. Iimura, T. Kitaguchi, S. Higashijima, and A. Miyawaki. 2013. Visualization of an endogenous retinoic acid gradient across embryonic development. *Nature*. 496:363-366.

Sive, H.L., and P.F. Cheng. 1991. Retinoic acid perturbs the expression of Xhox.lab genes and alters mesodermal determination in Xenopus laevis. *Genes Dev*. 5:1321-1332.

Slape, C., and P.D. Aplan. 2004. The role of NUP98 gene fusions in hematologic malignancy. *Leuk Lymphoma*. 45:1341-1350.

Slusarski, D.C., J. Yang-Snyder, W.B. Busa, and R.T. Moon. 1997. Modulation of embryonic intracellular Ca2+ signaling by Wnt-5A. *Dev Biol*. 182:114-120.

So, C.W., H. Karsunky, P. Wong, I.L. Weissman, and M.L. Cleary. 2004. Leukemic transformation of hematopoietic progenitors by MLL-GAS7 in the absence of Hoxa7 or Hoxa9. *Blood*. 103:3192-3199.

Staal, F.J., and T.C. Luis. 2010. Wnt signaling in hematopoiesis: crucial factors for self-renewal, proliferation, and cell fate decisions. *Journal of cellular biochemistry*. 109:844-849.

Staal, F.J., T.C. Luis, and M.M. Tiemessen. 2008. WNT signalling in the immune system: WNT is spreading its wings. *Nature reviews. Immunology*. 8:581-593.

Stadler, H.S., J.C. Murray, N.J. Leysens, P.J. Goodfellow, and M. Solursh. 1995. Phylogenetic conservation and physical mapping of members of the H6 homeobox gene family. *Mammalian genome : official journal of the International Mammalian Genome Society*. 6:383-388.

Stadler, H.S., and M. Solursh. 1994. Characterization of the homeobox-containing gene GH6 identifies novel regions of homeobox gene expression in the developing chick embryo. *Dev Biol*. 161:251-262.

Sumoy, L., J.B. Keasey, T.D. Dittman, and D. Kimelman. 1997. A role for notochord in axial vascular development revealed by analysis of phenotype and the expression of VEGR-2 in zebrafish flh and ntl mutant embryos. *Mech Dev*. 63:15-27.

Takada, S., K.L. Stark, M.J. Shea, G. Vassileva, J.A. McMahon, and A.P. McMahon. 1994. Wnt-3a regulates somite and tailbud formation in the mouse embryo. *Genes Dev*. 8:174-189.

Taketani, T., T. Taki, R. Ono, Y. Kobayashi, K. Ida, and Y. Hayashi. 2002. The chromosome translocation t(7;11)(p15;p15) in acute myeloid leukemia results in fusion of the NUP98 gene with a HOXA cluster gene, HOXA13, but not HOXA9. *Genes, chromosomes & cancer*. 34:437-443.

Tallafuss, A., L.A. Hale, Y.L. Yan, L. Dudley, J.S. Eisen, and J.H. Postlethwait. 2006. Characterization of retinoid-X receptor genes rxra, rxrba, rxrbb and rxrg during zebrafish development. *Gene expression patterns : GEP*. 6:556-565.

Tavian, M., L. Coulombel, D. Luton, H.S. Clemente, F. Dieterlen-Lievre, and B. Peault. 1996. Aorta-associated CD34+ hematopoietic cells in the early human embryo. *Blood*. 87:67-72.

Thompson, M.A., D.G. Ransom, S.J. Pratt, H. MacLennan, M.W. Kieran, H.W. Detrich, 3rd, B. Vail, T.L. Huber, B. Paw, A.J. Brownlie, A.C. Oates, A. Fritz, M.A. Gates, A. Amores, N. Bahary, W.S. Talbot, H. Her, D.R. Beier, J.H. Postlethwait, and L.I. Zon. 1998. The cloche and spadetail genes differentially affect hematopoiesis and vasculogenesis. *Dev Biol*. 197:248-269.

Thorsteinsdottir, U., E. Kroon, L. Jerome, F. Blasi, and G. Sauvageau. 2001. Defining roles for HOX and MEIS1 genes in induction of acute myeloid leukemia. *Mol Cell Biol*. 21:224-234.

Thorsteinsdottir, U., G. Sauvageau, M.R. Hough, W. Dragowska, P.M. Lansdorp, H.J. Lawrence, C. Largman, and R.K. Humphries. 1997. Overexpression of HOXA10 in murine hematopoietic cells perturbs both myeloid and lymphoid differentiation and leads to acute myeloid leukemia. *Mol Cell Biol*. 17:495-505.

Troussard, X., F. Valensi, F. Salomon-Nguyen, C. Debert, G. Flandrin, and E. MacIntyre. 1995. Correlation of cytoplasmic Ig mu (C mu) and E2A-PBX1 fusion transcripts in t(1;19) B lineage ALL: discrepancy in C mu detection by slide immunofluorescence and flow cytometry. *Leukemia*. 9:518-519.

Tsai, F.Y., G. Keller, F.C. Kuo, M. Weiss, J. Chen, M. Rosenblatt, F.W. Alt, and S.H. Orkin. 1994. An early haematopoietic defect in mice lacking the transcription factor GATA-2. *Nature*. 371:221-226.

Tyurina, O.V., B. Guner, E. Popova, J. Feng, A.F. Schier, J.D. Kohtz, and R.O. Karlstrom. 2005. Zebrafish Gli3 functions as both an activator and a repressor in Hedgehog signaling. *Dev Biol*. 277:537-556.

Uhl, J.D., T.A. Cook, and B. Gebelein. 2010. Comparing anterior and posterior Hox complex formation reveals guidelines for predicting cis-regulatory elements. *Dev Biol*. 343:154-166.

Vaclavik, V., D.F. Schorderet, F.X. Borruat, and F.L. Munier. 2011. Retinal dystrophy in the oculo-auricular syndrome due to HMX1 mutation. *Ophthalmic genetics*. 32:114-117.

Van Bockstaele, D.R., M. Lenjou, H.W. Snoeck, F. Lardon, and M.E. Peetermans. 1994. Effect of retinoic acid (RA) on myeloid progenitors in normal bone marrow (BM). *Leukemia*. 8:214-215.

Villa, N., L. Walker, C.E. Lindsell, J. Gasson, M.L. Iruela-Arispe, and G. Weinmaster. 2001. Vascular expression of Notch pathway receptors and ligands is restricted to arterial vessels. *Mech Dev*. 108:161-164.

Vlachakis, N., S.K. Choe, and C.G. Sagerstrom. 2001. Meis3 synergizes with Pbx4 and Hoxb1b in promoting hindbrain fates in the zebrafish. *Development*. 128:1299-1312.

von Lintig, J., and K. Vogt. 2000. Filling the gap in vitamin A research. Molecular identification of an enzyme cleaving beta-carotene to retinal. *J Biol Chem*. 275:11915-11920.

von Lintig, J., and K. Vogt. 2004. Vitamin A formation in animals: molecular identification and functional characterization of carotene cleaving enzymes. *The Journal of nutrition*. 134:251S-256S.

Wada, M.R., Y. Ohtani, Y. Shibata, K.J. Tanaka, N. Tanimoto, and T. Nishikata. 1998. An alternatively spliced gene encoding a Y-box protein showing maternal expression and tissue-specific zygotic expression in the ascidian embryo. *Development, growth & differentiation*. 40:631-640.

Wagner, G.P., C. Amemiya, and F. Ruddle. 2003. Hox cluster duplications and the opportunity for evolutionary novelties. *Proc Natl Acad Sci U S A*. 100:14603-14606.

Wang, G.V., G.J. Dolecki, R. Carlos, and T. Humphreys. 1990. Characterization and expression of two sea urchin homeobox gene sequences. *Developmental genetics*. 11:77-87.

Wang, J., I.C. Weaver, A. Gauthier-Fisher, H. Wang, L. He, J. Yeomans, F. Wondisford, D.R. Kaplan, and F.D. Miller. 2010. CBP histone acetyltransferase activity regulates embryonic neural differentiation in the normal and Rubinstein-Taybi syndrome brain. *Dev Cell*. 18:114-125.

Wang, Q., T. Stacy, J.D. Miller, A.F. Lewis, T.L. Gu, X. Huang, J.H. Bushweller, J.C. Bories, F.W. Alt, G. Ryan, P.P. Liu, A. Wynshaw-Boris, M. Binder, M. Marin-Padilla, A.H. Sharpe, and N.A. Speck. 1996a. The CBFbeta subunit is essential for CBFalpha2 (AML1) function in vivo. *Cell*. 87:697-708.

Wang, W., E.K. Chan, S. Baron, T. Van de Water, and T. Lufkin. 2001. Hmx2 homeobox gene control of murine vestibular morphogenesis. *Development*. 128:5017-5029.

Wang, W., J.F. Grimmer, T.R. Van De Water, and T. Lufkin. 2004. Hmx2 and Hmx3 homeobox genes direct development of the murine inner ear and hypothalamus and can be functionally replaced by Drosophila Hmx. *Dev Cell*. 7:439-453.

Wang, W., P. Lo, M. Frasch, and T. Lufkin. 2000. Hmx: an evolutionary conserved homeobox gene family expressed in the developing nervous system in mice and Drosophila. *Mech Dev*. 99:123-137.

Wang, W., and T. Lufkin. 1997. Assignment of the murine Hmx2 and Hmx3 homeobox genes to the distal region of mouse chromosome 7. *Chromosome research : an international journal on the molecular, supramolecular and evolutionary aspects of chromosome biology*. 5:501-502.

Wang, W., and T. Lufkin. 2005. Hmx homeobox gene function in inner ear and nervous system cell-type specification and development. *Experimental cell research*. 306:373-379.

Wang, W., T. Van De Water, and T. Lufkin. 1998. Inner ear and maternal reproductive defects in mice lacking the Hmx3 homeobox gene. *Development*. 125:621-634.

Wang, X.D., R.M. Russell, C. Liu, F. Stickel, D.E. Smith, and N.I. Krinsky. 1996b. Beta-oxidation in rabbit liver in vitro and in the perfused ferret liver contributes to retinoic acid biosynthesis from beta-apocarotenoic acids. *J Biol Chem*. 271:26490-26498.

Warrell, R.P., Jr., H. de The, Z.Y. Wang, and L. Degos. 1993. Acute promyelocytic leukemia. *The New England journal of medicine*. 329:177-189.

Waskiewicz, A.J., H.A. Rikhof, R.E. Hernandez, and C.B. Moens. 2001. Zebrafish Meis functions to stabilize Pbx proteins and regulate hindbrain patterning. *Development*. 128:4139-4151.

Waskiewicz, A.J., H.A. Rikhof, and C.B. Moens. 2002. Eliminating zebrafish pbx proteins reveals a hindbrain ground state. *Dev Cell*. 3:723-733.

Waxman, J.S., and D. Yelon. 2007. Comparison of the expression patterns of newly identified zebrafish retinoic acid and retinoid X receptors. *Dev Dyn*. 236:587-595.

Weinstein, B.M., and N.D. Lawson. 2002. Arteries, veins, Notch, and VEGF. *Cold Spring Harbor symposia on quantitative biology*. 67:155-162.

White, R.J., and T.F. Schilling. 2008. How degrading: Cyp26s in hindbrain development. *Dev Dyn*. 237:2775-2790.

Wilkinson, R.N., M.J. Koudijs, R.K. Patient, P.W. Ingham, S. Schulte-Merker, and F.J. van Eeden. 2012. Hedgehog signaling via a calcitonin receptor-like receptor can induce arterial differentiation independently of VEGF signaling in zebrafish. *Blood*. 120:477-488.

Willert, K., J.D. Brown, E. Danenberg, A.W. Duncan, I.L. Weissman, T. Reya, J.R. Yates, 3rd, and R. Nusse. 2003. Wnt proteins are lipid-modified and can act as stem cell growth factors. *Nature*. 423:448-452.

Willert, K., and K.A. Jones. 2006. Wnt signaling: is the party in the nucleus? *Genes Dev*. 20:1394-1404.

Williams, C., S.H. Kim, T.T. Ni, L. Mitchell, H. Ro, J.S. Penn, S.H. Baldwin, L. Solnica-Krezel, and T.P. Zhong. 2010. Hedgehog signaling induces arterial endothelial cell formation by repressing venous cell fate. *Dev Biol*. 341:196-204.

Williams, T.M., M.E. Williams, and J.W. Innis. 2005. Range of HOX/TALE superclass associations and protein domain requirements for HOXA13:MEIS interaction. *Dev Biol*. 277:457-471.

Wilson, D.S., G. Sheng, S. Jun, and C. Desplan. 1996. Conservation and diversification in homeodomain-DNA interactions: a comparative genetic analysis. *Proc Natl Acad Sci U S A*. 93:6886-6891.

Yanagawa, S., Y. Matsuda, J.S. Lee, H. Matsubayashi, S. Sese, T. Kadowaki, and A. Ishimoto. 2002. Casein kinase I phosphorylates the Armadillo protein and induces its degradation in Drosophila. *EMBO J*. 21:1733-1742.

Yin, H.C., H.P. Tseng, H.Y. Chung, C.Y. Ko, W.S. Tzou, D.R. Buhler, and C.H. Hu. 2008. Influence of TCDD on zebrafish CYP1B1 transcription during development. *Toxicological sciences : an official journal of the Society of Toxicology*. 103:158-168.

Yoshiura, K., N.J. Leysens, R.S. Reiter, and J.C. Murray. 1998. Cloning, characterization, and mapping of the mouse homeobox gene Hmx1. *Genomics*. 50:61-68.

Yu, C., Y. Liu, Z. Miao, M. Yin, W. Lu, Y. Lv, M. Ding, and H. Deng. 2010. Retinoic acid enhances the generation of hematopoietic progenitors from human embryonic stem cell-derived hemato-vascular precursors. *Blood*. 116:4786-4794.

Zhang, Y., H. Jin, L. Li, F.X. Qin, and Z. Wen. 2011. cMyb regulates hematopoietic stem/progenitor cell mobilization during zebrafish hematopoiesis. *Blood*. 118:4093-4101.

Zhao, B., F.P. Guengerich, M. Voehler, and M.R. Waterman. 2005. Role of active site water molecules and substrate hydroxyl groups in oxygen activation by cytochrome P450 158A2: a new mechanism of proton transfer. *J Biol Chem*. 280:42188-42197.

Zhu, J., M. Gianni, E. Kopf, N. Honore, M. Chelbi-Alix, M. Koken, F. Quignon, C. Rochette-Egly, and H. de The. 1999. Retinoic acid induces proteasome-dependent degradation of retinoic acid receptor alpha (RARalpha) and oncogenic RARalpha fusion proteins. *Proc Natl Acad Sci U S A*. 96:14807-14812.

Chapter 2

Materials and Methods

2.1 Ethics statement

Embryonic and adult zebrafish were cared for in accordance with Canadian Council for Animal Care (CCAC) guidelines. This study was approved by the University of Alberta Animal Care and Use Committee for Biosciences (protocol 427).

2.2. Animal care, fish lines and general procedures

Care of adult and embryonic zebrafish was conducted according to standard protocols (Westerfield, 2000). Embryos were grown at room temperature (RT), 25.5°C, 28.5°C, or 33°C in embryo media (EM) and staged according to standardized morphological criteria (Kimmel et al., 1995). EM was supplemented with 0.003% – 0.006% 1-phenyl 2-thiourea (PTU) (Sigma) to prevent pigment formation in post-24 hours post fertilization (hpf) embryos.

Unless otherwise noted, AB strain zebrafish were used for all experiments. Transgenic fish lines used in experiments include *Tg*(*gata1*:*DsRed*)^{sd2Tg}, and *Tg*(*fli1a*:E*GFP*)^{y1Tg}. Mutant fish lines used in experiments include *lazarus* (*lzr*/*pbx4*^{b557}), *kugelig* (*kgg*/*cdx4*^{tv205c}), *hmx4*^{ua1003}, and *hmx4*^{ua1004}.

The ua1003, and ua1004 alleles of H6 family homeobox 4 (*hmx4*) were generated using ZFN technology (2.19; 2.22). The ua1004 allele contains a 2 base pair (bp) deletion, while the ua1003 allele contains a 4 bp insertion. Both sequence alterations generate frameshift mutations that produce premature stop codons immediately upstream of the Hmx4 homeodomain (Figure 5.10). These sequence alterations represent loss-of-function mutations in Hmx4, as the mutant proteins exhibit no activity in mRNA overexpression assays (Figure 5.15). Genotyping of *hmx4*-mutant embryos was conducted by high-resolution melt curve analysis, and/or sequencing of isolated genomic DNA. Hmx-depleted embryos were generated by injecting one-cell stage *hmx4*-mutant embryos with translation-blocking *hmx1* morpholino (Table 2.1). *hmx4*-morphants were generated by injecting one-cell stage embryos with a combination of two previously-described translation-blocking morpholinos (Table 2.1; (Gongal et al., 2011).

The b557 allele of pre-B-cell leukemia transcription factor 4 (*pbx4*; also known as *lazarus* or *lzr*) was originally identified through the altered hindbrain expression pattern of *egr2b* (*krox20*), as previously described (Popperl et al., 2000). Pbx-depleted embryos were

generated by injecting one-cell stage embryos from a heterozygous mutant *lzr*$^{+/-}$ (*pbx4*$^{+/-}$) incross with a combination of four previously described Pbx translation-blocking morpholinos (Table 2.1; Erickson et al., 2007). This method yields 75% Pbx-depleted embryos (*lzr*$^{+/-}$ and *lzr*$^{-/-}$) and 25% partially-depleted embryos (*lzr*$^{+/+}$). The effectiveness of this approach at removing >95% of total Pbx protein in Pbx-depleted embryos has been documented using a pan-Pbx antibody (Maves et al., 2007; Waskiewicz et al., 2002). Pbx-depleted embryos are phenotypically indistinguishable from maternally and zygotically mutant *lzr* embryos injected with pre-B-cell leukemia transcription factor 2 (*pbx2*) morpholinos, and were identified through *in situ* hybridization assays for the downregulation of *eng2a* (Erickson et al., 2007; Maves and Kimmel, 2005) and abrogation of *egr2b* expression (Popperl et al., 2000; Waskiewicz et al., 2002).

Myeloid ecotropic integration site (Meis1)-deficient embryos were generated by injecting one-cell AB embryos with 4 ng of translation-blocking *meis1* morpholino (Table 2.1), as previously described (French et al., 2007). The specificity of this morpholino was assessed through the observation of expected hindbrain phenotypes, mRNA rescue experiments (French et al., 2007), and immunohistochemical analysis of Meis1 protein levels using the P2A6 monoclonal antibody.

GATA binding protein 1a (Gata1)-deficient embryos were generated by injecting one-cell AB embryos with approximately 5 ng of translation-blocking *gata1* morpholino (Table 2.1) as previously described (Galloway et al., 2005).

The tv205 allele of *caudal type homeobox 4* (*cdx4;* also known as *kugelig* or *kgg*) was originally identified because of impaired development of the posterior body axis, as previously described (Hammerschmidt et al., 1996). Cdx-depleted embryos were generated by injecting one-cell *cdx4*$^{tv205c/tv205c}$ embryos with approximately 5 ng of translation-blocking *caudal type homeobox 1a* (*cdx1a*) morpholino (Table 2.1), as previously described (Davidson and Zon, 2006).

Aldehyde dehydrogenase 1 family, member A2 (Aldh1a2)-depleted embryos were generated by injecting one-cell AB embryos with approximately 5 ng of previously-described translation-blocking *aldh1a2* morpholino (Table 2.1; Alexa et al., 2009).

Manual dechorionation of fixed or live embryos was preformed using Dumont No. 5 forceps. Enzymatic dechorionation of live embryos was performed by incubating embryos in a 1 mg/ml solution of Pronase E (Sigma) at RT, with gentle swirling until chorions began to crumple. Embryos were then washed three times successively in EM.

Prior to mRNA in situ hybridization or immunohistochemical analyses, embryos were fixed in 4% paraformaldehyde (PFA)/phosphate-buffered saline (PBS) overnight at 4 °C or 4-5 hours (h) at RT with gentle agitation on a rotating platform.

2.3 Morpholinos

Translation-blocking morpholino antisense oligonucleotides (MO; GeneTools) were used to knockdown targeted proteins in zebrafish embryos. Morpholino sequences and injected dosages are listed in Table 2.1. MO stocks were diluted to a concentration of 10 mg/ml in water, and were stored at -80 °C, -20 °C or 4 °C. Working morpholino stocks were diluted to the appropriate concentration in Danieau solution (17.4 mM NaCl + 0.21 mM KCl + 0.12 mM MgSO4 • 7H2O + 0.18 mM Ca(NO3)2 + 1.5 mM HEPES) and were stored at 4 °C. Prior to injection, working morpholino stocks were heated to 65 °C for 5 to 10 minutes (min), then cooled to RT. All morpholinos were injected into the yolk or cell of single-cell zebrafish embryos.

2.4 Pharmacological treatments

All compounds were dissolved in Dimethyl sulfoxide (DMSO), and diluted to a working concentration in EM. Equivalent solutions of DMSO/EM were used as solvent controls. A 2-10 μM solution of Diethylaminobenzaldehyde (DEAB; Sigma) was used to inhibit retinoic acid (RA) synthesis by retinaldehyde dehydrogenase enzymes (Maves and Kimmel, 2005; Perz-Edwards et al., 2001). A 1-10 nM solution of all-trans RA (Sigma) was applied to live, dechorionated embryos at 4 hpf to activate retinoic acid signaling. All embryos were then grown to various stages at 28.5 °C in the dark, and were assessed for phenotypes, washed into EM, or fixed in 4% PFA/PBS overnight at 4 °C.

2.5 O-dianisidine histochemical staining

Histochemical staining of hemoglobin by o-dianisidine was preformed as previously described (Lieschke et al., 2001). Briefly, 48 hpf dechorionated embryos were incubated in staining solution (0.6 mg/ml o-dianisidine (Sigma) + 40% ethanol + 0.01 M sodium acetate, pH 5.2 + 0.65% hydrogen peroxide) for 15 min at RT, with gentle agitation on a rotating platform. Embryos were then washed four times 5 min each in water at RT, with gentle agitation on a rotating platform, and stored at 4 °C.

2.6 Real-time quantitative PCR (qPCR)

Total mRNA was extracted from 25-100 embryos using RNAqueous-4PCR (Ambion) according to the manufacturer's specifications: Embryos were homogenized by vortex-based agitation in 350 μl of Lysis/Binding solution. 350 μl of 64% Ethanol was added, and the solution was vortexed for 30 seconds (s). The solution was transferred to a filter column in a collection tube, and centrifuged for 1 min at full speed. The flow-through was discarded. 700 μl of Wash Solution #1 was added to the column, which was then centrifuged for 1 min at full speed. The flow-through was discarded. 500 μl of Wash Solution #2/3 was added to the column, which was centrifuged for 1 min at full speed, and the flow-through was discarded. This last step was repeated once. The column was transferred to a new collection tube. 40 μl of 70 °C Elution Solution was added to the column, which was then centrifuged for 30 s at full speed. 30 μl of 70 °C Elution Solution was added to the column, which was then centrifuged for 30 s at full speed. DNA was removal was performed by adding 19 μl of diethylpyrocarbonate-treated water, 10 μl of 10X DNase I Buffer (Ambion), and 1 μl DNase I (Ambion) to the eluted RNA. This solution was incubated for 30 min with gentle agitation in a 37 °C water bath.

Extracted mRNA was purified using the RNeasy Mini Kit (Qiagen) according to the manufacturer's specifications:. 350 μl of Buffer RLT + 1% beta mercaptoethanol was added to the DNAse I-treated RNA. The solution was vortexed. 250 μl of 100% ethanol was added to the solution, which was then mixed by pippetting up and down. The solution was placed in a column inside a collection tube, and centrifuged for 15 s at 10,000 revolutions per minute

(rpm). The flow-through was discarded, and the column was transferred to a new collection tube. 500 µl of Buffer RPE was added to the column, which was centrifuged for 15 s at 10,000 rpm. The flow-through was discarded. 500 µl of Buffer RPE was added to the column, which was centrifuged 2 min at 10,000 rpm. The column was transferred to a new collection tube, and this was centrifuged for 1 min at maximum speed. The column was transferred to a new collection tube. To elute RNA, 10 µl of diethylpyrocarbonate (DEPC)-treated water was added to the column, which was then centrifuged 1 min at 10,000 rpm. Isolated, purified RNA was stored at -80 °C. RNA quantity and quality was assessed by spectrophotometry.

First-strand cDNA synthesis was performed using the AffinityScript QPCR cDNA Synthesis Kit (Agilent), with random primers, according to the manufacturer's specifications. 3 µg of isolated, purified RNA was added to a PCR tube containing RNase-free water, 10 µl 2X cDNA Synthesis Master Mix, 3 µl Random Primers, and 1 µl RT/RNase Block Enzyme Mixture (total volume 20 µl). The PCR cycle conditions were 25 °C for 5 min (primer annealing), 42 °C for 30 min (cDNA synthesis), 95 °C for 5 min (reaction termination). cDNA was stored at 20 °C.

qPCR analysis of cDNA was performed using Brilliant SYBR Green QPCR Master Mix (Stratagene) and the StepOnePlus Real-Time PCR System (Applied Biosystems). All cDNA samples were run in replicates of six to nine, and each experiment was repeated twice. The PCR cycle conditions were 95 °C for 10 min (initial denaturation), then 40 cycles of 95 °C for 20 s (denaturation), 55 °C for 1 min (annealing), and 72 °C for 30 s (extension). Fluorescence readings were taken after the 55 °C annealing step. The Ct value data were analyzed using the comparative Ct method ($2^{-\Delta\Delta Ct}$ method) (Livak and Schmittgen, 2001).

All qPCR primers were selected from the Universal Probe Library Assay Design Center for Zebrafish (Roche), with preference given to primers generating intron-spanning amplicons. qPCR primer sequences are listed in Table 2.2. Prior to real-time qPCR analysis, primer sets were validated as follows: For each primer set, an amplification plot was produced from a standard cDNA two-fold dilution series. This plot was used to generate a linear regression curve. Valid primer sets were shown to produce linear regression slopes of -3.3 ± 0.1 with a coefficient of determination (R^2) of 0.99. Furthermore, the endogenous control

primer set *eukaryotic translation elongation factor 1 alpha 1a* (*ef1a*) was shown to produce a slope within 0.1 of each test primer set slope.

2.7 Template mRNA extraction

Total mRNA was extracted as previously described (2.6), using RNAqueous-4PCR (Ambion) according to the manufacturer's specifications, or using TRIzol-based mRNA extraction. For the TRIzol-based extraction method, 50-100 dechorionated embryos were homogenized in 200 µl of TRIzol by vortexing. 300 µl of TRIzol was added to the homogenized samples. Samples were vortexed for an additional 30 s. Following the addition of 125 µl of chloroform, each sample was vortexed for 30 s, and centrifuged at 14,000 rpm for 20 min at 4 °C. 350 µl of chloroform was added to the reserved supernatant, which was then vortexed for 30 s, and centrifuged at 14,000 rpm for 20 min at 4 °C. 1 µl of 20 mg/ml RNAse-free glycogen (Roche) was added to the reserved supernatant. Samples were vortexed, and mRNA was precipitated at -20 °C for 1 h. The samples were centrifuged at 14,000 rpm for 20 min at 4 °C. The pelleted mRNA was washed with 70% ethanol. The samples were stored for 15 min at -20 °C, and centrifuged at 14,000 rpm for 5 min at 4 °C. Following supernatant removal, the dried, pelleted mRNA was resuspended in 90 µl of DEPC-treated water. Samples were treated with 10 µl of 10X DNAse I buffer (Ambion), and 1µl of DNAse I (Ambion) at 37 °C for 15 min. mRNA was purified using the RNeasy Mini Kit (Qiagen), as previously described (2.6), according to the manufacturer's specifications.

2.8 cDNA synthesis and cloning

First-strand cDNA synthesis was performed using the AffinityScript QPCR cDNA Synthesis Kit (Stratagene), with random primers, as previously described (2.6), according to the manufacturer's specifications. Using a cDNA template, DNA was PCR-amplified using Phusion high-fidelity DNA Polymerase (Thermo Scientific) and primers containing integrated restriction endonuclease sites. The PCR cycle conditions were 94 °C for 2 min (initial denaturation), then 40 cycles of 98 °C for 20 s (denaturation), 2-5 °C blow primer melting temperature (Tm) for 30 s (annealing), 72 °C for 30 s per kb of product (extension), then 72 °C for 3 min (final extension).

PCR products were analyzed by gel electrophoresis, and correctly sized product was gel-purified using a QIAquick (Qiagen) or GeneJET (Fermentas) gel extraction kit according to the manufacturer's specifications: 300 µl of Buffer QG (Qiagen) or Binding Buffer (Fermentas) was added to the excised DNA-containing gel slice. This was incubated in a 55 °C water bath, with intermittent vortexing until the gel dissolved. 100 µl isopropanol was added to the solution, which was then transferred to a filter column in a collection tube, and centrifuged 1 min at 13,000 rpm. The flow-through was discarded. 500 µl of Buffer QG (Qiagen) or 100 µl of Binding Buffer (Fermentas) was added to the column, which was then centrifuged 1 min at 13,000 rpm. The flow-through was discarded. 750 µl of Buffer PB (Qiagen), or 700 µl of Wash Buffer (Fermentas) was added to the column, which was then centrifuged 1 min at 13,000 rpm. The flow-through was discarded. The column was centrifuged for 1 min at maximum speed, and placed in a new collection tube. To elute DNA, 50 µl of Buffer EB (Qiagen) or Elution Buffer (Fermentas) was added to the column, which was then left to stand for 1 min, and centrifuged 1 min at full speed. Gel-purified DNA was stored at -20 °C.

Adenine tails were added to the gel-purified PCR product in the following manner: 15 µl of gel-purified PCR product was added to a PCR tube containing 2 µl 10X Ex Taq Buffer (TaKaRa), 1 µl 2.5 mM dNTP mix, 1 µl Taq DNA Polymerase (Life Technologies), and 1 µl water. The solution was incubated 10 min at 72 °C in a PCR machine. Tailed PCR product was then cloned into pCR4-TOPO using the TA TOPO Cloning Kit (Life Technologies), according to manufacturer's specifications, but using quarter reactions. Brifely, 60 µl of water was added to the tailed PCR product. 1 µl of the diluted product was added to 0.25 µl of pCR4-TOPO vector, and 1.25 µl water. The solution was left to sit for 5 min at RT. The product was then used to transform One Shot TOP10 chemically competent *E. Coli* (Life Technologies) according to manufacturer's specifications. Briefly, 2.5 µl of product was added to 10 µl of One Shot TOP10 chemically competent *E. Coli* cells, on ice. This solution was cooled on ice for 10 min. The cells were heat-shocked for 45 s in a 42 °C water bath, and were cooled on ice for 2 min. 150 µl of lysogeny broth (LB; 10 g Bacto-Tryptone + 5 g Bacto yeast extract + 10 g NaCl + 100 µl 1M NaOH) or super optimal broth (SOC; Life

Technologies) was added to the solution, which was then incubated for 30 min with gentle agitation in a 37 °C water bath. The solution was then plated on Carbenicillin plates (LB + 7.5 g agar + 50 μg/ml Carbenicillin), which were incubated at 37 °C overnight. To amplify DNA, colonies were picked from the plates and grown at 37 °C overnight in LB + Carbenicillin with agitation.

Plasmid DNA was isolated from liquid cultures using the QIAprep Spin Miniprep Kit (Qiagen) or the GeneJet Plasmid Miniprep Kit (Fermentas), according to the manufacturer's specifications: Briefly, 1.5 ml of cells were pelleted by 5 min of centrifugation at 4,000 rpm. Cells were resuspended in 250 μl of Buffer P1/Resuspension Solution, and the solution was gently inverted 5 times. 250 μl of Buffer P2/Lysis Solution was added, and the solution was gently inverted 5 times. 350 μl of Buffer N3/Neutralization Solution was added, and the solution was gently inverted 5 times. The reaction was centrifuged 10 min at maximum speed. The supernatant was transferred to a column, which was centrifuged 1 min at 13,000 rpm. The flowthrough was discarded. 500 μl of Buffer PB/Wash Solution was added to the column, and the solution was centrifuged 1 min at 13,000 rpm. The flowthrough was discarded. 750 μl of Buffer PE/Wash Solution was added to the column, and the solution was centrifuged 1 min at 13,000 rpm. The flowthrough was discarded, and the column was centrifuged 1 min at maximum speed. The column was transferred to a new collection tube. 50 μl of Buffer EB/Elution Buffer was added to the column. After 1 min, the solution was centrifuged 2 min at 10,000 rpm.

Constructs were verified by Sanger sequencing, and digested with appropriate restriction endonucleases. Digests were analyzed by gel electrophoresis, and correctly sized product was gel-purified (2.8) and ligated to appropriately digested expression vectors. Briefly, 10 μl of digested insert was added to 5 μl of digested vector, 4 μl of 5X T4 DNA Ligase Buffer (Promega), and 1 μl T4 DNA Ligase (Promega). The ligation reaction as incubated 4 h at RT, or overnight at 16 °C. Ligations were then used to transform One Shot TOP10 (Life Technologies) chemically competent *E. Coli* according to manufacturer's specifications (2.8).

2.9 Site-directed mutagenesis

Site directed mutagenesis primers are listed in Table 2.3. The PCR reaction contained: 500 ng of template plasmid DNA, 17 μl of master mix (100 μl 10X PFU buffer, 792 μl water, 2 μl each of 100 mM dNTPs), 1 μl (10 mM) NAD, 0.5 μl (200 ng) forward primer, 0.5 μl (200 ng) reverse primer, 0.5 μl DMSO, 0.3 μl Taq DNA Ligase (NEB), 1 μl PfuUltra DNA Polymerase (Agilent), and 1.5 μl water. The PCR cycle conditions were 95 °C for 2 min (initial denaturation), then 30 cycles of 95 °C for 1 min (denaturation), 55 °C for 1 min (annealing), and 65°C for 10 min (extension). PCR products were then treated with 1 μl of DpnI for 30 min at 37 °C to digest original plasmid. Cloned constructs were verified by Sanger sequencing.

2.10 *In vitro* mRNA synthesis

mRNA expression constructs are listed in Table 2.4. Prior to mRNA synthesis, linearized plasmid DNA (50 μl total volume) was incubated with 2.5 μl of 10% SDS and 2 μl of 10 mg/ml proteinase K at 50°C for 1 hour to denature any RNAses present. Plasmid DNA was then purified by phenol-chloroform-isoamyl alcohol extraction and ethanol precipitation. Briefly, DEPC-treated water, and 10 μl of NaOAc (pH 5.3) was added to the purified plasmid DNA (total volume 200 μl). 200 μl of phenol-chloroform-isoamyl alcohol (Fisher) was added, and the solution was vortexed for 20 s, then centrifuged for 5 min at maximum speed. The upper layer was transferred to a new tube. 200 μl of chloroform (Fisher) was added, and the solution was vortexed for 20 s, then centrifuged for 5 min at maximum speed. The upper layer was transferred to a new tube. To precipitate the DNA, 20 μl of 3M NaOAc (pH 5.2) and 600 μl of 95% ethanol was added to the tube, which was then incubated at -20 °C for 15 minutes. The solution was centrifuged for 20 min at -4 °C to pellet DNA. The DNA pellet was washed in 70% ethanol/DEPC-treated water and dried. DNA was resuspended in 10 μl of DEPC-treated water.

All mRNAs were transcribed from linearized, purified plasmid DNA templates using T7 or SP6 mMessage mMachine kits (Ambion) according to manufacturer's specifications. Briefly, 2 μg of template DNA was added to 10 μl of 2X NTP/CAP, 2 μl 10X Reaction Buffer,

2 μl of Enzyme Mix, and Nuclease-free water (total volume 20 μl). The reaction was incubated 2 h at 37 °C. 1 μl of TURBO DNase (Life Technologies) was added to degrade template DNA, and the solution was incubated 15 min at 37 °C.

mRNAs were purified using Amicon Ultra 50K centrifugal filters (Millipore) or Microcon YM-50 centrifugal filters (Millipore) according to manufacturer's specifications: 480 μl DEPC-treated water was added to the mRNA-containing solution. The solution was placed into a column in a collection tube, and centrifuged 15 min at 3,000 rpm. The flowthrough was discarded. 400 μl of DEPC-treated water was added to the column. The column was centrifuged 16 min at 3,000 rpm, and the flowthrough was discarded. The column was inverted into a new collection tube and centrifuged 3 min at 3,000 rpm. DEPC-treated water was added to the flowthrough (total volume 500 μl), which was placed in a new column in a new collection tube. The column was centrifuged 16 min at 3,000 rpm. The column was inverted into a new collection tube, and centrifuged 3 min at 3,000 rpm. mRNA concentration was determined via spectrophotometry, and mRNAs were diluted in DEPC-treated water.

2.11 RNA riboprobe synthesis

Antisense fluorescein or digoxigenin (DIG)-labeled riboprobes were transcribed either from purified, linearized plasmid DNA containing a gene-specific insert (Table 2.5), or from a gene-specific PCR product with an integrated T3 or T7 RNA polymerase site (Thisse and Thisse, 2008). Primers used to generate riboprobe PCR products are listed in Table 2.6.

200-400 ng of linearized, purified plasmid DNA or PCR product (with integrated T3 or T7 RNA polymerase site) was incubated with 2 μl of 10X transcription buffer (Roche), 2 μl of DIG or fluorescein RNA labeling mix (Roche), 1 μl RNA polymerase (T7, T3 or SP6; Roche), 1 μl RNaseOUT (Life Technologies), and DEPC-treated water (20 μl total volume) for 1 hour at 37 °C. Following the addition of 1 μl RNA polymerase, the reaction was incubated for 1 h at 37°C. 1 μl of TURBO DNase (Life Technologies) was added, and the reaction was incubated for 5 min at 37 °C. 2 μl of 0.2M EDTA, pH 8.0 in DEPC-treated water was then added to stop the reaction. Probe was purified using SigmaSpin post-reaction clean-up

columns (Sigma-Aldrich) according to manufacturer's specifications: The column was placed in a collection tube, and centrifuged at 2,500 rpm for two minutes. The base of the column was removed, and the column was centrifuged for another two minutes at 2,500 rpm. The probe synthesis reaction was placed in the column, which was placed in a new collection tube. This was centrifuged for four minutes at 2,500 rpm. 0.5 µl of RNase OUT (Life Technologies) was added to the purified probe to inhibit degradation by RNAses, and probe was stored at -80 °C. Alternatively, a working stock of probe diluted in pre-hybridization solution was stored at -20 °C.

2.12 mRNA *in situ* hybridization

Examination of gene expression by whole-mount *in situ* hybridization was performed essentially as previously described (Prince et al., 1998), except probes were not hydrolyzed. All washes and incubations were performed with gentle agitation on a rotating platform (RT or 4 °C), or in a water bath.

Fixed embryos were washed 4 times, 5 min each in PBS + 0.1% Tween-20 (PBST) at RT. Embryos were permeabilized in 10 µg/ml proteinase K for 10 s (10-12 hpf embryos), 30 s (14-16 hpf embryos), 3 min (24-30 hpf embryos), 30 min (48 hpf embryos), or 1 h (3 dpf embryos) at RT. Embryos were refixed in 4% PFA/PBS for 20 min at RT, and rewashed 4 times 5 min each in PBST at RT.

Embryos were incubated in hybridization solution (50% formamide + 5X sodium saline citrate [SSC] + 50 µg/ml heparin + 0.1% Tween-20 + 0.092 M citric acid) with 500 µg/ml tRNA, for 1-4 h at 65 °C. Embryos were then incubated in hybridization solution with or without tRNA, containing fluorescein and/or or DIG-labeled riboprobe(s) overnight at 65 °C. The following washes were then performed at 65 °C: 5 min in 66% hybridization solution, 33% 2X SSC. 5 min in 33% hybridization solution, 66% 2X SSC. 5 min in 2X SSC. 20 min in 0.2X SSC + 0.1% Tween-20. 2 times 20 min in 0.1X SSC + 0.1% Tween-20. The following washes were then performed at RT: 5 min in 66% 0.2X SSC, 33% PBST. 5 min in 33% 0.2X SSC, 66% PBST. 5 min in PBST. Embryos were then blocked in PBST containing 2% sheep serum and 2 mg/ml bovine serum albumin (BSA) for 1-4 h at RT. Embryos were incubated in a 1:5000 dilution of anti-DIG, alkaline phosphate-conjugated F(ab') fragments (Roche) in

blocking solution 2 h at RT, or overnight at 4 °C. Embryos were then washed 6 times 15 min each in PBST at RT, and stored at 4 °C overnight, or immediately coloured.

Embryos were washed 4 times 5 min each in colouration buffer (100 mM Tris-HCl, pH 9.5 + 50 mM MgCl2 + 100 mM NaCl + 0.1% Tween-20). Embryos were incubated in 45 µl 4-nitro blue tetrazolium chloride solution (NBT; Roche), and 35 µl 5-bromo-4-chloro-3-indolyl-phosphate, toluidine-salt solution (BCIP; Roche) diluted in 10 ml of colouration buffer, at RT or 4 °C until formation of visible coloured precipitate. The colouration reaction was stopped by washing embryos 2 times 5 min, then 2 times 15 min at RT in PBST, pH 5.5 or 100% MeOH + 0.1% Tween-20. Embryos were stored in PBST or 100% MeOH + 0.1% Tween-20, respectively at 4 °C.

2.13 Two-colour mRNA *in situ* hybridizations

The initial colouration reaction was stopped by washing embryos 4 times 5 min in water at RT. Embryos were then incubated in 0.1M glycine, pH 2.2 for 10 min at RT. Embryos were washed 4 times 5 min in PBST, and were re-blocked for 1 h at RT. Embryos were incubated in a 1:10,000 dilution of anti-fluorescein, alkaline phosphate-conjugated F(ab') fragments (Roche) in blocking solution 2 h at RT, or overnight at 4 °C. Embryos were washed 5 times, 15 min each in PBST at RT. Embryos were washed 4 times 5 min in colouration buffer. Embryos were incubated in 17.5 µl 2-(4-iodophenyl)-5-(4-nitrophenyl)-3-phenyltetrazolium chloride solution (INT; Roche), and 17.5 µl BCIP (Roche) diluted in 5 mL of colouration buffer at RT or 4 °C until formation of visible coloured precipitate. Washing embryos 2 times 5 min, then 2 times 15 min in water at RT stopped the colouration reaction. Embryos were then stored 4% PFA/PBS at 4 °C.

2.14 Immunohistochemistry

All incubations and washes were performed with gentle agitation on a nutator. Previously fixed 16 hpf embryos were permeablized for 5 min in 10 µg/ml Proteinase K/PBST, refixed in 4% PFA/PBS for 20 min, and washed 4 times 5 min in PBST. Embryos were then incubated in blocking solution (PBS + 0.1% Triton X-100 + 1% BSA + 5% goat serum) for 1 h. Embryos were incubated in a 1:5 dilution of P2A6 hybridoma

supernatant/blocking solution overnight at 4 °C. Embryos were washed 5 times 15 min in PBST + 1% DMSO + 0.1% Triton X-100 (PBSDTT), reblocked, and incubated overnight, in the dark at 4 °C in a 1:500 dilution of Alexa Fluor 488-conjugated goat anti-mouse secondary antibody (Molecular Probes). Embryos were then washed 4 times 15 min each in PBSDTT. Embryonic nuclei were stained in 10 μg/ml of Hoechst 33258 (Molecular Probes) in PBSDTT for 15 min. Embryos were then washed 4 times 5 min in PBSDTT and were stored at 4 °C in the dark.

2.15 Mounting and photography

Prior to mounting, embryos were manually deyolked, and cleared in 30%, then 50%, then 70% glycerol. Mounted *in situ* hybridizations were photographed using a Zeiss AxioImager Z1 compound microscope with an Axiocam HR digital camera. Mounted embryos stained by immunohistochemistry were photographed using a Zeiss LSM510 confocal microscope. Whole embryos were photographed with an Olympus stereoscope with a QImaging micropublisher camera, or a Leica stereoscope with a Leica DFC420C camera. Images were assembled in ImageJ, and figures were assembled in Photoshop (Adobe).

2.16 Cell lysate generation

All stages of the protocol, except centrifugation were performed on ice. Dechorionated zebrafish embryos were suspended in 1 ml deyolking buffer containing 55 mM NaCl + 1.8 mM KCl + 1.25 mM NaHCO3 + protease inhibitor (Pefabloc and Leupeptin; Sigma, or Complete, Mini, EDTA-free; Roche). Gentle pipetting, followed by vortexing at 1100 rpm for 30 s, was used to disrupt embryo yolk and cells. Cells were pelleted by 1 min of centrifugation at 3000 rpm. The supernatant was discarded. The cells were resuspended in 1 ml wash buffer (110 mM NaCl + 3.5 mM KCl +10 mM Tris, pH 8.5 + 2.7 mM CaCl2 + protease inhibitor. Cells were pelleted by 1 min of centrifugation at 3000 rpm. The supernatant was discarded. Cells were then resuspended in 1X NuPAGE LDS Sample Buffer (Life Technologies) + 2.5% beta mercaptoethanol, and the solution was vortexed to lyse cells. Cell lysates were stored at -20 °C or used immediately for Western analysis.

2.17 Co-immunoprecipitation analysis

Constructs were transcribed and translated using the TNT T7 or SP6 Coupled Rabbit Reticulocyte Lysate System (Promega) from 1 μg of plasmid DNA according to manufacturer's specifications. Briefly, all components were thawed on ice. 1 μg of plasmid DNA was mixed with 25 μl of TNT Rabbit Reticulocyte Lysate, 2 μl of TNT Reaction buffer, 1 μl of TNT RNA Polymerase, 1 μl of 1 mM Amino Acid Mixture Minus Leucine, 1 μl of 1 mM Amino Acid Mixture Minus Methionine, 1 μl of RNase OUT (Life Technologies), and water (total volume 50 μl). The reaction was incubated for 90 minutes with gentle agitation in a 30 °C water bath.

25 μl anti-Flag agarose was prepared in the following manner: 300 μl of binding buffer containing 50 mM Tris-HCl pH 7.4 + 75 mM NaCl + 1mM EDTA + 1% Triton X-100 + 1% BSA + 0.5 mM DTT + protease inhibitor (Pefabloc; Sigma), along with 1 μg of double stranded and single-stranded (forward) DNA oligonucleotide containing a canonical Cdx/Pbx-binding domain (5'-CTGCGATGATTTATGACCGC-3') was added to 150 μl of anti-Flag agarose (Sigma). The agarose was pelleted by 30 s of centrifugation at 5000 x g at 4 °C and the supernatant was discarded. The addition of binding buffer/centrifugation was repeated twice more.

20 μl each of *in vitro* translated crude protein lysate and/or rabbit reticulocyte lysate (control) was added to 40 μl of prepared anti-Flag agarose/binding buffer and incubated overnight at 4 °C with gentle agitation on a rotating platform. The anti-Flag agarose was then washed 7-10 times in 300 μl of binding buffer without BSA and DTT/pelleted by centrifugation 5000 x g at 4 °C. 20 μl of 1X NuPAGE LDS Sample Buffer (Life Technologies) + 2.5% beta mercaptoethanol was added to the mixture. The sample was then boiled and analyzed by Western analysis.

2.18 Western analysis

Boiled zebrafish cell lysates (2.16), or *in vitro* translated crude protein lysates (2.17) in 1X NuPAGE LDS Sample Buffer (Life Technologies) + 2.5% beta mercaptoethanol were run out on NuPAGE Novex Bis-Tris gels using the XCell Sure Lock Mini-Cell system

(Invitrogen) according to manufacturer's specifications. Proteins were transferred to PVDF membrane using a TE 77 ECL Semi-dry transfer apparatus (Amersham), or the XCell Blot Module wet transfer apparatus (Amersham). Membranes were blocked in 5% skim milk in Tris-buffered saline + 0.1% Tween-20 (TBST) (anti-Flag antibody), 1% ovalbumin, 1% sheep serum, 1% BSA (anti-Myc antibody), or 5% skim milk with 2% BSA and 2% goat serum in TBST (anti-HA antibody). Membranes were incubated in anti-Flag antibody (Sigma; 1:2,000 dilution), anti-Myc antibody (Sigma, 1:7,500 dilution), or anti-HA antibody (GenScript, Sigma or Covance; 1:1,000 or 1:2,000 dilution) in their respective blocking solutions. Following TBST washes; both membranes were incubated in 1:5,000 or 1:7,500 secondary antibody (goat, anti-mouse HRP-linked F(ab') fragments; Amersham) in TBST. Following TBST washes, an ECL reaction was performed using PicoSignal (Pierce).

2.19 Zinc finger nuclease construction

Algorithm-based (http://pgfe.umassmed.edu/ZFPsearch.html) detection of suitable zinc finger nuclease (ZFN) target sequences was performed as previously described (Meng et al., 2008), with preference given to purine-rich sequences, guanine-rich sequences, and sequences containing a six-nucleotide spacer region between ZFN recognition sites. Chosen ZFN target sequences for bacterial one-hybrid selection are listed in Table 2.7.

To identify and construct suitable ZFN arrays for *prp2*, *hmx4*, and *crx*, zinc finger library construction and two-stage omega-based bacterial one-hybrid selection of zinc finger arrays was performed as previously described (Meng et al., 2008), except for *hmx4* ZFNs, in which the bacterial one-hybrid selection target-site plasmids were modified so that the fourth base-pair on the opposite strand always corresponded to the *hmx4* zinc finger domain's recognition site (as opposed to the Zif268 scaffold zinc finger domain's recognition site) (Table 2.8). This was done to increase the context-dependent selection of individual zinc finger domains that bind to the *hmx4* target-site. Furthermore, the degeneracy of *hmx4* library primers was manually altered to encode an increased number of zinc finger protein motifs, which were previously shown to recognize triplets present within the *hmx4* target-site (Table 2.9) (Maeder et al., 2008). Refer to Appendix A for a comprehensive protocol detailing

bacterial one-hybrid ZFN array selection. The seven-amino acid target-site recognition motifs of each ZFN chosen for analyses *in vivo* are listed in Table 2.10.

All selected zinc finger arrays were cloned into the previously described pCS2-HA-GAAZFP-FokI-RR (5' arrays) or pCS2-Flag-TTGZFP-FokI-DD (3' arrays) ZFN expression vectors (Addgene)(Meng et al., 2008). The DD and RR cleavage domain mutations favor heterodimeric cleavage activity, and therefore reduce ZFN toxicity (Miller et al., 2007; Szczepek et al., 2007).

ZFNs containing the *Sharkey* FokI cleavage domain have previously been shown to exhibit greater *in vitro* activity than those containing the wild type FokI cleavage domain (Guo et al., 2010). *Sharkey* variants of the aforementioned heterodimeric ZFN expression vectors (pCS2-Flag-TTGZFP-*Sharkey*FokI-DD; pCS2-HA-GAAZFP-*Sharkey*FokI-RR) were synthesized through site-directed mutagenesis of the original expression vectors using primers listed in Table 2.3. All constructs were confirmed by Sanger sequencing. ZFN mRNA expression constructs are listed in Table 2.11.

2.20 Transcription activator-like effector nuclease construction

All transcription activator-like (TAL) effector arrays were designed essentially as previously described (Cermak et al., 2011), using the TAL Effector Nucleotide Targeter 2.0 (https://tale-nt.cac.cornell.edu) to select the TAL effector nuclease (TALEN) target-sites (Doyle et al., 2012). Preference was given to sequences occurring on or near the translation start site of targeted genes. Chosen TALEN target sequences are listed in Table 2.12.

Assembly of custom TAL effector arrays was performed essentially as previously described (Cermak et al., 2011). All TAL Effector arrays were cloned into the previously described pCS2TAL3-RR or pCS2TAL3-DD TALEN expression vectors (Addgene) (Dahlem et al., 2012). *Sharkey* variants of the aforementioned heterodimeric ZFN expression vectors (pCS2TAL3-*Sharkey*FokI-RR; pCS2TAL3-*Sharkey*FokI-DD) were synthesized through site-directed mutagenesis of the original expression vectors using the same mutagenic primers used to make the heterodimeric *Sharkey* ZFN expression constructs. Constructs were confirmed by Sanger sequencing. TALEN mRNA expression constructs are listed in Table 2.13.

2.21 Targeted endonuclease protein synthesis and *in vitro* DNA cleavage assay

The *in vitro* DNA cleavage assay was adapted from the *in vitro* transcription-translation assay for rapid screening of ZFNs for sequence-specific cleavage activity (Mani et al., 2005). ZFN or TALEN constructs were transcribed and translated using the TNT SP6 Coupled Rabbit Reticulocyte Lysate System (Promega) from 100-500 ng of pCS2-FokI ZFN (RR or DD; control or *Sharkey*) or pCS2TAL3 TALEN (RR or DD; control or *Sharkey*) plasmid DNA according to manufacturer's specifications (2.17). Following synthesis, 0.1-2 μl of 5' ZFN or TALEN (RR; control or *Sharkey*) and 3' ZFN or TALEN (DD; control or *Sharkey*) protein lysates were combined with 500 ng of target-site-containing plasmid DNA (pCR4-TOPO for *hmx4* and *wwtr1* constructs; pCR2.1-TOPO for *prp2*), 2 μl 10X Restriction Buffer 4 (NEB) or 10X FastDigest Buffer (Fermentas), and 0.5 μl of NcoI plasmid-linearizing restriction enzyme (20 μl total volume). This reaction was incubated at 37°C for 2 h. Digested plasmid DNA was purified using a gel extraction kit (QIAquick Gel Extraction Kit, QIAGEN; GeneJET Gel Extraction Kit, Fermentas), and digested DNA fragments were analyzed by agarose gel electrophoresis. Anecdotal evidence suggests that the plasmid purification step improves the resolution and separation of DNA fragments.

2.22 Zebrafish mutagenesis

The following amounts of 5' and 3' control or *Sharkey* ZFN mRNAs were injected into single-cell zebrafish embryos: *prp2* ZFN mRNA, 20 pg; *hmx4* ZFN mRNA, 200 pg; and *crx* ZFN mRNA, 100 pg. The dosage of each injected ZFN mRNA was titrated and chosen to minimize embryonic toxicity and lethality (producing 65%-75% 'normal' embryos for control ZFN mRNAs). For each category of injected embryos, genomic DNA was isolated from pooled 24 hpf embryos, essentially as previously described (Meeker et al., 2007). PCR fragments containing the ZFN recognition site were amplified and cloned into pCR4-TOPO (*hmx4, crx*) or pCR2.1-TOPO (*prp2*). The cloned product was used to transform TOP10 cells (Invitrogen). Following transformation, 96 independent colonies from each sample were picked, and from these the cloned PCR product was amplified using *Taq* DNA polymerase. The amplified clones were sequenced using M13R primer to determine the frequency and

type of mutations present at the ZFN target-site. Significant differences in mutation frequencies among embryos injected with *Sharkey* versus control ZFNs were determined using two-tailed Fisher's exact tests.

The following amounts of 5' and 3' control or *Sharkey* TALEN mRNAs were injected into single-cell zebrafish embryos: *wwtr1* TALEN mRNA, 200 pg; *hoxb1b* TALEN mRNA, 400 pg. For each category of injected embryos, genomic DNA was isolated from pooled 24 hpf embryos, essentially as previously described (Meeker et al., 2007). PCR fragments containing the ZFN recognition site were amplified and cloned into pCR4-TOPO. The cloned product was used to transform TOP10 cells (Invitrogen). Following transformation, 90 independent colonies from each sample were picked and diluted in 25 μl of water. High-resolution melt curve analysis (HRMA) was performed on each sample to detect TALEN-induced mutations. Each 10 μl HRMA reaction contained: 2 μl of diluted plasmid DNA, 5 μl of MeltDoctor HRM Master Mix (Applied Biosystems), 0.6 μl each of 5 μM forward and reverse primer, and 1.8 μl of water. Each reaction was run using the 7500 Fast Real-Time PCR System (Applied Biosystems), with the following PCR cycle conditions: intial denaturation 95 °C, 10 min; 40 cycles of amplification (95°C, 15 s; 60°C, 20 s); disassociation curve at 95°C, 15 s; 60°C, 1 min; 95°C, 15 s; 60°C, 15 s. Melting profiles were analyzed using HRM v.2.0 software (Life Technologies) Representatives of detected variants were sequenced using M13R or M13F primer to determine the frequency and type of mutations present at the TALEN target-site. Significant differences in mutation frequencies among embryos injected with *Sharkey* versus control TALENs were determined using two-tailed Fisher's exact tests.

2.23 Analyses of targeted endonuclease toxicity

The following amounts of 5' and 3' control or *Sharkey* ZFN mRNAs were injected into single-cell zebrafish embryos: *prp2* ZFN mRNA, 20 pg; *hmx4* ZFN mRNA, 200 pg; and *crx* ZFN mRNA, 100 pg. 200 pg each of 5' and 3' control or *Sharkey wwtr1* TALEN mRNAs were injected into single-cell zebrafish embryos. At 24 hpf, embryos were categorized according to morphological phenotype (normal, 'monster', which indicates any morphological phenotype that differs from wild type, or dead) and counted. The morphological phenotypes of control, uninjected embryos were likewise assessed. Each set of injections/assessment was conducted

in triplicate. Significant differences in morphology and lethality among treatments were determined using two-tailed Fisher's exact tests with Bonferroni correction on pooled datasets.

2.24 Tables

Table 2.1: Translation-blocking morpholino sequence and injected dosage.

Gene	Morpholino sequence (5'-3')	Dosage per embryo (ng)
aldh1a2	GCAGTTCAACTTCACTGGAGGTCAT	5
cdx1a	CAGCAGATAGCTCACGGACATTTTC	5
gata1	CTGCAAGTGTAGTATTGAAGATGTC	5
hmx1	GCATGTCTTGAGCAAATATACCAGT	5
hmx4	CGCGTCCTCCTTGCTCATATTCTCC	1
hmx4	GGGTCCGTGTCTGTGCCTCTTTTTC	1
meis1	GTATATCTTCGTACCTCTGCGCCAT	4
pbx2	CCGTTGCCTGTGATGGGCTGCTGCG	1
pbx2	GCTGCAACATCCTGAGCACTACATT	2
pbx4	AATACTTTTGAGCCGAATCTCTCCG	3
pbx4	CGCCGCAAACCAATGAAAGCGTGTT	3

Table 2.2: Real-time quantitative PCR primer sequences.

Gene	Forward Primer (5'-3')	Reverse Primer (5'-3')
aldh1a2	AACCACTGAACACGGACCTC	ATGAGCTCCAGCACACGTC
efla	CCTTCGTCCCAATTTCAGG	CCTTGAACCAGCCCATGT
gata1	GAGACTGACCTACTGCCATCG	TCCCAGAATTGACTGAGATGAG

Table 2.3: Site-directed mutagenesis primers.

Gene	Mutation	Forward Primer (5'-3')	Reverse Primer (5'-3')
cdx4^{W135S}*	W135S	GGCGTAATTCCTATCAATCGAT GAGCAAAACCGTCCAGTCGTC	GACGACTGGACGGTTTTGCTCA TCGATTGATAGGAATTACGCC
SharkeyFokI-DD	S418P	AAATCCCACTCAGGATAGAATT CTTG	ATTTCTGGCAATTTCAATTAATT CAAT
SharkeyFokI-RR	K441E	GAAAGTTTATGGATATAGAGGTG AACATTTGGGTGGATCAAGGAA	TTCCTTGATCCACCCAAATGTTC ACCTCTATATCCATAAACTTTC

*Indicates design by author.

Altered nucleotide sequence is underlined.

Table 2.4: Plasmids used for mRNA and/or protein synthesis.

Gene	Vector	Linearize	Promoter	N-terminal Tag
*cdx4**	Flag-T7TS*	BamHI	T7	Flag
cdx4^{W135S}*	Flag-T7TS*	BamHI	T7	Flag
*gata1**	pCS2+MT	XbaI	SP6	Myc
*hmx4**	pCS3+MT	NotI	SP6	Myc
hmx4^{ua1003}*	pCS3+MT	NotI	SP6	Myc
hmx4^{ua1004}*	pCS3+MT	NotI	SP6	Myc
*hoxb7a**	Flag-T7TS*	BamHI	T7	Flag
meis1	pCS3+MT	NotI	SP6	Myc
pbx4	pCS2+MT	NotI	SP6	Myc

*Indicates construction by author.

Table 2.5: Plasmids used for RNA riboprobe synthesis.

Gene	Vector	Antibiotic	Linearize	Promoter
aldh1a2	pSport	Carbenicillin	EcoRI	SP6
*cdx1**	pCR4-TOPO	Carbenicillin	NotI	T3
*cdx4**	pCR4-TOPO	Carbenicillin	NotI	T3
cyp26a1	pBS KS+	Carbenicillin	Sal1	T7
*efnb2a**	pCR4-TOPO	Carbenicillin	NotI	T3
gata1	unknown	Carbenicillin	XbaI	T7
gata2	unknown	Carbenicillin	XbaI	T7
*hbae3**	pCR4-TOPO	Carbenicillin	PmeI	T7
hmx1	pCR4-TOPO	Carbenicillin	NotI	T3
hmx4	pSport	Carbenicillin	EcoRI	SP6
*hoxa9a**	pCR4-TOPO	Carbenicillin	NotI	T3
*hoxb6b**	pCR4-TOPO	Carbenicillin	NotI	T3
*hoxb7a**	pCR4-TOPO	Carbenicillin	NotI	T3
*ikaros**	pCR4-TOPO	Carbenicillin	NotI	T3
*kdrl**	pCR4-TOPO	Carbenicillin	NotI	T3
*lcp1**	pCR4-TOPO	Carbenicillin	NotI	T3
*lmo2**	pCR4-TOPO	Carbenicillin	PmeI	T7
meis1	pSport	Carbenicillin	EcoRI	SP6
pax2a	unknown	Carbenicillin	BamHI	T7
*pu.1**	pCR4-TOPO	Carbenicillin	NotI	T3
*rag1**	pCR4-TOPO	Carbenicillin	NotI	T3
*runx1**	pCR4-TOPO	Carbenicillin	NotI	T3
*scl**	pCR4-TOPO	Carbenicillin	NotI	T3

*Indicates construction by author

Table 2.6: Primer sequences used for PCR-based RNA riboprobe synthesis.

Gene	Forward Primer (5'-3')	Reverse Primer (5'-3')[1]	Promoter	Size (bp)	T(m)
*cmyb**	GAAGAAGACCAACG GGTGATTGAG	CAGTGTGGATTTGA ATGGAGTGGG	T3	1020	57.8
*dlc**	ATCTGGAGCACCTC AAACACCAGTGG	AGTGAATGTTGACA GGATGGCCGCTG	T3	888	66.7
*dld**	GCAGAGGAGCCAGC AAATCGATAGCC	TCTTCCTCTCGCGA TCCAAGGATCCG	T3	832	67.6
*foxn1**	CCTGGCTTTGAGGA ACAGTAAAAC	AAGAGGAGTCTTTC TCATAGCAGAGG	T3	1023	55.0
*her6**	TACACCTGATAAAC CCAAAACGGC	ATCACAACGTGGAA AAGATACCGC	T3	1007	61.6
*her9**	TCCGCATCTAATCCT AAGAGCCCG	TGCCCAACAGAAGG TCAACAAAGTC	T3	1074	63.9
*lyz**	ATGAGGCTGGCAGT GGTGTTTTTG	AATCAGGCTCGGAG GCTTTGTTTG	T3	458	61.0
*notch1a**	ACACGGCTAAGAAA ACACGCAAAC	CAGACAAGTTGGAA TGTGGAGATGAG	T3	837	61.8
*notch1b**	CGTAAGCCCAGCAC TAAAGGCATCGG	ATTTGTGACTGCAT GCTGGTGGGAGG	T3	968	67.5
*notch2**	TCACTGACAGCCCA AGTTCAGCCAAG	TCGCCACTCTGGTT AACCGATGCATG	T3	851	67.1
*notch3**	AGTCCAGTAAGCGT GCCGTTTGACTG	GGATACGGCAGATG GTCTTCTTGACGC	T3	897	67.3
*wnt16**	ATAACAGTGAGGCT GGGAGACAGG	GGGAAAAAGTGAA GAGGTGAGTTG	T3	885	55.1

*Indicates construction by author.

[1]T3 promoter sequence (5'-AATTAACCCTCACTAAAGGGA-3') added to the end of each reverse primer.

Table 2.7: ZFN target sequences.

Gene	Sequence (5'-3')[1]
crx	AGCCCCATTATGCTGTGAACGGGTTA
hmx4	TAAACTCAACAGAGAGGGGGATGCGA
prp2	CCACCTCCCTACCCTGGTGCTGGAGG

[1]ZFN recognition sites are underlined.

Table 2.8: Algorithm-generated and manually altered *hmx4* bacterial-one-hybrid array selection target-site sequences.

Sequence	Algorithm-Generated			Altered[1]		
***hmx4* 5' target-site**	**GTT**	**GAG**	**TTTa**	**GTT**	**GAG**	**TTTa**
5'-1 target-site	GCG	TGG	TTT	GCG	TGG	TTTa
5'-2 target-site	GCA	GAG	AGG	GCA	GAG	TGG
5'-3 target-site	GTT	TGG	GCG	GTT	GGG	GCG
***hmx4* 3' target-site**	**GGG**	**GAT**	**GCG**	**GGG**	**GAT**	**GCGa**
3'-1 target-site	GCG	TGG	GCGa	GCG	TGG	GCGa
3'-2 target-site	GCA	GAT	AGG	GCA	GAT	GGG
3'-3 target-site	GGG	TGG	GCG	GGG	GGG	GCG

Target-sites were modified so that the fourth base on the opposite strand corresponds to the *hmx4* zinc finger domain's recognition site.

[1]Altered bases are underlined.

Table 2.9: Algorithm-generated and manually altered *hmx4* zinc finger library bacterial-one-hybrid array selection sequences.

	Algorithm-Generated ZF Motif							Altered ZF Motif						
Position	-1	1	2	3	4	5	6	-1	1	2	3	4	5	6
ZF 5'-1	**NNS** 20	**VNT** 12	**NNW** 18	**KST** S A C G	**CTG** L	**ACC** T	**AMG** T K	**ABS** I M T S R	**VNT** 12	**MHG** L P Q M T K	**RBC** I T S V A G	**CTG** L	**VNT** 12	**RKA** I R V G
ZF 5'-2	**CGT** R	**TCT** S	**GAT** D	**AAC** N	**CTG** L	**ACC** T	**CGT** R	**CGT** R	**VNS** 16	**GAC** D	**AAC** N	**CTG** L	**VNS** 16	**CGT** R
ZF 5'-3	**NNS** 20	**VNT** 12	**NNW** 18	**KST** S A C G	**CTG** L	**ACC** T	**CGT** R	**VWS** 10	**VNT** 12	**VNS** 16	**RBS** 8	**CTG** L	**ACC** T	**CGT** R
ZF 3'-1	**ARA** K R	**VNS** 16	**NNW** 18	**RVT** T N S A D G	**CTG** L	**ACC** T	**CGT** R	**ARA** K R	**MDC** L H R I N S	**SAC** H D	**RNS** 12	**CTG** L	**VHC** 9	**ARA** K R
ZF 3'-2	**NNS** 20	**VNT** 12	**NNW** 18	**AAC** N	**CTG** L	**ACC** T	**CGT** R	**VWA** L K V E	**VNS** 16	**SAS** H Q D E	**AAC** N	**CTG** L	**VNS** 16	**CGT** R
ZF 3'-3	**CGT** R	**TCT** S	**GAT** D	**CAC** H	**CTG** L	**ACC** T	**CGT** R	**CGT** R	**VNS** 16	**SAS** H Q D E	**MRS** H Q R N K S	**CTG** L	**SDC** L H R V D G	**SSC** P R A G

Shown are degenerate library primer sequences, and the corresponding possible seven amino-acid target-site recognition motifs that they encode. When more than six possible amino acids are encoded by a single degenerate codon, the number of possible amino acids are provided instead of the amino acid identity.

Table 2.10: Target-site recognition motifs of select bacterial one-hybrid derived zinc finger nuclease (ZFN) arrays.

prp2								
Triplet	**ZF**	**Recognition Motif**						
		-1	**1**	**2**	**3**	**4**	**5**	**6**
GTG	5'-1	R	S	D	A	L	T	R
GAG	5'-2	R	S	D	N	L	T	R
AGG	5'-3	R	S	D	H	L	P	Q
GAG	3'-1	R	S	D	N	L	T	R
CTG	3'-2	R	S	D	A	L	T	E
GTG	3'-3	R	M	D	G	L	T	R
crx								
Triplet	**ZF**	**Recognition Motif**						
		-1	**1**	**2**	**3**	**4**	**5**	**6**
GGC	5'-1	S	H	S	H	L	T	R
TGG	5'-2	R	S	D	H	L	T	K
TAA	5'-3	Q	K	S	N	L	T	K
GTT	3'-1	S	D	A	A	L	T	R
CGG	3'-2	R	S	D	H	L	S	D
GAA	3'-3	Q	L	G	N	L	T	R
hmx4								
Triplet	**ZF**	**Recognition Motif**						
		-1	**1**	**2**	**3**	**4**	**5**	**6**
TTT	5'-1	T	H	T	G	L	T	V
GAG	5'-2	R	G	D	N	L	R	R
GTT	5'-3	H	R	T	A	L	T	R
GCG	3'-1	R	H	D	T	L	L	R
GAT	3'-2	V	K	H	N	L	H	R
GGG	3'-3	R	S	D	K	L	L	G

Shown are seven amino-acid target-site recognition motifs for zinc fingers in the *prp2*, *crx*, and *hmx4* 5' and 3' ZFNs, as well as their corresponding target-site DNA triplets.

Table 2.11: Plasmids used for ZFN mRNA and/or protein synthesis.

Target Gene	Vector	Linearize	Promoter	N-terminal Tag
crx	pCS2-FLAG-Fok1-DD	NotI	SP6	Flag
crx	pCS2-FLAG-*Sharkey*Fok1-DD	NotI	SP6	Flag
crx	pCS2-HA-Fok1-RR	NotI	SP6	HA
crx	pCS2-HA-*Sharkey*Fok1-RR	NotI	SP6	HA
*hmx4**	pCS2-FLAG-Fok1-DD	NotI	SP6	Flag
*hmx4**	pCS2-FLAG-*Sharkey*Fok1-DD	NotI	SP6	Flag
*hmx4**	pCS2-HA-Fok1-RR	NotI	SP6	HA
*hmx4**	pCS2-HA-*Sharkey*Fok1-RR	NotI	SP6	HA
prp2	pCS2-FLAG-Fok1-DD	NotI	SP6	Flag
prp2	pCS2-FLAG-*Sharkey*Fok1-DD	NotI	SP6	Flag
prp2	pCS2-HA-Fok1-RR	NotI	SP6	HA
prp2	pCS2-HA-*Sharkey*Fok1-RR	NotI	SP6	HA

*Indicates construction by author.

Table 2.12: TALEN target sequences.

Gene	Sequence (5'-3')[1]
wwtr1	TGAGCGGTAATCCTCTCCAGCCGATACCGGGCCACCAGGTGATCCATGTCGCCA
hoxb1b	GGTTCTAACACTTATAGTTCGAAAGTTGGGTGTTTTCCTGTAGAGCAAGAATACTTGCC

[1]TALEN recognition sites are underlined.

Table 2.13: Plasmids used for TALEN mRNA and/or protein synthesis.

Target Gene	Vector	Linearize	Promoter	N-terminal Tag
hoxb1b	pCS2TAL3-DD	NotI	SP6	Flag
hoxb1b	pCS2TAL3-RR	NotI	SP6	HA
hoxb1b	pCS2TAL3-*Sharkey*FokI-DD	NotI	SP6	Flag
hoxb1b	pCS2TAL3-*Sharkey*FokI-RR	NotI	SP6	HA
wwtr1	pCS2TAL3-DD	NotI	SP6	Flag
wwtr1	pCS2TAL3-RR	NotI	SP6	HA
wwtr1	pCS2TAL3-*Sharkey*FokI-DD	NotI	SP6	Flag
wwtr1	pCS2TAL3-*Sharkey*FokI-RR	NotI	SP6	HA

2.25 References

Alexa, K., S.K. Choe, N. Hirsch, L. Etheridge, E. Laver, and C.G. Sagerstrom. 2009. Maternal and zygotic aldh1a2 activity is required for pancreas development in zebrafish. *PloS one*. 4:e8261.

Cermak, T., E.L. Doyle, M. Christian, L. Wang, Y. Zhang, C. Schmidt, J.A. Baller, N.V. Somia, A.J. Bogdanove, and D.F. Voytas. 2011. Efficient design and assembly of custom TALEN and other TAL effector-based constructs for DNA targeting. *Nucleic Acids Res*. 39:e82.

Dahlem, T.J., K. Hoshijima, M.J. Jurynec, D. Gunther, C.G. Starker, A.S. Locke, A.M. Weis, D.F. Voytas, and D.J. Grunwald. 2012. Simple methods for generating and detecting locus-specific mutations induced with TALENs in the zebrafish genome. *PLoS Genet*. 8:e1002861.

Davidson, A.J., and L.I. Zon. 2006. The caudal-related homeobox genes cdx1a and cdx4 act redundantly to regulate hox gene expression and the formation of putative hematopoietic stem cells during zebrafish embryogenesis. *Dev Biol*. 292:506-518.

Doyle, E.L., N.J. Booher, D.S. Standage, D.F. Voytas, V.P. Brendel, J.K. Vandyk, and A.J. Bogdanove. 2012. TAL Effector-Nucleotide Targeter (TALE-NT) 2.0: tools for TAL effector design and target prediction. *Nucleic Acids Res*. 40:W117-122.

Erickson, T., S. Scholpp, M. Brand, C.B. Moens, and A.J. Waskiewicz. 2007. Pbx proteins cooperate with Engrailed to pattern the midbrain-hindbrain and diencephalic-mesencephalic boundaries. *Dev Biol*. 301:504-517.

French, C.R., T. Erickson, D. Callander, K.M. Berry, R. Koss, D.W. Hagey, J. Stout, K. Wuennenberg-Stapleton, J. Ngai, C.B. Moens, and A.J. Waskiewicz. 2007. Pbx homeodomain proteins pattern both the zebrafish retina and tectum. *BMC Dev Biol*. 7:85.

Galloway, J.L., R.A. Wingert, C. Thisse, B. Thisse, and L.I. Zon. 2005. Loss of gata1 but not gata2 converts erythropoiesis to myelopoiesis in zebrafish embryos. *Dev Cell*. 8:109-116.

Gongal, P.A., L.D. March, V.L. Holly, L.M. Pillay, K.M. Berry-Wynne, H. Kagechika, and A.J. Waskiewicz. 2011. Hmx4 regulates Sonic hedgehog signaling through control of retinoic acid synthesis during forebrain patterning. *Dev Biol*. 355:55-64.

Guo, J., T. Gaj, and C.F. Barbas, 3rd. 2010. Directed evolution of an enhanced and highly efficient FokI cleavage domain for zinc finger nucleases. *Journal of molecular biology*. 400:96-107.

Hammerschmidt, M., F. Pelegri, M.C. Mullins, D.A. Kane, M. Brand, F.J. van Eeden, M. Furutani-Seiki, M. Granato, P. Haffter, C.P. Heisenberg, Y.J. Jiang, R.N. Kelsh, J. Odenthal, R.M. Warga, and C. Nusslein-Volhard. 1996. Mutations affecting morphogenesis during gastrulation and tail formation in the zebrafish, Danio rerio. *Development*. 123:143-151.

Kimmel, C.B., W.W. Ballard, S.R. Kimmel, B. Ullmann, and T.F. Schilling. 1995. Stages of embryonic development of the zebrafish. *Dev Dyn*. 203:253-310.

Lieschke, G.J., A.C. Oates, M.O. Crowhurst, A.C. Ward, and J.E. Layton. 2001. Morphologic and functional characterization of granulocytes and macrophages in embryonic and adult zebrafish. *Blood*. 98:3087-3096.

Livak, K.J., and T.D. Schmittgen. 2001. Analysis of relative gene expression data using real-time quantitative PCR and the 2(-Delta Delta C(T)) Method. *Methods*. 25:402-408.

Maeder, M.L., S. Thibodeau-Beganny, A. Osiak, D.A. Wright, R.M. Anthony, M. Eichtinger, T. Jiang, J.E. Foley, R.J. Winfrey, J.A. Townsend, E. Unger-Wallace, J.D. Sander, F. Muller-Lerch, F. Fu, J. Pearlberg, C. Gobel, J.P. Dassie, S.M. Pruett-Miller, M.H. Porteus, D.C. Sgroi, A.J. Iafrate, D. Dobbs, P.B. McCray, Jr., T. Cathomen, D.F. Voytas, and J.K. Joung. 2008. Rapid "open-source" engineering of customized zinc-finger nucleases for highly efficient gene modification. *Mol Cell*. 31:294-301.

Mani, M., K. Kandavelou, F.J. Dy, S. Durai, and S. Chandrasegaran. 2005. Design, engineering, and characterization of zinc finger nucleases. *Biochem Biophys Res Commun*. 335:447-457.

Maves, L., and C.B. Kimmel. 2005. Dynamic and sequential patterning of the zebrafish posterior hindbrain by retinoic acid. *Dev Biol*. 285:593-605.

Maves, L., A.J. Waskiewicz, B. Paul, Y. Cao, A. Tyler, C.B. Moens, and S.J. Tapscott. 2007. Pbx homeodomain proteins direct Myod activity to promote fast-muscle differentiation. *Development*. 134:3371-3382.

Meeker, N.D., S.A. Hutchinson, L. Ho, and N.S. Trede. 2007. Method for isolation of PCR-ready genomic DNA from zebrafish tissues. *BioTechniques*. 43:610, 612, 614.

Meng, X., M.B. Noyes, L.J. Zhu, N.D. Lawson, and S.A. Wolfe. 2008. Targeted gene inactivation in zebrafish using engineered zinc-finger nucleases. *Nat Biotechnol*. 26:695-701.

Miller, J.C., M.C. Holmes, J. Wang, D.Y. Guschin, Y.L. Lee, I. Rupniewski, C.M. Beausejour, A.J. Waite, N.S. Wang, K.A. Kim, P.D. Gregory, C.O. Pabo, and E.J. Rebar. 2007. An improved zinc-finger nuclease architecture for highly specific genome editing. *Nat Biotechnol*. 25:778-785.

Perz-Edwards, A., N.L. Hardison, and E. Linney. 2001. Retinoic acid-mediated gene expression in transgenic reporter zebrafish. *Dev Biol*. 229:89-101.

Popperl, H., H. Rikhof, H. Chang, P. Haffter, C.B. Kimmel, and C.B. Moens. 2000. lazarus is a novel pbx gene that globally mediates hox gene function in zebrafish. *Mol Cell*. 6:255-267.

Szczepek, M., V. Brondani, J. Buchel, L. Serrano, D.J. Segal, and T. Cathomen. 2007. Structure-based redesign of the dimerization interface reduces the toxicity of zinc-finger nucleases. *Nat Biotechnol*. 25:786-793.

Waskiewicz, A.J., H.A. Rikhof, and C.B. Moens. 2002. Eliminating zebrafish pbx proteins reveals a hindbrain ground state. *Dev Cell*. 3:723-733.

Westerfield, M. 2000. The zebrafish book. A guide for the library use of zebrafish (Danio rerio). University of Oregon Press, Eugene.

Chapter 3

The Hox cofactors Meis1 and Pbx act upstream of *gata1* to regulate primitive hematopoiesis

A version of this chapter has been published. Laura M. Pillay, A. Michael Forrester, Timothy Erickson, Jason N. Berman, and Andrew J. Waskiewicz (2010). The Hox cofactors Meis1 and Pbx act upstream of *gata1* to regulate primitive hematopoiesis. *Developmental Biology*, 340(2):306-317.

3.1 Introduction

During vertebrate development, the initial wave of hematopoiesis produces cells that help to shape the developing circulatory system (Baumann and Dragon, 2005; Hove et al., 2003) and oxygenate the early embryo (Orkin and Zon, 2008). The differentiation of primitive erythroid and myeloid cells occurs within a short transitory period, and is subject to precise molecular regulation by a hierarchical cascade of transcription factors. However, the upstream mechanisms by which these factors are regulated remain largely unclear. Previous research has shown that overexpressing posteriorly-expressed *hox* genes partially rescues erythropoietic gene expression in mutants with defects in primitive blood cell differentiation (Davidson et al., 2003; Davidson and Zon, 2006). These data support a model whereby Hox transcription factors serve to regulate primitive hematopoiesis.

Hox proteins require the TALE-class homeodomain transcription factors Pbx and Meis to activate transcription (Uhl et al., 2010). Embryos lacking Meis and Pbx display phenotypes that are consistent with a total lack of Hox function. For example, loss of both Pbx2 and Pbx4 in the zebrafish hindbrain generates an anteriorizing homeotic transformation of the neural tube, in which rhombomeres 2-6 take on the molecular and neuronal identity of rhombomere 1 (Popperl et al., 2000; Waskiewicz et al., 2002). A nearly identical phenotype results from the knockdown of *Hoxa1, Hoxb1,* and *Hoxd1* gene products in *Xenopus* (McNulty et al., 2005). Combined, these data illustrate the significant role that TALE-class proteins play as Hox cofactors *in vivo.*

The Hox cofactors Meis1 and Pbx have also been implicated in hematopoiesis; *Pbx1*-knockout and *Meis1*-deficient mice exhibit profound embryonic anemia (Azcoitia et al., 2005; DiMartino et al., 2001; Hisa et al., 2004). Notably, the precise molecular function of Meis1 and Pbx in regulating primitive hematopoiesis remains to be elucidated, and it is not yet known where Meis1, Pbx, and Hox participate in the hematopoietic transcription factor hierarchy. In this chapter, we analyze the function of Meis1 and Pbx by ablating these proteins and characterizing their molecular effects on known regulators of zebrafish primitive hematopoiesis.

3.1.1 Summary

We provide evidence that Meis and Pbx proteins are essential regulators of zebrafish primitive hematopoiesis. We demonstrate that inhibiting zebrafish Meis1 and Pbx protein synthesis cripples the production of circulating erythrocytes, and generates defects in erythropoietic gene expression. We also demonstrate that Meis-Pbx complexes are required for proper expression of *gata1*, but are not required to initiate *scl* expression. This phenotype is strikingly different from that of a Cdx1a/Cdx4-depleted zebrafish embryo, which completely lacks early *scl* expression. We propose a model placing Meis1 and Hox downstream of Cdx, and upstream of *gata1* in the molecular hierarchy of primitive hematopoiesis.

3.2 Results

3.2.1 Loss of Meis1 results in the production of erythropoietic defects

meis1 is expressed broadly in the posterior mesoderm and intermediate cell mass (ICM) during primitive hematopoiesis (Minehata et al., 2008; Waskiewicz et al., 2001). To assess the requirement for Meis1 in zebrafish primitive hematopoiesis, we generated embryos that lack Meis1 protein (hereafter called *meis1*-morphants). *meis1*-morphant embryos possess fewer visible circulating blood cells than their wild type counterparts at 48 hours post fertilization (hpf), and 67% (n = 181) of *meis1*-morphant embryos fail to produce any visible circulating blood cells by 48 hpf (Figure 3.1A, B; Table 3.1). Furthermore, *meis1*-morphant embryos also display a severe reduction in the number of differentiated erythrocytes, as visualized through o-dianisidine staining of 48 hpf embryos (Figure 3.1D, E).

In order to determine if Meis1 is required to initiate hematopoietic gene expression, we compared the expression of *scl*, *lmo2*, *gata1*, and *kdrl* in the posterior lateral-plate mesdoderm (PLM) of 16 hpf wild type and *meis1*-morphant embryos (Figure 3.2; Table 3.2). *meis1*-morphant embryos exhibit reduced expression of the erythroid precursor marker *gata1* (Figure 3.2A, A'), but maintain near normal expression of the endothelial marker *kdrl* (Figure 3.2B, B'), as shown through *in situ* hybridization. These data suggest that Meis1 regulates early erythroid-specific gene expression. *scl* and *lmo2* are expressed in a region of the PLM that gives rise to both blood and endothelial precursors (Dooley et al., 2005; Gering et al., 1998; Gering et al., 2003; Patterson et al., 2007). Although the overall level of *lmo2* and *scl* expression is near normal in 16 hpf *meis1*-morphant embryos, the lateral-most domain of expression is reduced or absent (Figure 3.2C-D'; arrowheads). In wild type embryos, this lateral domain of *scl* expression colocalizes with the pronephric mesoderm marker *pax2a* (Figure 3.3; arrowheads), suggesting that it gives rise to kidney progenitor cells.

We next examined *scl*, *lmo2*, and *gata1* expression at 24 hpf to determine if Meis1 is required to maintain hematopoietic gene expression. By 24 hpf, approximately one hour prior to the initiation of circulation, *meis1*-morphant embryos exhibit reduced hematopoietic gene expression in the ICM, as shown through *in situ* hybridization (Figure 3.2E-G'; Table

3.2). In comparison to wild type embryos, *meis1*-morphant embryos demonstrate decreased *gata1* (Figure 3.2E, E'), *scl* (Figure 3.2F, F'), and *lmo2* (Figure 3.2G, G') expression.

3.2.2 Pbx stabilizes Meis1 and is required for its nuclear localization

Meis1 forms stable heterodimeric complexes with the TALE-class homeodomain protein Pbx (Berthelsen et al., 1998b; Chang et al., 1997; Rieckhof et al., 1997). Of the zebrafish *pbx* genes, only *lazarus* (*lzr/pbx4*) and *pbx2* are expressed ubiquitously in the PLM and ICM during primitive hematopoiesis (Maves et al., 2007; Popperl et al., 2000; Vlachakis et al., 2001; Waskiewicz et al., 2002). To assess the requirement for Pbx in zebrafish primitive hematopoiesis, we generated embryos that are deficient for both Pbx2 and Pbx4 (hereafter referred to as Pbx-depleted) by injecting one-cell stage embryos from a heterozygous mutant *pbx4*$^{+/-}$ incross with *pbx2* and *pbx4* translation-blocking morpholinos. Like *meis1*-morphants, Pbx-depleted embryos possess fewer visible circulating blood cells than their wild type counterparts at 48 hpf, and 45% (n = 66) of Pbx-depleted embryos fail to produce any visible circulating blood cells by 48 hpf (Figure 3.1A, C; Table 3.1), and display a severe reduction in the number of differentiated erythrocytes, as visualized through o-dianisidine staining of 48 hpf embryos (Figure 3.1D, F). Furthermore, Pbx-depleted and *meis1*-morphant embryos exhibit nearly identical defects in primitive hematopoietic gene expression, as shown through *in situ* hybridization (Figure 3.4; Table 3.3).

Given the phenotypes that *meis1*-morphant and Pbx-depleted embryos share with regards to hematopoietic gene expression, we wanted to investigate further the relationship between these two heterodimeric partners. In zebrafish, overexpressing *pbx4* generates an increase in Meis1 protein levels (Waskiewicz et al., 2001). In a reciprocal fashion, overexpressing *meis1* generates an increase in Pbx4 protein levels (Waskiewicz et al., 2001). This bidirectional stabilization is dependent upon the N-terminal MH domain of Meis1, and the PBC domains of Pbx4 (Waskiewicz et al., 2001), the exact domains that mediate Pbx4-Meis1 heterodimer formation (Knoepfler et al., 1997). This stabilization is observed following the injection of mRNA constructs (Waskiewicz et al., 2001), suggesting that it occurs post-transcriptionally. Given this stabilization phenotype, it is plausible that Pbx-depleted and *meis1*-morphant embryos each possess reduced levels of Meis1 protein. To test this

hypothesis *in vivo* under conditions where neither protein is overexpressed, we examined Meis1 protein levels in 14 hpf wild type and Pbx-depleted zebrafish embryos through immunohistochemical staining with the P2A6 anti-Meis1 monoclonal antibody. At 14 hpf, this antibody stains nuclei in a tissue-specific pattern that is consistent with *meis1* mRNA expression (Figure 3.5A; Erickson et al., 2010). P2A6 antibody staining is nearly abolished in *meis1*-morphants (Figure 3.5B; Figure 3.6), and is rescued by *meis1*-overexpression (Figure 3.5). Combined, these data suggest that the P2A6 antibody specifically labels Meis1 protein. In the PLM of 14 hpf wild type embryos, anti-Meis1 antibody staining is punctate and colocalizes with Hoechst nuclear staining (Figure 3.6A-C), indicating that Meis1 is present primarily within the nucleus. Conversely, Pbx-depleted embryos exhibit extremely low levels of anti-Meis1 antibody staining in the PLM at 14 hpf (Figure 3.6G). In Pbx-depleted embryos, this low level of anti-Meis1 antibody staining does not colocalize with Hoechst nuclear staining (Figure 3.6G-I), indicating that Meis1 is predominantly excluded from the nucleus. As Pbx-depletion and *meis1*-morpholino injection does not fully eliminate anti-Meis1 antibody staining, we next sought to combine these manipulations in order to generate a more complete loss of Meis1 protein. As predicted, Pbx-depleted; *meis1*-morphant embryos (Figure 3.6J) display less anti-Meis1 antibody staining than *meis1*-morphant (Figure 3.6D) or Pbx-depleted (Figure 3.6G) embryos. Combined, these data suggest that Meis1 requires Pbx for its nuclear localization and stabilization *in vivo*.

3.2.3 Effects of combined Meis1 and Pbx knockdown

Given that the simultaneous depletion of Pbx and Meis1 generates a more profound effect on Meis1 protein levels than through removal of either protein alone, we next sought to investigate erythropoietic gene expression in Pbx-depleted; *meis1*-morphant embryos. To do this, we examined the expression of *gata1* and *hbae3* in the PLM of 16 hpf embryos lacking both Pbx and Meis1. In comparison to wild type embryos, embryos partially depleted of Pbx or Meis1 (injected with a half-dose of *pbx2/4* MO or *meis1* MO respectively) exhibit subtle decreases in *gata1* and *hbae3* erythroid gene expression at 16 hpf, as shown through *in situ* hybridization (Figure 3.7A-C, E-G). Embryos partially depleted of both Pbx and Meis1 exhibit a severe decrease in *gata1* expression (Figure 3.7D) and nearly abolished *hbae3*

expression (Figure 3.7H), defects that are more severe than through knockdown of either protein alone.

To measure quantitatively the observed changes in *gata1* expression, we performed real-time quantitative PCR on 16 hpf wild type embryos, *lzr/pbx4*$^{+/-}$ incross progeny injected with *pbx2/4* MO, *meis1*-morphant embryos, and *lzr/pbx4*$^{+/-}$ incross progeny injected with both *pbx2/4* MO and *meis1* MO. Consistent with the *in situ* hybridization analysis, Pbx-depleted embryos exhibit a 28% decrease in *gata1* expression when compared to wild type embryos ($P < 0.0001$, Figure 3.7I). *meis1*-morphants exhibit a 26% decrease in *gata1* expression when compared to wild type embryos ($P < 0.0001$, Figure 3.7I). Embryos depleted of both Pbx and Meis1 exhibit a 50% decrease in *gata1* expression when compared to wild type embryos ($P < 0.0001$, Figure 3.7I). As one-quarter of the embryos injected with *pbx2/4* MO alone or in combination with *meis1* MO are on a *lzr/pbx4*$^{+/+}$ background, these embryos are not completely devoid of Pbx protein. Since embryo pools are collected at 16 hpf, a stage when phenotypic differences are not detectable, this quantitative PCR analysis likely under-represents the actual loss of *gata1* expression that occurs in both Pbx-depleted, and Pbx-depleted; *meis1*-morphant embryos.

3.2.4 Meis1 functions in association with Hox to regulate primitive erythropoiesis

Overexpressing *hoxb7a* or *hoxa9a* is sufficient to rescue *gata1* erythroid gene expression in embryos depleted of both Cdx1a and Cdx4 (Davidson and Zon, 2006), suggesting that these posteriorly-expressed *hox* genes act upstream of *gata1* to regulate erythropoiesis. Pbx and Meis proteins typically act as Hox protein cofactors (Moens and Selleri, 2006), and the posterior Hox proteins Hoxb7, Hoxa9, and Hoxd9 are able to form heterodimeric and heterotrimeric complexes with Pbx and Meis *in vitro* (Chang et al., 1997; Shanmugam et al., 1999). To determine if the posterior Hox proteins require Meis1 for their *in vivo* function, we injected *hoxb7a* mRNA into *meis1*-morphant embryos (Figure 3.8; Table 3.4). As shown through *in situ* hybridization, overexpressing *hoxb7a* does not restore *gata1* erythroid gene expression in the PLM of 16 hpf *meis1*-morphant embryos (Figures 3.8A-C). To measure *gata1* expression quantitatively, we performed real-time quantitative PCR on 16 hpf wild type embryos, *meis1*-morphant embryos, and embryos injected with both *meis1* MO

and *hoxb7a* mRNA. Consistent with the *in situ* hybridization analysis, both *meis1*-morphant embryos and *hoxb7a*-overexpressing *meis1*-morphant embryos exhibit a 28% decrease in *gata1* expression when compared to wild type embryos ($P < 0.0001$ for each, Figure 3.8D). Pbx-depleted and *meis1*-morphant embryos possess wild type levels of *hoxb6b*, *hoxb7a*, and *hoxa9a* gene expression at 16 hpf, as shown through *in situ* hybridization (Figure 3.9). Western immunoblotting reveals that Hoxb7a protein stability is not dependent on the presence of Pbx or Meis1 (Figure 3.10). Taken together, these data suggest that Hoxb7a requires Meis1 in order to activate *gata1* erythroid gene expression.

3.2.5 Meis1 and Pbx regulate primitive myelopoiesis

Overexpressing the zinc finger transcription factor GATA1 in myeloid cells inhibits myeloid differentiation, and induces a switch to megakaryocyte-erythroid cell fate (Iwasaki et al., 2003). Gata1-depleted zebrafish embryos display reduced numbers of erythrocytes, and expanded populations of granulocytic neutrophils and macrophages (Galloway et al., 2005; Rhodes et al., 2005), indicating that *gata1* represses myeloid differentiation, and is crucial for specifying erythroid cell fate. The molecular phenotype of Pbx-depleted and *meis1*-morphant embryos is similar to that of a Gata1-depleted embryo with regards to erythropoietic gene expression. Consequently, in order to determine if Pbx and Meis1 also serve to regulate myelopoiesis, we analyzed the expression of *pu.1* (*spi1b*) in the anterior lateral-plate mesoderm (ALPM) of 24 hpf wild type, Pbx-depleted, and *meis1*-morphant embryos (Figure 3.11A-G; Table 3.5). *pu.1* is an Ets-family transcription factor that is responsible for specifying myeloid cell fate (Anderson et al., 1998; McKercher et al., 1996; Scott et al., 1994; Zhang et al., 1996). In comparison to their wild type counterparts (Figure 3.11A, E), *meis1*-morphant embryos exhibit a significant 1.86-fold increase ($P < 0.0001$) in the number of *pu.1*-expressing cells at 24 hpf, as shown through *in situ* hybridization analysis (Figure 3.11B, E;). Pbx-depleted embryos exhibit a significant 2.05-fold increase in the number of *pu.1*-expressing cells in comparison to wild type embryos ($P < 0.0001$; Figure 3.11A, C, E). Embryos depleted of both Pbx and Meis1 exhibit a more severe (2.60-fold) increase in the number of *pu.1*-positive cells than through removal of either protein alone ($P < 0.0001$ for each when compared to wild type, Pbx-depleted, and *meis1*-morphant embryos; Figure

3.11A-E). Consistent with our ALPM results, Pbx-depleted; *meis1*-morphant embryos also exhibit increased levels of ICM *pu.1* expression when compared to wild type embryos, as shown through *in situ* hybridization (Figure 3.11F, G).

We next used *in situ* hybridization to analyze the expression *l-plastin* (*lcp1*) and *lysozyme C* (*lyz*) in the ALPM of 24 hpf wild type, Pbx-depleted, and *meis1*-morphant embryos. *lcp1* and *lyz* label macrophage and granulocyte progenitors (Hall et al., 2007; Le Guyader et al., 2008). In comparison to their wild type counterparts, both Pbx-depleted and *meis1*-morphant embryos exhibit an increase in the number of cells expressing *lcp1* (Figure 3.11H-J) and *lyz* (Figure 3.11K-M). Combined, these data suggest that Pbx and Meis1 act in a cooperative fashion to repress myeloid cell fate.

3.2.6 Pbx and Meis1 act upstream of *gata1*

Our findings that Pbx-depleted and *meis1*-morphant embryos fail to initiate proper *gata1* expression, and possess similar defects in myelopoiesis to Gata1-depleted embryos imply that Pbx and Meis1 act upstream of *gata1* to regulate primitive hematopoiesis. To test this hypothesis, we first analyzed the maintenance of *scl* and *lmo2* in the ICM of 24 hpf g*ata1*-morphant embryos. In comparison to their wild type counterparts, *gata1*-morphant embryos exhibit reduced *scl* expression at 24 hpf (Figure 3.12C, D). These data suggest that, like Pbx and Meis1, Gata1 is required to maintain normal levels of *scl* expression at 24 hpf. Unlike Pbx-depleted (Figure 3.4G') and *meis1*-morphant (Figure 3.2G') embryos, *gata1*-morphant embryos exhibit wild type levels of *lmo2* expression at 24 hpf (Figure 3.12A, B). Taken together, these data suggest that although Pbx and Meis1 are required to maintain normal levels of *lmo2* expression at 24 hpf, Gata1 is not.

In order to determine if the biological activity of *gata1* is dependent on the presence of Pbx and Meis1 protein, we first examined *scl* expression in the ICM of 24 hpf *gata1*-overexpressing *meis1*-morphant and Pbx-depleted embryos. As shown through *in situ* hybridization, *gata1*-overexpressing *meis1*-morphant (Figure 3.12F) and Pbx-depleted (Figure 3.12H) embryos display a greater level of *scl* expression than their *meis1*-morphant (Figure 3.12E) and Pbx-depleted (Figure 3.12G) counterparts, indicating that *gata1* is able to drive *scl* expression in the near absence of Pbx and Meis1. We next examined *hbae3*

expression in the PLM of 16 hpf *gata1*-overexpressing Pbx-depleted; *meis1*-morphant embryos. As shown through *in situ* hybridization, *gata1*-overexpression restores *hbae3* expression to near wild type levels in Pbx-depleted; *meis1*-morphant embryos (Figure 3.12I-K), indicating that *gata1* is able to drive *hbae3* gene expression in the absence of Pbx and Meis1. Combined, these data suggest that Pbx and Meis1 act upstream of *gata1* to regulate the expression of *scl* and *hbae3*, but function independently of *gata1* to regulate *lmo2* expression.

3.2.7 Pbx interacts with Cdx4 through a tryptophan-containing hexapeptide motif

Previous research has shown that *cdx4*-mutant (*kgg*^{tv205}) embryos injected with *cdx1* morpholino (hereafter referred to as Cdx-depleted) are deficient for ICM blood precursors, and fail to properly initiate *scl* and *gata1* expression in the PLM at 12 hpf (Davidson and Zon, 2006), phenotypes that are highly reminiscent of loss of Pbx/Meis1. Pbx binds Hox paralogue groups 1-4 through both its TALE motif and a tryptophan-containing hexapeptide motif termed the Pbx-Interaction Domain (PID). Cdx proteins also possess a putative PID. Based on their common hematopoietic defects, we hypothesized that Pbx/Meis1 and Cdx may interact to regulate primitive erythropoiesis. We therefore sought to determine if Pbx4 and Cdx4 have the capacity to interact *in vitro*. To do this, we attempted to co-immunoprecipitate Myc-Pbx4 with Flag-Cdx4 using anti-Flag agarose (Figure 3.13).

Western immunoblotting demonstrates that Myc-Pbx4 is successfully immunoprecipitated in the presence of wild type Cdx4 and a canonical Cdx/Pbx-binding DNA oligonucleotide (Figure 3.13; Lane 7). Conversely, Pbx4 is not immunoprecipitated in the presence of a mutant version of Cdx4 (Cdx4^{W135S}), in which the PID tryptophan residue has been replaced with serine (Figure 3.13; Lane 8). Combined, these results suggest that Pbx4 and Cdx4 have the capacity to interact *in vitro.* These results also suggest that this interaction requires an intact Cdx4 PID.

To determine if this interaction between Pbx4 and Cdx4 may also occur *in vivo*, we assessed the morphological phenotypes of zebrafish embryos overexpressing *pbx4* alone or in combination with wild type or PID-mutant *cdx4* (*cdx4*^{W135S}). Compared to wild type uninjected embryos, overexpression of Pbx4 alone generates no morphological abnormalities

(Figure 3.14A, B). Overexpression of wild type *cdx4* or *cdx4*^{W135S} generates nearly identical phenotypes, whereby the embryo exhibits moderate posteriorization (Figure 3.14C, D; Skromne et al., 2007). Overexpression of wild type *cdx4* with *pbx4* (Figure 3.14E) generates a much more severe morphological phenotype than overexpression of wild type *cdx4* alone (Figure 3.14C), whereby both the anterior and posterior regions of the embryo are affected. Conversely, the morphological phenotype generated by overexpression of both *cdx4*^{W135S} and *pbx*4 (Figure 3.14F) closely resembles the posteriorization observed by the overexpression of *cdx4*^{W135S} alone (Figure 3.14D).

We also examined the contribution of endogenous Pbx to the morphological defects generated by *cdx4* overexpression (Figure 3.15). Overexpression of *cdx4* in Pbx-depleted embryos (Figure 3.15D) produces a milder phenotype than overexpression of *cdx4* in wild type embryos (Figure 3.15C). Combined, these data suggest that Pbx4 and Cdx4 have the capacity to interact *in vivo*, and that this interaction is at least partially dependent upon the PID of Cdx4.

3.2.8 Pbx/Meis1-depleted and Cdx-depleted embryos exhibit distinct phenotypes

In addition to their primitive hematopoietic defects, Cdx-depleted embryos exhibit severe defects in *hoxb7a* and *hoxa9a* expression (Davidson and Zon, 2006). Furthermore, overexpressing these posteriorly-expressed *hox* genes partially rescues *gata1* expression in a Cdx-depleted embryo (Davidson and Zon, 2006). These data suggest that *hox* genes act upstream of *gata1* to specify erythroid cell fate. Pbx and Meis proteins typically act as Hox protein cofactors (Moens and Selleri, 2006), and are essential for proper Hox function in the developing hindbrain (McNulty et al., 2005; Popperl et al., 2000; Vlachakis et al., 2001; Waskiewicz et al., 2002). We therefore wanted to determine if Cdx-depleted embryos and Pbx-depleted; *meis1*-morphant embryos exhibit comparable defects in erythropoietic gene expression. To do this, we examined the expression of *gata1* and *scl* in the PLM of wild type, Pbx-depleted; *meis1*-morphant, and Cdx-depleted embryos at 12 hpf, shortly after the initiation of *gata1* expression. As shown through *in situ* hybridization, *scl* is expressed at wild type levels in the PLM of 12 hpf Pbx-depleted; *meis1*-morphant embryos (Figure 3.16A, B), but is abolished in the PLM of 12 hpf Cdx-depleted embryos (Figure 3.16E, F). In contrast,

gata1 expression is abolished in Pbx-depleted; *meis1*-morphant (Figure 3.16C, D) and Cdx-depleted (Figure 3.16G, H) embryos at 12 hpf. *gata1* expression is also nearly abolished in Pbx-depleted embryos and *meis1*-morphants at 12 hpf (Figure 3.17). To determine if the loss of *gata1* expression in Cdx-depleted embryos is attributable to a loss of Meis1, we examined *meis1* expression levels and Meis1 protein levels in 14 hpf Cdx-depleted embryos. Cdx-depleted embryos exhibit mildly upregulated *meis1* expression and slightly increased levels of anti-Meis1 antibody staining in comparison to wild type embryos (Figure 3.18). Combined, these data suggest that Cdx functions independently of Meis1/Pbx to initiate the expression of *scl* and *gata1*.

Primitive erythropoietic gene expression is completely dependent on *scl* (Patterson et al., 2007; Shivdasani et al., 1995*)*. It is therefore plausible that the erythropoietic defects of Cdx-depleted embryos (i.e. loss of *gata1* and *hbae3*) represent indirect results of abolished *scl* expression. *hoxb7a* overexpression can partially rescue *gata1* expression in a Cdx-depleted embryo (Davidson and Zon, 2006). *hoxb7a* overexpression fails to rescue *gata1* expression in *meis1*-morphant embryos (Figure 3.8), or Pbx depleted; *meis1*-morphant embryos (Figure 3.19A-C), suggesting that Hox function depends on the presence of Meis1 protein. Taken together, these results are consistent with a model that places *hox* and its cofactor *meis1* on a parallel pathway to *scl*, and upstream of *gata1* (Figure 3.20).

3.3 Discussion

Previous research has shown that the TALE-class homeodomain transcription factors Meis and Pbx function as critical regulators of definitive hematopoiesis (Azcoitia et al., 2005; Di Rosa et al., 2007; DiMartino et al., 2001; Ferretti et al., 2006; Hisa et al., 2004). Our study describes a novel role for Meis1 and Pbx in primitive hematopoiesis. We propose that Meis1 and Pbx function near the top of a hierarchy of transcription factors that regulate the development of primitive erythrocytes (Figure 3.20). Through targeted ablation of Meis1 and Pbx proteins, we demonstrate that Meis1 and Pbx are required for the transcriptional activation of *gata1*, a gene that has an evolutionarily conserved role in specifying erythroid cell fate (Galloway et al., 2005; Pevny et al., 1991; Rhodes et al., 2005; Shivdasani et al., 1997). Consequently, in the absence of Meis1 and Pbx, embryos exhibit severe defects in primitive erythropoiesis, and are unable to produce visible circulating blood cells. Concomitant with a loss of *gata1*, Meis1 and Pbx-depleted embryos also exhibit increased numbers of myelocytes, and fail to maintain wild type levels of *scl*, a broad marker of hematopoietic cell fate.

3.3.1 Meis1 and Pbx in the erythropoietic transcription factor hierarchy

Inhibiting Meis1 and Pbx function reduces the expression of genes that specify primitive erythrocyte identity. *meis1*-morphant and Pbx-depleted embryos fail to properly initiate *gata1*, a transcription factor that is essential for erythrocyte development (Galloway et al., 2005; Lyons et al., 2002; Pevny et al., 1991; Rhodes et al., 2005; Shivdasani et al., 1997). These embryos also exhibit downregulated expression of the embryonic hemoglobin gene *hbae3*, which is a downstream target of *gata1* (Figure 3.21). The expression of *scl*, a broad marker of hematopoietic cell fate, is initiated normally, but not maintained at wild type levels in embryos lacking Meis1 and Pbx. Gata transcription factors act as part of multiprotein complexes that bind the autoregulatory enhancer of *scl* (Gottgens et al., 2002; Orkin, 1992). We demonstrate that *gata1*-morphant embryos likewise fail to maintain normal levels of *scl* expression, and this molecular phenotype is also observed in *gata1*-mutant (vlt^{m651}) embryos (Lyons et al., 2002). We also demonstrate that *gata1* overexpression is able to drive *scl* and *hbae3* expression in *meis1*-morphant and Pbx-depleted embryos. Taken together, these data

support a model in which Meis1 and Pbx regulate erythropoiesis by activating *gata1*, which is subsequently required to activate *hbae3* and maintain wild type levels of *scl* expression in maturing erythrocytes (Figure 3.20).

Although *lmo2* is a broad marker of hematopoietic cell fate, previous research has highlighted its importance in specifying the erythroid lineage. For example, *Lmo2*-mutant mice possess severe embryonic-lethal defects in erythropoiesis (Warren et al., 1994). Like with *scl*, the expression of *lmo2* is initiated normally, but not maintained at wild type levels in *meis1*-morphant and Pbx-depleted embryos. However, we demonstrate that *lmo2* expression, unlike *scl* expression, is maintained normally in Gata1-depleted embryos. These data suggest that Meis1 and Pbx act in a *gata1*-independent fashion to regulate the expression of *lmo2*. The transcriptional regulation of *scl* and *lmo2* is also uncoupled in *cloche* (*clo*^{m39}) mutant zebrafish (Dooley et al., 2005). Consequently, our study identifies Meis1 and Pbx as novel targets for elucidating the mechanisms by which *lmo2* and *scl* are independently regulated.

3.3.2 Pbx and Meis1 in primitive myelopoiesis

The interplay between *gata1* and *pu.1* in specifying erythroid versus myeloid cell fate is well characterized. Biochemical evidence suggests that GATA1 and PU.1 proteins physically interact to inhibit the transcriptional regulation of each other's target genes (Nerlov et al., 2000; Rekhtman et al., 1999; Stopka et al., 2005; Zhang et al., 1999; Zhang et al., 2000). Furthermore, Pu.1-depleted zebrafish embryos exhibit ectopic *gata1* expression in the anterior lateral-plate mesoderm (ALPM) (Rhodes et al., 2005), suggesting that Pu.1 transcriptionally represses *gata1*. In a reciprocal fashion, Gata1-depleted zebrafish embryos demonstrate increased numbers of *pu.1*-positive cells in the intermediate cell mass (ICM) and ALPM (Galloway et al., 2005; Lyons et al., 2002; Rhodes et al., 2005). As previously mentioned, *meis1*-morphant and Pbx-depleted embryos exhibit diminished *gata1* expression. In key with these findings, these embryos also exhibit increased numbers of *pu.1*-positive ALPM and ICM cells. Consequently, because *meis1*-morphant and Pbx-depleted embryos phenocopy Gata1-depleted embryos with regards to both erythropoietic and myelopoietic gene expression defects, we can place Meis1 and Pbx upstream of *gata1* in the primitive myelopoietic transcription factor hierarchy. Furthermore, given that *pu.1* expression is

upregulated in the ICM of Pbx-depleted; *meis1*-morphant embryos, we postulate that the loss of *gata1* expression in these embryos represents a switch from erythroid to myeloid cell fate.

3.3.3 Distinct requirements for Pbx and Meis1 in primitive hematopoiesis

Pbx and Meis/Prep1 proteins associate with each other through conserved motifs situated N-terminal to their respective homeodomains (Berthelsen et al., 1998b; Knoepfler et al., 1997). This interaction occurs even in the absence of DNA (Knoepfler et al., 1997). Previous research has demonstrated a role for Meis/Prep1 in stabilizing Pbx, and regulating its nuclear import (Abu-Shaar et al., 1999; Berthelsen et al., 1999; Mercader et al., 1999; Stevens and Mann, 2007; Waskiewicz et al., 2001). In a reciprocal fashion, recent work in *Drosophila* has demonstrated that Hth (Homothorax; orthologue of Meis) requires Exd (Extrandenticle; orthologue of Pbx) to achieve nuclear import and stability (Stevens and Mann, 2007). In zebrafish, we similarly demonstrate that Pbx stabilizes Meis1, and is required for its nuclear import *in vivo*. Pbx-depleted zebrafish exhibit wild type levels of *meis1* expression at 12 hpf, and downregulated *meis1* expression at 24 hpf, as shown through *in situ* hybridization analyses (T. Erickson, unpublished). Taken together, these data suggest that Pbx acts in a pre- and post-transcriptional fashion to regulate Meis1 protein levels.

Other Meis-family proteins, such as Prep1, are present in the developing embryo during primitive hematopoiesis. Furthermore, previous research has demonstrated the capacity of Pbx to be nuclear-localized in the absence of Meis/Prep1 (Kilstrup-Nielsen et al., 2003). It is therefore unlikely that Pbx is dependent solely on Meis1 for its stabilization and nuclear import. For these reasons, we hypothesize that the hematopoietic defects we observe in *meis1*-morphant and Pbx-depleted embryos are due to a specific transcriptional requirement for Meis1. Our immunohistochemical data suggests that *meis1*-morphant embryos mimic hypomorphs, providing an explanation for why Pbx-depleted; *meis1*-morphant embryos exhibit more severe defects in *gata1* and *hbae3* expression than Pbx-depleted or *meis1*-morphant embryos.

3.3.4 Pbx and Meis1 as Hox cofactors in primitive hematopoiesis

Pbx and Meis proteins form heterodimeric and heterotrimeric complexes with Hox proteins (Berthelsen et al., 1998a; Chang et al., 1996; Chang et al., 1995; Ferretti et al., 2000; Jacobs et al., 1999; Mann and Chan, 1996; Ryoo et al., 1999; Sarno et al., 2005; Shanmugam et al., 1999; Shen et al., 1997a; Shen et al., 1999; Shen et al., 1997b; Vlachakis et al., 2001; Williams et al., 2005). These interactions are necessary for proper anteroposterior patterning of the developing hindbrain (Cooper et al., 2003; Vlachakis et al., 2001; Waskiewicz et al., 2001; Waskiewicz et al., 2002). In zebrafish, the posteriorly expressed *hox* genes *hoxb6b*, *hoxb7a*, and *hoxa9a* have been implicated in the transcriptional regulation of primitive erythropoietic genes such as *gata1* (Davidson et al., 2003; Davidson and Zon, 2006). Biochemical analyses have demonstrated the capacity of Pbx and Meis proteins to bind posterior Hox proteins *in vitro* (Chang et al., 1996; Chang et al., 1995; Mann and Chan, 1996; Sarno et al., 2005; Shanmugam et al., 1999; Shen et al., 1997a; Shen et al., 1999; Shen et al., 1997b; Williams et al., 2005). We demonstrate that overexpressing *hoxb7a* fails to rescue the *gata1* erythroid gene expression defects of *meis1*-morphant embryos. Given that *meis1*-morphant embryos exhibit wild type levels of *hoxb7a* expression and normal levels of overexpressed Hoxb7a protein, these data suggest that Hoxb7a specifically requires Meis1 protein in order to transcriptionally regulate *gata1*.

3.3.5 Implications for Hox function in primitive hematopoiesis

The role of Hox function in hematopoiesis has been studied extensively in mice with targeted deletions in *Hoxb3*, *Hoxb4*, *Hoxb6*, *Hoxa7*, *Hoxc8,* and *Hoxa9* respectively (Bjornsson et al., 2003; Brun et al., 2004; Izon et al., 1998; Kappen, 2000; Ko et al., 2007; Lawrence et al., 1997; Magnusson et al., 2007a; Shimamoto et al., 1999; So et al., 2004). Mice with mutations in *Hoxa9*, *Hoxb4*, or *Hoxb3* exhibit similar defects in the capacity of hematopoietic stem cells to repopulate (Bjornsson et al., 2003; Brun et al., 2004; Lawrence et al., 1997). The hematopoietic defects observed in mice with compound mutations in *Hoxb3*, *Hoxb4* and *Hoxa9* are more severe than those observed in *Hoxa9*-mutant mice (Magnusson et al., 2007a), suggesting that Hox transcription factors perform overlapping functions in hematopoiesis. A more global analysis of Hox function in primitive hematopoiesis is achieved

through knockdown of the homeodomain transcription factor Cdx. Previous research has shown that *cdx4*-mutant (*kgg*^{tv205}) zebrafish exhibit decreased expression of the posteriorly-expressed *hox* genes *hoxb6b*, *hoxb7a*, *hoxb8b*, and *hoxa9a* (Davidson et al., 2003). Notably, the expression of many *hox* genes is normal in Cdx-depleted embryos, and the expression of some posteriorly-expressed *hox* genes, such as *hoxb5a,* is markedly expanded (Davidson et al., 2003; Davidson and Zon, 2006). These embryos also possess severe defects in primitive erythropoiesis (Davidson et al., 2003; Davidson and Zon, 2006) that are in some ways similar to those observed in *meis1*-morphant and Pbx-depleted embryos. For example, Cdx-depleted embryos fail to initiate *gata1* erythroid gene expression, but exhibit normal rostral angioblast expression of *kdrl* (Davidson and Zon, 2006). Cdx-depleted embryos are also strikingly different from *meis1*-morphant and Pbx-depleted embryos. The posterior *hox* genes *hoxb6b*, *hoxb7a*, and *hoxa9a* are expressed at normal levels in *meis1*-morphant and Pbx-depleted embryos. Furthermore, whereas Cdx-depleted embryos exhibit defects in the initiation of *scl* expression (Davidson and Zon, 2006), *scl* expression is initiated normally, but not maintained at proper levels in embryos lacking Meis1 and Pbx. *scl* overexpression generates increased populations of *gata1*-expressing cells in a Cdx4-dependent manner (Davidson et al., 2003). Conversely, *hox* overexpression drives *gata1* expression in the absence of Cdx4 (Davidson et al., 2003; Davidson and Zon, 2006). Taken together with our own data, these data place Hox upstream of *gata1* in the primitive hematopoietic transcription factor hierarchy. These data also suggest that Cdx acts in a *hox*-independent fashion to initiate *scl* expression. We therefore propose a model whereby Cdx activates Hox, which together with Meis1 activates *gata1* erythroid gene expression (Figure 3.20). Previous research has shown that Hoxa10 has the capacity to bind directly to the *gata1* promoter (Magnusson et al., 2007b). Meis1 and Pbx form heterotrimeric complexes with posterior Hox proteins including Hoxa10 (Shanmugam et al., 1999). Consequently, the transcriptional activation of *gata1* by Pbx and Meis1 may occur in a direct fashion.

3.3.6 Hoxd4a acts upstream of *meis1* in primitive hematopoiesis

Amali et al. (2013) recently examined the role of Hoxd4a in primitive hematopoiesis. They demonstrate that *hoxd4a*-morphant zebrafish embryos exhibit impaired erythropoiesis,

with a concomitant decrease in *gata1* expression. *meis1* expression is downregulated in *hoxd4a*-morphants, and *meis1*-overexpression is able to rescue *gata1* expression in *hoxd4a*-morphants (Amali et al., 2013). Combined, these data place Hoxd4a upstream of *meis1* in the primitive hematopoietic transcription factor hierarchy. *hoxd4a*-morphants exhibit wild type levels of *cdx4* expression (Amali et al., 2013), placing *hoxd4a* genetically downstream of, or on a parallel pathway to Cdx4 in primitive hematopoiesis. Notably, *hoxd4a*-morphants also exhibit reduced *scl* and *kdrl* expression, along with defects in endothelial development and intersegmental vessel sprouting (Amali et al., 2013). These data support a role for Hoxd4a in hemangioblast formation. *hoxd4a*-morphants exhibit diminished expression of numerous *hox* genes that have been implicated in primitive hematopoiesis. These include *hoxd3a*, *hoxb4a*, *hoxb6b*, *hoxb7a*, and *hoxa9a* (Amali et al., 2013). Consequently, the *hoxd4a*-morphant phenotype represents a combination of diminished Meis1 activity, in concert with the reduced function of numerous Hox proteins.

3.3.7 Unknown biological significance of a Pbx-Cdx interaction

Pbx binds Hox paralogue groups 1-4 through both its TALE motif and a tryptophan-containing hexapeptide motif termed the Pbx-Interaction Domain (PID). Cdx proteins possess a putative PID. We demonstrate that Pbx4 and Cdx4 proteins have the capacity to interact both *in vitro* and *in vivo*. This interaction requires an intact Cdx4 PID. As previously mentioned, the hematopoietic and *hox* gene expression defects of Cdx-depleted embryos differ from those of Pbx-depleted embryos. Our data therefore support a model whereby Pbx/Meis1 and Cdx function at disparate points in the hematopoietic transcription factor hierarchy (Figure 3.20). Consequently, the biological significance of a Pbx-Cdx interaction currently remains unclear and requires further analyses. It would therefore be of interest to identify common, direct transcriptional targets of Pbx4 and Cdx4 using chromatin immunoprecipitation and massively parallel sequencing (ChIP-seq).

3.3.8 Discrepancies with other accounts of Meis1/Pbx function in hematopoiesis

Subsequent to our study, Cvejic et al. (2011) conducted their own analyses of Meis1 and Pbx function in zebrafish primitive hematopoiesis. Consistent with our results, they

demonstrate that *meis1*-morphants exhibit reduced numbers of terminally differentiated erythrocytes. However, they also demonstrate that *meis1*-morphants exhibit wild type levels of *gata1* expression at 14 hpf, and increased expression of *gata1* and *scl* at 24 hpf (Cvejic et al., 2011). These data lead them to conclude that Meis1 regulates primitive erythropoiesis independent of *gata1*. Conversely, our data clearly demonstrate that Meis1 acts upstream of *gata1* to regulate primitive erythropoiesis. These conflicting results can likely be attributed to technical differences between our two studies. Using a translation-blocking *meis1* morpholino, Cvejic et al. (2011) observe a 55% reduction in the number of Meis1-positive cells within the ICM. This was shown through immunohistochemistry using a polyclonal Meis1 antibody that does not accurately recapitulate endogenous zebrafish *meis1* mRNA expression. Our *meis1*-morpholino injections are far more effective, nearly eliminating Meis1 protein within the embryo, as shown through immunohistochemistry using a highly specific Meis1-monoclonal antibody (Figure 3.5; Figure 3.6). It is possible that very little Meis1 protein is required to initiate *gata1* expression, and that the incomplete knockdown of Meis1 protein by Cvejic et al. (2011) was insufficient to generate observable defects in *gata1* expression.

Notably, Cvejic et al. (2011) further demonstrate that *scl*-morphants exhibit nearly abolished Meis1 protein levels, placing *scl* upstream of *meis1* in the hematopoietic transcription factor hierarchy. We did not specifically evaluate whether or not Meis1 levels are influenced by Scl-depletion. However, Amali et al. (2013) recently demonstrated that *meis1*-overexpression is able to rescue both *gata1*, and *scl* expression in *hoxd4a*-morphants. These data support our findings, placing Meis1 upstream of *gata1* and (indirectly) *scl*.

Cvejic et al. (2011) also demonstrate that *pbx1*-morphants and *meis1*-morphants possess nearly identical primitive hematopoietic defects. This leads them to postulate that Pbx1 is acting as the preferred binding partner of Meis1 in zebrafish primitive hematopoiesis. However, zebrafish *pbx1* expression is not initiated until 24 hpf, whereupon it becomes enriched only within non-hematopoietic tissues (Teoh et al., 2010). These include the central nervous system, pharyngeal arches, and swim bladder (Teoh et al., 2010). Furthermore, alternative analyses of *pbx1*-morphants have shown that these embryos mature normally until 3 dpf, at which point they develop a curved body and fail to produce a swim bladder

(Teoh et al., 2010). These combined data suggest that Pbx1 is not likely involved in zebrafish primitive hematopoiesis. Conversely, *pbx4* is expressed fairly ubiquitously throughout the somitogenic embryo (Vlachakis et al., 2000). Combined with our analyses of Pbx2/4 function, these data suggest that Pbx2 and Pbx4 are the preferred binding partners of Meis1 in primitive hematopoiesis.

3.4 Figures

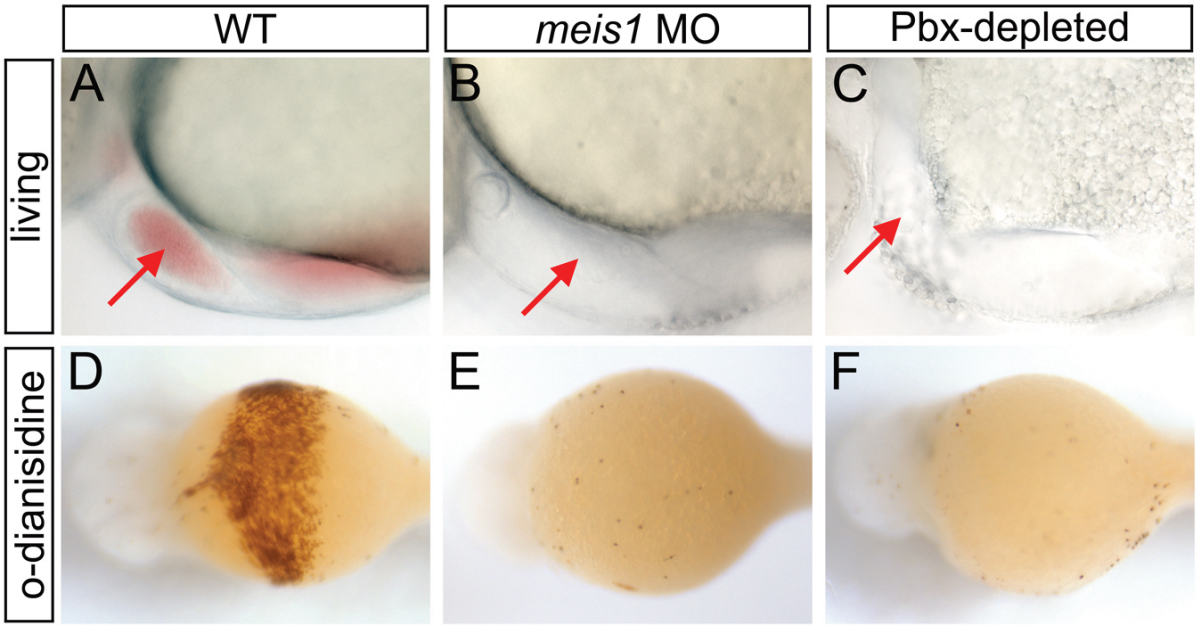

Figure 3.1. *meis1*-morphant and Pbx-depleted embryos fail to produce visible circulating erythrocytes. (A-C) Lateral view of live 48 hours post fertilization (hpf) embryos showing close-up of heart region; anterior to left. Unlike their wild type (WT) counterparts (A), *meis1*-morphant (B), and Pbx-depleted (C) embryos lack visible circulating blood cells. Arrows indicate heart. (D-F) o-dianisidine staining of differentiated erythrocytes in 48 hpf whole-mount embryos; ventral view with anterior to left. o-dianisidine staining is abolished in *meis1*-morphant (E) and Pbx-depleted (F) embryos when compared to WT embryos (D).

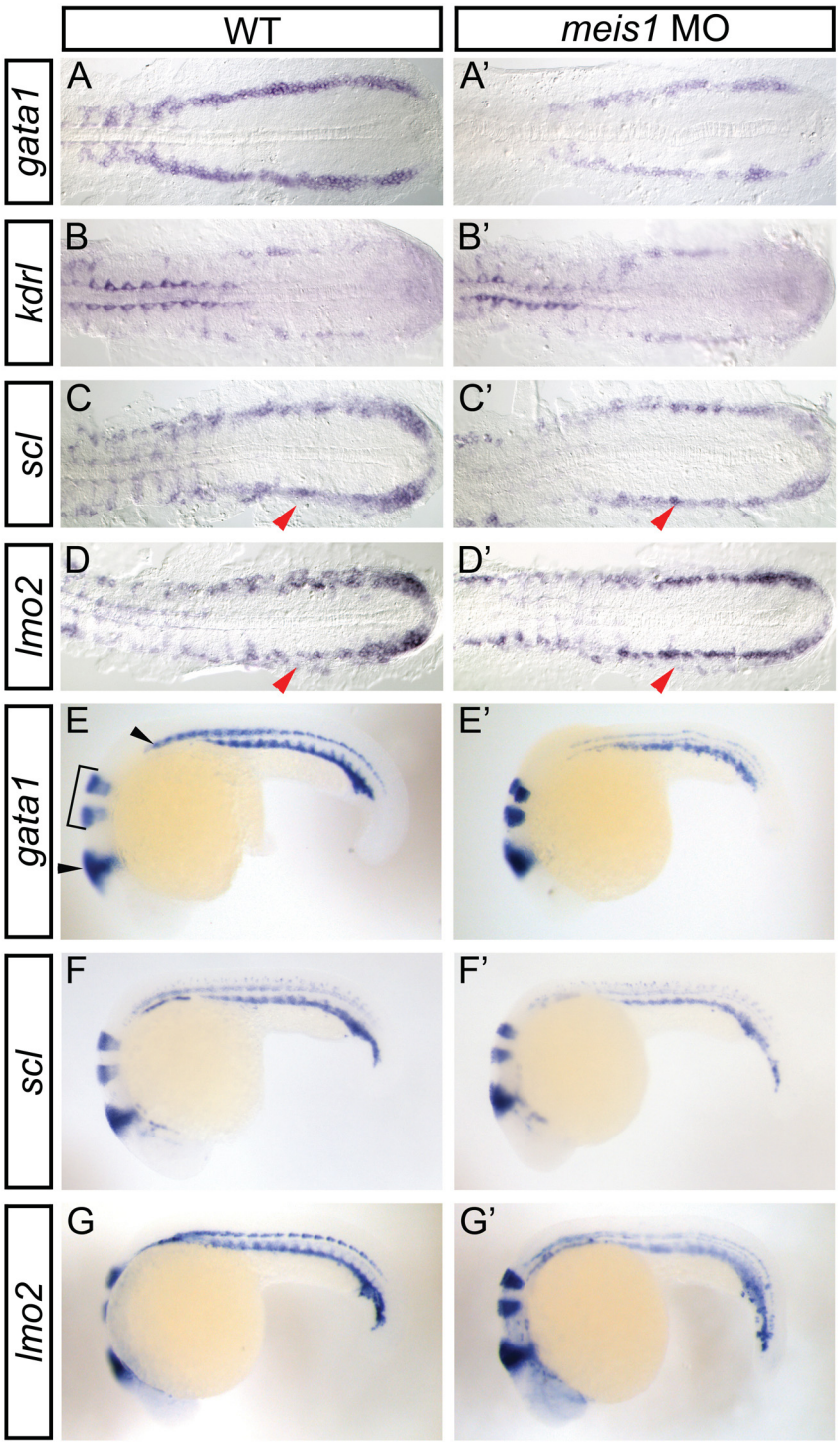
WT
meis1 MO
gata1
kdrl
scl
lmo2
gata1
scl
lmo2
A
A'
B
B'
C
C'
D
D'
E
E'
F
F'
G
G'

Figure 3.2. *meis1*-morphant embryos exhibit defects in primitive hematopoietic gene expression. Shown are representative embryos following *in situ* hybridization analysis of hematopoietic marker expression in wild type (WT; A-G) compared with *meis1*-morphant (A'-G') embryos. (A-D') The PLM of 16 hours post fertilization (hpf) flat-mounted, deyolked embryos is shown in dorsal view with anterior to left. *gata1* expression is severely reduced in *meis1*-morphant embryos (A') when compared to WT (A). *kdrl* expression is unchanged in *meis1*-morphant embryos (B') when compared to WT (B). Lateral domain of *scl* and *lmo2* expression is abolished in *meis1*-morphant embryos (C', D'; red arrowheads), while the medial domain of *scl* and *lmo2* expression is near normal. (E-G') 24 hpf whole-mount embryos are shown in lateral view with anterior to left. *eng2a* expression in the midbrain hindbrain boundary and muscle pioneers (E; black arrowheads) and *egr2b* expression in hindbrain rhombomeres 3 and 5 (E; bracket) is shown in all panels. *gata1* (E'), *scl* (F'), and *lmo2* (G') expression is reduced in the ICM of *meis1*-morphant embryos when compared to WT (E-G).

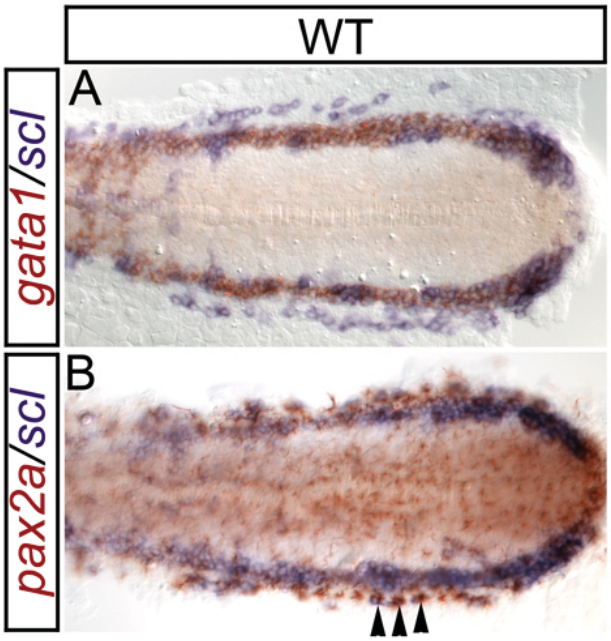

Figure 3.3. Lateral domain of *scl* expression colocalizes with *pax2a* expression. Shown are representative embryos following *in situ* hybridization analysis of *scl* and *gata1* (A) or *scl* and *pax2a* (B) expression in wild type embryos. The PLM of 16 hours post fertilization (hpf) flat-mounted, deyolked embryos is shown in dorsal view with anterior oriented to the left. Arrowheads indicate *scl* and *pax2a* colocalization.

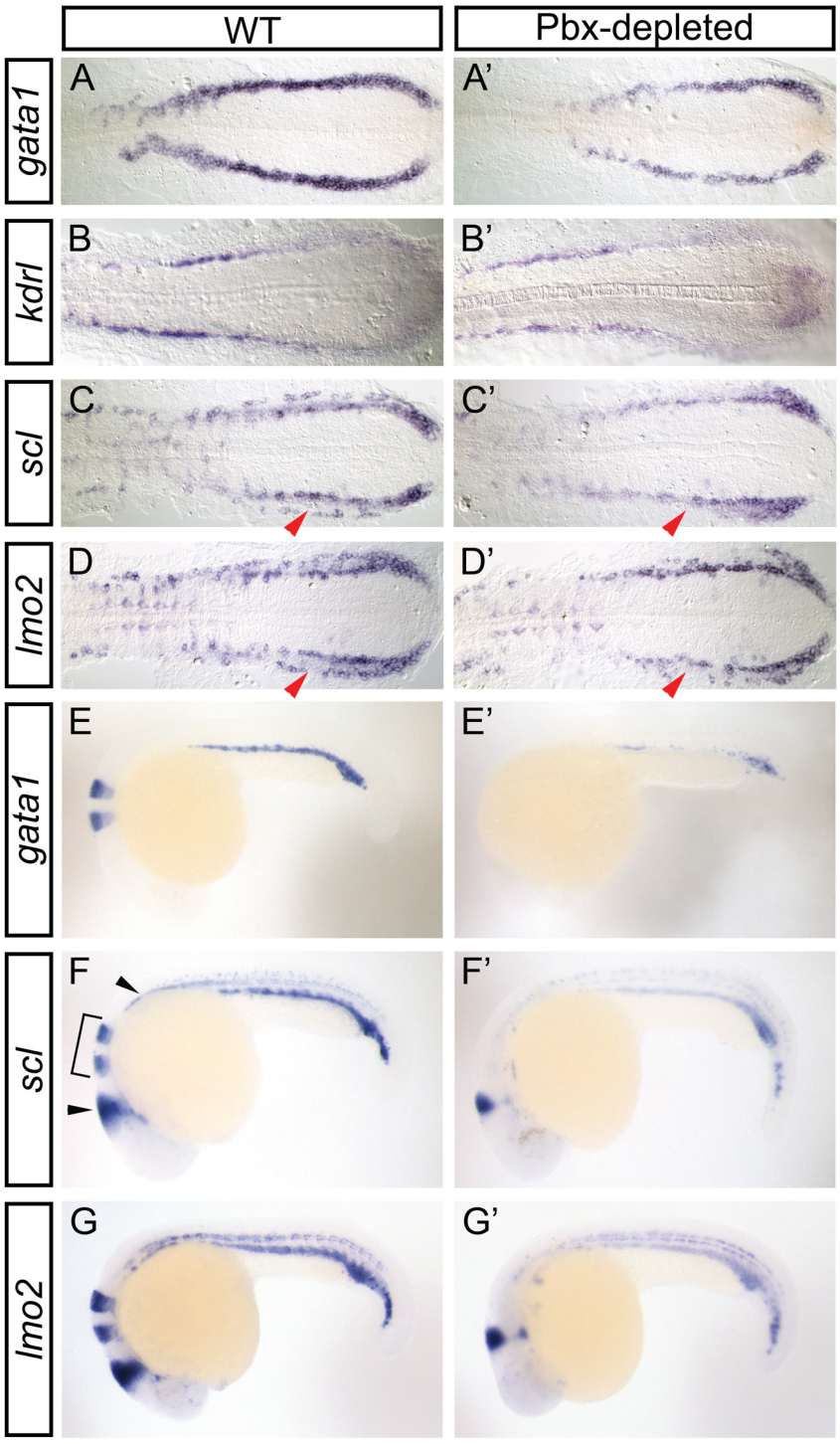
WT
Pbx-depleted
gata1
kdrl
scl
lmo2
gata1
scl
lmo2
A
A'
B
B'
C
C'
D
D'
E
E'
F
F'
G
G'

Figure 3.4. Pbx-depleted embryos exhibit defects in primitive hematopoietic gene expression. Shown are representative embryos following *in situ* hybridization analysis of hematopoietic marker expression in wild type (WT; A-G) compared with Pbx-depleted (A'-G') embryos. (A-D') The PLM of 16 hours post fertilization (hpf) flat-mounted, deyolked embryos is shown in dorsal view with anterior to left. *gata1* expression is severely reduced in Pbx-depleted embryos (A') when compared to WT (A). *kdrl* expression is unchanged in Pbx-depleted embryos (B') when compared to WT (B). Lateral domain of *scl* and *lmo2* expression is abolished in Pbx-depleted embryos (C', D'; red arrowheads), while the medial domain of *scl* and *lmo2* expression is near normal. (E-G') 24 hpf whole-mount embryos are shown in lateral view with anterior to left. *eng2a* expression in the midbrain hindbrain boundary and muscle pioneers (F; black arrowheads) is shown in panels F-G', and *egr2b* expression in hindbrain rhombomeres 3 and 5 (F; bracket) is shown in all panels. *gata1* (E'), *scl* (F'), and *lmo2* (G') expression is reduced in the ICM of Pbx-depleted embryos when compared to WT (E-G).

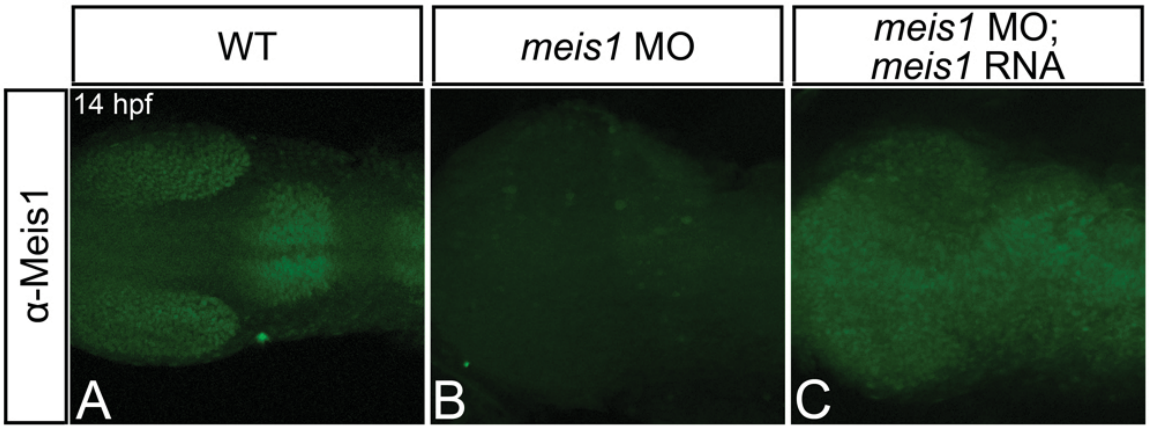

Figure 3.5. The P2A6 monoclonal antibody specifically labels Meis1. Shown are representative embryos following immunohistochemical staining with the P2A6 monoclonal antibody to visualize Meis1 protein levels in 14 hours post fertilization (hpf) wild type embryos (WT; A), *meis1*-morphant embryos (B), and *meis1*-morphant embryos injected with *meis1* RNA (C). Flat-mount; dorsal view of embryo; anterior to left. All embryos visualized under a 20X objective. In wild type (WT; A) embryos, α-Meis1 antibody staining is punctate, and resembles *meis1* expression (Erickson et al., 2010). *meis1*-morphant embryos (B) exhibit severely decreased α-Meis1 antibody staining when compared to WT embryos (A). α-Meis1 antibody staining is restored in *meis1*-morphant embryos injected with *meis1* RNA (C).

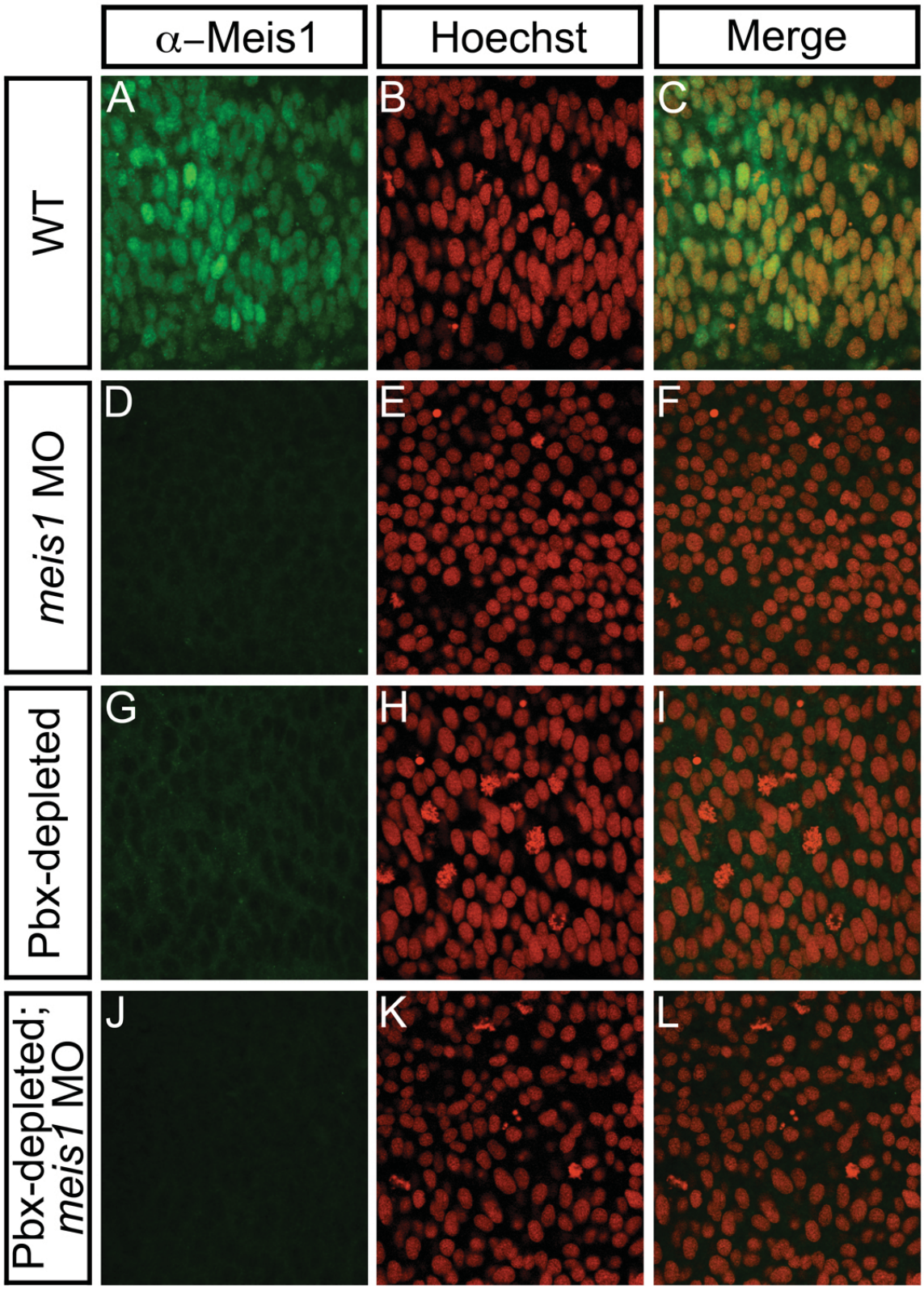
α–Meis1
Hoechst
Merge
WT
meis1 MO
Pbx-depleted
Pbx-depleted; meis1 MO
A
B
C
D
E
F
G
H
I
J
K
L

Figure 3.6. Meis1 protein levels are severely diminished in the posterior mesoderm of Pbx-depleted and *meis1*-morphant embryos. Shown are representative embryos following immunohistochemical staining with the P2A6 antibody (green; A, D, G, J) to visualize Meis1 protein levels, and Hoechst 33258 (red; B, E, H, K) to visualize nuclei in 14 hours post fertilization (hpf) wild type (WT; A-C), *meis1*-morphant (D-F), Pbx-depleted (G-I), and Pbx-depleted; *meis1*-morphant (J-L) embryos. Flat-mount; dorsal view of posterior mesoderm; anterior to left. All embryos visualized under a 100X objective. In wild type (WT; A-C) embryos, α-Meis1 antibody staining is punctate, and colocalizes with Hoechst nuclear staining. *meis1*-morphant (D) and Pbx-depleted (G) embryos exhibit severely decreased α-Meis1 antibody staining when compared to WT embryos (A). α-Meis1 antibody staining is further abolished in Pbx-depleted; *meis1*-morphant embryos (J). α-Meis1 antibody staining does not colocalize with Hoechst nuclear staining in Pbx-depleted embryos (G-I).

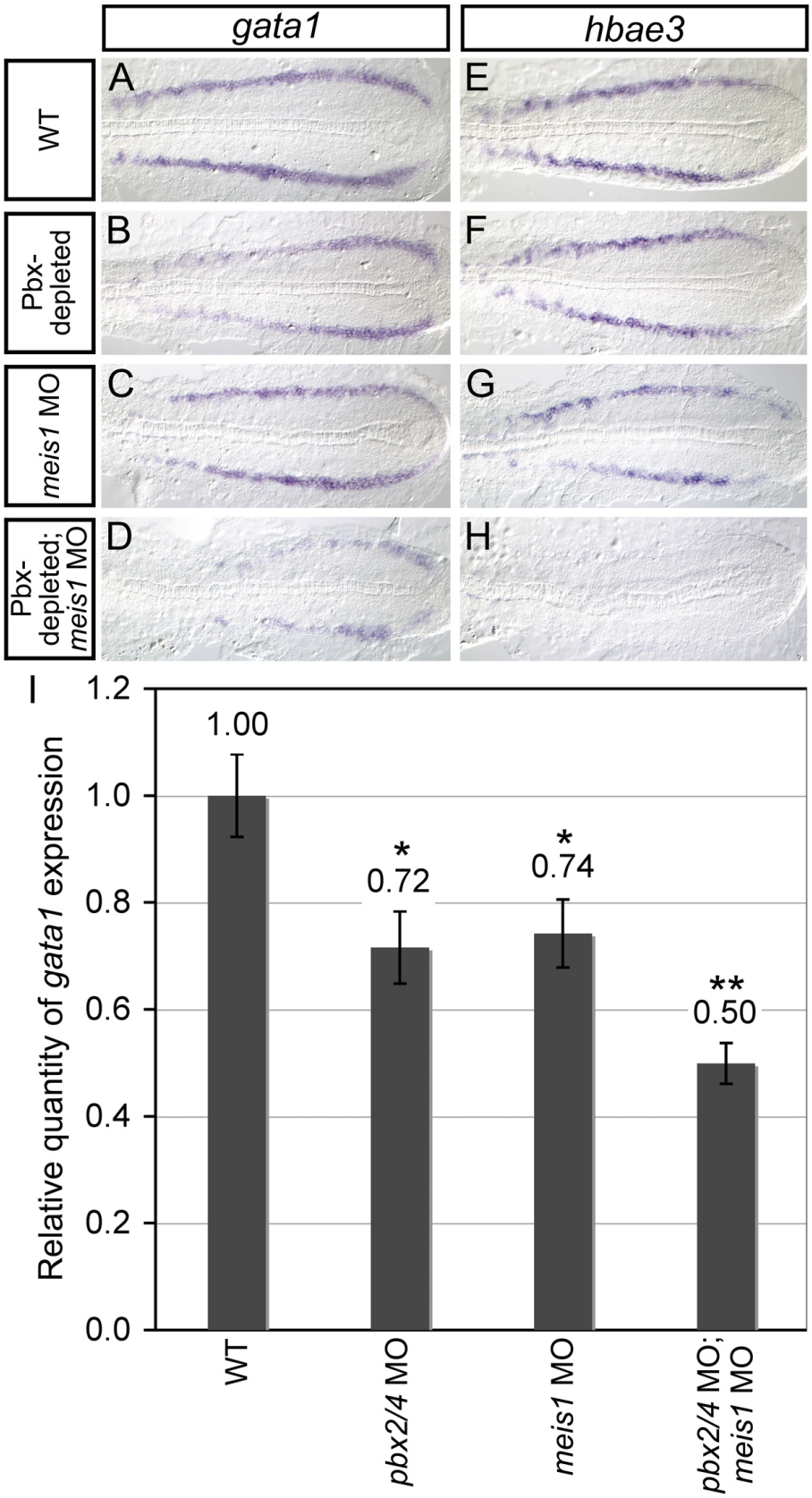
gata1
hbae3
WT
Pbx-depleted
meis1 MO
Pbx-depleted; meis1 MO
A
B
C
D
E
F
G
H
I
Relative quantity of gata1 expression
1.2
1.0
0.8
0.6
0.4
0.2
0.0
1.00
*
0.72
*
0.74
**
0.50
WT
pbx2/4 MO
meis1 MO
pbx2/4 MO; meis1 MO

Figure 3.7. Pbx and Meis1 act in a cooperative fashion to regulate erythroid gene expression. (A-H) Shown are representative embryos following *in situ* hybridization analysis of *gata1* (A-D) and *hbae3* (E-H) expression in 16 hours post fertilization (hpf) embryos. Embryos shown are deyolked and flat-mounted with a dorsal view of gene expression in the PLM and anterior oriented to the left. Embryos partially depleted of Pbx (injected with 4.5 ng of *pbx2/4* MO) exhibit subtle decreases in *gata1* (B) and *hbae3* (F) expression. Embryos partially depleted of Meis1 (injected with 2 ng of *meis1* MO) exhibit subtle decreases in *gata1* (C) and *hbae3* (G) expression. Embryos partially depleted of both Pbx and Meis1 exhibit profoundly reduced *gata1* (D) and *hbae3* (H) expression. (I) Real-time quantitative PCR analysis of *gata1* expression in 16 hpf wild type embryos (WT), *lzr/pbx4*$^{+/-}$ incross progeny injected with a full dose of *pbx2/4* MO (*pbx2/4* MO), *meis1*-morphant embryos (*meis1* MO), and *lzr/pbx4*$^{+/-}$ incross progeny injected with a full dose of both *pbx2/4* MO and *meis1* MO (*pbx2/4* MO; *meis1* MO). Shown is the relative quantity of *gata1* expression. Samples were normalized to *ef1a* and WT was set to 1. Error bars indicate standard deviation from the mean. *Indicates the difference compared with WT is significant by Student *t* test, $P < 0.0001$. **Indicates the difference compared with all other samples is significant by Student *t* test, $P < 0.0001$.

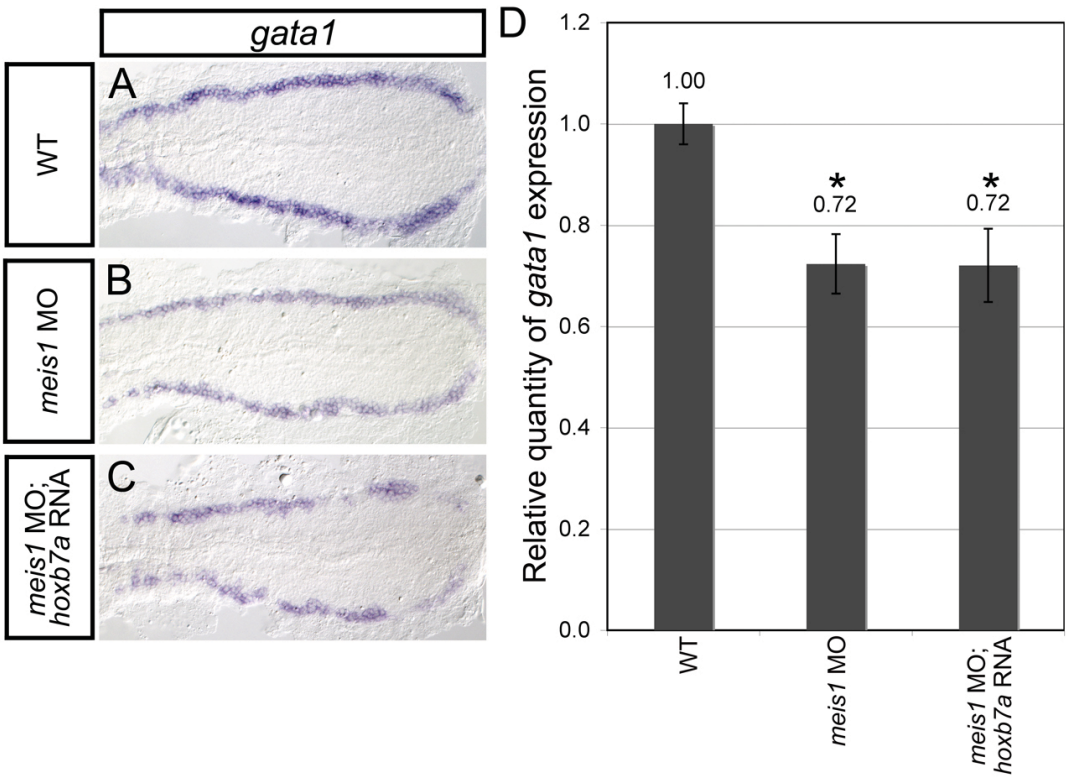

Figure 3.8. Overexpressing *hoxb7a* does not rescue *gata1* erythroid gene expression in *meis1*-morphant embryos. (A-C) Shown are representative embryos following *in situ* hybridization analysis of *gata1* expression in 16 hours post fertilization (hpf) embryos. Dorsal view of PLM gene expression is shown in flat-mounted and deyolked embryos, with anterior oriented to the left. Both *meis1*-morphant embryos (B) and *hoxb7a* RNA-injected *meis1*-morphant embryos (C) exhibit a severe decrease in *gata1* expression when compared to wild type embryos (WT; A). (D) Real-time quantitative PCR analysis of *gata1* expression in 16 hpf wild type embryos (WT), *meis1*-morphant embryos (*meis1* MO), and *hoxb7a* RNA-injected *meis1*-morphant embryos (*meis1* MO; *hoxb7a* RNA). Shown is the relative quantity of *gata1* expression. Samples were normalized to *ef1a* and WT was set to 1. Error bars indicate standard deviation from the mean. *Indicates the difference compared with WT is significant by Student *t* test; $P < 0.0001$.

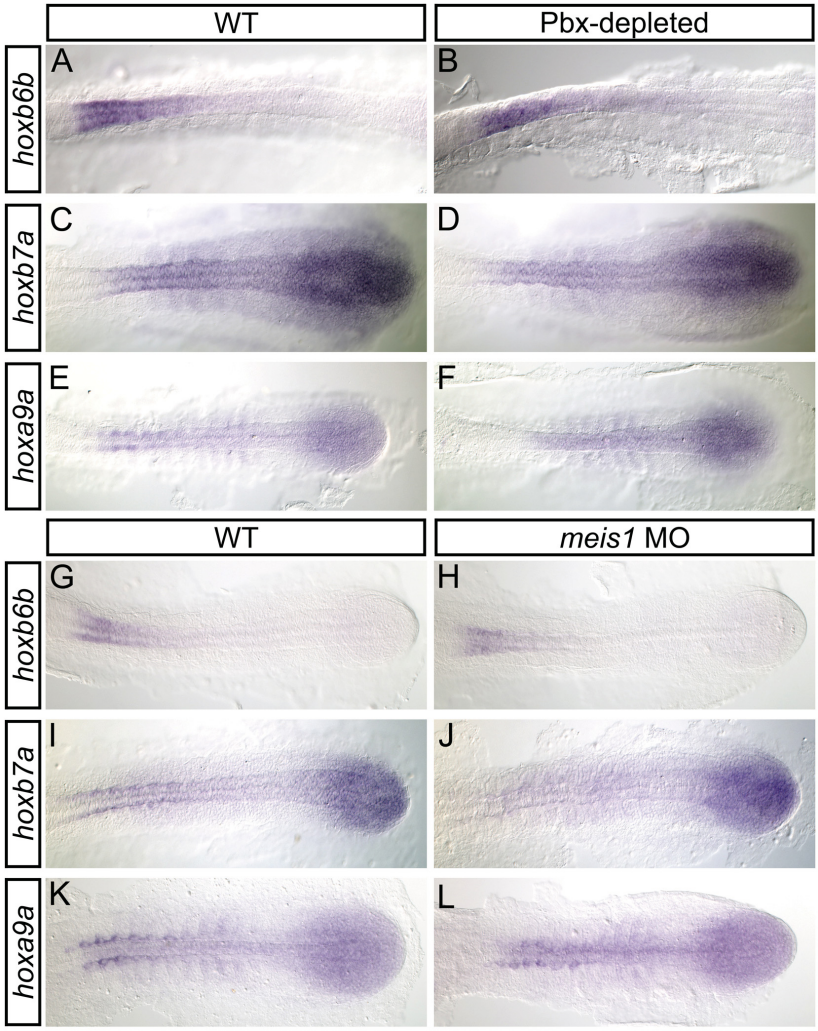

Figure 3.9. Pbx-depleted and *meis1*-morphant embryos exhibit normal posterior *hox* gene expression. Shown are representative embryos following *in situ* hybridization analyses of *hoxb6b* (A, B, G, H), *hoxb7a* (C, D, I, J), and *hoxa9a* (E, F, K, L) expression in wild type (WT; A, C, E, G, I, K), Pbx-depleted (B, D, F), and *meis1*-morphant (H, J, L) embryos. The PLM of 16 hours post fertilization (hpf) flat-mounted, deyolked embryos is shown in dorsal view with anterior oriented to left. In comparison to WT embryos, Pbx-depleted and *meis1*-morphant embryos exhibit normal *hoxb6b*, *hoxb7a*, and *hoxa9a* expression.

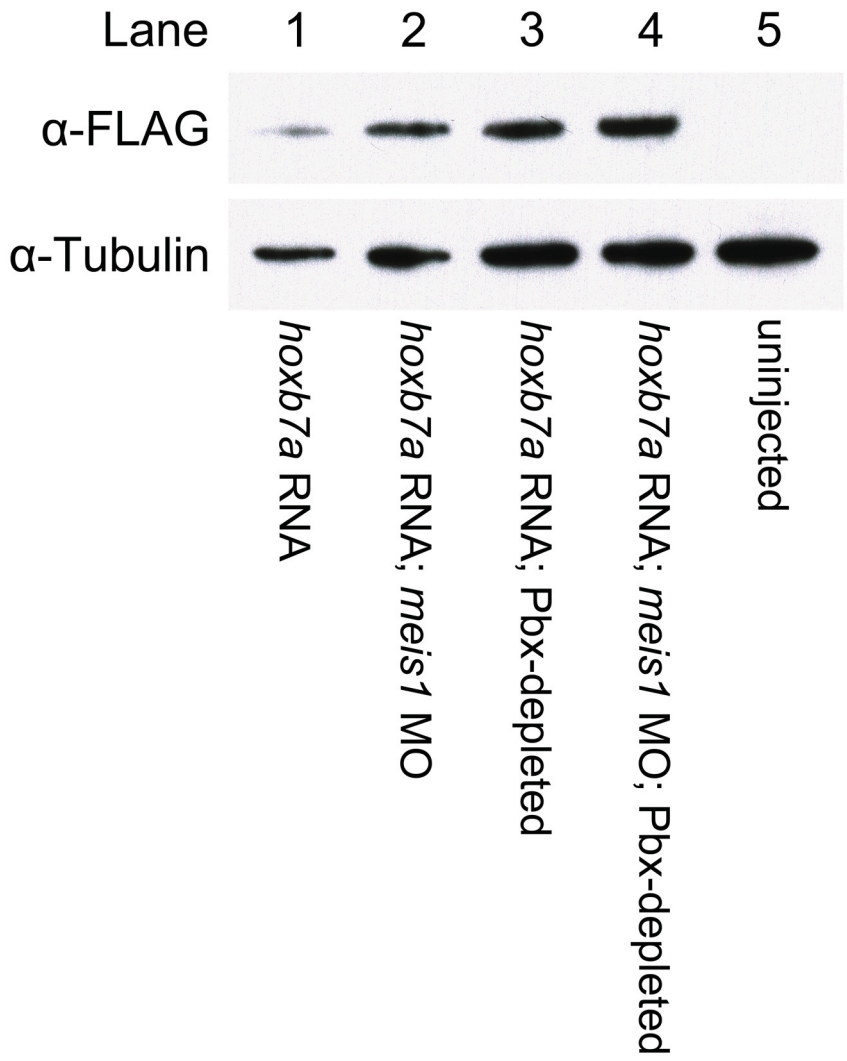

Figure 3.10. Hoxb7a stability is not dependent on the presence of Pbx or Meis1. Wild type, *meis1*-morphant, Pbx-depleted, or *meis1*-morphant; Pbx-depleted embryos were injected with FLAG-tagged *hoxb7a* RNA. Cell lysates from 14 hours post fertilization (hpf) embryos were analyzed by Western blot with α-FLAG antibody, and α-Tubulin antibody (loading control). Hoxb7a is present in roughly equivalent amounts in wild type (Lane 1), *meis1*-morphant (Lane 2), Pbx-depleted (Lane 3), and *meis1*-morphant; Pbx-depleted (Lane 4) embryos.

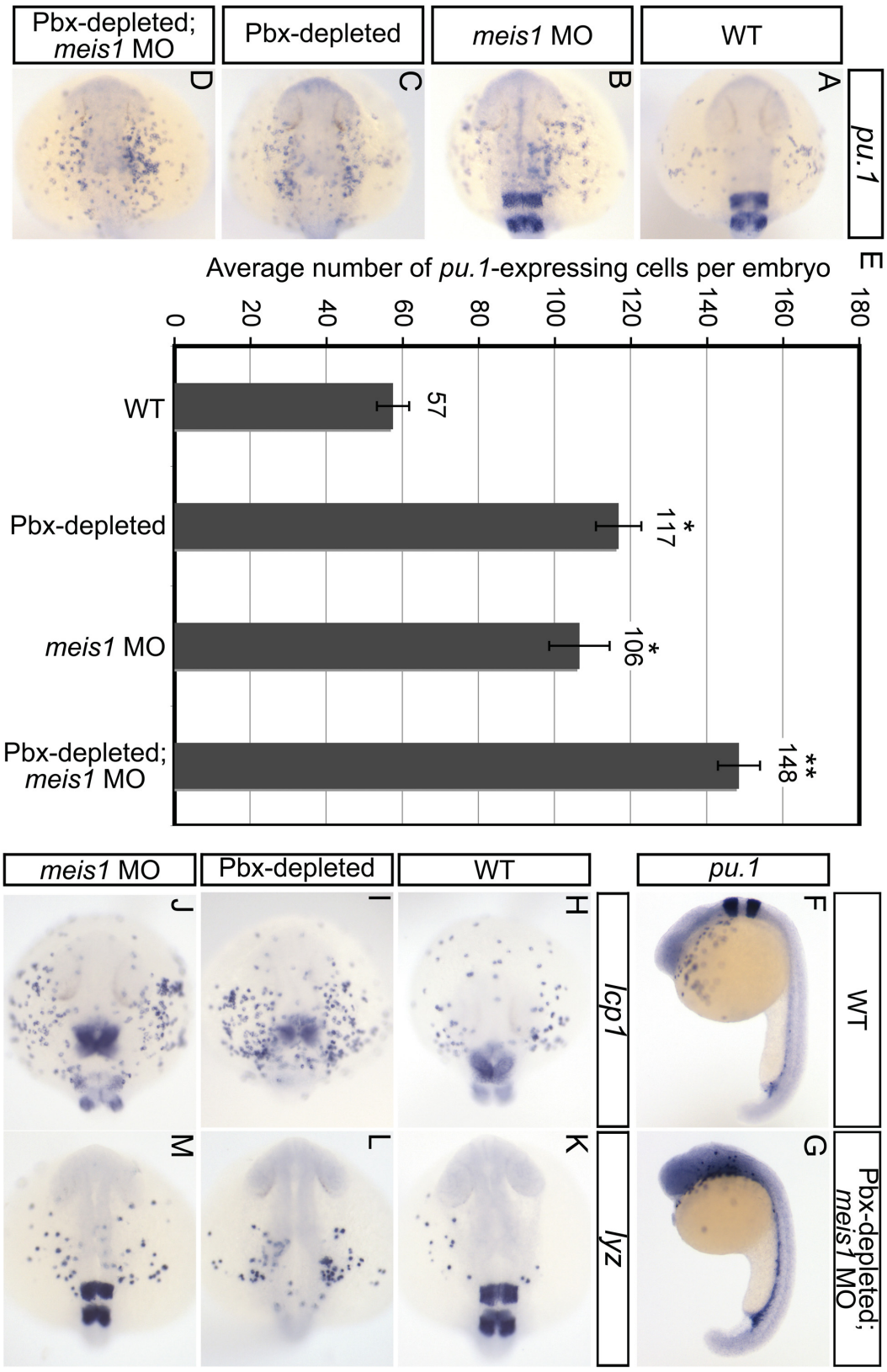
Pbx-depleted; meis1 MO
Pbx-depleted
meis1 MO
WT
A
B
C
D
pu.1
E
Average number of pu.1-expressing cells per embryo
0
20
40
60
80
100
120
140
160
180
WT
Pbx-depleted
meis1 MO
Pbx-depleted; meis1 MO
57
*
117
*
106
**
148
meis1 MO
Pbx-depleted
WT
pu.1
J
I
H
F
lcp1
WT
M
L
K
G
lyz
Pbx-depleted; meis1 MO

Figure 3.11. Pbx and Meis1 act in a cooperative fashion to regulate primitive myelopoietic gene expression. (A-D) Shown are representative embryos following *in situ* hybridization analysis of *pu.1* expression in 24 hours post fertilization (hpf) embryos. Dorsal view of gene expression in the anterior lateral-plate mesoderm (ALPM) is shown in whole-mount embryos with anterior oriented to the left. *meis1*-morphant (B), Pbx-depleted (C), and *meis1*-morphant; Pbx-depleted (D) embryos exhibit a severe increase in the number of *pu.1*-expressing cells when compared to wild type (WT; A) embryos. (E) Quantification of the phenotypes shown in A-D. Shown is the average number of *pu.1*-expressing cells in the ALPM of 24 hpf embryos as determined by *in situ* hybridization. Error bars indicate standard error of the mean. *Indicates the difference compared with WT is significant by Student *t* test; $P < 0.0001$. **Indicates the difference compared to all other samples is significant by Student *t* test; $P < 0.001$. (F-M) Shown are representative embryos following *in situ* hybridization analysis of *pu.1* (F, G) in lateral view, and *l-plastin* (*lcp1*; H-J) and *lysozyme C* (*lyz*; K-M) expression in dorsal view 24 hpf whole-mount embryos. Pbx-depleted; *meis1*-morphant embryos (G) exhibit upregulated *pu.1* expression in the intermediate cell mass when compared to WT embryos (F). Pbx-depleted (I, L), and *meis1*-morphant (J, M) embryos exhibit increased numbers of *lcp1* and *lyz*-positive cells in the ALPM when compared to WT embryos (H, K). Genotype of embryos was determined by *in situ* hybridization analysis of *egr2b* (F-M) and *eng2a* (H-J) expression.

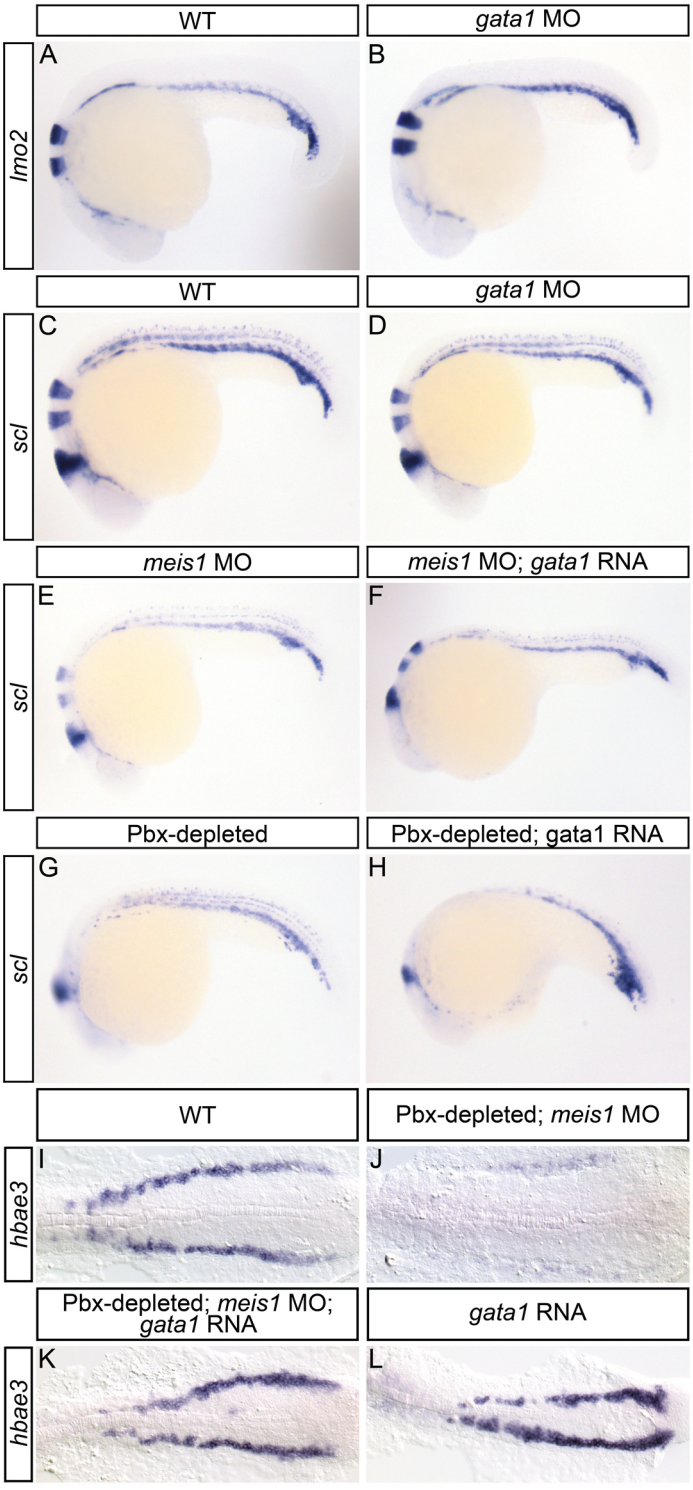
WT
gata1 MO
A
B
lmo2
WT
gata1 MO
C
D
scl
meis1 MO
meis1 MO; gata1 RNA
E
F
scl
Pbx-depleted
Pbx-depleted; gata1 RNA
G
H
scl
WT
Pbx-depleted; meis1 MO
I
J
hbae3
Pbx-depleted; meis1 MO; gata1 RNA
gata1 RNA
K
L
hbae3

Figure 3.12. Pbx and Meis1 act upstream of *gata1* to regulate the expression of *hbae3* and *scl*, but not *lmo2*. (A-H) Shown are representative embryos following *in situ* hybridization analyses of *lmo2* and *scl* expression in lateral view 24 hours post fertilization (hpf) whole-mount embryos. *gata1*-morphant embryos (B) exhibit near normal *lmo2* expression when compared to WT embryos (A). *gata1*-morphant (D), *meis1*-morphant (E), and Pbx-depleted (G) embryos exhibit diminished *scl* expression in the ICM when compared to wild type (WT; C) embryos. *meis1*-morphant, *gata1* RNA-injected embryos (F), and Pbx-depleted, *gata1* RNA-injected embryos (H) exhibit greater levels of *scl* expression than respective *meis1*-morphant (E) and Pbx-depleted (G) counterparts. Genotype of embryos was determined by *in situ* hybridization analysis of *egr2b* expression in hindbrain rhombomeres 3 and 5 (A-H), and *eng2a* expression in the midbrain hindbrain boundary and muscle pioneers (C-H). (I-L) Shown are representative embryos following *in situ* hybridization analysis of *hbae3* expression in 16 hpf embryos. Dorsal view of PLM gene expression is shown in deyolked, flat-mounted embryos with anterior oriented to the left. Pbx-depleted; *meis1*-morphant embryos (J) exhibit nearly abolished *hbae3* expression when compared to WT embryos (I). *gata1* RNA-injected, Pbx-depleted; *meis1*-morphant embryos (K) exhibit near normal *hbae3* expression. *gata1* RNA-injected embryos (L) exhibit slightly increased *hbae3* expression when compared to WT embryos (I).

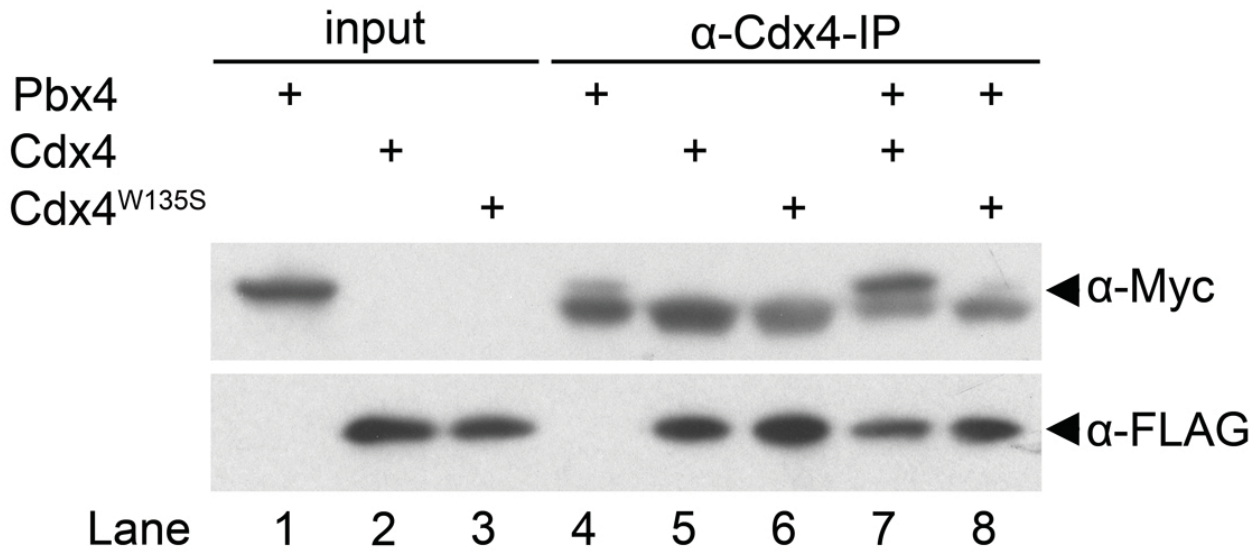

Figure 3.13. Pbx4 interacts with wild type, but not mutant Cdx4. Myc-tagged Pbx4 and FLAG-tagged wild type (WT) or mutant Cdx4 *in vitro* transcribed and translated proteins were co-immunoprecipitated with anti-FLAG agarose in the presence of a canonical Cdx/Pbx-binding DNA oligonucleotide, then analyzed by Western blot. A low level of Pbx4 is detected in the absence of Cdx4 (Lane 4), indicating that some non-specific binding of Pbx4 to the anti-FLAG agarose has occurred. Pbx4 is detected in the presence of WT Cdx4 (Lane 7). Pbx4 protein is not detected in the presence of a mutant form Cdx4 ($Cdx4^{W135S}$), in which the putative Pbx-interaction domain (PID) tryptophan residue is replaced with serine (Lane 8; compare to Lane 7).

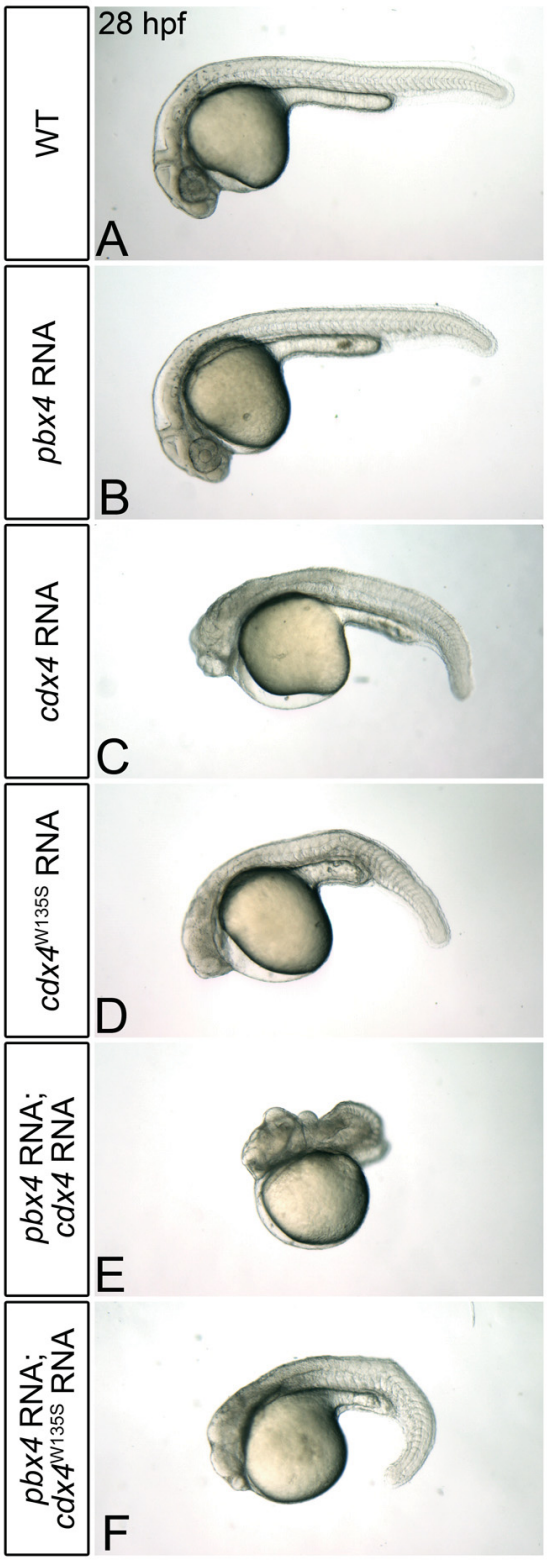

Figure 3.14. Pbx4 has the capacity to interact with wild type, but not mutant Cdx4 *in vivo*. (A-F) Shown are representative 28 hours post fertilization (hpf) embryos following the injection of wild type or mutant *cdx4* RNA and/or *pbx4* RNA. For *cdx4*^{W135S} RNA, the putative Pbx-interaction domain (PID) tryptophan residue was replaced with serine. Compared to wild type uninjected embryos (WT; A), overexpression of *pbx4* generates no morphological abnormalities (B). Overexpression of *cdx4* (C) or *cdx4*^{W135S} (D) produces mild posteriorization. Overexpression of *cdx4* with *pbx4* generates a severe morphological phenotype (E). Overexpression of *cdx4*^{W135S} with *pbx4* produces mild posteriorization (F).

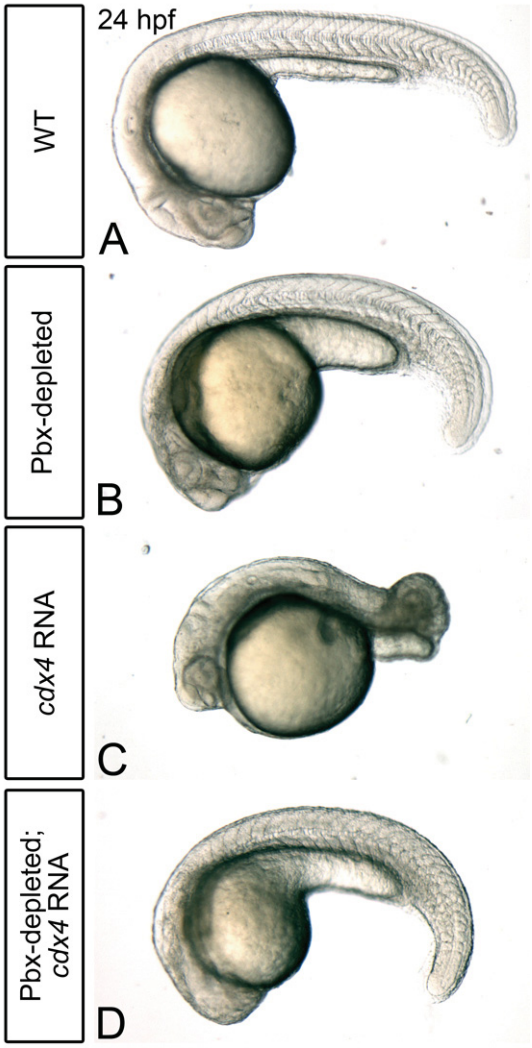

Figure 3.15. The *cdx4*-overexpression phenotype is partially rescued by loss of Pbx. (A-D) Shown are representative 28 hours post fertilization (hpf) uninjected or *cdx4*-overexpressing wild type (WT) or Pbx-depleted embryos. Compared to WT uninjected embryos (A), and Pbx-depleted embryos (B), *cdx4* overexpression (C) produces mild posteriorization. *cdx4* overexpression in Pbx-depleted embryos (D) produces a less severe phenotype than *cdx4* overexpression on a WT background (C).

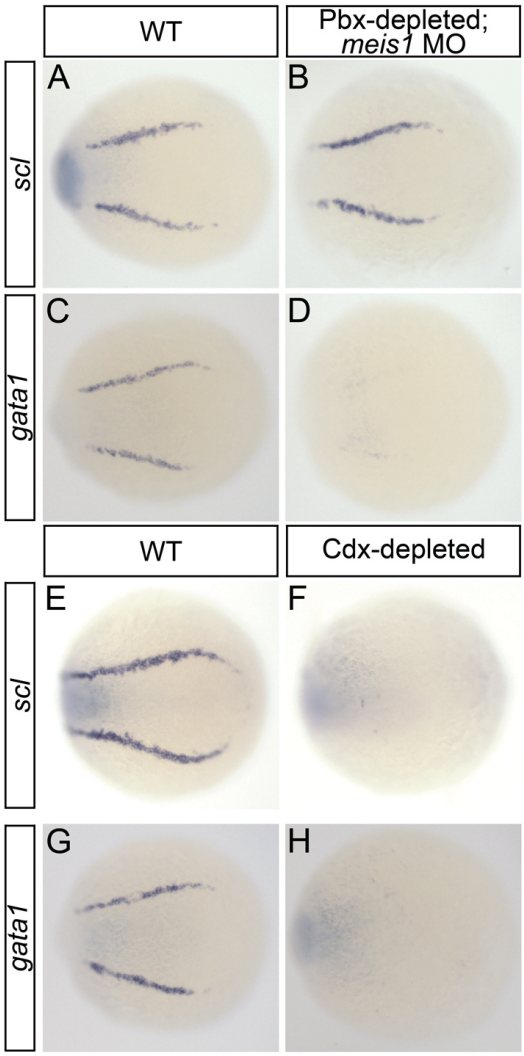

Figure 3.16. Unlike Cdx, Meis1 and Pbx function downstream of *scl* to activate *gata1* expression. (A-H) Shown are representative embryos following *in situ* hybridization analysis of *scl* and *gata1* expression in 12 hours post fertilization (hpf) embryos. Dorsal view of gene expression in the posterior lateral-plate mesoderm (PLM) is shown in whole-mount embryos with anterior oriented to the left. Pbx-depleted; *meis1*-morphant embryos exhibit wild type (WT) levels of *scl* expression (B) and abolished *gata1* expression (D) when compared to WT (A, C) embryos. Genotype of Pbx-depleted; *meis1*-morphant embryos was determined by *in situ* hybridization analysis of *egr2b* expression. Cdx-depleted embryos exhibit abolished *scl* (F) and *gata1* (H) expression when compared to WT (E, G) embryos.

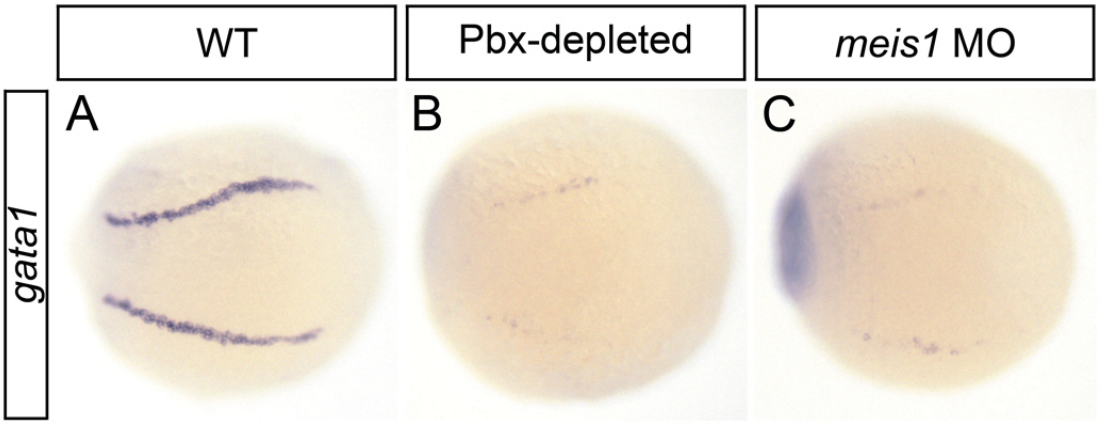

Figure 3.17. Meis1 and Pbx are required for normal activation of *gata1* expression. Shown are representative embryos following *in situ* hybridization analysis of *gata1* expression in 12 hours post fertilization (hpf) embryos. Dorsal view of gene expression in the posterior lateral-plate mesoderm is shown in whole-mount embryos with anterior oriented to the left. Pbx-depleted (B) and *meis1*-morphant (C) embryos exhibit abolished *gata1* expression when compared to wild type (WT; A).

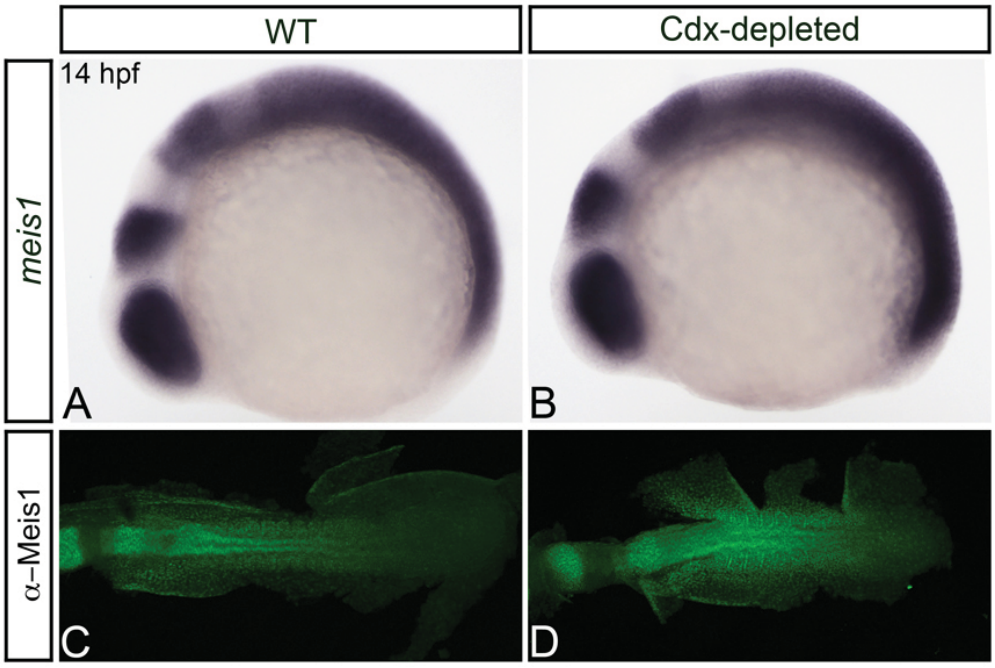

Figure 3.18. Cdx-depleted embryos exhibit slightly increased levels of Meis1. (A, B) Shown are representative embryos following *in situ* hybridization analysis of *meis1* expression in wild type (WT; A) compared with Cdx-depleted (B) embryos. The PLM of 14 hours post fertilization (hpf) flat-mounted, deyolked embryos is shown in dorsal view with anterior to left. *meis1* expression is increased in the posterior of Cdx-depleted embryos (B) when compared to WT (A). (C, D) Shown are representative embryos following immunohistochemical staining with the P2A6 antibody to visualize Meis1 protein levels in 14 hpf wild type (C) and Cdx-depleted (D) embryos. Flat-mount; dorsal view of embryo; anterior to left. Embryos are visualized under a 10X objective. Meis1 antibody staining is increased in Cdx-depleted embryos (D) when compared to WT (C).

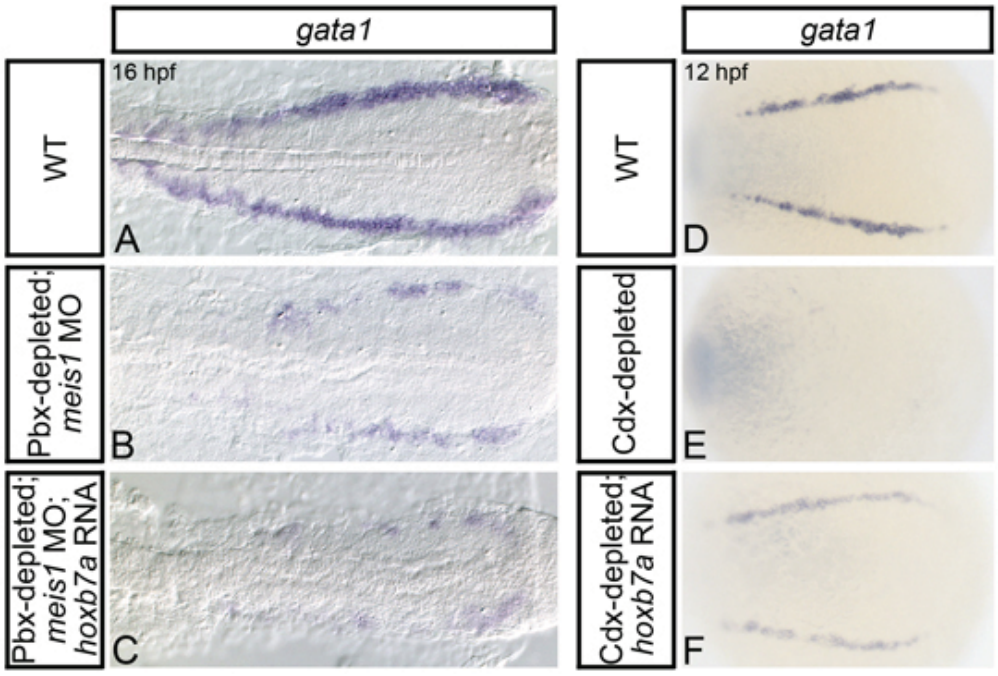

Figure 3.19. Overexpressing *hoxb7a* rescues *gata1* erythroid gene expression in Cdx-depleted embryos, but not in Pbx-depleted; *meis1*-morphant embryos. Shown are representative embryos following *in situ* hybridization analysis of *gata1* expression. (A-C) Dorsal view of PLM gene expression is shown in 16 hours post fertilization (hpf) flat-mounted and deyolked embryos, with anterior oriented to the left. Both Pbx-depleted; *meis1*-morphant embryos (B) and *hoxb7a* RNA-injected Pbx-depleted; *meis1*-morphant embryos (C) exhibit a severe decrease in *gata1* expression when compared to wild type embryos (WT; A). (D-F) Dorsal view of PLM gene expression is shown 12 hpf whole-mount embryos, with anterior oriented to the left. Cdx-depleted embryos (E) exhibit a notable decrease in *gata1* expression when compared to WT embryos (D). Cdx-depleted, *hoxb7a* RNA-injected embryos (F) exhibit greater levels of *gata1* expression than Cdx-depleted embryos (E).

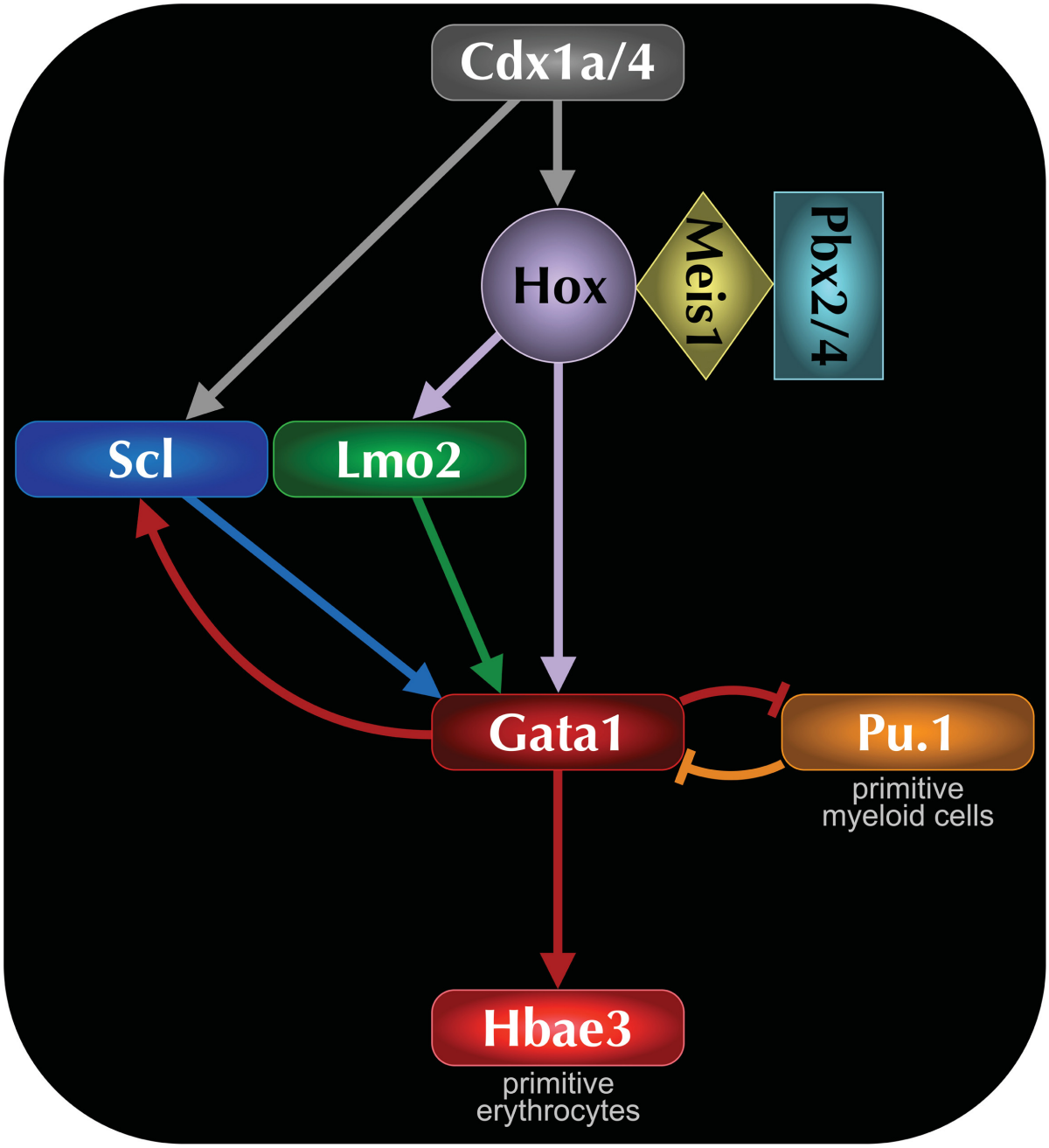

Figure 3.20. Model of Pbx and Meis1 function in primitive hematopoiesis. Hierarchical model indicating the genetic interactions that occur between a subset of transcription factors that regulate zebrafish primitive hematopoiesis. Arrows do not necessarily represent direct interactions.

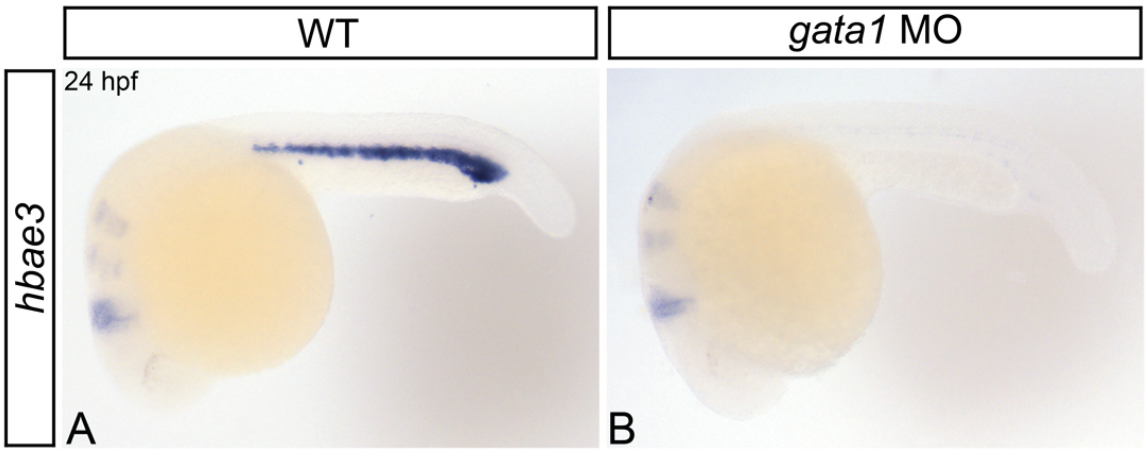

Figure 3.21. *gata1*-morphant embryos exhibit nearly abolished *hbae3* expression. Shown are representative embryos following *in situ* hybridization analysis of *hbae3* expression in wild type (WT; A) compared with *gata1*-morphant (B) embryos. 24 hours post fertilization (hpf) whole-mount embryos are shown in lateral view with anterior to left. *eng2a* expression in the midbrain hindbrain boundary and muscle pioneers and *egr2b* expression in hindbrain rhombomeres 3 and 5 is shown in all panels. *hbae3* expression is nearly abolished in the ICM of *gata1*-morphant embryos (B) when compared to WT (A).

3.5 Tables

Table 3.1: Quantification of blood phenotypes of 48 hpf *meis1*-morphant and Pbx-depleted embryos.

Treatment	Wild type	No blood	Total	Two-tailed *P*-value
WT	140	0	140	
meis1 MO	60	121	181	<0.0001*
Pbx-depleted	36	30	66	<0.0001*

*Indicates significant result compared to wild type (WT), by Fisher's Exact Test on cumulative raw counts.

Table 3.2: Quantification of primitive hematopoietic gene expression defects of *meis1*-morphants.

Gene	Stage	Treatment	Wild type	Abnormal	Total	Two-tailed *P*-value
gata1	16 hpf	WT	48	0	48	
		meis1 MO	6	33	39	<0.0001*
gata1	24 hpf	WT	53	0	53	
		meis1 MO	4	48	52	<0.0001*
kdrl	16 hpf	WT	34	0	34	
		meis1 MO	21	0	21	1.000
scl	16 hpf	WT	43	0	43	
		meis1 MO	3	26	29	<0.0001*
scl	24 hpf	WT	40	0	40	
		meis1 MO	1	34	35	<0.0001*
lmo2	16 hpf	WT	48	0	48	
		meis1 MO	5	19	24	<0.0001*
lmo2	24 hpf	WT	41	0	41	
		meis1 MO	3	33	36	<0.0001*

*Indicates significant result compared to wild type (WT), by Fisher's Exact Test on cumulative raw counts.

Table 3.3: Quantification of primitive hematopoietic gene expression defects of Pbx-depleted embryos.

Gene	Stage	Treatment	Wild type	Abnormal	Total	Two-tailed *P*-value
gata1	16 hpf	WT	36	0	36	
		Pbx-depleted	7	24	31	<0.0001*
gata1	24 hpf	WT	64	0	64	
		Pbx-depleted	8	58	66	<0.0001*
kdrl	16 hpf	WT	32	0	32	
		Pbx-depleted	31	0	31	1.000
scl	16 hpf	WT	43	0	43	
		Pbx-depleted	2	18	20	<0.0001*
scl	24 hpf	WT	36	0	36	
		Pbx-depleted	3	27	30	<0.0001*
lmo2	16 hpf	WT	48	0	48	
		Pbx-depleted	3	28	31	<0.0001*
lmo2	24 hpf	WT	43	0	43	
		Pbx-depleted	2	30	32	<0.0001*

*Indicates significant result compared to wild type (WT), by Fisher's Exact Test on cumulative raw counts.

Table 3.4: Quantification of *gata1* expression in 16 hpf *meis1*-morphants with and without *hoxb7a* overexpression.

Treatment	Wild type	Reduced	Total	Two-tailed *P*-value
WT	54	0	54	
meis1 MO	4	59	63	<0.0001*
meis1 MO; *hoxb7a* RNA	4	39	43	<0.0001*

*Indicates significant result compared to wild type (WT), by Fisher's Exact Test on cumulative raw counts.

Table 3.5: Quantification of primitive myeloid defects of *meis1*-morphant and Pbx-depleted embryos.

Treatment	Mean cell number	SEM	*n*	Two-tailed *P*-value	Two-tailed *P*-value	Two-tailed *P*-value
WT	57	4	14			
meis1 MO	106	8	14	<0.0001*		
Pbx-depleted	117	6	18	<0.0001*		
meis1 MO; Pbx-depleted	148	6	15	<0.0001*	0.0006**	0.0002***

*Indicates significant result compared to wild type (WT) by Student *t* test.

**Indicates a significant result compared to *meis1*-morphants by Student *t* test.

***Indicates a significant result compared to Pbx-depleted embryos by Student *t* test.

3.6 References

Abu-Shaar, M., H.D. Ryoo, and R.S. Mann. 1999. Control of the nuclear localization of Extradenticle by competing nuclear import and export signals. *Genes Dev*. 13:935-945.

Amali, A.A., L. Sie, C. Winkler, and M. Featherstone. 2013. Zebrafish hoxd4a acts upstream of meis1.1 to direct vasculogenesis, angiogenesis and hematopoiesis. *PloS one*. 8:e58857.

Anderson, K.L., K.A. Smith, K. Conners, S.R. McKercher, R.A. Maki, and B.E. Torbett. 1998. Myeloid development is selectively disrupted in PU.1 null mice. *Blood*. 91:3702-3710.

Azcoitia, V., M. Aracil, A.C. Martinez, and M. Torres. 2005. The homeodomain protein Meis1 is essential for definitive hematopoiesis and vascular patterning in the mouse embryo. *Dev Biol*. 280:307-320.

Baumann, R., and S. Dragon. 2005. Erythropoiesis and red cell function in vertebrate embryos. *Eur J Clin Invest*. 35 Suppl 3:2-12.

Berthelsen, J., C. Kilstrup-Nielsen, F. Blasi, F. Mavilio, and V. Zappavigna. 1999. The subcellular localization of PBX1 and EXD proteins depends on nuclear import and export signals and is modulated by association with PREP1 and HTH. *Genes Dev*. 13:946-953.

Berthelsen, J., V. Zappavigna, E. Ferretti, F. Mavilio, and F. Blasi. 1998a. The novel homeoprotein Prep1 modulates Pbx-Hox protein cooperativity. *EMBO J*. 17:1434-1445.

Berthelsen, J., V. Zappavigna, F. Mavilio, and F. Blasi. 1998b. Prep1, a novel functional partner of Pbx proteins. *EMBO J*. 17:1423-1433.

Bjornsson, J.M., N. Larsson, A.C. Brun, M. Magnusson, E. Andersson, P. Lundstrom, J. Larsson, E. Repetowska, M. Ehinger, R.K. Humphries, and S. Karlsson. 2003. Reduced proliferative capacity of hematopoietic stem cells deficient in Hoxb3 and Hoxb4. *Mol Cell Biol*. 23:3872-3883.

Brun, A.C., J.M. Bjornsson, M. Magnusson, N. Larsson, P. Leveen, M. Ehinger, E. Nilsson, and S. Karlsson. 2004. Hoxb4-deficient mice undergo normal hematopoietic development but exhibit a mild proliferation defect in hematopoietic stem cells. *Blood*. 103:4126-4133.

Chang, C.P., L. Brocchieri, W.F. Shen, C. Largman, and M.L. Cleary. 1996. Pbx modulation of Hox homeodomain amino-terminal arms establishes different DNA-binding specificities across the Hox locus. *Mol Cell Biol*. 16:1734-1745.

Chang, C.P., Y. Jacobs, T. Nakamura, N.A. Jenkins, N.G. Copeland, and M.L. Cleary. 1997. Meis proteins are major in vivo DNA binding partners for wild-type but not chimeric Pbx proteins. *Mol Cell Biol*. 17:5679-5687.

Chang, C.P., W.F. Shen, S. Rozenfeld, H.J. Lawrence, C. Largman, and M.L. Cleary. 1995. Pbx proteins display hexapeptide-dependent cooperative DNA binding with a subset of Hox proteins. *Genes Dev*. 9:663-674.

Cooper, K.L., W.M. Leisenring, and C.B. Moens. 2003. Autonomous and nonautonomous functions for Hox/Pbx in branchiomotor neuron development. *Dev Biol*. 253:200-213.

Cvejic, A., J. Serbanovic-Canic, D.L. Stemple, and W.H. Ouwehand. 2011. The role of meis1 in primitive and definitive hematopoiesis during zebrafish development. *Haematologica*. 96:190-198.

Davidson, A.J., P. Ernst, Y. Wang, M.P. Dekens, P.D. Kingsley, J. Palis, S.J. Korsmeyer, G.Q. Daley, and L.I. Zon. 2003. cdx4 mutants fail to specify blood progenitors and can be rescued by multiple hox genes. *Nature*. 425:300-306.

Davidson, A.J., and L.I. Zon. 2006. The caudal-related homeobox genes cdx1a and cdx4 act redundantly to regulate hox gene expression and the formation of putative hematopoietic stem cells during zebrafish embryogenesis. *Dev Biol*. 292:506-518.

Di Rosa, P., J.C. Villaescusa, E. Longobardi, G. Iotti, E. Ferretti, V.M. Diaz, A. Miccio, G. Ferrari, and F. Blasi. 2007. The homeodomain transcription factor Prep1 (pKnox1) is required for hematopoietic stem and progenitor cell activity. *Dev Biol*. 311:324-334.

DiMartino, J.F., L. Selleri, D. Traver, M.T. Firpo, J. Rhee, R. Warnke, S. O'Gorman, I.L. Weissman, and M.L. Cleary. 2001. The Hox cofactor and proto-oncogene Pbx1 is required for maintenance of definitive hematopoiesis in the fetal liver. *Blood*. 98:618-626.

Dooley, K.A., A.J. Davidson, and L.I. Zon. 2005. Zebrafish scl functions independently in hematopoietic and endothelial development. *Dev Biol*. 277:522-536.

Ferretti, E., H. Marshall, H. Popperl, M. Maconochie, R. Krumlauf, and F. Blasi. 2000. Segmental expression of Hoxb2 in r4 requires two separate sites that integrate cooperative interactions between Prep1, Pbx and Hox proteins. *Development*. 127:155-166.

Ferretti, E., J.C. Villaescusa, P. Di Rosa, L.C. Fernandez-Diaz, E. Longobardi, R. Mazzieri, A. Miccio, N. Micali, L. Selleri, G. Ferrari, and F. Blasi. 2006. Hypomorphic mutation of the TALE gene Prep1 (pKnox1) causes a major reduction of Pbx and Meis proteins and a pleiotropic embryonic phenotype. *Mol Cell Biol*. 26:5650-5662.

Galloway, J.L., R.A. Wingert, C. Thisse, B. Thisse, and L.I. Zon. 2005. Loss of gata1 but not gata2 converts erythropoiesis to myelopoiesis in zebrafish embryos. *Dev Cell*. 8:109-116.

Gering, M., A.R. Rodaway, B. Gottgens, R.K. Patient, and A.R. Green. 1998. The SCL gene specifies haemangioblast development from early mesoderm. *EMBO J*. 17:4029-4045.

Gering, M., Y. Yamada, T.H. Rabbitts, and R.K. Patient. 2003. Lmo2 and Scl/Tal1 convert non-axial mesoderm into haemangioblasts which differentiate into endothelial cells in the absence of Gata1. *Development*. 130:6187-6199.

Gottgens, B., A. Nastos, S. Kinston, S. Piltz, E.C. Delabesse, M. Stanley, M.J. Sanchez, A. Ciau-Uitz, R. Patient, and A.R. Green. 2002. Establishing the transcriptional programme for blood: the SCL stem cell enhancer is regulated by a multiprotein complex containing Ets and GATA factors. *EMBO J*. 21:3039-3050.

Hall, C., M.V. Flores, T. Storm, K. Crosier, and P. Crosier. 2007. The zebrafish lysozyme C promoter drives myeloid-specific expression in transgenic fish. *BMC Dev Biol*. 7:42.

Hisa, T., S.E. Spence, R.A. Rachel, M. Fujita, T. Nakamura, J.M. Ward, D.E. Devor-Henneman, Y. Saiki, H. Kutsuna, L. Tessarollo, N.A. Jenkins, and N.G. Copeland. 2004. Hematopoietic, angiogenic and eye defects in Meis1 mutant animals. *EMBO J*. 23:450-459.

Hove, J.R., R.W. Koster, A.S. Forouhar, G. Acevedo-Bolton, S.E. Fraser, and M. Gharib. 2003. Intracardiac fluid forces are an essential epigenetic factor for embryonic cardiogenesis. *Nature*. 421:172-177.

Iwasaki, H., S. Mizuno, R.A. Wells, A.B. Cantor, S. Watanabe, and K. Akashi. 2003. GATA-1 converts lymphoid and myelomonocytic progenitors into the megakaryocyte/erythrocyte lineages. *Immunity*. 19:451-462.

Izon, D.J., S. Rozenfeld, S.T. Fong, L. Komuves, C. Largman, and H.J. Lawrence. 1998. Loss of function of the homeobox gene Hoxa-9 perturbs early T-cell development and induces apoptosis in primitive thymocytes. *Blood*. 92:383-393.

Jacobs, Y., C.A. Schnabel, and M.L. Cleary. 1999. Trimeric association of Hox and TALE homeodomain proteins mediates Hoxb2 hindbrain enhancer activity. *Mol Cell Biol*. 19:5134-5142.

Kappen, C. 2000. Disruption of the homeobox gene Hoxb-6 in mice results in increased numbers of early erythrocyte progenitors. *Am J Hematol*. 65:111-118.

Kilstrup-Nielsen, C., M. Alessio, and V. Zappavigna. 2003. PBX1 nuclear export is regulated independently of PBX-MEINOX interaction by PKA phosphorylation of the PBC-B domain. *EMBO J*. 22:89-99.

Knoepfler, P.S., K.R. Calvo, H. Chen, S.E. Antonarakis, and M.P. Kamps. 1997. Meis1 and pKnox1 bind DNA cooperatively with Pbx1 utilizing an interaction surface disrupted in oncoprotein E2a-Pbx1. *Proc Natl Acad Sci U S A*. 94:14553-14558.

Ko, K.H., Q.L. Lam, M. Zhang, C.K. Wong, C.K. Lo, M. Kahmeyer-Gabbe, W.H. Tsang, S.L. Tsang, L.C. Chan, M.H. Sham, and L. Lu. 2007. Hoxb3 deficiency impairs B lymphopoiesis in mouse bone marrow. *Exp Hematol*. 35:465-475.

Lawrence, H.J., C.D. Helgason, G. Sauvageau, S. Fong, D.J. Izon, R.K. Humphries, and C. Largman. 1997. Mice bearing a targeted interruption of the homeobox gene HOXA9 have defects in myeloid, erythroid, and lymphoid hematopoiesis. *Blood*. 89:1922-1930.

Le Guyader, D., M.J. Redd, E. Colucci-Guyon, E. Murayama, K. Kissa, V. Briolat, E. Mordelet, A. Zapata, H. Shinomiya, and P. Herbomel. 2008. Origins and unconventional behavior of neutrophils in developing zebrafish. *Blood*. 111:132-141.

Lyons, S.E., N.D. Lawson, L. Lei, P.E. Bennett, B.M. Weinstein, and P.P. Liu. 2002. A nonsense mutation in zebrafish gata1 causes the bloodless phenotype in vlad tepes. *Proc Natl Acad Sci U S A*. 99:5454-5459.

Magnusson, M., A.C. Brun, H.J. Lawrence, and S. Karlsson. 2007a. Hoxa9/hoxb3/hoxb4 compound null mice display severe hematopoietic defects. *Exp Hematol*. 35:1421-1428.

Magnusson, M., A.C. Brun, N. Miyake, J. Larsson, M. Ehinger, J.M. Bjornsson, A. Wutz, M. Sigvardsson, and S. Karlsson. 2007b. HOXA10 is a critical regulator for hematopoietic stem cells and erythroid/megakaryocyte development. *Blood*. 109:3687-3696.

Mann, R.S., and S.K. Chan. 1996. Extra specificity from extradenticle: the partnership between HOX and PBX/EXD homeodomain proteins. *Trends Genet*. 12:258-262.

Maves, L., A.J. Waskiewicz, B. Paul, Y. Cao, A. Tyler, C.B. Moens, and S.J. Tapscott. 2007. Pbx homeodomain proteins direct Myod activity to promote fast-muscle differentiation. *Development*. 134:3371-3382.

McKercher, S.R., B.E. Torbett, K.L. Anderson, G.W. Henkel, D.J. Vestal, H. Baribault, M. Klemsz, A.J. Feeney, G.E. Wu, C.J. Paige, and R.A. Maki. 1996. Targeted disruption of

the PU.1 gene results in multiple hematopoietic abnormalities. *EMBO J*. 15:5647-5658.

McNulty, C.L., J.N. Peres, N. Bardine, W.M. van den Akker, and A.J. Durston. 2005. Knockdown of the complete Hox paralogous group 1 leads to dramatic hindbrain and neural crest defects. *Development*. 132:2861-2871.

Mercader, N., E. Leonardo, N. Azpiazu, A. Serrano, G. Morata, C. Martinez, and M. Torres. 1999. Conserved regulation of proximodistal limb axis development by Meis1/Hth. *Nature*. 402:425-429.

Minehata, K., A. Kawahara, and T. Suzuki. 2008. meis1 regulates the development of endothelial cells in zebrafish. *Biochem Biophys Res Commun*. 374:647-652.

Moens, C.B., and L. Selleri. 2006. Hox cofactors in vertebrate development. *Dev Biol*. 291:193-206.

Nerlov, C., E. Querfurth, H. Kulessa, and T. Graf. 2000. GATA-1 interacts with the myeloid PU.1 transcription factor and represses PU.1-dependent transcription. *Blood*. 95:2543-2551.

Orkin, S.H. 1992. GATA-binding transcription factors in hematopoietic cells. *Blood*. 80:575-581.

Orkin, S.H., and L.I. Zon. 2008. Hematopoiesis: an evolving paradigm for stem cell biology. *Cell*. 132:631-644.

Patterson, L.J., M. Gering, C.E. Eckfeldt, A.R. Green, C.M. Verfaillie, S.C. Ekker, and R. Patient. 2007. The transcription factors Scl and Lmo2 act together during development of the hemangioblast in zebrafish. *Blood*. 109:2389-2398.

Pevny, L., M.C. Simon, E. Robertson, W.H. Klein, S.F. Tsai, V. D'Agati, S.H. Orkin, and F. Costantini. 1991. Erythroid differentiation in chimaeric mice blocked by a targeted mutation in the gene for transcription factor GATA-1. *Nature*. 349:257-260.

Popperl, H., H. Rikhof, H. Chang, P. Haffter, C.B. Kimmel, and C.B. Moens. 2000. lazarus is a novel pbx gene that globally mediates hox gene function in zebrafish. *Mol Cell*. 6:255-267.

Rekhtman, N., F. Radparvar, T. Evans, and A.I. Skoultchi. 1999. Direct interaction of hematopoietic transcription factors PU.1 and GATA-1: functional antagonism in erythroid cells. *Genes Dev*. 13:1398-1411.

Rhodes, J., A. Hagen, K. Hsu, M. Deng, T.X. Liu, A.T. Look, and J.P. Kanki. 2005. Interplay of pu.1 and gata1 determines myelo-erythroid progenitor cell fate in zebrafish. *Dev Cell*. 8:97-108.

Rieckhof, G.E., F. Casares, H.D. Ryoo, M. Abu-Shaar, and R.S. Mann. 1997. Nuclear translocation of extradenticle requires homothorax, which encodes an extradenticle-related homeodomain protein. *Cell*. 91:171-183.

Ryoo, H.D., T. Marty, F. Casares, M. Affolter, and R.S. Mann. 1999. Regulation of Hox target genes by a DNA bound Homothorax/Hox/Extradenticle complex. *Development*. 126:5137-5148.

Sarno, J.L., H.J. Kliman, and H.S. Taylor. 2005. HOXA10, Pbx2, and Meis1 protein expression in the human endometrium: formation of multimeric complexes on HOXA10 target genes. *J Clin Endocrinol Metab*. 90:522-528.

Scott, E.W., M.C. Simon, J. Anastasi, and H. Singh. 1994. Requirement of transcription factor PU.1 in the development of multiple hematopoietic lineages. *Science*. 265:1573-1577.

Shanmugam, K., N.C. Green, I. Rambaldi, H.U. Saragovi, and M.S. Featherstone. 1999. PBX and MEIS as non-DNA-binding partners in trimeric complexes with HOX proteins. *Mol Cell Biol*. 19:7577-7588.

Shen, W.F., J.C. Montgomery, S. Rozenfeld, J.J. Moskow, H.J. Lawrence, A.M. Buchberg, and C. Largman. 1997a. AbdB-like Hox proteins stabilize DNA binding by the Meis1 homeodomain proteins. *Mol Cell Biol*. 17:6448-6458.

Shen, W.F., S. Rozenfeld, A. Kwong, L.G. Kom ves, H.J. Lawrence, and C. Largman. 1999. HOXA9 forms triple complexes with PBX2 and MEIS1 in myeloid cells. *Mol Cell Biol*. 19:3051-3061.

Shen, W.F., S. Rozenfeld, H.J. Lawrence, and C. Largman. 1997b. The Abd-B-like Hox homeodomain proteins can be subdivided by the ability to form complexes with Pbx1a on a novel DNA target. *J Biol Chem*. 272:8198-8206.

Shimamoto, T., Y. Tang, Y. Naot, M. Nardi, P. Brulet, C.J. Bieberich, and K. Takeshita. 1999. Hematopoietic progenitor cell abnormalities in Hoxc-8 null mutant mice. *J Exp Zool*. 283:186-193.

Shivdasani, R.A., Y. Fujiwara, M.A. McDevitt, and S.H. Orkin. 1997. A lineage-selective knockout establishes the critical role of transcription factor GATA-1 in megakaryocyte growth and platelet development. *EMBO J*. 16:3965-3973.

Shivdasani, R.A., E.L. Mayer, and S.H. Orkin. 1995. Absence of blood formation in mice lacking the T-cell leukaemia oncoprotein tal-1/SCL. *Nature*. 373:432-434.

Skromne, I., D. Thorsen, M. Hale, V.E. Prince, and R.K. Ho. 2007. Repression of the hindbrain developmental program by Cdx factors is required for the specification of the vertebrate spinal cord. *Development*. 134:2147-2158.

So, C.W., H. Karsunky, P. Wong, I.L. Weissman, and M.L. Cleary. 2004. Leukemic transformation of hematopoietic progenitors by MLL-GAS7 in the absence of Hoxa7 or Hoxa9. *Blood*. 103:3192-3199.

Stevens, K.E., and R.S. Mann. 2007. A balance between two nuclear localization sequences and a nuclear export sequence governs extradenticle subcellular localization. *Genetics*. 175:1625-1636.

Stopka, T., D.F. Amanatullah, M. Papetti, and A.I. Skoultchi. 2005. PU.1 inhibits the erythroid program by binding to GATA-1 on DNA and creating a repressive chromatin structure. *EMBO J*. 24:3712-3723.

Teoh, P.H., A.C. Shu-Chien, and W.K. Chan. 2010. Pbx1 is essential for growth of zebrafish swim bladder. *Dev Dyn*. 239:865-874.

Uhl, J.D., T.A. Cook, and B. Gebelein. 2010. Comparing anterior and posterior Hox complex formation reveals guidelines for predicting cis-regulatory elements. *Dev Biol*. 343:154-166.

Vlachakis, N., S.K. Choe, and C.G. Sagerstrom. 2001. Meis3 synergizes with Pbx4 and Hoxb1b in promoting hindbrain fates in the zebrafish. *Development*. 128:1299-1312.

Vlachakis, N., D.R. Ellstrom, and C.G. Sagerstrom. 2000. A novel pbx family member expressed during early zebrafish embryogenesis forms trimeric complexes with Meis3 and Hoxb1b. *Dev Dyn*. 217:109-119.

Warren, A.J., W.H. Colledge, M.B. Carlton, M.J. Evans, A.J. Smith, and T.H. Rabbitts. 1994. The oncogenic cysteine-rich LIM domain protein rbtn2 is essential for erythroid development. *Cell*. 78:45-57.

Waskiewicz, A.J., H.A. Rikhof, R.E. Hernandez, and C.B. Moens. 2001. Zebrafish Meis functions to stabilize Pbx proteins and regulate hindbrain patterning. *Development*. 128:4139-4151.

Waskiewicz, A.J., H.A. Rikhof, and C.B. Moens. 2002. Eliminating zebrafish pbx proteins reveals a hindbrain ground state. *Dev Cell*. 3:723-733.

Williams, T.M., M.E. Williams, and J.W. Innis. 2005. Range of HOX/TALE superclass associations and protein domain requirements for HOXA13:MEIS interaction. *Dev Biol*. 277:457-471.

Zhang, D.E., S. Hohaus, M.T. Voso, H.M. Chen, L.T. Smith, C.J. Hetherington, and D.G. Tenen. 1996. Function of PU.1 (Spi-1), C/EBP, and AML1 in early myelopoiesis: regulation of multiple myeloid CSF receptor promoters. *Curr Top Microbiol Immunol*. 211:137-147.

Zhang, P., G. Behre, J. Pan, A. Iwama, N. Wara-Aswapati, H.S. Radomska, P.E. Auron, D.G. Tenen, and Z. Sun. 1999. Negative cross-talk between hematopoietic regulators: GATA proteins repress PU.1. *Proc Natl Acad Sci U S A*. 96:8705-8710.

Zhang, P., X. Zhang, A. Iwama, C. Yu, K.A. Smith, B.U. Mueller, S. Narravula, B.E. Torbett, S.H. Orkin, and D.G. Tenen. 2000. PU.1 inhibits GATA-1 function and erythroid differentiation by blocking GATA-1 DNA binding. *Blood*. 96:2641-2648.

Chapter 4

Retinoic acid regulates definitive hematopoiesis

4.1 Introduction

All adult vertebrate hematopoietic lineages arise from a common multipotent progenitor, the hematopoietic stem cell (HSC). This definitive hematopoietic cell type is able to self renew, differentiate into all major blood lineages, and maintain adult hematopoiesis for life. HSC transplants are used to treat a spectrum of disease that ranges from anemia and other congenital blood disorders, to acute leukemia. Unfortunately, these cells are present in restrictive quantities, and recent *ex vivo* methods for expanding human HSCs for clinical therapies have achieved limited success. Identifying the molecular pathways that regulate HSC formation is therefore a major goal of both basic and clinical biology.

Although much is known about the cellular and functional properties of vertebrate HSCs, little information exists about the genetic pathways that govern HSC induction, expansion, and homeostasis. However, loss and gain of function analyses in mouse have implicated the retinoic Acid (RA) signaling pathway in vertebrate HSC formation. The Vitamin A derivative RA is an extremely potent diffusible morphogen. Consequently, its levels are tightly regulated within the developing embryo. The *aldehyde dehydrogenase 1a* (*aldh1a/Raldh*) genes encode the rate-limiting enzymes in RA synthesis, and high levels of RA occur in tissues that express them (Begemann and Meyer, 2001; Niederreither et al., 1999; Niederreither et al., 2000). Mouse *Aldh1a2* (*Raldh2*) mutants strongly recapitulate phenotypes associated with vitamin A deficiency, suggesting that Aldh1a2 is the main source of RA in the vertebrate embryo (Niederreither et al., 1999; Niederreither et al., 2000). Once synthesized, RA binds nuclear retinoic acid receptor and retinoid X receptor heterodimers to activate target gene transcription (reviewed by Belandia and Parker, 2003; Glass and Rosenfeld, 2000; Xu et al., 1999).

Evidence for the role of RA signaling in definitive hematopoiesis has emerged from analyses of *Aldh1a2*-mutant mice. These mice exhibit decreased numbers of yolk sac hemogenic endothelial cells, and a corresponding loss in the formation of multipotent blood progenitors that give rise to myeloid and erythroid lineages (Goldie et al., 2008). At embryonic day 8.0, *Aldh1a2*-mutants exhibit normal endothelial cell-specific gene expression, and normal circulation (Goldie et al., 2008; Lai et al., 2003). These data suggest

that RA signaling is not required for general endothelial cell formation, but rather for yolk sac vascular endothelial cells to adopt a hemogenic fate. Support for this hypothesis comes from recent analyses of mice with a conditional deletion of *Aldh1a2* in VE-cadherin-positive endothelial cells (Chanda et al., 2013), as yolk sac vascular endothelial cells isolated from these mice fail to reconstitute lethally irradiated recipients. Notably, *Aldh1a2*-mutant mice die of severe vascular defects by embryonic day 10.5 (Niederreither et al., 1999), prior to HSC emergence. This early embryonic lethality makes mice a challenging model in which to examine the native developmental functions of RA in definitive hematopoiesis. Consequently, although existing studies suggest that endothelial cells require RA in order to adopt a hemogenic fate, they fail to elucidate other potential molecular functions of RA signaling in specifying HSCs *in vivo*.

4.1.1 Summary

In the present study, we provide evidence that RA is an essential regulator of zebrafish HSC specification. We demonstrate that RA regulates the formation of HSCs prior to hemogenic endothelial cell formation, at a time when *aldh1a2* is expressed in the paraxial mesoderm and somites. Previous studies in both mouse and zebrafish have implicated the Notch signaling pathway as a critical regulator of HSC formation (Clements et al., 2011; Gering and Patient, 2010; Hadland et al., 2004; Kim et al., 2014; Kumano et al., 2003; Robert-Moreno et al., 2005; Robert-Moreno et al., 2008). The yolk sac endothelial cells of *Aldh1a2*-mutant mice exhibit downregulated *Notch1* and Notch1-target gene expression (Marcelo et al., 2013), implicating RA as a potential modulator of murine Notch1 signaling. Conversely, we demonstrate that components of the Notch1 signaling pathway remain intact in RA-depleted zebrafish embryos. We therefore propose a model whereby RA signaling acts outside of the pre-hemogenic endothelium, in a Notch1-independent fashion to regulate zebrafish HSC formation.

4.2 Results

4.2.1 Retinoic acid regulates hematopoietic stem cell formation

We initially wanted to assess the requirement for RA in zebrafish HSC formation. Of the known *aldh1a* genes expressed in early zebrafish development, only *aldh1a2* is expressed in pre-hematopoietic posterior mesoderm. We therefore generated RA-deficient embryos by injecting embryos with *aldh1a2* morpholino (hereafter referred to as *aldh1a2*-morphants) (Begemann et al., 2001; Lieschke et al., 2001), or by treating them with Diethylaminobenzaldehyde (DEAB), a competitive inhibitor of aldehyde dehydrogenases including Aldh1a2 (Maves and Kimmel, 2005; Perz-Edwards et al., 2001). Zebrafish HSCs first emerge from dorsal aorta hemogenic endothelium, a region analogous to the mammalian aorta-gonad-mesonephros, by 30 hours post fertilization (hpf) (Burns et al., 2002; Kalev-Zylinska et al., 2002; Thompson et al., 1998; Zhang et al., 2011). These cells express *cmyb,* a transcription factor essential for HSC emergence (Zhang et al., 2011). As shown by *in situ* hybridization, both *aldh1a2*-morphants and DEAB-treated embryos display a severe reduction in the number of dorsal aorta *cmyb*-expressing cells at 32 hpf (Figure 4.1A-C; Table 4.1), suggesting that RA regulates zebrafish HSC formation.

Following their emergence, zebrafish HSCs migrate posteriorly to the caudal hematopoietic tissues, before becoming established in the thymus by 3 dpf (Jin et al., 2007; Murayama et al., 2006), where they differentiate to form *rag1*- and *ikaros*-expressing lymphoid progenitors (Jin et al., 2007; Murayama et al., 2006). Subsequently, in order to further determine if HSCs are specified in RA-deficient zebrafish embryos, we examined their *rag1* and *ikaros* expression. *aldh1a2*-morphant embryos completely lack thymic *rag1* and *ikaros* expression at 3 dpf, as shown by *in situ* hybridization (Figure 4.1D-E'; Table 4.2).

Thymic epithelial cells support lymphoid progenitor development and maturation. These cells differentiate from the thymus primordium, which is derived from the third pharyngeal endodermal pouch in zebrafish (Ma et al., 2013). As perturbations in RA signaling have been shown to produce defects in endodermal pouch morphogenesis (Kopinke et al., 2006), we wanted to verify that the thymic epithelium of RA-deficient embryos is correctly specified. We therefore examined expression of the thymic epithelial cell

marker *foxn1*, and find that it is expressed at wild type levels in 4 dpf *aldh1a2*-morphant embryos (Figure 4.1F, F'). Combined, our data suggest that RA is required to properly specify zebrafish HSCs and their thymocyte progeny.

As HSC formation is also dependent upon intact blood flow (North et al., 2009), and HSCs originate from dorsal aorta hemogenic endothelium (Burns et al., 2002; Kalev-Zylinska et al., 2002; Thompson et al., 1998), we next wanted to determine if the hematopoietic defects that we observe in RA-deficient embryos are due to aberrant vasculogenesis. To do this, we first visualized circulating primitive erythrocytes in *Tg*(*gata1*:*DsRed*)^{sd2Tg} transgenic zebrafish embryos (Traver et al., 2003). Examination of live 48 hpf, *aldh1a2*-morphant *gata1*:*DsRed* embryos reveals beating hearts, intact circulation, and a functional dorsal aorta (Figure 4.2A'). As shown by *in situ* hybridization, *aldh1a2*-morphants also exhibit wild type *kdrl* vasculature marker expression at 28 hpf (Figure 4.2B, B'). Combined, these data suggest that RA is not required for gross development of the embryonic vasculature.

4.2.2 RA is dispensable for zebrafish dorsal aorta Notch1 signaling

Previous studies have revealed an essential role for the Notch signaling pathway in regulating vertebrate HSC development (reviewed in Bertrand et al., 2010; Burns et al., 2005; Clements et al., 2011; Gering and Patient, 2010; Robert-Moreno et al., 2008; Weinstein and Lawson, 2002). Notch is a transmembrane surface receptor. Binding of the receptor to its Delta or Jagged transmembrane ligand on a neighboring cell induces a conformational change in the Notch receptor that renders it susceptible to cleavage by γ-secretase. This cleavage event releases the Notch intracellular domain (NICD), permitting it to enter the nucleus where it acts as a transcriptional activator (Kopan and Ilagan, 2009; Lai, 2002). The basic helix-loop-helix transcription factors *hairy and enhancer of split* (*Hes*) are transcriptional targets of the Notch signaling pathway. These proteins act as Notch-dependent transcriptional regulators, and serve to mediate the majority of Notch function (Iso et al., 2003).

Research in both mouse and zebrafish has established a cell-autonomous function for Notch signaling in HSC specification, whereby Notch1-expressing cells within the dorsal aorta are instructed by adjacent cells to form HSCs (Gering and Patient, 2010; Hadland et al.,

2004; Kim et al., 2014; Kumano et al., 2003; Robert-Moreno et al., 2005; Robert-Moreno et al., 2008). The yolk sac endothelial cells of *Aldh1a2*-mutant mice exhibit downregulated *Notch1* and Notch1-target gene (*Hes1*) expression (Marcelo et al., 2013), implicating RA as a potential modulator of Notch signaling. We therefore wanted to determine if the hematopoietic defects that we observe in RA-deficient zebrafish are the result of impaired Notch signaling. To do this, we first examined the expression of dorsal aorta Notch signaling pathway components and their downstream transcriptional targets in RA-deficient embryos.

Zebrafish possess four Notch receptors: *notch1a*, *notch1b*, *notch2*, and *notch3*. Of these, only Notch2 is completely dispensable for HSC formation (Hadland et al., 2004; Kim et al., 2014; Kumano et al., 2003). *notch1a*, *notch1b*, and *notch3* are initially expressed within the somitic mesoderm (Kim et al., 2014; Ma and Jiang, 2007). As development proceeds, their domain of expression expands to include nascent endothelial cells and, eventually, the dorsal aorta (Bertrand et al., 2010; Kim et al., 2014; Ma and Jiang, 2007). As shown through *in situ* hybridization, RA-deficient embryos exhibit wild type expression of *notch1a*, and *notch1b*, while the somitic expression of *notch3* is mildly increased at 26 hpf (Figure 4.3; Table 4.3). Our combined data suggest that RA is dispensable for dorsal aorta Notch receptor expression in zebrafish.

Previous research has shown that both global NICD induction after 20 hpf, and vascular (but not somite)-specific NICD induction rescues the HSC gene expression defects of *notch1a*- and *notch1b*-morphant zebrafish embryos (Kim et al., 2014). Conversely, global or somite-specific NICD induction at 14 hpf, but not 20 hpf rescues HSC formation in *notch3*-morphant embryos (Kim et al., 2014). As the dorsal aorta begins to form at 20 hpf (Ellertsdottir et al., 2010), these combined data suggest that the definitive hematopoietic roles of zebrafish Notch1a/b and murine Notch1 are likely functionally conserved. These data also suggest that there is a distinct temporal and spatial requirement for Notch3 in zebrafish hematopoiesis, which occurs prior to formation of the dorsal aorta. Consequently, to further determine if RA regulates zebrafish dorsal aorta Notch signaling, we next examined the expression of transcriptional targets of the Notch1-signaling pathway in RA-deficient embryos (Figure 4.4; Table 4.4).

gata2, a transcription factor essential for the production and maintenance of HSCs (Tsai et al., 1994; Tsai and Orkin, 1997), is a direct transcriptional target of the Notch1 signaling pathway (Da'as et al., 2012; Robert-Moreno et al., 2005). As shown through *in situ* hybridization, *gata2* expression is unchanged in *aldh1a2*-morphant embryos at 24 hpf (Figure 4.4A, A'). Expression of the Notch ligand *deltaC* (*dlc*) is strongly reduced in the dorsal aorta of *notch1a*- and *notch1b*-morphant zebrafish embryos (Kim et al., 2014). We therefore examined its expression in RA-deficient embryos. As shown by in situ hybridization, *dlc* is expressed at wild type levels in 26 hpf DEAB-treated embryos (Figure 4.4B, B'). We also examined the expression of *her6* (the zebrafish orthologue of mammalian *Hes1;* Gates et al., 1999; Jouve et al., 2000), finding that is also expressed at wild type levels in 24 hpf *aldh1a2*-morphant embryos (Figure 4.4C, C'). These data suggest that, unlike its mammalian orthologue *Hes1*, zebrafish *her6* is not RA-responsive. These combined data also suggest that RA does not regulate the Notch1-signaling pathway in zebrafish.

4.2.3 RA signaling regulates HSC formation prior to 19 hpf

Our analyses indicate that the hematopoietic defects of RA-deficient embryos are not due to impaired dorsal aorta Notch signaling. Consequently, to gain a better understanding of how RA regulates zebrafish definitive hematopoiesis, we next wanted to elucidate the temporal requirement for RA signaling in HSC formation. To accomplish this, we treated *aldh1a2*-morphant embryos with RA at different time points, and examined their *cmyb* HSC gene expression at 32 hpf through *in situ* hybridization (Figure 4.5; Table 4.5). We demonstrate that RA treatment beginning at 4 hpf rescues dorsal aorta *cmyb* gene expression in *aldh1a2*-morphant embryos (Figure 4.5C). Conversely, RA treatment beginning at 19 hpf (Figure 4.5E) or 24 hpf (Figure 4.5F) fails to rescue *cmyb* expression in *aldh1a2*-morphant embryos. Combined, these data suggest that RA is required prior to 19 hpf to specify HSCs. Notably, *aldh1a2* is expressed in the paraxial mesoderm and later somites during this period, and the dorsal aorta has not yet formed (Ellertsdottir et al., 2010).

4.2.4 RA does not regulate *wnt16* or Notch signaling within the somites.

The human *wingless-type MMTV integration site family, member* 16 (WNT16) orthologue was initially identified as a gene misexpressed in pre-B-cell acute lymphoblastic leukemia cells generated by the E2A-PBX1 (t1:19) chromosomal translocation (McWhirter et al., 1999). Wnt16 participates in a non-canonical Wnt signaling pathway, as its depletion has no effect on the expression of β-catenin/Tcf-dependent reporter transgene expression (Clements et al., 2011). Previous research has shown that *wnt16*-morphant zebrafish embryos exhibit defects in Notch signaling and HSC formation. NICD induction from 15-19 hpf is able to rescue *cmyb* expression in *wnt16*-morphant embryos (Clements et al., 2011), suggesting that Wnt16-mediated Notch signaling is required for HSC formation prior to formation of the dorsal aorta. Similar to RA-depleted embryos, *wnt16*-morphant embryos exhibit normal vasculogenesis and Notch1-target gene expression. Given that RA and Wnt16 are required for HSC formation prior to 19 hpf, and *aldh1a2* and *wnt16* are both expressed in the paraxial mesoderm and somites at this time (Clements et al., 2011), we hypothesized that pertubations in Wnt16 or its downstream effectors may be responsible for the hematopoietic defects that we observe in RA-depleted embryos. To test this hypothesis, we first examined *wnt16* expression in RA-deficient embryos by *in situ* hybridization. We demonstrate that *wnt16* is expressed at wild type levels in DEAB-treated embryos at 17 hpf (Figure 4.6A-B'; Table 4.6).

In addition to hematopoietic defects, Wnt16-depleted embryos exhibit reduced somitic expression of the Notch ligands *dlc* and *dld*, and *dlc/dld* overexpression rescues HSC gene expression in *wnt16*-morphants (Clements et al., 2011). These combined data place *dlc* and *dld* downstream of Wnt16 in definitive hematopoiesis. Dlc and Dld participate in a Notch1-independent signaling pathway to specify zebrafish HSCs (Clements et al., 2011). Given that *aldh1a2*, and *dlc*/*dld* are expressed within the posterior somitic mesoderm at common time points (Clements et al., 2011), we examined their expression in RA-deficient embryos at 17 hpf through *in situ* hybridization (Figure 4.6; Table 4.6). In comparison to wild type embryos, DEAB-treated embryos exhibit normal levels of somitic *dlc* expression (Figure 4.6C-D'), and

mildly upregulated *dld* expression (Figure 4.6E-F'). Combined, our data suggest that RA is not required for posterior somitic mesoderm *dlc* and *dld* Notch ligand expression.

dlc/*dld* overexpression fails to rescue HSC gene expression in *notch3*-morphants, or *notch3*/*wnt16*-double morphant zebrafish embryos (Kim et al., 2014). Notch3 does not regulate *dlc* and *dld* expression (Kim et al., 2014), and *notch3* expression is not downregulated in *wnt1*6-morphants (Clements et al., 2011). Furthermore, Dlc/Dld and Notch3 proteins synergize, as partial loss of Dlc and Notch3 or Dld and Notch3 produces greater HSC gene expression defects than partial loss of Dlc, Dld, or Notch3 alone (Kim et al., 2014). These combined data suggest that Notch3 is required by Wnt16-induced Dlc/Dld to regulate HSC formation. Like RA-deficient embryos, *notch3*-morphants display normal *dlc* and *dld* expression (Kim et al., 2014). As NICD induction prior to 20 hpf rescues HSC gene expression in *notch3*-morphant embryos, both RA and Notch3-signaling regulate HSC formation at similar time points. We therefore postulated that RA regulates *notch3* expression at this time, and so examined its expression by *in situ* hybridization (Figure 4.6G-H'; Table 4.6). Compared to wild type embryos (Figure 4.6G, G'), DEAB-treated embryos exhibit increased somitic *notch3* expression at 17 hpf (Figure 4.6H, H').

her9 is expressed within the somitic mesoderm (Bae et al., 2005; Bertrand et al., 2010; Chen et al., 2007; Liu et al., 2007; Ma et al., 2007). Its expression is partially downregulated in both *notch1a*-mutant and *notch3*-morphant zebrafish embryos (Liu et al., 2007; Ma and Jiang, 2007). Like *notch3*, *her9* is expressed at wild type levels in 17 hpf DEAB-treated embryos (Figure 4.6I-J'; Table 4.6). Our combined data suggests that RA does not regulate Wnt16-Notch3 pathway signaling.

4.3 Discussion

Previous research has shown that RA is a critical regulator of definitive hematopoiesis (Chanda et al., 2013; Goldie et al., 2008). RA treatment of hematovascular precursors increases their ability to generate definitive hematopoietic precursors (Chanda et al., 2013; Yu et al., 2010), suggesting that RA signaling plays an instructive role in definitive hematopoiesis. This data is in line with previous analyses of RA function in mice, as *Aldh1a2*-mutants fail to correctly specify yolk sac hemogenic endothelial cells (Goldie et al., 2008), and loss of *Aldh1a2* in VE-cadherin-positive endothelial cells is sufficient to abrogate HSC formation (Chanda et al., 2013). *Aldh1a2*-mutant mice die of severe vascular defects prior to HSC emergence (Niederreither et al., 1999), precluding global analyses of *Aldh1a2*-function in murine definitive hematopoiesis. We therefore used zebrafish as a model to study the role of RA signaling in definitive hematopoiesis.

Our study describes a novel role for RA signaling in definitive hematopoiesis. We propose that RA functions in the somites, prior to formation of the dorsal aorta, to regulate hematopoietic stem cell (HSC) formation. By impairing RA synthesis in the developing zebrafish embryo, we demonstrate that RA is required for proper HSC gene expression. In the absence of RA, embryos exhibit a severe reduction in HSC number and a corresponding failure to produce thymic lymphoid progenitors.

4.3.1 RA regulates HSC formation independent of the Notch1-signaling pathway

Previous research in both mouse and zebrafish has established a model whereby Notch1-expressing cells within the dorsal aorta are instructed by adjacent cells to form HSCs (Gering and Patient, 2010; Hadland et al., 2004; Kumano et al., 2003; Robert-Moreno et al., 2005; Robert-Moreno et al., 2008). *Notch1*-mutant embryonic stem cells fail to contribute to the wild type adult hematopoietic system in mouse chimeras (Hadland et al., 2004), supporting this cell-autonomous role for Notch1 in definitive hematopoiesis. The yolk sac endothelial cells of *Aldh1a2*-mutant mice exhibit downregulated *Notch1* and Notch-target gene expression (Marcelo et al., 2013), implicating RA as a critical regulator of murine Notch1 signaling. Notch1 specifies HSCs, in part, by activating *gata2* expression (Gering and

Patient, 2010; Hadland et al., 2004; Robert-Moreno et al., 2005; Robert-Moreno et al., 2008). We, however, demonstrate that both *notch1a/b* and *gata2* expression are unaffected by loss of RA in zebrafish. We further demonstrate that RA is required for HSC formation prior to the formation of dorsal aorta hemogenic endothelium. Our combined results therefore suggest that, unlike in mice, zebrafish RA does not regulate Notch1-signaling. RA is therefore functioning independently of the Notch1 signaling pathway to regulate zebrafish definitive hematopoiesis.

4.3.2 RA does not regulate the Wnt16-Notch pathway

Recently, Clements et al. (2011) demonstrated a requirement for Wnt16 in zebrafish hematopoiesis. RA-deficient and *wnt16*-morphant embryos display common hematopoietic phenotypes; both demonstrate proper vascular gene expression and produce a functional dorsal aorta, but exhibit a severe reduction in HSC and common lymphoid progenitor gene expression (Clements et al., 2011). These data suggest that both RA and Wnt16 are required for HSC formation. Our data, and previous results also suggest that both RA and Wnt16 function outside of dorsal aorta pre-hemogenic endothelium to regulate zebrafish HSC formation prior to 19 hpf (Clements et al., 2011). Furthermore, both *aldh1a2* and *wnt16* are expressed in the somitic mesoderm at this time (Clements et al., 2011). In addition to hematopoietic defects, *wnt16*-depleted embryos exhibit reduced somitic expression of the Notch ligands *dlc* and *dld* (Clements et al., 2011). HSC gene expression is lost in Dlc-mutants injected with *dld* morpholino, and *dlc*/*dld* overexpression rescues HSC gene expression in *wnt16*-morphants (Clements et al., 2011). NICD induction from 15-19 hpf is also able to rescue *cmyb* expression in *wnt16*-morphant embryos (Clements et al., 2011). These combined data suggest that Wnt16 acts upstream of the Notch signaling pathway to regulate definitive hematopoiesis, and that Notch signaling downstream of Wnt16 is required to specify HSCs prior to 19 hpf. We demonstrate that RA-deficient embryos possess wild type levels *wnt16*, *dlc* and *dld* expression within the segmental plate and somites at 17 hpf. Our data therefore indicate that, despite their similar localization and their common temporal requirement in definitive hematopoiesis, RA does not regulate *wnt16* or its downstream targets *dlc* and *dld*.

Notch3 is required by Wnt16-induced Dlc/Dld to regulate HSC formation (Kim et al., 2014). NICD induction prior to 20 hpf rescues HSC gene expression in *notch3*-morphant embryos, and *notch3* is expressed robustly within the somites at this time. Consequently, both RA and Notch3-signaling regulate HSC formation at similar time points, and are present in the same tissues. We demonstrate that the expression of *notch3*, and its transcriptional target *her9* are normal in RA-deficient embryos at 17 hpf. Our combined results therefore suggest that RA and Wnt16/Notch3 participate in convergent pathways to regulate HSC formation. Alternatively, RA may function downstream of the Wnt16-Notch3 pathway in zebrafish definitive hematopoiesis. By determining if NICD induction is able to rescue HSC gene expression in RA-deficient embryos, we can determine if RA is acting in a Notch-dependent or independent fashion to regulate HSC formation. Furthermore, to determine if RA is modulating Notch signaling within the developing embryo, it would be useful to monitor Notch signaling within the somitic mesoderm and pre-hemogenic endothelium of wild type versus RA-deficient embryos using the *TP1:GFP* Notch reporter line, which expresses GFP under the control of a Notch-responsive promoter (Parsons et al., 2009).

4.3.3 Alternative mechanisms by which RA may regulate HSC formation

Using a photo-convertible Kaede protein under the control of a Notch-responsive promoter, Clements et al. (2011) demonstrated that cells photoconverted prior to 19.5 hpf are never fated to become HSCs. It is therefore currently unclear how these cells contribute to the hematopoietic system. Both *wnt16*-morphants and *dlc*-mutants injected with *dld* morpholino exhibit defects in sclerotomal gene expression (Clements et al., 2011), suggesting that Wnt16 may contribute indirectly to HSC specification by participating in sclerotome specification or morphogenesis. Support for the role of RA in sclerotome specification comes from an examination of vitamin A-deficient quail, which demonstrate apoptosis in the sclerotomal half of each somite (Maden et al., 2000). However, it is currently unclear if/how the sclerotome contributes to HSC formation. It is also unclear if RA-deficient zebrafish embryos possess sclerotomal gene expression defects.

Close morphological examination of 32 hpf RA-deficient embryos reveals an absent or mispatterned hypochord (Figure 4.1), although further analyses should be conducted to

determine the extent of this defect. The dorsal aorta forms in close physical and temporal proximity to the hypochord. Consequently, although little is known about the relationship between these two structures, it is hypothesized that the hypochord may serve to accurately position or pattern the dorsal aorta (Eriksson and Lofberg, 2000).

Many of the Notch pathway components that are essential for HSC formation are also required for hypochord development (Appel et al., 1999; Appel et al., 2003; Latimer et al., 2002). For example, *notch1a*-morphants exhibit reduced hypochord cell numbers, while *dlc* mutants injected with *dld* morpholino fail to produce a hypochord (Appel et al., 2003; Latimer et al., 2002). Furthermore, embryos treated with the γ-secretase inhibitor DAPT at or before 12 hpf exhibit severe hypochord defects (Latimer and Appel, 2006). Hypochord cells develop between axial and paraxial mesoderm, adjacent to where *aldh1a2* is expressed (Latimer et al., 2002). RA-supplementation between 4 hpf and 19 hpf rescues the HSC gene expression defects of RA-deficient embryos. Notch signaling is required for hypochord development during this period. It is therefore possible that the hematopoietic defects of Notch-deficient or RA-deficient embryos are due to, in part, to impaired hypochord formation.

The dorsal aorta forms from angioblasts that arise from bilateral stripes of posterior lateral-plate mesoderm. These angioblasts migrate towards the midline and aggregate (Ellertsdottir et al., 2010). Recently, Kobayashi et al. (2014) determined that the junctional adhesion molecules Jam1a and Jam2a are required for zebrafish HSC formation. *jam1a* is expressed within angioblasts that migrate across j*am2a*-, *dlc*-, and *dld*-expressing somites (Kobayashi et al., 2014). Jam1a and Jam2a proteins physically interact (Kobayashi et al., 2014). Jam1a- and Jam2a-deficient embryos possess defects in Notch signal transduction, and their hematopoietic defects are rescued by heat-shock induction of the NICD during angioblast migration (Kobayashi et al., 2014). Notably, Jam1a- and Jam2a-deficient embryos display normal expression of *notch1a*, *notch1b*, *notch3*, *dlc*, and *dld* (Kobayashi et al., 2014). The data generated by Kobayashi et al. (2014) therefore suggest that Notch signal transduction in pre-hematopoietic angioblasts requires Jam-mediated intercellular contact.

Angioblast migration occurs between 14 and 18 hpf. We demonstrate that RA is required between prior to 19 hpf for HSC formation. RA is a diffusible morphogen. It is

therefore plausible that RA signaling within the somites or migrating angioblats may render them competent to form hemogenic endothelium and or HSCs. Like Jam1a/2a-depleted embryos, RA-deficient embryos exhibit wild type expression of *notch1a*, *notch1b*, *notch3*, and *dlc*. It would therefore be of interest to determine if RA is an upstream regulator of *jam1a* and/or *jam2a*.

4.4 Figures

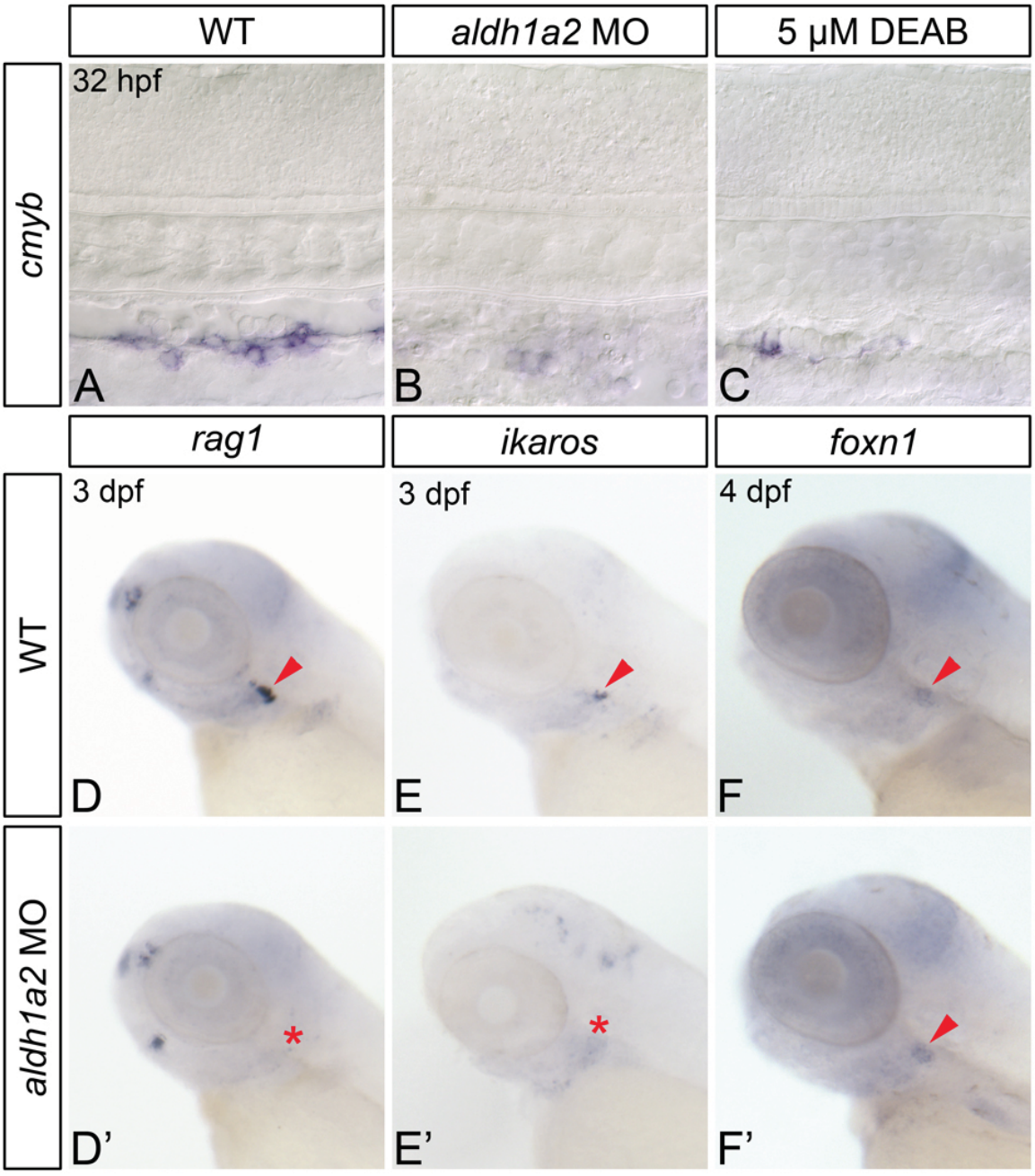
WT
aldh1a2 MO
5 μM DEAB
cmyb
32 hpf
A
B
C
rag1
ikaros
foxn1
WT
3 dpf
3 dpf
4 dpf
D
E
F
aldh1a2 MO
D'
E'
F'

Figure 4.1. RA-deficient embryos demonstrate impaired HSC formation. (A-C) Shown are representative embryos following *in situ* hybridization analysis of *cmyb* gene expression in 32 hours post fertilization (hpf) embryos. Lateral view of gene expression in the dorsal aorta region of the trunk is shown; anterior to the left. Compared to wild type embryos (WT; A) *aldh1a2*-morphants (B), and DEAB-treated embryos (C) exhibit nearly abolished *cmyb* expression. (D-E') Shown are representative embryos following *in situ* hybridization analyses of common lymphoid progenitor gene expression in 3 days post fertilization (dpf) embryos. Lateral view of gene expression in the head is shown; anterior to the left. Arrows and asterisks indicate thymus. Compared to WT embryos (D, E) *aldh1a2*-morphants exhibit nearly abolished thymic *rag1* (D') and *ikaros* (E') expression. (F, F') Shown are representative embryos following *in situ* hybridization analyses of *foxn1* thymic epithelial cell gene expression in 4 dpf embryos. Lateral view of gene expression in the head is shown; anterior to the left. Arrows indicate thymus. WT embryos (F) and aldh1a2-morphants (F') exhibit similar thymic *foxn1* expression levels.

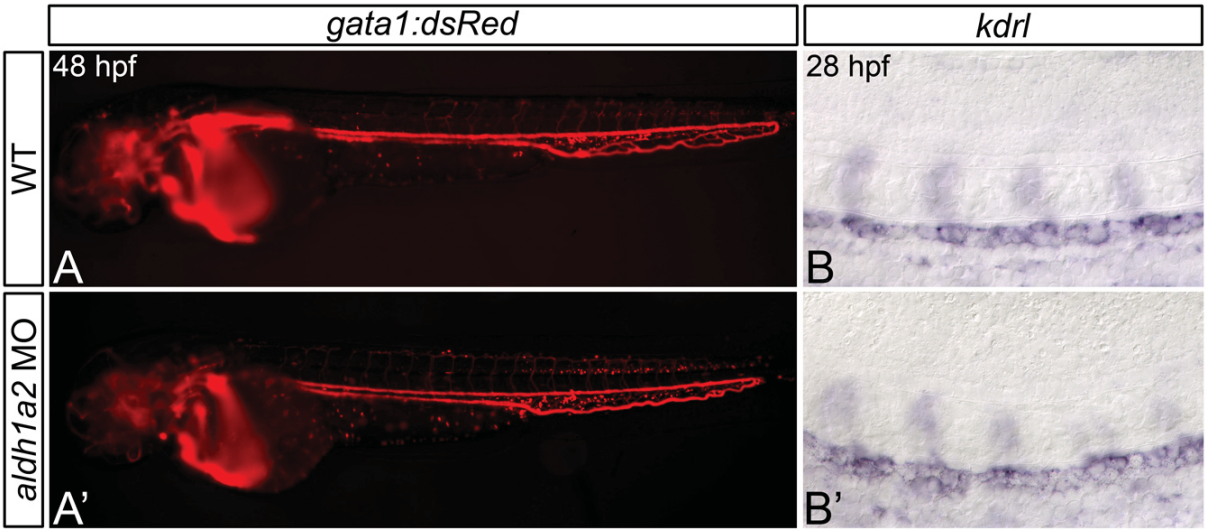

Figure 4.2. RA-deficient embryos demonstrate normal vasculogenesis. (A, A') Lateral view of live 48 hours post fertilization (hpf) *gata1:dsRed* embryos; anterior to left. Compared to wild type (WT) embryos (A), *aldh1a2*-morphants (A') display visible circulating blood cells, and an intact dorsal aorta and posterior cardinal vein. (B-B') Shown are representative embryos following *in situ* hybridization analysis of *kdrl* gene expression in 28 hpf embryos. Lateral view of gene expression in the dorsal aorta region of the trunk is shown; anterior to the left. Compared to WT embryos (B) *aldh1a2*-morphants (B') exhibit normal dorsal aorta *kdrl* gene expression.

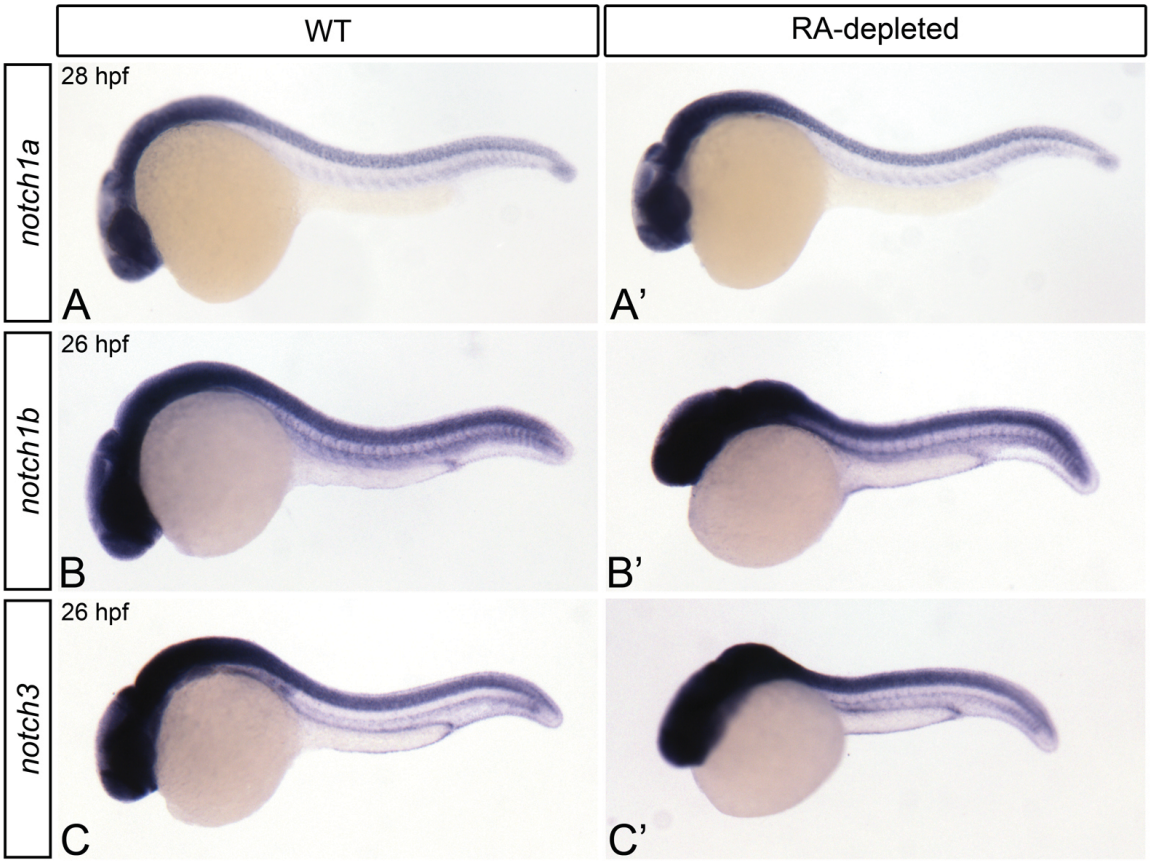

Figure 4.3. RA-deficient embryos demonstrate normal dorsal aorta *notch* expression. 28 hours post fertilization (hpf) (A, A') or 26 hpf (B-C') whole-mount embryos are shown in lateral view with anterior to left. Compared to wild type embryos (WT; A) or WT DMSO-treated control embryos (B, C), *aldh1a2*-morphants (A') or embryos treated with 5 μM DEAB (B', C') exhibit normal *notch1a* (A'), and *notch1b* (B') gene expression within the trunk and dorsal aorta. *notch3* is expressed at normal levels in the dorsal aorta, but is mildly upregulated in the somites of DEAB-treated (C') versus WT DMSO-treated comtrol embryos (C).

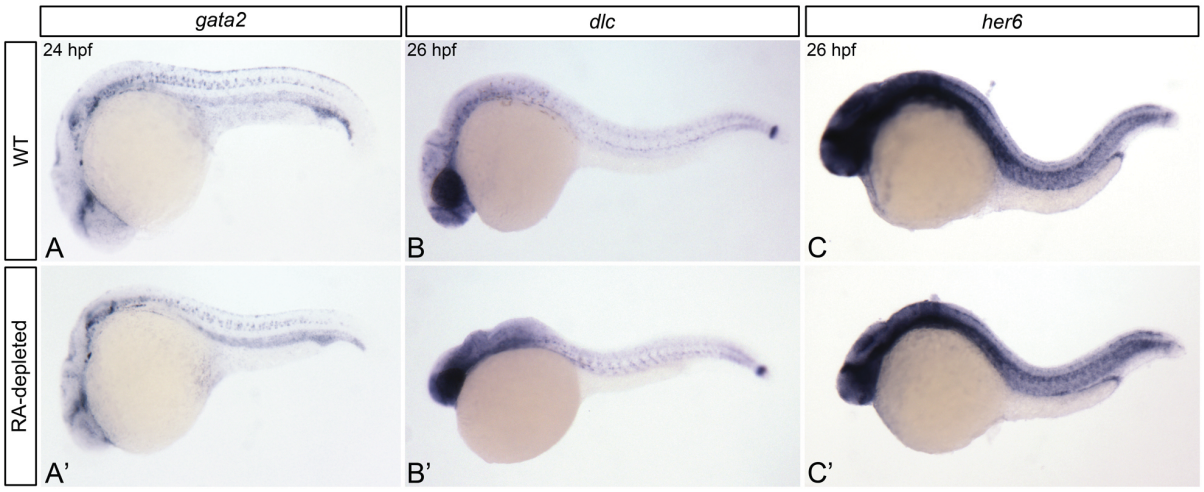

Figure 4.4. RA-deficient embryos demonstrate normal Notch1-target gene expression. 24 hours post fertilization (hpf; A, A') or 26 hpf (B-C') whole-mount embryos are shown in lateral view with anterior to left. Compared to wild type embryos (WT; A, C), or WT DMSO-treated control embryos (B), *aldh1a2*-morphants (A', C') or embryos treated with 5 μM DEAB (B') exhibit normal *gata2* (A'), *dlc* (B') and *her6* (C') gene expression levels within the trunk and dorsal aorta.

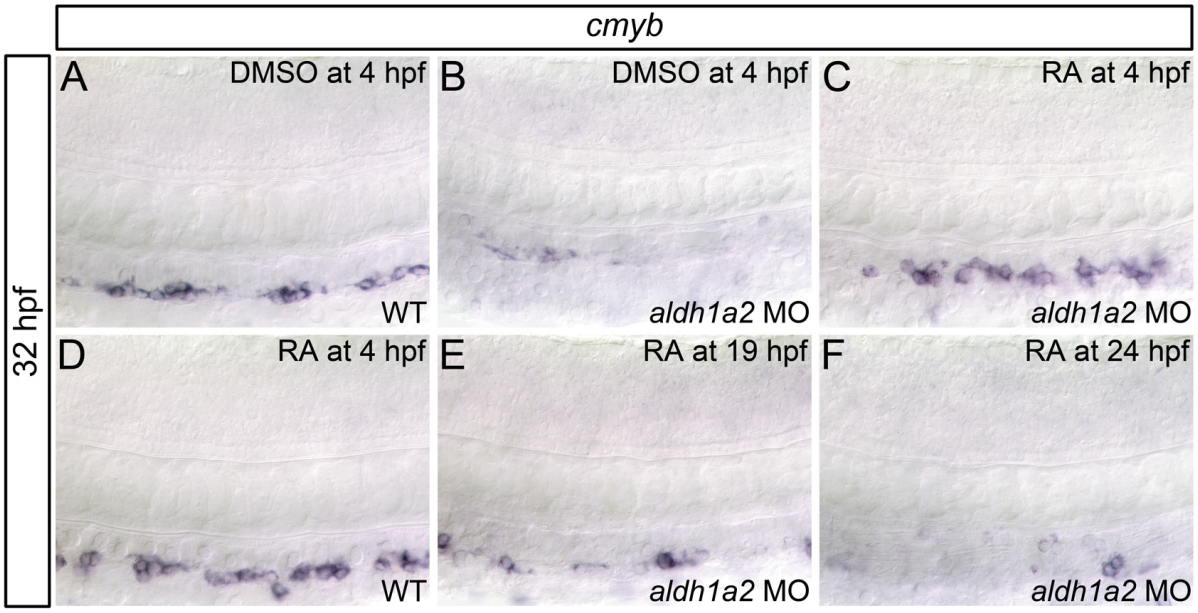

Figure 4.5. RA is required prior to 19 hpf for HSC formation. Shown are representative embryos following *in situ* hybridization analysis of *cmyb* gene expression in wild type (WT; A, D) or *aldh1a2*-morphant (B, C, E, F) 32 hours post fertilization (hpf) embryos treated with DMSO (A, B) or 1 nM RA (C-F) at various time points. Lateral view of gene expression in the dorsal aorta region of the trunk is shown; anterior to the left. Compared to WT embryos (A) and embryos treated with 1 nM RA (D) *aldh1a2*-morphants (B) exhibit nearly abolished *cmyb* expression. *cmyb* expression is restored in *aldh1a2*-morphant embryos treated with 1 nM RA at 4 hpf (C). *cmyb* expression is not significantly restored in *aldh1a2*-morphants treated with 1 nM RA at 19 hpf (E) or 24 hpf (F).

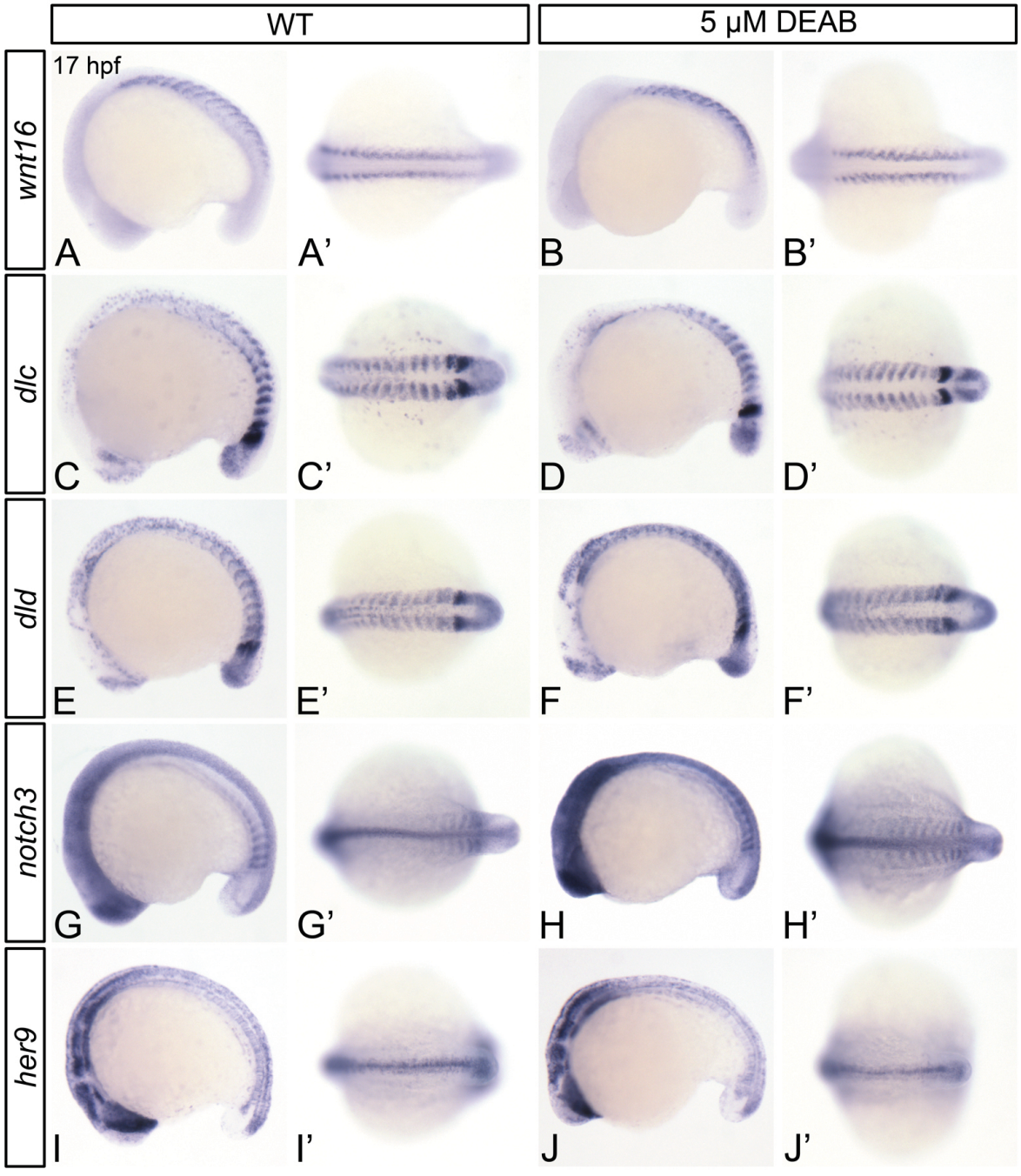
WT
5 µM DEAB
17 hpf
wnt16
dlc
dld
notch3
her9
A
A'
B
B'
C
C'
D
D'
E
E'
F
F'
G
G'
H
H'
I
I'
J
J'

Figure 4.6. RA does not regulate the somitic expression of Wnt16-Notch signaling pathway components. Shown are representative embryos following *in situ* hybridization analyses in 17 hours post fertilization (hpf) embryos. Dorsal view (A'-J') or lateral view (A-J) of gene expression is shown with anterior oriented to the left. A'-J' represent different views of the embryos shown in A-J. Compared to wild type DMSO-treated control embryos (WT; A, A', C, C', E, E', G, G'), DEAB-treated embryos exhibit normal somitic expression levels of *wnt16* (B, B'), and *dlc* (D, D'), mildly increased *dld* expression (F, F'), and increased *notch3* somitic gene expression (H, H'). DEAB-treated embryos also exhibit normal levels of *her9* expression (J, J'), when compared to DMSO-treated controls (I, I').

4.5 Tables

Table 4.1: Quantification of *cmyb* expression in 32 hpf wild type (WT) and RA-deficient embryos.

Treatment	Wild type	Reduced	Total	Mean % Reduced	SEM (%)	Two-tailed *P*-value
WT; DMSO	60	7	67	8.7	7.2	
aldh1a2 MO; DMSO	10	27	37	69	11	<0.0002*
5 µM DEAB	12	42	54	78	10	<0.0002*

*Indicates significant result compared to wild type (WT), by Fisher's Exact Test with Bonferroni correction on cumulative raw counts.

Table 4.2: Quantification of thymic lymphoid progenitor gene expression defects of 3 dpf RA-deficient embryos.

Gene	Treatment	Wild type	Abolished	Total	Mean % Abolished	SEM (%)	Two-tailed *P*-value
ikaros	WT	62	0	66	0.0	0.0	
	aldh1a2 MO	8	37	46	80	3.5	<0.0001*
rag1	WT	72	0	72	0.0	0.0	
	aldh1a2 MO	14	21	45	47	3.0	<0.0001*

*Indicates significant result compared to wild type (WT), by Fisher's Exact Test on cumulative raw counts.

Table 4.3: Quantification of Notch receptor gene expression phenotypes of 26 hpf RA-deficient embryos.

Gene	Treatment	Wild type	Abnormal	Total	Two-tailed *P*-value
notch1a	WT	16	0	16	
	aldh1a2 MO	16	0	16	1.000
notch1b	WT; DMSO	21	0	21	
	5 µM DEAB	29	0	29	1.000
notch3	WT; DMSO	60	0	60	
	5 µM DEAB	4	38	42	<0.0001*

*Indicates significant result compared to wild type (WT), by Fisher's Exact Test on cumulative raw counts.

Table 4.4: Quantification of Notch1-target gene expression phenotypes of RA-deficient embryos.

Gene	Stage	Treatment	Wild type	Abnormal	Total	Two-tailed *P*-value
gata2	24 hpf	WT	11	2	13	
		aldh1a2 MO	11	1	12	1.000
dlc	26 hpf	WT; DMSO	21	0	21	
		5 µM DEAB	29	0	29	1.000
her6	26 hpf	WT; DMSO	7	0	7	
		aldh1a2 MO	8	0	8	1.000

*Indicates significant result compared to wild type (WT), by Fisher's Exact Test on cumulative raw counts.

Table 4.5: Quantification of *cmyb* gene expression defects in 32 hpf *aldh1a2*-morphants embryos treated with 1 nM RA at various time points.

Treatment	Wild type	Reduced	Total	Two-tailed *P*-value
WT; DMSO	12	0	12	
WT; 1 nm RA at 4 hpf	10	1	11	1.000
aldh1a2 MO; DMSO	5	7	12	0.0230*
aldh1a2 MO; 1 nM RA at 4 hpf	10	1	11	1.000
aldh1a2 MO; 1 nM RA at 19 hpf	7	7	14	0.0320*
aldh1a2 MO; 1 nM RA at 24 hpf	3	7	10	0.0035*

*Indicates significant result compared to wild type (WT), DMSO-treated controls by Fisher's Exact Test with Bonferroni correction on cumulative raw counts.

Table 4.6: Quantification of Wnt16-Notch3 signaling pathway component gene expression phenotypes of 17 hpf RA-deficient embryos.

Gene	Treatment	Wild type	Abnormal	Total	Two-tailed *P*-value
wnt16	WT; DMSO	28	0	28	
	5 µM DEAB	27	0	27	1.000
dlc	WT; DMSO	29	0	29	
	5 µM DEAB	33	0	33	1.000
dld	WT; DMSO	27	1	28	
	5 µM DEAB	1	23	24	<0.0001*
notch3	WT; DMSO	36	0	36	
	5 µM DEAB	0	24	24	<0.0001*
her9	WT; DMSO	27	0	27	
	5 µM DEAB	31	0	31	1.000

*Indicates significant result compared to wild type (WT), by Fisher's Exact Test on cumulative raw counts.

4.6 References

Appel, B., A. Fritz, M. Westerfield, D.J. Grunwald, J.S. Eisen, and B.B. Riley. 1999. Delta-mediated specification of midline cell fates in zebrafish embryos. *Current biology : CB*. 9:247-256.

Appel, B., P. Marasco, L.E. McClung, and A.J. Latimer. 2003. lunatic fringe regulates Delta-Notch induction of hypochord in zebrafish. *Dev Dyn*. 228:281-286.

Bae, Y.K., T. Shimizu, and M. Hibi. 2005. Patterning of proneuronal and inter-proneuronal domains by hairy- and enhancer of split-related genes in zebrafish neuroectoderm. *Development*. 132:1375-1385.

Begemann, G., and A. Meyer. 2001. Hindbrain patterning revisited: timing and effects of retinoic acid signalling. *Bioessays*. 23:981-986.

Begemann, G., T.F. Schilling, G.J. Rauch, R. Geisler, and P.W. Ingham. 2001. The zebrafish neckless mutation reveals a requirement for raldh2 in mesodermal signals that pattern the hindbrain. *Development*. 128:3081-3094.

Belandia, B., and M.G. Parker. 2003. Nuclear receptors: a rendezvous for chromatin remodeling factors. *Cell*. 114:277-280.

Bertrand, J.Y., J.L. Cisson, D.L. Stachura, and D. Traver. 2010. Notch signaling distinguishes 2 waves of definitive hematopoiesis in the zebrafish embryo. *Blood*. 115:2777-2783.

Burns, C.E., T. DeBlasio, Y. Zhou, J. Zhang, L. Zon, and S.D. Nimer. 2002. Isolation and characterization of runxa and runxb, zebrafish members of the runt family of transcriptional regulators. *Exp Hematol*. 30:1381-1389.

Burns, C.E., D. Traver, E. Mayhall, J.L. Shepard, and L.I. Zon. 2005. Hematopoietic stem cell fate is established by the Notch-Runx pathway. *Genes Dev*. 19:2331-2342.

Chanda, B., A. Ditadi, N.N. Iscove, and G. Keller. 2013. Retinoic acid signaling is essential for embryonic hematopoietic stem cell development. *Cell*. 155:215-227.

Chen, J., C. Jette, J.P. Kanki, J.C. Aster, A.T. Look, and J.D. Griffin. 2007. NOTCH1-induced T-cell leukemia in transgenic zebrafish. *Leukemia*. 21:462-471.

Clements, W.K., A.D. Kim, K.G. Ong, J.C. Moore, N.D. Lawson, and D. Traver. 2011. A somitic Wnt16/Notch pathway specifies haematopoietic stem cells. *Nature*. 474:220-224.

Da'as, S.I., A.J. Coombs, T.B. Balci, C.A. Grondin, A.A. Ferrando, and J.N. Berman. 2012. The zebrafish reveals dependence of the mast cell lineage on Notch signaling in vivo. *Blood*. 119:3585-3594.

Ellertsdottir, E., A. Lenard, Y. Blum, A. Krudewig, L. Herwig, M. Affolter, and H.G. Belting. 2010. Vascular morphogenesis in the zebrafish embryo. *Dev Biol*. 341:56-65.

Eriksson, J., and J. Lofberg. 2000. Development of the hypochord and dorsal aorta in the zebrafish embryo (Danio rerio). *Journal of morphology*. 244:167-176.

Gates, M.A., L. Kim, E.S. Egan, T. Cardozo, H.I. Sirotkin, S.T. Dougan, D. Lashkari, R. Abagyan, A.F. Schier, and W.S. Talbot. 1999. A genetic linkage map for zebrafish: comparative analysis and localization of genes and expressed sequences. *Genome research*. 9:334-347.

Gering, M., and R. Patient. 2010. Notch signalling and haematopoietic stem cell formation during embryogenesis. *Journal of cellular physiology*. 222:11-16.

Glass, C.K., and M.G. Rosenfeld. 2000. The coregulator exchange in transcriptional functions of nuclear receptors. *Genes Dev*. 14:121-141.

Goldie, L.C., J.L. Lucitti, M.E. Dickinson, and K.K. Hirschi. 2008. Cell signaling directing the formation and function of hemogenic endothelium during murine embryogenesis. *Blood*. 112:3194-3204.

Hadland, B.K., S.S. Huppert, J. Kanungo, Y. Xue, R. Jiang, T. Gridley, R.A. Conlon, A.M. Cheng, R. Kopan, and G.D. Longmore. 2004. A requirement for Notch1 distinguishes 2 phases of definitive hematopoiesis during development. *Blood*. 104:3097-3105.

Iso, T., L. Kedes, and Y. Hamamori. 2003. HES and HERP families: multiple effectors of the Notch signaling pathway. *Journal of cellular physiology*. 194:237-255.

Jin, H., J. Xu, and Z. Wen. 2007. Migratory path of definitive hematopoietic stem/progenitor cells during zebrafish development. *Blood*. 109:5208-5214.

Jouve, C., I. Palmeirim, D. Henrique, J. Beckers, A. Gossler, D. Ish-Horowicz, and O. Pourquie. 2000. Notch signalling is required for cyclic expression of the hairy-like gene HES1 in the presomitic mesoderm. *Development*. 127:1421-1429.

Kalev-Zylinska, M.L., J.A. Horsfield, M.V. Flores, J.H. Postlethwait, M.R. Vitas, A.M. Baas, P.S. Crosier, and K.E. Crosier. 2002. Runx1 is required for zebrafish blood and vessel development and expression of a human RUNX1-CBF2T1 transgene advances a model for studies of leukemogenesis. *Development*. 129:2015-2030.

Kim, A.D., C.H. Melick, W.K. Clements, D.L. Stachura, M. Distel, D. Panakova, C. MacRae, L.A. Mork, J.G. Crump, and D. Traver. 2014. Discrete Notch signaling requirements in the specification of hematopoietic stem cells. *EMBO J*. 33:2363-2373.

Kobayashi, I., J. Kobayashi-Sun, A.D. Kim, C. Pouget, N. Fujita, T. Suda, and D. Traver. 2014. Jam1a-Jam2a interactions regulate haematopoietic stem cell fate through Notch signalling. *Nature*. 512:319-323.

Kopan, R., and M.X. Ilagan. 2009. The canonical Notch signaling pathway: unfolding the activation mechanism. *Cell*. 137:216-233.

Kopinke, D., J. Sasine, J. Swift, W.Z. Stephens, and T. Piotrowski. 2006. Retinoic acid is required for endodermal pouch morphogenesis and not for pharyngeal endoderm specification. *Dev Dyn*. 235:2695-2709.

Kumano, K., S. Chiba, A. Kunisato, M. Sata, T. Saito, E. Nakagami-Yamaguchi, T. Yamaguchi, S. Masuda, K. Shimizu, T. Takahashi, S. Ogawa, Y. Hamada, and H. Hirai. 2003. Notch1 but not Notch2 is essential for generating hematopoietic stem cells from endothelial cells. *Immunity*. 18:699-711.

Lai, E.C. 2002. Notch cleavage: Nicastrin helps Presenilin make the final cut. *Current biology : CB*. 12:R200-202.

Lai, L., B.L. Bohnsack, K. Niederreither, and K.K. Hirschi. 2003. Retinoic acid regulates endothelial cell proliferation during vasculogenesis. *Development*. 130:6465-6474.

Latimer, A.J., and B. Appel. 2006. Notch signaling regulates midline cell specification and proliferation in zebrafish. *Dev Biol*. 298:392-402.

Latimer, A.J., X. Dong, Y. Markov, and B. Appel. 2002. Delta-Notch signaling induces hypochord development in zebrafish. *Development*. 129:2555-2563.

Lieschke, G.J., A.C. Oates, M.O. Crowhurst, A.C. Ward, and J.E. Layton. 2001. Morphologic and functional characterization of granulocytes and macrophages in embryonic and adult zebrafish. *Blood*. 98:3087-3096.

Liu, Y., N. Pathak, A. Kramer-Zucker, and I.A. Drummond. 2007. Notch signaling controls the differentiation of transporting epithelia and multiciliated cells in the zebrafish pronephros. *Development*. 134:1111-1122.

Ma, A., M. Boulton, B. Zhao, C. Connon, J. Cai, and J. Albon. 2007. A role for notch signaling in human corneal epithelial cell differentiation and proliferation. *Investigative ophthalmology & visual science*. 48:3576-3585.

Ma, D., Y. Wei, and F. Liu. 2013. Regulatory mechanisms of thymus and T cell development. *Developmental and comparative immunology*. 39:91-102.

Ma, M., and Y.J. Jiang. 2007. Jagged2a-notch signaling mediates cell fate choice in the zebrafish pronephric duct. *PLoS Genet*. 3:e18.

Maden, M., A. Graham, M. Zile, and E. Gale. 2000. Abnormalities of somite development in the absence of retinoic acid. *The International journal of developmental biology*. 44:151-159.

Marcelo, K.L., T.M. Sills, S. Coskun, H. Vasavada, S. Sanglikar, L.C. Goldie, and K.K. Hirschi. 2013. Hemogenic endothelial cell specification requires c-Kit, Notch signaling, and p27-mediated cell-cycle control. *Dev Cell*. 27:504-515.

Maves, L., and C.B. Kimmel. 2005. Dynamic and sequential patterning of the zebrafish posterior hindbrain by retinoic acid. *Dev Biol*. 285:593-605.

McWhirter, J.R., S.T. Neuteboom, E.V. Wancewicz, B.P. Monia, J.R. Downing, and C. Murre. 1999. Oncogenic homeodomain transcription factor E2A-Pbx1 activates a novel WNT gene in pre-B acute lymphoblastoid leukemia. *Proc Natl Acad Sci U S A*. 96:11464-11469.

Murayama, E., K. Kissa, A. Zapata, E. Mordelet, V. Briolat, H.F. Lin, R.I. Handin, and P. Herbomel. 2006. Tracing hematopoietic precursor migration to successive hematopoietic organs during zebrafish development. *Immunity*. 25:963-975.

Niederreither, K., V. Subbarayan, P. Dolle, and P. Chambon. 1999. Embryonic retinoic acid synthesis is essential for early mouse post-implantation development. *Nat Genet*. 21:444-448.

Niederreither, K., J. Vermot, B. Schuhbaur, P. Chambon, and P. Dolle. 2000. Retinoic acid synthesis and hindbrain patterning in the mouse embryo. *Development*. 127:75-85.

North, T.E., W. Goessling, M. Peeters, P. Li, C. Ceol, A.M. Lord, G.J. Weber, J. Harris, C.C. Cutting, P. Huang, E. Dzierzak, and L.I. Zon. 2009. Hematopoietic stem cell development is dependent on blood flow. *Cell*. 137:736-748.

Parsons, M.J., H. Pisharath, S. Yusuff, J.C. Moore, A.F. Siekmann, N. Lawson, and S.D. Leach. 2009. Notch-responsive cells initiate the secondary transition in larval zebrafish pancreas. *Mech Dev*. 126:898-912.

Perz-Edwards, A., N.L. Hardison, and E. Linney. 2001. Retinoic acid-mediated gene expression in transgenic reporter zebrafish. *Dev Biol*. 229:89-101.

Robert-Moreno, A., L. Espinosa, J.L. de la Pompa, and A. Bigas. 2005. RBPjkappa-dependent Notch function regulates Gata2 and is essential for the formation of intra-embryonic hematopoietic cells. *Development*. 132:1117-1126.

Robert-Moreno, A., J. Guiu, C. Ruiz-Herguido, M.E. Lopez, J. Ingles-Esteve, L. Riera, A. Tipping, T. Enver, E. Dzierzak, T. Gridley, L. Espinosa, and A. Bigas. 2008. Impaired embryonic haematopoiesis yet normal arterial development in the absence of the Notch ligand Jagged1. *EMBO J*. 27:1886-1895.

Thompson, M.A., D.G. Ransom, S.J. Pratt, H. MacLennan, M.W. Kieran, H.W. Detrich, 3rd, B. Vail, T.L. Huber, B. Paw, A.J. Brownlie, A.C. Oates, A. Fritz, M.A. Gates, A. Amores, N. Bahary, W.S. Talbot, H. Her, D.R. Beier, J.H. Postlethwait, and L.I. Zon. 1998. The cloche and spadetail genes differentially affect hematopoiesis and vasculogenesis. *Dev Biol*. 197:248-269.

Traver, D., B.H. Paw, K.D. Poss, W.T. Penberthy, S. Lin, and L.I. Zon. 2003. Transplantation and in vivo imaging of multilineage engraftment in zebrafish bloodless mutants. *Nature immunology*. 4:1238-1246.

Tsai, F.Y., G. Keller, F.C. Kuo, M. Weiss, J. Chen, M. Rosenblatt, F.W. Alt, and S.H. Orkin. 1994. An early haematopoietic defect in mice lacking the transcription factor GATA-2. *Nature*. 371:221-226.

Tsai, F.Y., and S.H. Orkin. 1997. Transcription factor GATA-2 is required for proliferation/survival of early hematopoietic cells and mast cell formation, but not for erythroid and myeloid terminal differentiation. *Blood*. 89:3636-3643.

Weinstein, B.M., and N.D. Lawson. 2002. Arteries, veins, Notch, and VEGF. *Cold Spring Harbor symposia on quantitative biology*. 67:155-162.

Xu, L., C.K. Glass, and M.G. Rosenfeld. 1999. Coactivator and corepressor complexes in nuclear receptor function. *Curr Opin Genet Dev*. 9:140-147.

Yu, C., Y. Liu, Z. Miao, M. Yin, W. Lu, Y. Lv, M. Ding, and H. Deng. 2010. Retinoic acid enhances the generation of hematopoietic progenitors from human embryonic stem cell-derived hemato-vascular precursors. *Blood*. 116:4786-4794.

Zhang, Y., H. Jin, L. Li, F.X. Qin, and Z. Wen. 2011. cMyb regulates hematopoietic stem/progenitor cell mobilization during zebrafish hematopoiesis. *Blood*. 118:4093-4101.

Chapter 5

Hmx4 regulates primitive and definitive hematopoiesis

Some of the data within this chapter was published. Patricia A. Gongal, Lindsey D. March, Vanessa L. Holly, Laura M. Pillay, Karyn M. Berry-Wynne, Hiroyuki Kagechika, and Andrew J. Waskiewicz (2011). Hmx4 regulates Sonic hedgehog signaling through control of retinoic acid synthesis during forebrain patterning. *Developmental Biology*, 355(1): 55-64.

5.1 Introduction

Morpholino-based analyses have shown that the homeodomain transcription factor H6 homeobox 4 (*hmx4; soho1*) participates in eye and forebrain development (K. Berry-Wynne, unpublished; Boisset and Schorderet, 2012; Gongal et al., 2011). *hmx4*-morphant zebrafish display a host of defects, which include micropthalmia, narrowed eye-field, loss of pectoral fins, open neural tube, small ear, and reduced numbers of vagal motor neurons (Gongal et al., 2011). A portion of these phenotypes are attributable to defects in the sonic hedgehog signaling (Shh) pathway, as *hmx4*-morphants display a marked reduction in the forebrain expression domains of the Shh pathway targets *ptc1* and *nkx2.2a*, and the Shh transcriptional effector *gli3* (Gongal et al., 2011). Retinoic acid (RA) treatment rescues the Shh signaling defects of *hmx4*-morphants, as well as their forebrain patterning defects (Gongal et al., 2011). These data implicate *hmx4* as a regulator of the RA signaling pathway. Given that RA is an essential regulator of both primitive and definitive hematopoiesis, we wanted to determine the contribution of *hmx4* to embryonic hematopoiesis.

5.1.1 Summary

We analyzed the role of *hmx4* in hematopoiesis using both *hmx4*-morphant and *hmx4*-mutant zebrafish embryos. We provide evidence that *hmx4* is required for proper RA synthesis in the developing embryo, as *hmx4*-morphants demonstrate reduced *aldh1a2* expression, and an expansion in the domain of *cyp26a1* expression. Consistent with defects in RA signaling, *hmx4*-morphant embryos also exhibit defects in hematopoietic stem cell (HSC) formation. Supplementation of *hmx4*-morphants with a biologically relevant dose of RA rescues their *runx1* HSC gene expression defects, placing Hmx4 upstream of the RA signaling pathway in zebrafish definitive hematopoiesis. *hmx4*-morphants also exhibit primitive hematopoietic gene expression defects. We demonstrate that while the primitive myeloid phenotype of *hmx4*-morphants can be explained by reduced RA levels, their erythropoietic gene expression defects cannot be rescued with RA treatment, and do not resemble a loss of RA. Our analyses of *hmx4*-morphants therefore indicate that Hmx4 regulates primitive erythropoiesis in an RA-independent fashion. Surprisingly, *hmx4*-mutants fail to exhibit any

overt morphological or hematopoietic defects, confounding our understanding of the role of Hmx4 in RA signaling and embryonic hematopoiesis.

5.2 Results

5.2.1 Hmx4-depleted embryos are RA-deficient

We used a morpholino oligonucleotide-based protein knockdown approach to generate Hmx4-depleted zebrafish embryos (hereafter referred to as *hmx4*-morphants). *hmx4*-morphants exhibit a narrowed eyefield (Figure 5.1A', C') and neural tube defects, along with concomitant gene expression defects in Sonic hedgehog signaling (Gongal et al., 2011). In addition to these defects, *hmx4*-morphants also exhibit loss of pectoral fins (Figure 5.1A'), small ears (Figure 5.1B'), and misshapen somites (Figure 5.2; Gongal et al., 2011), phenotypes that are highly reminiscent of those obtained through loss of RA signaling.

To assess RA signaling in *hmx4*-morphant embryos, we analyzed the expression of genes involved in RA metabolism. As shown through *in situ* hybridization, *hmx4*-morphant embryos exhibit strongly reduced expression of the RA synthesis gene *aldh1a2* in the posterior mesoderm and dorsal retina at 11 hours post fertilization (hpf; Figure 5.2A-B'), 16 hpf (Figure 5.2C-D'), and 20 hpf (Figure 5.2E-F'). To more accurately measure the observed changes in *aldh1a2* expression, we performed real-time quantitative PCR (qPCR) on wild type and *hmx4*-morphant embryos. Consistent with the *in situ* hybridization analyses, 18 hpf *hmx4*-morphants exhibit a 50% decrease in *aldh1a2* expression when compared to wild type embryos ($P < 0.0001$; Figure 5.2G).

Cyp26 proteins hydroxylate RA, targeting it for degradation (reviewed in White and Schilling, 2008). As shown through *in situ* hybridization, *hmx4*-morphant embryos exhibit a broadened domain of tailbud *cyp26a1* expression at 11 hpf (Figure 5.3B) and increased anterior neurectoderm *cyp26a1* expression at 16 hpf and 20 hpf (Figure 5.3D', F'), compared to wild type embryos (Figure 5.3A, C', E'). Combined, these data suggest that *hmx4*-morphant embryos are RA-deficient. We therefore wanted to determine if they exhibit hematopoietic defects that are consistent with a loss in RA signaling.

5.2.2 Hmx4 regulates zebrafish definitive hematopoiesis

To assess the requirement of Hmx4 in zebrafish definitive hematopoiesis, we conducted analyses of definitive hematopoietic gene expression in wild type and *hmx4*-morphant

embryos using whole-mount *in situ* hybridization. The Runx1 transcription factor is essential for HSC formation (Burns et al., 2002; Burns et al., 2005; Gering and Patient, 2005; Kalev-Zylinska et al., 2002; Okuda et al., 1996; Thompson et al., 1998). In comparison to wild type embryos, *hmx4*-morphants exhibit a severe reduction in *runx1* gene expression at 28 hpf (Figure 5.4A, A'; Table 5.1). We next wanted to determine if this loss in gene expression represents a permanent loss of HSCs. To do this, we examined common lymphoid progenitor (CLP) marker (*rag1*, *ikaros*) gene expression in the thymus of *hmx4*-morphant embryos. CLPs represent the earliest detectable progeny of differentiating HSCs. We demonstrate that in comparison to wild type embryos, *hmx4*-morphants exhibit nearly abolished *rag1* and *ikaros* gene expression at 3 days post fertilization (dpf; Figure 5.4B-C'; Table 5.1). Combined, these data suggest that Hmx4 is required for proper HSC formation.

As HSCs develop from dorsal aorta hemogenic endothelium, we next wanted to determine if the defects that we observe in *hmx4*-morphant embryos are due to aberrant vasculogenesis. To do this, we examined the vasculature of *fli1a:EGFP* transgenic embryos. The vasculature of *hmx4*-morphants appears relatively normal at 48 hpf, although their intersegmental vessels are present in an atypical pattern that reflects the square shape of their somites (Figure 5.5A, A'; Gongal et al., 2011). As shown by *in situ* hybridization, *hmx4*-morphants also exhibit wild type *efnb2a* arterial gene expression at 25 hpf (Figure B-C'). Combined, these data suggest that Hmx4 is not required for gross development of the dorsal aorta.

5.2.3 Hmx4 acts upstream of RA signaling in definitive hematopoiesis

Given that *hmx4*-morphant embryos exhibit reduced *aldh1a2*-expression, we next wanted to determine if their definitive hematopoietic defects are due to a loss of RA signaling. To answer this question, we treated *hmx4*-morphant embryos with RA, and used *in situ* hybridization to analyze *runx1* expression. Treatment of *hmx4*-morphant embryos with a biologically relevant, low dose of RA (1 nM) partially rescues their *runx1* gene expression defects at 28 hpf (Figure 5.6A-C; Table 5.2). These data suggest that Hmx4 acts genetically upstream of the RA signaling pathway in definitive hematopoiesis. Notably, compared to wild type controls (Figure 5.6A), embryos treated with 10 nM RA (Figure 5.6E) exhibit

reduced *runx1* expression (Table 5.2). Combined, these data suggest that *runx1* expression is extremely sensitive to RA levels.

hmx4-morphants do not exhibit a complete loss of *aldh1a2* expression, making it possible that they possess residual, low levels of RA. They also possess reduced, but not abolished *runx1* and CLP gene expression. We therefore wanted to determine the contribution of any remaining RA in specifying HSCs within *hmx4*-morphant embryos. To do this, we examined *runx1* expression in *hmx4*-morphant embryos treated with the Alhdehyde dehydrogenase inhibitor diethylaminobenzaldehyde (DEAB). As shown through *in situ* hybridization, we demonstrate that DEAB-treated *hmx4*-morphants (Figure 5.7D) exhibit a more severe reduction in dorsal aorta *runx1* gene expression than untreated *hmx4*-morphants (Figure 5.7B) at 28 hpf. Notably, these embryos also demonstrate ectopic *runx1* gene expression in a region lying both lateral and ventral to the dorsal aorta (Figure 5.6D). These data suggest that *hmx4*-morphants are not completely devoid of RA. Our combined data also suggest that Hmx4 regulates definitive hematopoiesis by modulating RA signaling.

5.2.4 Hmx4 regulates zebrafish primitive hematopoiesis

Previous research has demonstrated an inhibitory role for RA signaling in both primitive erythropoiesis and primitive myelopoiesis (de Jong et al., 2010; Liang et al., 2012; Ma et al., 2010; Sive and Cheng, 1991). Zebrafish treated with exogenous RA exhibit reduced primitive erythroid gene expression (Ma et al., 2010), and reduced numbers of anterior lateral-plate primitive myeloid cells (Liang et al., 2012). Conversely, embryos treated with DEAB exhibit strongly upregulated primitive erythroid gene expression and increased numbers of primitive myeloid cells (Liang et al., 2012; Ma et al., 2010). Consequently, given that *hmx4*-morphant embryos exhibit defects in RA signaling, we next wanted to determine if they possess corresponding primitive hematopoietic defects.

We first examined primitive erythropoiesis in *hmx4*-morphant embryos. As shown through qPCR, 18 hpf *hmx4*-morphant embryos exhibit a significant 77% decrease ($P < 0.0001$) in *gata1* expression when compared to their wild type counterparts (Figure 5.8A). These embryos also display a severe reduction in the number of differentiated erythrocytes, as visualized through o-dianisidine staining of 48 hpf embryos (Figure 5.8D, F; Table 5.3).

Combined, these results demonstrate that *hmx4*-morphants possess defects in primitive erythropoiesis. As RA-deficient embryos exhibit increased *gata1* expression (de Jong et al., 2010; Ma et al., 2010), the *hmx4*-morphant erythroid phenotype is not likely due to defects in RA-signaling. To support this hypothesis, we attempted to rescue erythrocyte differentiation in *hmx4*-morphants by treating them with 1 nM RA (Figure 5.8; Table 5.3). No control embryos ($n = 23$) demonstrate reduced or abolished o-diansidine staining at 48 hpf (Figure 5.8B, F). 8% of control embryos treated with 1 nM RA ($n = 24$) exhibit reduced o-dianisidine staining (Figure 5.8C, F). 16% of *hmx4*-morphant embryos ($n = 25$) exhibit reduced o-dianisidine staining (Figure 5.8F), while 68% of these embryos demonstrate abolished staining (Figure 5.8D, F). The proportion of affected *hmx4*-morphant embryos is statistically significant when compared to control embryos ($P < 0.0004$) and control embryos treated with 1 nM RA ($P < 0.0004$). When *hmx4*-morphants are treated with 1 nM RA, these frequencies remain comparable (13% reduced, 70% abolished; $n = 23$), and the proportion of affected embryos is not statistically different from untreated *hmx4*-morphants ($P = 1.000$; Figure 5.8E, F). RA-treatment fails to rescue o-dianisidine staining in *hmx4*-morphants, and *gata1* expression is nearly abolished in these embryos. Our combined results therefore indicate that the primitive erythropoietic defects of *hmx4*-morphants are not due to reduced RA levels.

We next used *in situ* hybridization to examine primitive myeloid gene expression in the anterior lateral-plate mesoderm (ALPM) of 24 hpf *hmx4*-morphant embryos (Figure 5.9; Table 5.4). In comparison to their wild type counterparts (Figure 5.9A, D), *hmx4*-morphant embryos exhibit a significant 1.28-fold increase ($P = 0.0037$) in the number of *pu.1*-expressing cells (Figure 5.9A', D). These embryos also exhibit a significant 1.34-fold increase ($P = 0.0041$) in the number of cells expressing the more mature myeloid gene *lcp1* (Figure 5.9B', D; Berman et al., 2005; Le Guyader et al., 2008). Following their emergence from the rostral blood islands, primitive myeloid cells begin to express the macrophage and granulocyte progenitor marker *lyz* (Hall et al., 2007). In comparison to wild type embryos (Figure 5.9C, D), *hmx4*-morphant embryos exhibit a significant 1.45-fold decrease ($P = 0.0152$) in the number of *lyz*-expressing cells (Figure 5.9C', D). Combined, these data suggest that Hmx4 represses early myeloid cell fate, but may be required for proper myeloid progenitor maturation.

5.2.5 Generation of *hmx4*-mutant zebrafish using ZFN technology

Although our morpholino-based studies of have been useful, *hmx4*-morphants do not represent true nulls, and display incomplete penetrance of hematopoietic defects. Furthermore, *hmx4*-morphants exhibit increased cell death, an off-target morpholino effect that results from aberrant activation of the p53 apoptotic pathway (Robu et al., 2007). The p53 pathway has previously been implicated in maintaining steady-state hematopoiesis (Liu et al., 2009), making usage of p53 control morpholino non-ideal for our analyses. *hmx4* mRNA is incredibly toxic and generates extremely severe morphological defects. This makes mRNA rescue of *hmx4*-morphants (the ideal morpholino control) unachievable. Consequently, in order to better evaluate the role of Hmx4 in regulating hematopoiesis, we generated *hmx4*-mutant zebrafish using zinc finger nuclease (ZFN) targeted mutagenesis technology (Chapter 6).

Using a previously published bacterial-one-hybrid system (Meng et al., 2008), we identified arrays that bind the *hmx4* target sequence with high affinity and specificity. We injected ZFN mRNA into zebrafish embryos at the one-cell stage, raised them to sexual maturity, and screened their progeny for mutations in *hmx4.* Carriers of ideal germline mutations were outcrossed to wild type embryos, and their progeny were identified for mutations in *hmx4* using a combination of high resolution melt curve analysis and sequencing. We generated embryos containing either a two base pair deletion, or a four base pair insertion in *hmx4*. Both of these frameshift mutations generate a premature stop codon immediately upstream of the *hmx4* homeodomain (Figure 5.10).

5.2.6 Analyses of *hmx4*-mutant zebrafish embryos

hmx4-morphant zebrafish embryos exhibit a myriad of readily-observable morphological phenotypes including cyclopia, neural tube defects, loss of pectoral fins, misshapen somites, small ears, and a mildly compressed anteroposterior body axis (Figure 5.1, Gongal et al., 2011). We therefore examined the morphology of *hmx4*$^{-/-}$ embryos to determine if they exhibit defects that are consistent with those obtained through our morpholino-based analyses. Surprisingly, compared to wild type embryos (Figure 5.11A)

maternal-zygotic *hmx4*$^{-/-}$ embryos fail to exhibit any overt morphological defects by 5 dpf (Figure 5.11B, C).

We next wanted to determine if our *hmx4*$^{-/-}$ embryos recapitulate the hematopoietic defects observed in *hmx4*-morphants. To do this, we examined definitive hematopoietic gene expression in our mutants. Unlike *hmx4*-morphants, *hmx4*$^{-/-}$ embryos exhibit wild type levels of *runx1* gene expression at 28 hpf (Figure 5.12A, A'), as shown through *in situ* hybridization. We further demonstrate that *hmx4*$^{-/-}$ embryos possess wild type *ikaros* CLP thymic gene expression at 3 dpf (Figure 5.12B, B'). Combined, these data suggest that *hmx4*$^{-/-}$ zebrafish embryos do not possess defects in definitive hematopoiesis.

5.2.7 *hmx1* is upregulated in *hmx4*-mutants

As *hmx4*$^{-/-}$ embryos have no discernable morphological or hematopoietic phenotypes, we next wanted to determine if something is compensating for the loss of Hmx4 within our mutant embryos. Zebrafish *hmx4* and *hmx1* display nearly identical, overlapping temporal and spatial expression patterns from 5 hpf (Boisset and Schorderet, 2012; Deitcher et al., 1994; Gongal et al., 2011; Yoshiura et al., 1998). Furthermore, the ocular defects of *hmx4*-morphant zebrafish embryos are further compounded by loss of Hmx1 (K. Berry-Wynne, unpublished). Combined, these data suggest that zebrafish Hmx1 and Hmx4 possess partially redundant developmental functions. We therefore used *in situ* hybridization to examine the expression of both *hmx1* and *hmx4* in our *hmx4*$^{-/-}$ embryos. We demonstrate that, in comparison to *hmx4*$^{+/-}$ siblings, *hmx4*$^{-/-}$ embryos display increased and expanded ocular *hmx1* expression at 18 hpf (Figure 5.13A, A'). These data suggest that Hmx4 represses *hmx1* transcription. Notably, *hmx4* is expressed at normal levels in *hmx4*$^{-/-}$ embryos (Figure 5.13B, B'), indicating that the *hmx4*-mutant mRNA transcript does not undergo nonsense-mediated decay.

We hypothesized that the increase in *hmx1* that we observe in our *hmx4*-mutants is sufficient to compensate for loss of Hmx4 function in these embryos. To test this hypothesis, we examined the morphology of *hmx4*$^{-/-}$ embryos injected with *hmx1* morpholino. As with *hmx4*$^{-/-}$ embryos (Figure 5.14B), and *hmx1*-morphants (Figure 5.14C), *hmx4*$^{-/-}$ embryos injected with *hmx1*-morpholino do not exhibit any overt morphological defects by 5 dpf

(Figure 5.14D). These data suggest that *hmx1* upregulation does not serve to veil *hmx4*$^{-/-}$ phenotypes.

5.2.8 *hmx4*$^{-/-}$ embryos possess loss-of-function mutations in *hmx4*

Our *hmx4*$^{-/-}$ embryos fail to exhibit phenotypes obtained through our analyses of *hmx4*-morphants. Furthermore, we do not detect reduced *hmx4* transcript levels in *hmx4*$^{-/-}$ embryos. We therefore sought to determine if our mutant Hmx4 proteins retain some level of function. To do this, we examined 48 hpf embryos injected with either wild type *hmx4* RNA, or mutant *hmx4* RNA harboring the aforementioned 2 bp deletion (*hmx4*^{ua1004}) or 4 bp insertion (*hmx4*^{ua1003}) mutations, and quantified the proportion of embryos that exhibit developmental defects (Figure 5.15; Table 5.5). The majority of embryos overexpressing wild type *hmx4* RNA exhibit severe morphological defects, which include a severely shortened anteroposterior body axis (Figure 5.15B, E). Conversely, when compared to uninjected control embryos, embryos injected with *hmx4*^{ua1003} RNA or *hmx4*^{ua1004} RNA demonstrate a comparable (negligible) level of morphological defects (Fig 5.15C, D, E; corrected $P = 1.000$ for each). Combined, these data suggest that our *hmx4*^{ua1003} and *hmx4*^{ua1003} alleles both represent loss-of-function mutations in *hmx4*.

5.3 Discussion

Previous research by our lab has implicated Hmx4 as a critical regulator of zebrafish forebrain and ocular development (Gongal et al., 2011). Using a morpholino-based approach to block Hmx4 translation, we have elucidated novel roles for Hmx4 in zebrafish primitive and definitive hematopoiesis. We propose a model whereby Hmx4 regulates primitive myeloid cell development and hematopoietic stem cell (HSC) formation by modulating retinoic acid (RA) signaling. We further demonstrate that Hmx4 acts in an RA-independent fashion to regulate primitive erythropoiesis.

5.3.1 Hmx4 regulates definitive hematopoiesis by modulating RA signaling

Previous research has implicated sonic hedgehog (Shh) signaling in definitive, but not primitive hematopoiesis, as zebrafish *smo* mutants (Barresi et al., 2001; Chen et al., 2002) and embryos treated with cyclopamine during gastrulation exhibit a severe reduction in HSCs (Gering and Patient, 2005). Notably, these embryos also exhibit severe vascular defects, and fail to produce a dorsal aorta (Gering and Patient, 2005; Wilkinson et al., 2012; Williams et al., 2010). *hmx4*-morphants possess Shh signaling defects (Gongal et al., 2011). However, these defects are limited to the extreme anterior of the embryo, as *hmx4*-morphants exhibit wild type *ptc1* expression in the posterior mesoderm (K. Berry-Wynne, unpublished). Furthermore, we demonstrate that *hmx4*-morphant embryos possess wild type dorsal aorta gene expression and relatively normal vasculature. Consequently, it is improbable that the definitive hematopoietic defects of *hmx4*-morphants are due to deficiencies in Shh signaling.

hmx4-morphants demonstrate morphological defects that include a small ear and loss of pectoral fins (Figure 5.1; Gongal et al., 2011). Our results suggest that these embryos also exhibit HSC and thymic common lymphoid progenitor (CLP) gene expression defects. Consistent with a loss of RA signaling, *hmx4*-morphants display reduced expression of the RA synthesis gene *aldh1a2*, and an expansion in the domain of *cyp26a1* expression. Supplementation of *hmx4*-morphants with a biologically relevant dose of RA partially rescues their *runx1* HSC gene expression defects, placing Hmx4 upstream of the RA signaling pathway in zebrafish definitive hematopoiesis.

5.3.2 Hmx4 in primitive hematopoiesis

In addition to defects in definitive hematopoiesis, Hmx4 also appears to act earlier in development as a regulator of primitive hematopoesis. *hmx4*-morphants exhibit severely reduced expression of *gata1*, a gene that is required to specify erythroid cell fate (Galloway et al., 2005; Pevny et al., 1991; Rhodes et al., 2005; Shivdasani et al., 1997). These embryos also demonstrate reduced numbers of differentiated erythrocytes, as evidenced by nearly abolished o-dianisidine staining. These data therefore suggest that Hmx4 regulates primitive erythropoiesis.

Concomitant with a loss of *gata1* expression, *hmx4*-morphants also exhibit increased numbers of *pu.1*-expressing myelocytes in the anterior lateral-plate mesoderm (ALPM). The specification of erythroid versus myeloid cell fate is dependent on the interplay between Gata1 and Pu.1 transcription factors. These proteins transcriptionally repress each other's target genes (Nerlov et al., 2000; Rekhtman et al., 1999; Stopka et al., 2005; Zhang et al., 1999; Zhang et al., 2000) and in zebrafish, loss of either protein produces ectopic or increased expression of the other (Galloway et al., 2005; Kitaguchi et al., 2009; Lyons et al., 2002; Rhodes et al., 2005). It is therefore possible that the increase in *pu.1*-expressing myelocytes that we observe in the ALPM of *hmx4*-morphants is the indirect result of reduced *gata1* expression, and represents a conversion of erythroid to myeloid cell fate.

Although *hmx4*-morphants exhibit increased numbers of *pu.1*- and *lcp1*-expressing primitive myeloid cells when compared to their wild type counterparts, they exhibit reduced numbers of *lyz*-expressing myeloid cells. *pu.1* represents the earliest known marker of myeloid progenitor fate, and is detectable in the ALPM by 12 hpf in zebrafish (Crowhurst et al., 2002; Hsu et al., 2004; Lieschke et al., 2002; Ward et al., 2003). As myeloid progenitors mature and migrate across the yolk sac, they begin to express the monocyte and neutrophil lineage marker *lyz* (Bennett et al., 2001; Herbomel et al., 1999; Herbomel et al., 2001; Lieschke et al., 2002; Liu and Wen, 2002; Xu et al., 2012; Zakrzewska et al., 2010). Our results may therefore indicate that the myeloid progenitors of *hmx4*-morphants are specified correctly, but fail to mature properly.

Previous research in zebrafish has shown that specification of macrophage versus neutrophil cell fate is dependent on the regulation of Pu.1 levels by Runx1. High levels of

Pu.1 favour macrophage development, and suppress granulocyte and neutrophil formation (Jin et al., 2012; Su et al., 2007). Runx1 promotes neutrophil over macrophage cell fate by negatively regulating *pu.1* expression (Jin et al., 2012). Runx1 may also promote neutrophil fate by directly activating *lyz* transcription, as the zebrafish *lyz* promoter possesses an essential Runx1-binding element, and *lyz* expression is lost in *runx1*-morphants (Kitaguchi et al., 2009). We observe increased numbers of *pu.1*-expressing cells, but reduced numbers of *lyz*-expressing myeloid cells in our *hmx4*-morphants. These phenotypes are consistent with a conversion of granulocyte and neutrophil to macrophage cell fate. As *hmx4*-morphants exhibit reduced levels of *runx1* expression, our combined results suggest that the myeloid defects that we observe in *hmx4*-morphants may be the consequence of decreased Runx1 levels. Determining if *runx1* overexpression rescues the myeloid defects of *hmx4*-morphants would serve to test this hypothesis.

5.3.3 RA-independent functions of Hmx4 in primitive hematopoiesis

Previous research has shown that RA plays an inhibitory role in vertebrate primitive hematopoiesis, as zebrafish embryos treated with exogenous RA exhibit reduced *gata1* and *pu.1* gene expression (de Jong et al., 2010; Sive and Cheng, 1991). Conversely, zebrafish treated with the Aldehyde dehydrogenase inhibitor DEAB exhibit strongly upregulated *gata1* and *pu.1* gene expression (Ma et al., 2010). Our *hmx4*-morphants display RA metabolism gene expression defects that are consistent with a loss of RA signaling. Consequently, the increase in *pu.1*-expressing myeloid cell number that we observe in our *hmx4*-morphants may be due to a loss of RA signaling in these embryos. Conversely, the reduced *gata1* expression and o-dianisidine staining that we observe in *hmx4*-morphants lie in direct opposition to phenotypes obtained by loss of RA signaling. Furthermore, we demonstrate that RA-supplementation does not rescue o-dianisidine staining in *hmx4*-morphants. Our results therefore indicate that Hmx4 regulates primitive erythropoiesis through an RA-independent mechanism. The identification of direct transcriptional targets of Hmx4 using chromatin immunoprecipitation and massively parallel sequencing (ChIP-seq) could generate useful insights into how this transcription factor regulates primitive erythropoiesis.

5.3.4 *hmx4*$^{-/-}$ embryos fail to recapitulate *hmx4*-morphant phenotypes

Using zinc finger nuclease technology, we generated *hmx4*$^{-/-}$ zebrafish embryos. Overexpression of wild type, but not mutant *hmx4* mRNAs generates severe morphological defects. Our results therefore indicate that our embryos possess loss-of-function mutations in *hmx4*. Surprisingly, our maternal zygotic *hmx4*$^{-/-}$ embryos do not recapitulate *hmx4* morpholino-induced phenotypes. Unlike *hmx4*-morphants, *hmx4*$^{-/-}$ embryos possess no overt morphological or hematopoietic defects. Our mutants exhibit an increase in *hmx1* gene expression. However, this increase is not sufficient to explain the lack of phenotype in *hmx4*$^{-/-}$ embryos, as *hmx1*-morphant; *hmx4*$^{-/-}$ embryos also do not exhibit any overt morphological defects.

Several other possibilities exist to explain the discrepancy between *hmx4*-morphant and *hmx4*$^{-/-}$ phenotypes. Firstly, we do not currently have an antibody against Hmx4. This makes it impossible to accurately determine the effectiveness of our morpholinos at knocking down Hmx4 protein levels. We speculate that our *hmx4*-morphants retain some level of Hmx4 protein function. If this is the case, some compensatory mechanism may exist to differentially upregulate *hmx4* and/or *hmx4*-target RNA levels in *hmx4*-morphants versus mutants.

A second possibility to explain the discrepancy between *hmx4*-morphant and mutant phenotypes is that our morpholinos may bind to, and inhibit the function of unintended target genes. Our morpholino-based analyses of Hmx4 make use of two translation-blocking morpholinos with non-overlapping target sites. These morpholinos prevent the translation of target sequence-containing *EGFP* contructs, generate identical phenotypes when used independently, and synergize when used together at suboptimal dosages (Gongal et al., 2011). Furthermore, BLAST searching confirms that our *hmx4*-morpholino sequences do not exist outside of the *hmx4* locus in zebrafish. Thus, it appears that our *hmx4*-morphant phenotypes are specific to Hmx4-depletion, and are not likely the result of off-target effects. However, as *hmx4* overexpression generates morphological defects that are more severe than those observed in our *hmx4*-morphants (Figure 5.1; Figure 5.15; Gongal et al., 2011), we are unable to conduct the ideal morpholino control – to rescue *hmx4*-morphants by injecting them with *hmx4* RNA. Consequently, we cannot completely omit the possibility that our morpholinos

act on targets other than Hmx4. Notably, we are unable to use splice-blocking morpholinos against *hmx4*, as removal of its single exon generates an in-frame product.

Finally, although our overexpression analyses indicate that *hmx4*$^{-/-}$ embryos possess loss-of-function mutations in *hmx4*, it is possible that these embryos retain some level of Hmx4 protein function. Our *hmx4*$^{-/-}$ embryos possess a nonsense mutation that generates a premature stop codon immediately upstream of the Hmx4 homeodomain (Figure 5.10). These embryos therefore possess 72 (*hmx4*^{ua1004})/75 (*hmx4*^{ua1003}) amino acids (or 216/225 base pairs) of intact, wild type sequence N-terminal to the homeodomain. Although unlikely, it is therefore possible that our *hmx4*$^{-/-}$ embryos retain homeodomain-independent Hmx4 functions that are revealed by our analyses of *hmx4*-morphants. To test this hypothesis, we could ascertain if overexpressing our mutant *hmx4* RNAs in *hmx4*-morphants rescues their morphological defects.

Both transcription activator-like effector nucleases (TALENs) and the clustered regularly interspaced short palindromic repeats (CRISPR)/Cas9 system have successfully been used to delete whole loci from the zebrafish genome (Auer and Del Bene, 2014; Gupta et al., 2013; Liu et al., 2014; Ma et al., 2013; Xiao et al., 2013). These targeted endonuclease technologies could potentially be used to generate *hmx4*-null zebrafish. These mutants could then be used to more confidently assess Hmx4 function in zebrafish hematopoiesis.

5.4 Figures

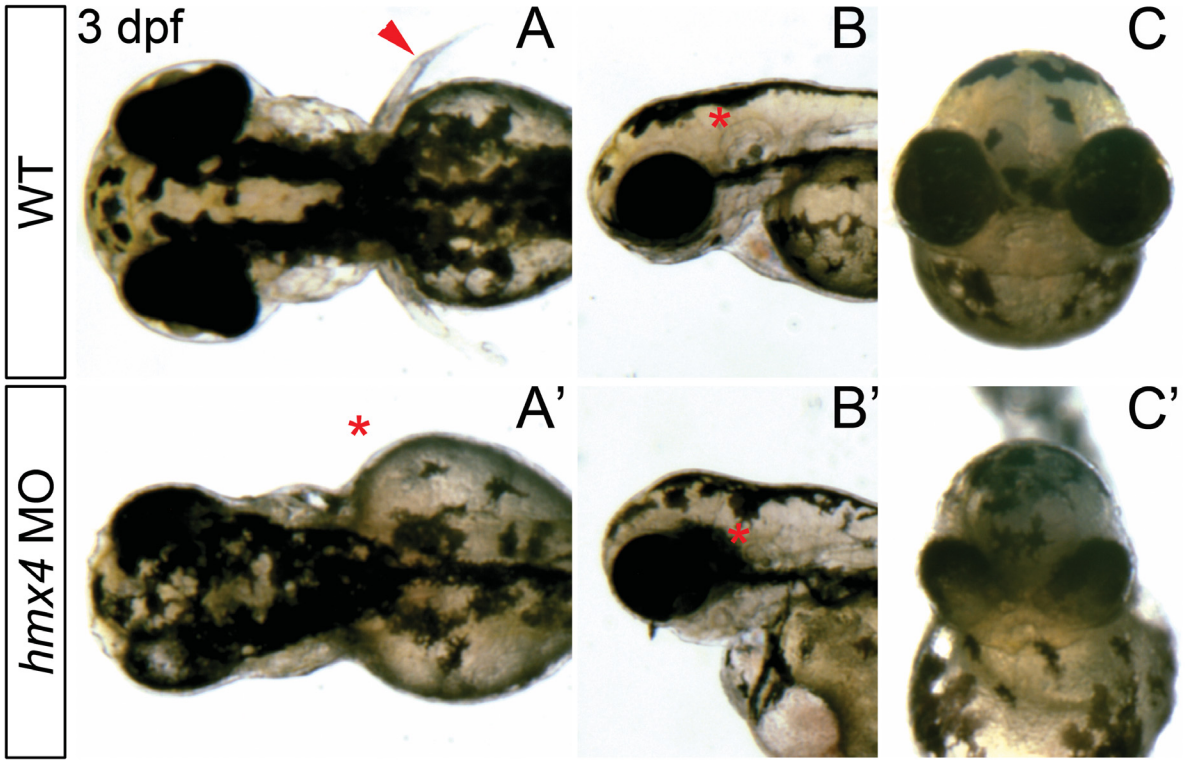

Figure 5.1. *hmx4*-morphants exhibit a host of morphological defects. (A,A') Dorsal view of live 3 days post fertilization (dpf) embryos; anterior to left. Unlike their wild type (WT) counterparts (A), *hmx4*-morphants (A') display a narrowed eyefield and loss of pectoral fins. Asterisk indicates absent pectoral fins. (B,B') Lateral view of live 3 dpf embryos; anterior to left. *hmx4*-morphants (B') display small ears compared to WT embryos (B). Asterisks indicate ears. (C,C') Frontal view of live 3 dpf embryos. *hmx4*-morphants (C') display a narrowed eyefield when compared to WT embryos (C).

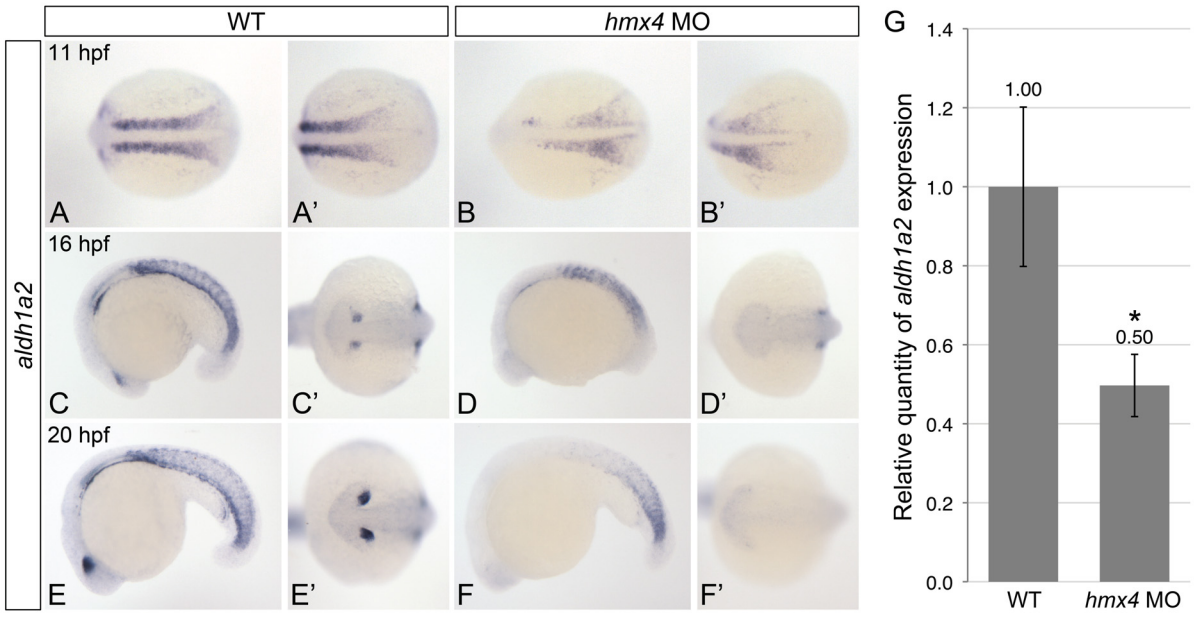

Figure 5.2. *hmx4*-morphant embryos exhibit reduced *aldh1a2* RA-synthesis gene expression. Shown are representative embryos following *in situ* hybridization analysis of *aldh1a2* expression in 11 hours post fertilization (hpf) (A-B'), 16 hpf (C-D') and 20 hpf (E-F') embryos. Dorsal view (A-B', C', D', E', F') or lateral view (C, D, E, F) of gene expression is shown with anterior oriented to the left. A', B', C', D', E' and F' represent different views of the embryos shown in A, B, C, D, E and F. *hmx4*-morphant embryos (B, B', D, D', F, F') exhibit a severe decrease in *aldh1a2* expression when compared to wild type embryos (WT; A, A', C, C', E, E') at all stages examined. (G) Real-time quantitative PCR analysis of *aldh1a2* expression in 18 hpf WT and *hmx4*-morphant embryos Shown is the relative quantity of *aldh1a2* expression. Samples were normalized to *ef1a* and WT was set to 1. Error bars indicate standard deviation from the mean. *Indicates the difference compared to WT is significant by Student *t* test; $P < 0.0001$.

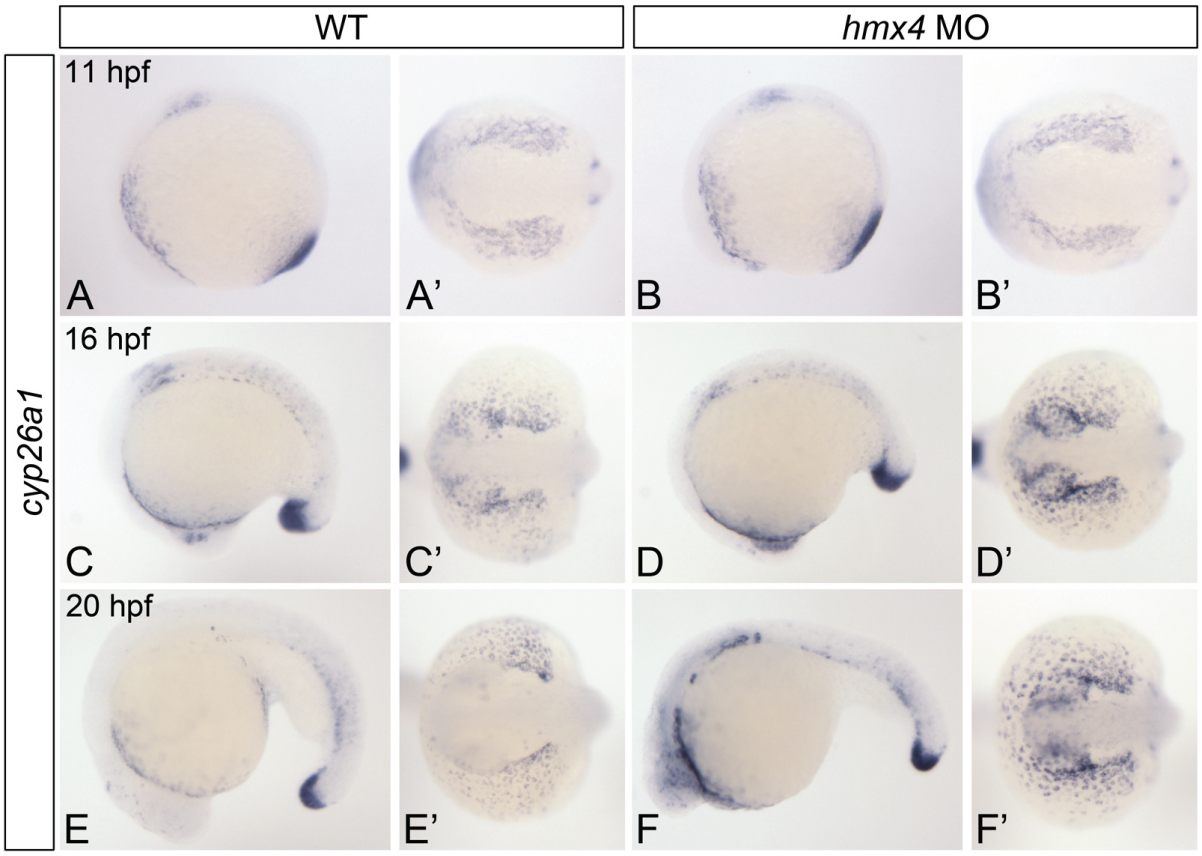

Figure 5.3. *hmx4*-morphant embryos exhibit expanded *cyp26a1* RA-metabolism gene expression. Shown are representative embryos following *in situ* hybridization analyses of *cyp26a1* expression in 11 hours post fertilization (hpf; A-B'), 16 hpf (C-D') and 20 hpf (E-F') embryos. Dorsal view (A', B', C', D', E', F') or lateral view (A, B, C, D, E, F) of gene expression is shown with anterior oriented to the left. A', B', C', D', E' and F' represent different views of the embryos shown in A, B, C, D, E and F. *hmx4*-morphant embryos exhibit a broadened domain of tailbud *cyp26a1* expression at 11 hpf (B), and increased anterior neurectoderm *cyp26a1* expression at 16 hpf and 20 hpf (D', F'), compared to wild type embryos (WT; A, C', E').

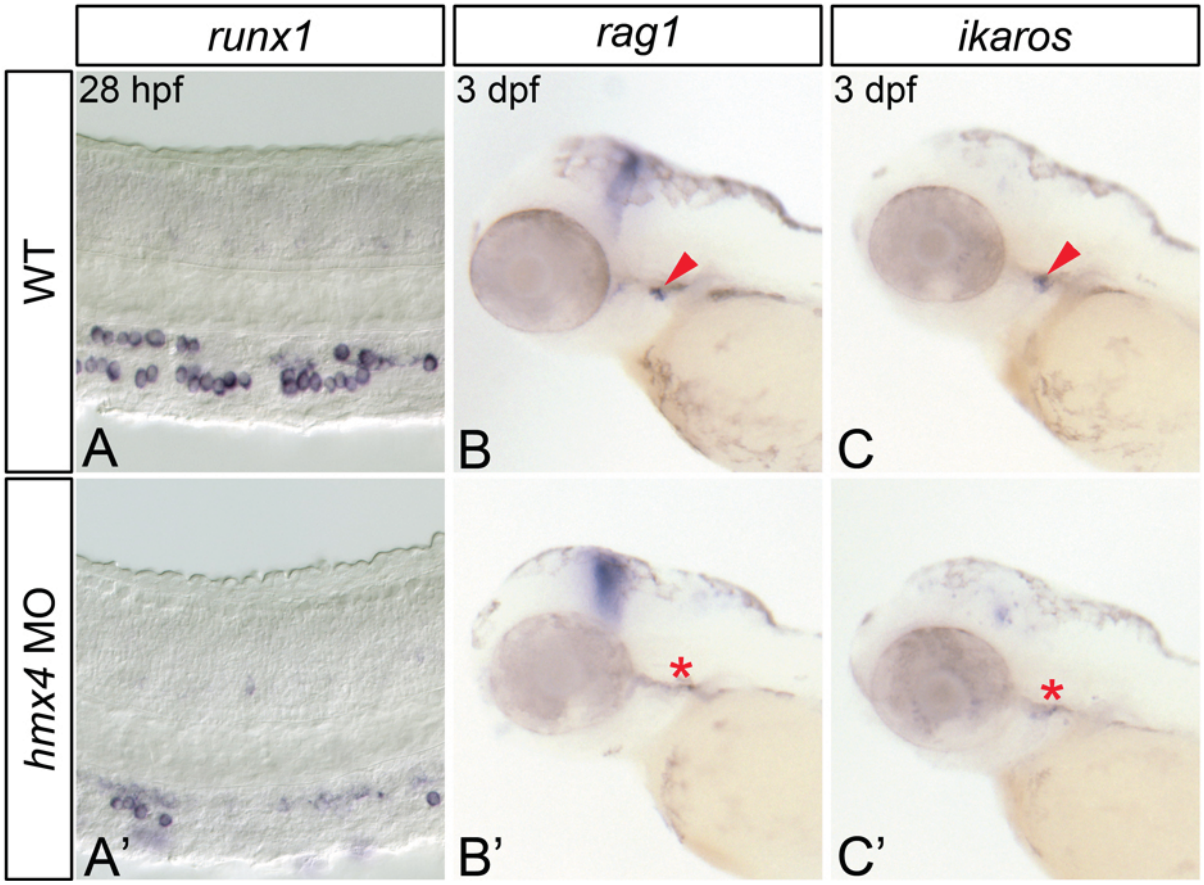

Figure 5.4. *hmx4*-morphant embryos demonstrate impaired HSC formation. (A, A') Shown are representative embryos following *in situ* hybridization analysis of *runx1* gene expression in 28 hours post fertilization (hpf) embryos. Lateral view of gene expression in the dorsal aorta region of the trunk is shown; anterior to the left. Compared to wild type embryos (WT; A) *hmx4*-morphants (A') exhibit reduced *runx1* expression. (B-C') Shown are representative embryos following *in situ* hybridization analyses of common lymphoid progenitor gene expression in 3 days post fertilization (dpf) embryos. Lateral view of gene expression in the head is shown; anterior to the left. Arrows and asterisks indicate thymus. Compared to WT embryos (B, C) *hmx4*-morphants exhibit nearly abolished thymic *rag1* (B') and *ikaros* (C') expression. *eng2a* expression in the midbrain hindbrain boundary is shown in B and B'.

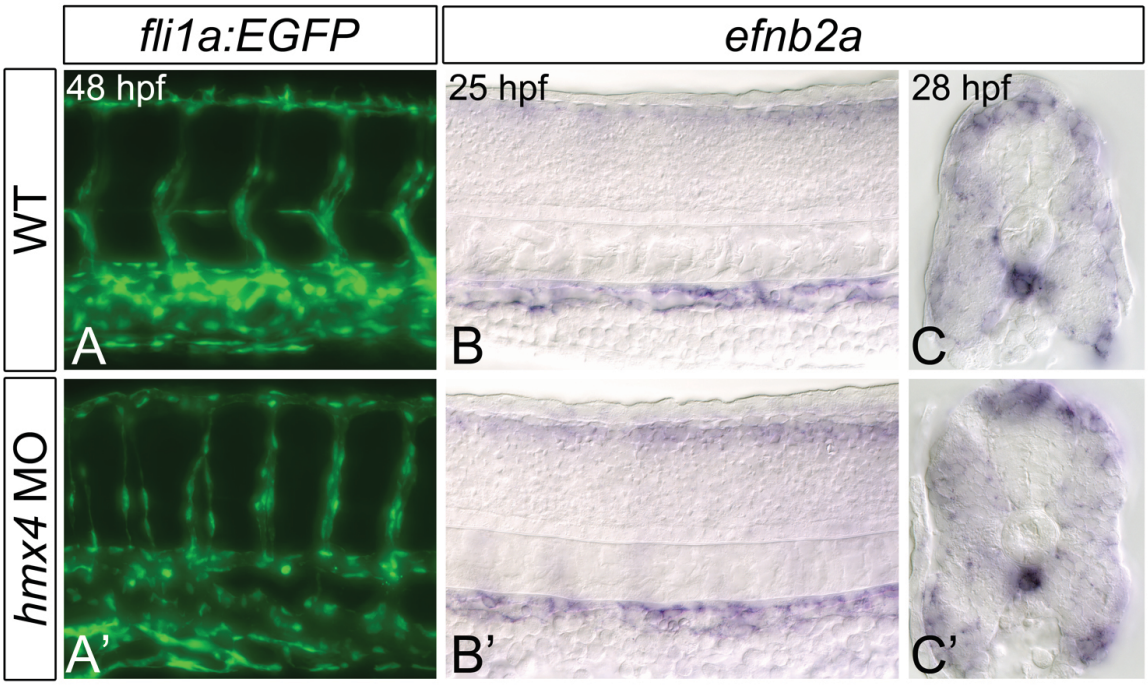

Figure 5.5. *hmx4*-morphant embryos demonstrate relatively normal vasculogenesis. (A, A') Lateral view of 48 hours post fertilization (hpf) *fli1a:EGFP* embryos; anterior to left. Compared to wild type (WT) embryos (A), *hmx4*-morphants (A') display relatively normal vasculature. The atypical intersegmental vessel patterning of *hmx4*-morphants reflects the square shape of their somites. (B-C') Shown are representative embryos following *in situ* hybridization analysis of *efnb2a* gene expression in 25 hpf (B, B') and 28 hpf (C, C') embryos. (B, B') Lateral view of gene expression in the dorsal aorta region of the trunk is shown; anterior to the left. (C, C') Transverse section of expression in the dorsal aorta region of the trunk is shown; anterior to the front. Compared to WT embryos (B, C), *hmx4*-morphants (B', C') exhibit normal dorsal aorta *efnb2a* gene expression.

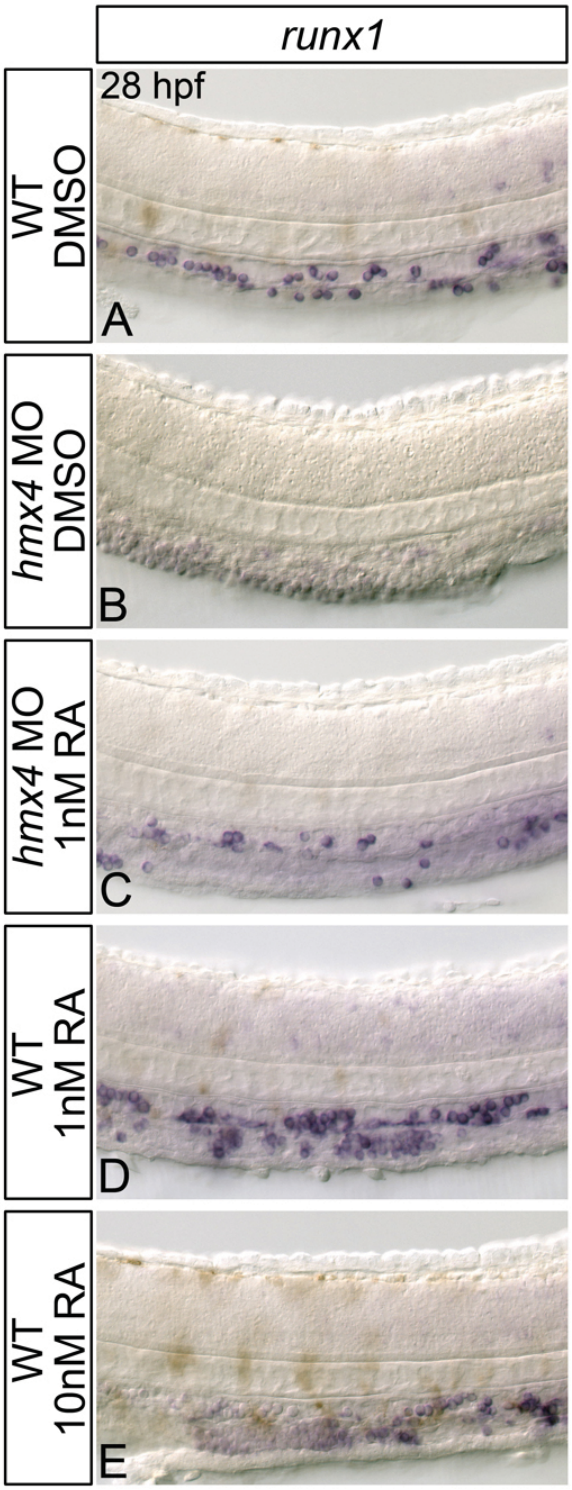

Figure 5.6. RA-treatment rescues *runx1* gene expression in *hmx4*-morphants. Shown are representative embryos following *in situ* hybridization analysis of *runx1* gene expression at 28 hpf. Lateral view of gene expression in the dorsal aorta region of the trunk is shown; anterior to the left. Compared to wild type (WT) control embryos (A) *hmx4*-morphants (B) exhibit nearly abolished *runx1* expression. This expression is partially restored in *hmx4*-morphants treated with 1 nM retinoic acid (RA; C). WT embryos treated with 1 nM RA exhibit ectopic *runx1* expression (D), while those treated with 10 nM RA exhibit reduced *runx1* expression (E).

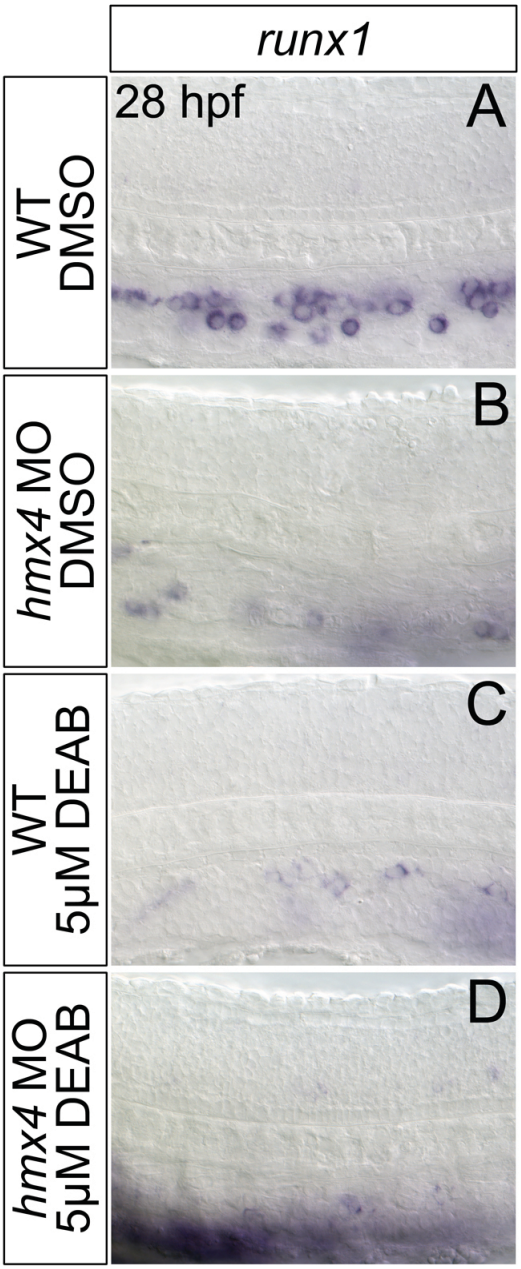

Figure 5.7. DEAB-treated *hmx4*-morphants exhibit more severe *runx1* gene expression defects than *hmx4*-morphants. Shown are representative embryos following *in situ* hybridization analysis of *runx1* gene expression at 28 hpf. Lateral view of gene expression in the dorsal aorta region of the trunk is shown; anterior to the left. Compared to wild type (WT) control embryos (A), *hmx4*-morphants (B) and embryos treated with 5 μM DEAB (C) exhibit strongly reduced *runx1* expression. This expression is further reduced in 5 μM DEAB-treated *hmx4*-morphants (D).

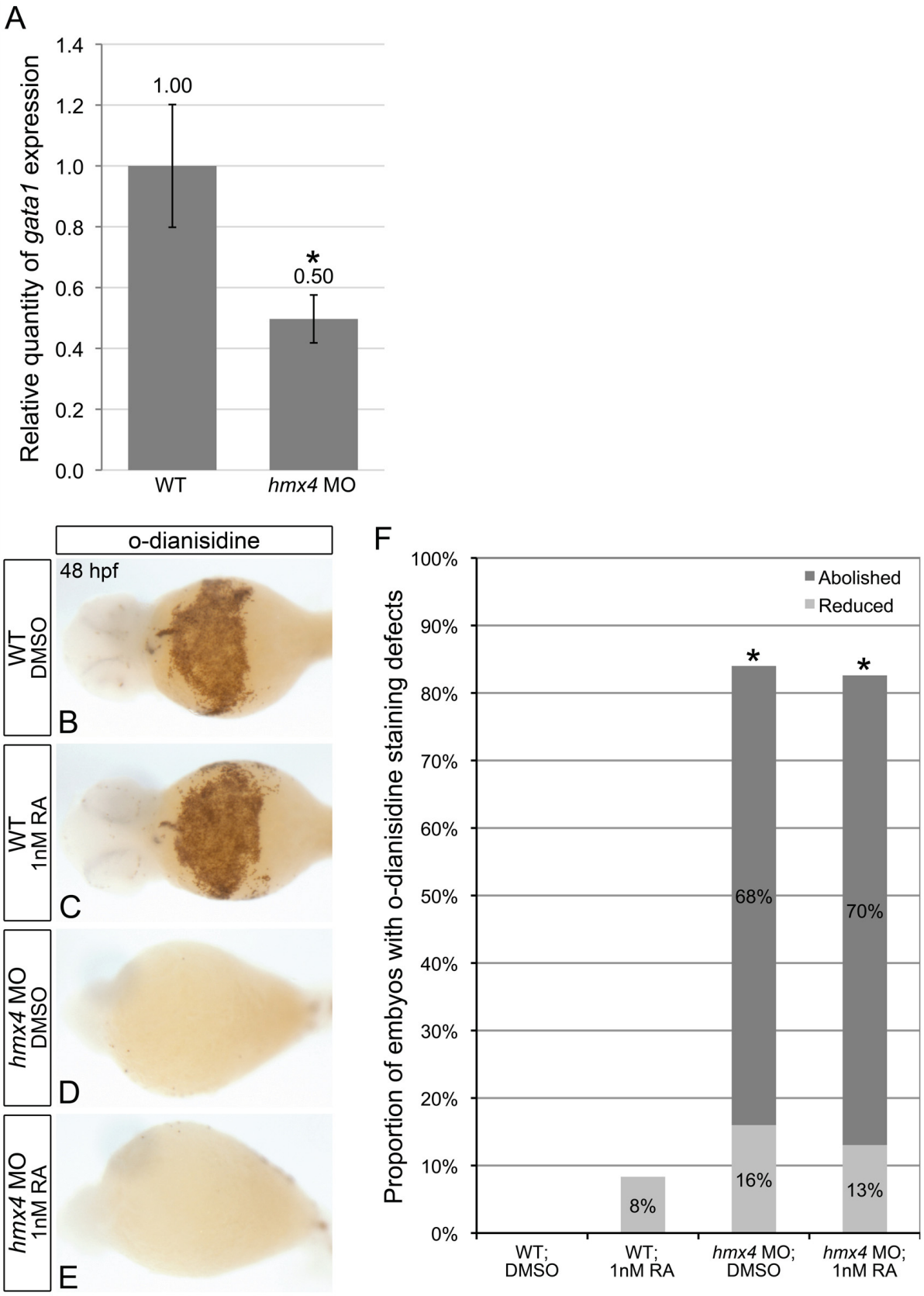
A
Relative quantity of gata1 expression
1.4
1.2
1.0
0.8
0.6
0.4
0.2
0.0
1.00
*
0.50
WT
hmx4 MO
o-dianisidine
48 hpf
WT DMSO
B
WT 1nM RA
C
hmx4 MO DMSO
D
hmx4 MO 1nM RA
E
F
Proportion of embyos with o-dianisidine staining defects
100%
90%
80%
70%
60%
50%
40%
30%
20%
10%
0%
Abolished
Reduced
*
*
68%
70%
16%
13%
8%
WT; DMSO
WT; 1nM RA
hmx4 MO; DMSO
hmx4 MO; 1nM RA

Figure 5.8. *hmx4*-morphants exhibit RA-independent primitive erythropoietic defects. (A) Real-time quantitative PCR analysis of *aldh1a2* expression in 18 hpf WT and *hmx4*-morphant embryos. Shown is the relative quantity of *gata1* expression. Samples were normalized to *ef1a* and WT was set to 1. Error bars indicate standard deviation from the mean. *Indicates the difference compared with WT is significant by Student *t* test; $P < 0.0001$. (B-E) o-dianisidine staining of differentiated erythrocytes in 48 hpf whole-mount embryos; ventral view with anterior to left. o-dianisidine staining is abolished in *hmx4*-morphant embryos (D), when compared to WT control embryos (B) and embryos treated with 1 nM RA (C). o-dianisidine staining is not restored in *hmx4*-morphants treated with 1nM RA (E). (F) Quantification of the phenotypes shown in B-E. Shown is the proportion of 48 hpf embryos with reduced or abolished o-dianisidine staining. *Indicates significant result compared to WT, by Fisher's Exact test with Bonferroni correction on cumulative raw counts; $P < 0.0004$.

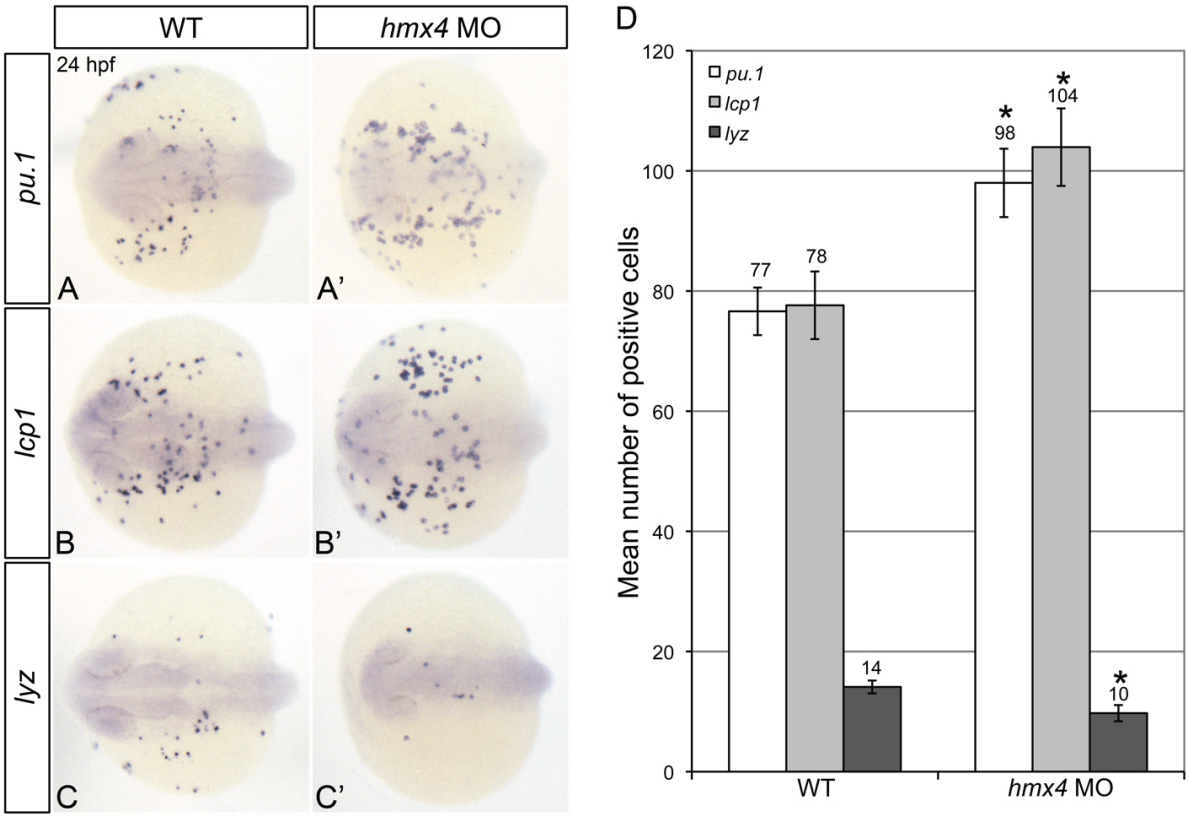

Figure 5.9. Hmx4 regulates primitive myelopoietic gene expression. (A-C') Shown are representative embryos following *in situ* hybridization analyses of *pu.1* (A, A'), *lcp1* (B, B'), and *lyz* (C, C') expression in 24 hours post fertilization (hpf) embryos. Dorsal view of gene expression in the anterior lateral-plate mesoderm (ALPM) is shown in whole-mount embryos with anterior oriented to the left. *hmx4*-morphant embryos (A', B') exhibit an increase in the number of *pu.1*- and *lcp1*-expressing cells, but a decrease in the number of *lyz*-expressing cells (C') when compared to wild type (WT; A, B, C) embryos. (D) Quantification of the phenotypes shown in A-C'. Shown is the average number of *pu.1*-, *lcp1*-, and *lyz*-expressing cells in the ALPM of 24 hpf embryos as determined by *in situ* hybridization. Error bars indicate standard error of the mean. *Indicates the difference compared to WT is significant by Student *t* test; $P < 0.05$.

A

Hmx4

DNA

5 ’- ATGAGCAAGGAGGACGCGTCATGTCGACCCGCTTCTTTGAAGTTCACCATTGACAAT
ATCCTCAACTCCAAGACGAGCAGCAGAAACTTTGACAGCTGTCATTCAAGGGCATCGCT
CGTGGTGTGTCGGGATGGCTGTCTTCATCACCCCGGAGAGAGCGAGGATCCATGTAAA
GAAGGGTCAGATGCAAGATTGCATGGCATTGATAAACTCAACAGAGAGGGGGATGCGA
CTGTGGACGCGCTCAAAGCCGTCGACATGCGCAGCGAGAGCGCGGACAGCTGCGAC
GACGCGCAGCAAAAGAACAACGGCAAGAAGAATAAACTGATGACGAAGAAGAAAACGC
GCACTATATTTTCAAAAAGACAGATCTTCCAACTGGAATCTACGTTTGACATGAAGCGCTA
CCTGAGCAGCGCGGAGCGCGCGTGCTTGGCGAACTCCTTGCAGCTTACCGAGACTCA
AGTCAAAATCTGGTTTCAGAATCGACGGAATAAATTAAAAAGACAACTGTCTACTGAACT
TGAAGGACCGAACAGCGAGTTCGGTGATATTGGAAAGACGGTGCCGCTTCCAGCTTTAT
ATAAAGAGAATAATCTGCTCGGAAGGTGCATGCTTCCAATGCCTTTACCAGTCGTGTATC
CTGGAGGTAGCGCGCCTTACTTTTATTTCTCAAATGCCAGCAAGTATTTCAGCCTGTTTG
ATGGAGATATATGA - 3’

Protein

N’ - MSKEDASCRPASLKFTIDNILNSKTSSRNFDSCHSRASLVVCRDGCLHHPGESEDPCK
EGSDARLHGIDKLNREGDATVDALKAVDMRSESADSCDDAQQKNNGKKNKLMTKKKTRTI
FSKRQIFQLESTFDMKRYLSSAERACLANSLQLTETQVKIWFQNRRNKLKRQLSTELEGPN
SEFGDIGKTVPLPALYKENNLLGRCMLPMPLPVVYPGGSAPYFYFSNASKYFSLFDGDI - C’

B

Hmx4^{ua1003}

DNA

5 ’- ATGAGCAAGGAGGACGCGTCATGTCGACCCGCTTCTTTGAAGTTCACCATTGACAAT
ATCCTCAACTCCAAGACGAGCAGCAGAAACTTTGACAGCTGTCATTCAAGGGCATCGCT
CGTGGTGTGTCGGGATGGCTGTCTTCATCACCCCGGAGAGAGCGAGGATCCATGTAAA
GAAGGGTCAGATGCAAGATTGCATGGCATTGATAAACTCAACAGAGAG**AGAG**GGGGAT
GCGACTGTGGACGCGCTCAAAGCCGTCGACATGCGCAGCGAGAGCGCGGACAGCTG
CGACGACGCGCAGCAAAAGAACAACGGCAAGAAGAATAAACTGATGACGAAGAAGAAA
ACGCGCACTATATTTTCAAAAAGACAGATCTTCCAACTGGAATCTACGTTTGACATGAAG
CGCTACCTGAGCAGCGCGGAGCGCGCGTGCTTGGCGAACTCCTTGCAGCTTACCGAG
ACTCAAGTCAAAATCTGGTTTCAGAATCGACGGAATAAATTAAAAAGACAACTGTCTACT
GAACTTGAAGGACCGAACAGCGAGTTCGGTGATATTGGAAAGACGGTGCCGCTTCCAG
CTTTATATAAAGAGAATAATCTGCTCGGAAGGTGCATGCTTCCAATGCCTTTACCAGTCGT
GTATCCTGGAGGTAGCGCGCCTTACTTTTATTTCTCAAATGCCAGCAAGTATTTCAGCCT
GTTTGATGGAGATATATGA - 3’

Protein

N’ - MSKEDASCRPASLKFTIDNILNSKTSSRNFDSCHSRASLVVCRDGCLHHPGESEDPCK
EGSDARLHGIDKLNRE**RGGCDCGRAQSRRHAQRERGQLRRRAAKEQRQEE** - C’

C

Hmx4^{ua1004}

DNA

5 ’- ATGAGCAAGGAGGACGCGTCATGTCGACCCGCTTCTTTGAAGTTCACCATTGACAAT
ATCCTCAACTCCAAGACGAGCAGCAGAAACTTTGACAGCTGTCATTCAAGGGCATCGCT
CGTGGTGTGTCGGGATGGCTGTCTTCATCACCCCGGAGAGAGCGAGGATCCATGTAAA
GAAGGGTCAGATGCAAGATTGCATGGCATTGATAAACTCAA**GAGAGGGGGATGCG**AC
TGTGGACGCGCTCAAAGCCGTCGACATGCGCAGCGAGAGCGCGGACAGCTGCGACGA
CGCGCAGCAAAAGAACAACGGCAAGAAGAATAAACTGATGACGAAGAAGAAAACGCGC
ACTATATTTTCAAAAAGACAGATCTTCCAACTGGAATCTACGTTTGACATGAAGCGCTACC
TGAGCAGCGCGGAGCGCGCGTGCTTGGCGAACTCCTTGCAGCTTACCGAGACTCAAG
TCAAAATCTGGTTTCAGAATCGACGGAATAAATTAAAAAGACAACTGTCTACTGAACTTG
AAGGACCGAACAGCGAGTTCGGTGATATTGGAAAGACGGTGCCGCTTCCAGCTTTATAT
AAAGAGAATAATCTGCTCGGAAGGTGCATGCTTCCAATGCCTTTACCAGTCGTGTATCCT
GGAGGTAGCGCGCCTTACTTTTATTTCTCAAATGCCAGCAAGTATTTCAGCCTGTTTGAT
GGAGATATATGA - 3’

Protein

N’ - MSKEDASCRPASLKFTIDNILNSKTSSRNFDSCHSRASLVVCRDGCLHHPGESEDPCK
EGSDARLHGIDKL**KRGGCDCGRAQSRRHAQRERGQLRRRAAKEQRQEE** - C’

D

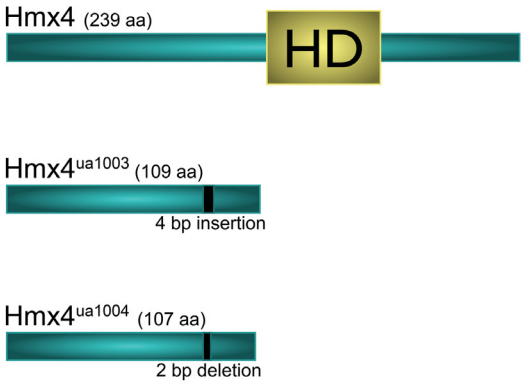

Figure 5.10. Mutations present in *hmx4*-mutant zebrafish generated using ZFN technology. (A-C) DNA and amino acid sequence of wild type (WT; Hmx4, A) and mutant (Hmx4^{ua1003}, B; Hmx4^{ua1004}, C) alleles of *hmx4* generated using zinc finger nuclease (ZFN) technology. ZFN target site is underlined. Homeodomain amino acid sequence is written in yellow. Modified amino acid sequence is bolded. (D) Diagrammatical representation of WT and mutant Hmx4 proteins. HD indicates homeodomain. Black bars represent placement of 4 bp insertion and 2 bp deletion, respectively. Both *hmx4* mutations produce frameshifts that generate premature stop codons immediately upstream of the *hmx4* homeodomain.

Figure 5.11. *hmx4*$^{-/-}$ embryos do not exhibit gross morphological defects. Lateral view of live 5 days post fertilization (dpf) embryos; anterior to left. Compared to wild type embryos (WT; A), maternal-zygotic (MZ) *hmx4*$^{ua1004/ua1004}$ (B) and *hmx4*$^{ua1003/ua1003}$ (C) embryos do not display any gross morphological defects.

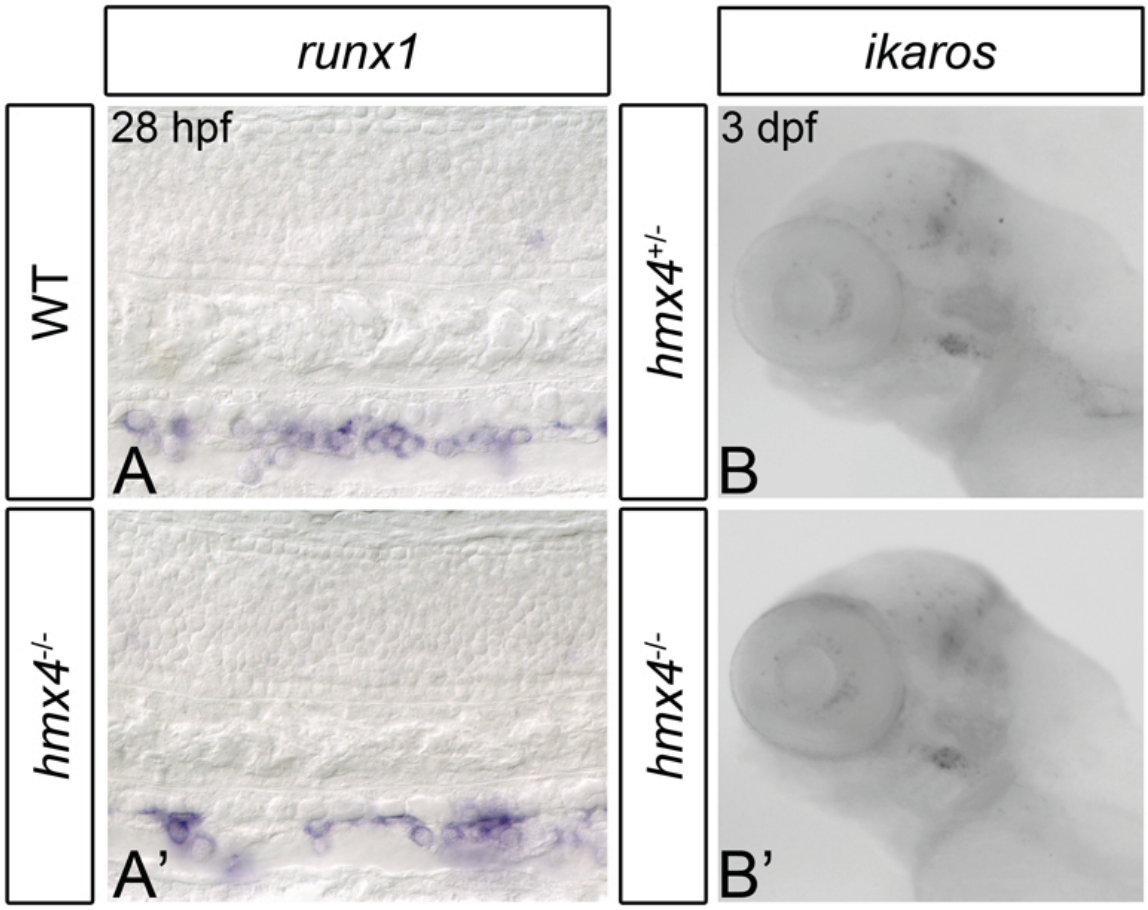

Figure 5.12. *hmx4*$^{-/-}$ embryos do not demonstrate impaired HSC formation. (A, A') Shown are representative embryos following *in situ* hybridization analysis of *runx1* gene expression in 28 hours post fertilization (hpf) embryos. Lateral view of gene expression in the dorsal aorta region of the trunk is shown; anterior to the left. Wild type embryos (WT; A) and *hmx4*$^{ua1004/ua1004}$ embryos (A') exhibit similar levels of *runx1* expression. (B, B') Shown are representative embryos following *in situ* hybridization analysis of *ikaros* common lymphoid progenitor gene expression in 3 days post fertilization (dpf) embryos. Lateral view of gene expression in the head is shown; anterior to the left. *hmx4*$^{ua1003/+}$ (A) and *hmx4*$^{ua1003/ua1004}$ embryos (A') exhibit similar levels of thymic *ikaros* expression.

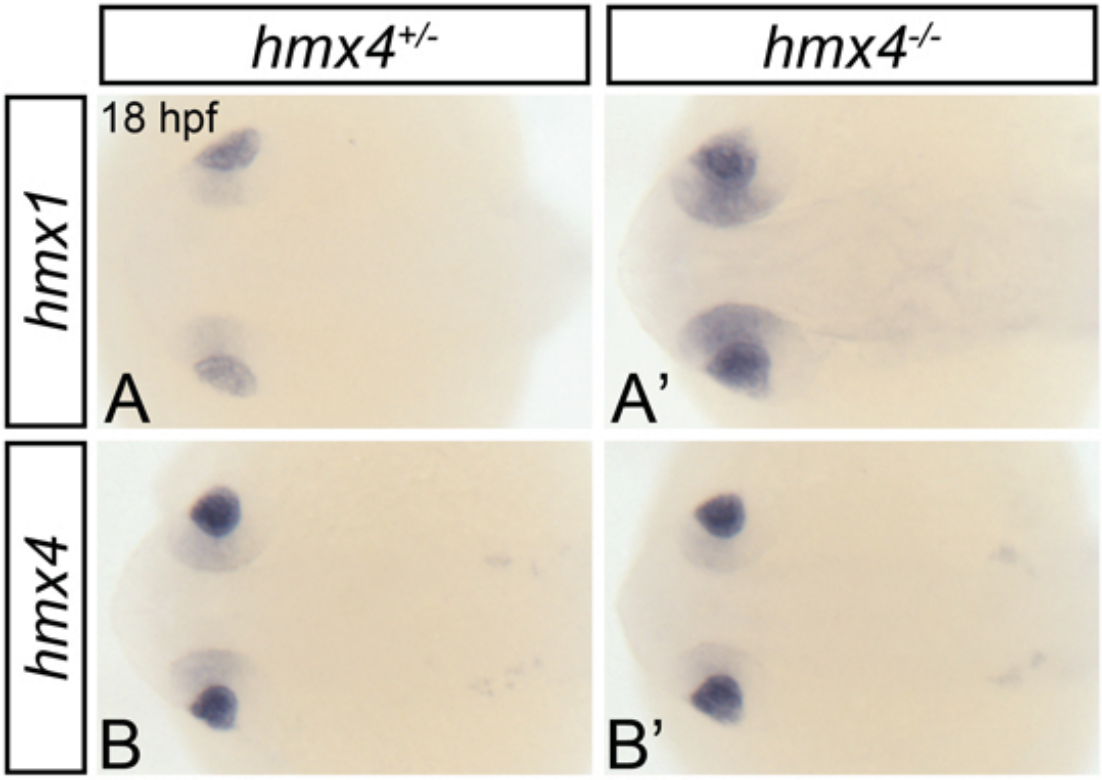

Figure 5.13. *hmx1*, but not *hmx4* expression is upregulated in *hmx4*$^{-/-}$ embryos. Shown are representative embryos following *in situ* hybridization analyses of *hmx1* (A, A') and *hmx4* (B, B') gene expression in 18 hours post fertilization (hpf) embryos. Dorsal view of gene expression in the head is shown; anterior to the left. Compared to *hmx4*$^{ua1003/+}$ siblings (A), *hmx4*$^{ua1003/ua1003}$ embryos (A') exhibit increased and expanded ocular *hmx1* expression. *hmx4*$^{ua1003/+}$ (B) and *hmx4*$^{ua1003/ua1003}$ embryos (B') exhibit similar levels of ocular *hmx4* expression.

Figure 5.14. *hmx1*-morphant; *hmx4*$^{-/-}$ embryos do not exhibit gross morphological defects. Lateral view of live 5 days post fertilization (dpf) embryos; anterior to left. Compared to wild type embryos (WT; A), maternal-zygotic (MZ) *hmx4*$^{ua1004/ua1004}$ (B), *hmx1*-morphant (C) and *hmx4*-morphant; MZ *hmx4*$^{ua1004/ua1004}$ (C) embryos do not display any gross morphological defects.

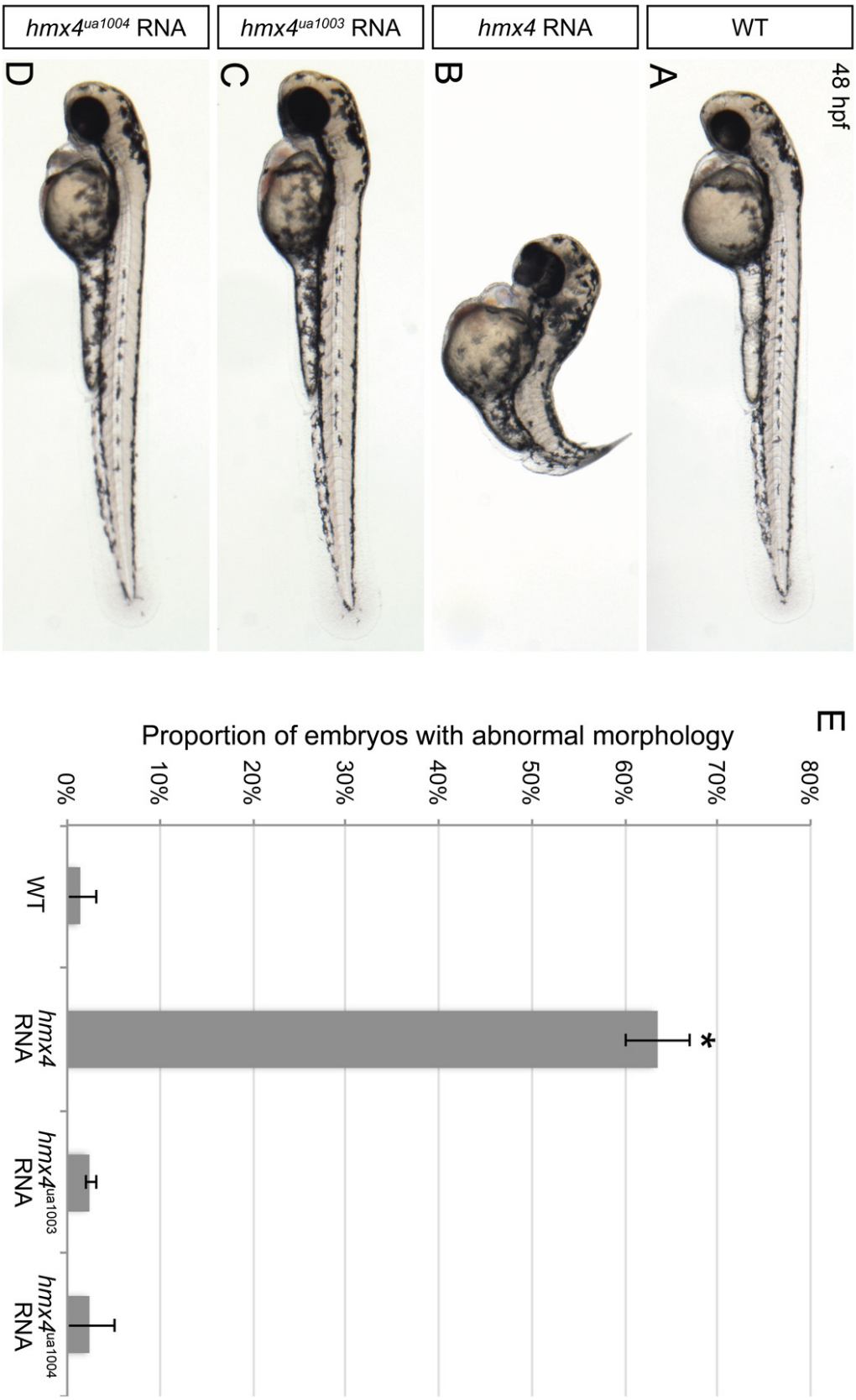
WT
hmx4 RNA
hmx4ua1003 RNA
hmx4ua1004 RNA
A
B
C
D
48 hpf
E
Proportion of embryos with abnormal morphology
0%
10%
20%
30%
40%
50%
60%
70%
80%
WT
hmx4 RNA
hmx4ua1003 RNA
hmx4ua1004 RNA
*

Figure 5.15. The *hmx4*^{ua1003} and *hmx4*^{ua1003} alleles represent loss-of-function mutations in *hmx4*. (A-D) Lateral view of live 48 hours post fertilization (hpf) embryos; anterior to left. Compared to wild type embryos (WT; A), embryos injected with *hmx4* RNA (B) display severe morphological defects. Embryos injected with *hmx4*^{ua1003} RNA (C) or *hmx4*^{ua1004} RNA (D) do not exhibit overt morphological defects. (E) Quantification of the phenotypes shown in A-D. Shown is the mean proportion of 48 hpf embryos with abnormal morphology. Error bars indicated standard error of the mean. *Indicates significant result compared to WT by Fisher's Exact test with Bonferroni correction on cumulative raw counts; $P < 0.0003$.

5.5 Tables

Table 5.1: Quantification of definitive hematopoietic gene-expression defects of *hmx4*-morphant embryos.

Gene	Stage	Treatment	Wild type	Reduced	Total	Two-tailed *P*-value
runx1	28 hpf	WT	15	1	16	
		hmx4 MO	5	26	31	<0.0001*
ikaros	3 dpf	WT	16	2	18	
		hmx4 MO	5	17	22	<0.0001*
rag1	3 dpf	WT	12	5	17	
		hmx4 MO	4	17	21	<0.0026*

*Indicates significant result compared to wild type (WT), by Fisher's Exact Test on cumulative raw counts.

Table 5.2: Quantification of *runx1* gene expression defects in 28 hpf *hmx4*-morphant embryos treated with RA.

Treatment	Wild type	Increased	Reduced	Total	Two-tailed *P*-value	Two-tailed *P*-value
WT; DMSO	12	0	0	12		
WT; 1 nM RA	9	3	1	13	1.000	
hmx4 MO; DMSO	3	0	12	15	<0.0005*	
hmx4 MO; 1 nM RA	9	0	8	17	0.0534	0.4554**
hmx4 MO; 10 nM RA	3	2	8	13	0.0096*	1.000**

*Indicates significant result compared to wild type (WT), by Fisher's Exact Test with Bonferroni correction on cumulative raw counts.

**Indicates not a significant result compared to DMSO-treated, *hmx4*-morphants by Fisher's Exact Test with Bonferroni correction on cumulative raw counts.

Table 5.3: Quantification of o-dianisidine staining defects in 28 hpf *hmx4*-morphant embryos treated with RA.

Treatment	Wild type	Reduced	Total	Two-tailed *P*-value	Two-tailed *P*-value
WT; DMSO	23	0	23		
WT; 1 nM RA	22	2	24	1.000	
hmx4 MO; DMSO	4	21	25	<0.0004*	
hmx4 MO; 1 nM RA	4	19	23	<0.0004*	1.000**

*Indicates significant result compared to wild type (WT), by Fisher's Exact Test with Bonferroni correction on cumulative raw counts.

**Indicates not a significant result compared to DMSO-treated *hmx4*-morphants, by Fisher's Exact Test with Bonferroni correction on cumulative raw counts.

Table 5.4: Quantification of primitive myeloid defects of *hmx4*-morphant embryos.

Gene	Treatment	Mean cell number	SEM	*n*	Two-tailed *P*-value
pu.1	WT	36	0	21	
	hmx4 MO	7	24	21	0.0037*
lyz	WT	64	0	20	
	hmx4 MO	8	58	19	0.0152*
lcp1	WT	32	0	19	
	hmx4 MO	31	0	20	0.0041*

*Indicates significant result compared to wild type (WT) by Student *t* test.

Table 5.5: Quantification of morphological phenotypes of 48 hpf embryos injected with wild type or mutant *hmx4* RNA.

Treatment	Wild type	Abnormal	Total	Two-tailed *P*-value
WT	254	6	260	
hmx4 RNA	81	132	213	<0.0003*
hmx4^{ua1003} RNA	140	4	144	1.000
hmx4^{ua1004} RNA	164	5	169	1.000

*Indicates significant result compared to wild type (WT), by Fisher's Exact Test with Bonferroni correction on cumulative raw counts.

5.6 References

Auer, T.O., and F. Del Bene. 2014. CRISPR/Cas9 and TALEN-mediated knock-in approaches in zebrafish. *Methods*. 69:142-150.

Barresi, M.J., J.A. D'Angelo, L.P. Hernandez, and S.H. Devoto. 2001. Distinct mechanisms regulate slow-muscle development. *Current biology : CB*. 11:1432-1438.

Bennett, C.M., J.P. Kanki, J. Rhodes, T.X. Liu, B.H. Paw, M.W. Kieran, D.M. Langenau, A. Delahaye-Brown, L.I. Zon, M.D. Fleming, and A.T. Look. 2001. Myelopoiesis in the zebrafish, Danio rerio. *Blood*. 98:643-651.

Berman, J.N., J.P. Kanki, and A.T. Look. 2005. Zebrafish as a model for myelopoiesis during embryogenesis. *Exp Hematol*. 33:997-1006.

Boisset, G., and D.F. Schorderet. 2012. Zebrafish hmx1 promotes retinogenesis. *Experimental eye research*. 105:34-42.

Burns, C.E., T. DeBlasio, Y. Zhou, J. Zhang, L. Zon, and S.D. Nimer. 2002. Isolation and characterization of runxa and runxb, zebrafish members of the runt family of transcriptional regulators. *Exp Hematol*. 30:1381-1389.

Burns, C.E., D. Traver, E. Mayhall, J.L. Shepard, and L.I. Zon. 2005. Hematopoietic stem cell fate is established by the Notch-Runx pathway. *Genes Dev*. 19:2331-2342.

Chen, J.K., J. Taipale, K.E. Young, T. Maiti, and P.A. Beachy. 2002. Small molecule modulation of Smoothened activity. *Proc Natl Acad Sci U S A*. 99:14071-14076.

Crowhurst, M.O., J.E. Layton, and G.J. Lieschke. 2002. Developmental biology of zebrafish myeloid cells. *The International journal of developmental biology*. 46:483-492.

de Jong, J.L., A.J. Davidson, Y. Wang, J. Palis, P. Opara, E. Pugach, G.Q. Daley, and L.I. Zon. 2010. Interaction of retinoic acid and scl controls primitive blood development. *Blood*. 116:201-209.

Deitcher, D.L., D.M. Fekete, and C.L. Cepko. 1994. Asymmetric expression of a novel homeobox gene in vertebrate sensory organs. *The Journal of neuroscience : the official journal of the Society for Neuroscience*. 14:486-498.

Galloway, J.L., R.A. Wingert, C. Thisse, B. Thisse, and L.I. Zon. 2005. Loss of gata1 but not gata2 converts erythropoiesis to myelopoiesis in zebrafish embryos. *Dev Cell*. 8:109-116.

Gering, M., and R. Patient. 2005. Hedgehog signaling is required for adult blood stem cell formation in zebrafish embryos. *Dev Cell*. 8:389-400.

Gongal, P.A., L.D. March, V.L. Holly, L.M. Pillay, K.M. Berry-Wynne, H. Kagechika, and A.J. Waskiewicz. 2011. Hmx4 regulates Sonic hedgehog signaling through control of retinoic acid synthesis during forebrain patterning. *Dev Biol*. 355:55-64.

Gupta, A., V.L. Hall, F.O. Kok, M. Shin, J.C. McNulty, N.D. Lawson, and S.A. Wolfe. 2013. Targeted chromosomal deletions and inversions in zebrafish. *Genome research*. 23:1008-1017.

Hall, C., M.V. Flores, T. Storm, K. Crosier, and P. Crosier. 2007. The zebrafish lysozyme C promoter drives myeloid-specific expression in transgenic fish. *BMC Dev Biol*. 7:42.

Herbomel, P., B. Thisse, and C. Thisse. 1999. Ontogeny and behaviour of early macrophages in the zebrafish embryo. *Development*. 126:3735-3745.

Herbomel, P., B. Thisse, and C. Thisse. 2001. Zebrafish early macrophages colonize cephalic mesenchyme and developing brain, retina, and epidermis through a M-CSF receptor-dependent invasive process. *Dev Biol*. 238:274-288.

Hsu, K., D. Traver, J.L. Kutok, A. Hagen, T.X. Liu, B.H. Paw, J. Rhodes, J.N. Berman, L.I. Zon, J.P. Kanki, and A.T. Look. 2004. The pu.1 promoter drives myeloid gene expression in zebrafish. *Blood*. 104:1291-1297.

Jin, H., L. Li, J. Xu, F. Zhen, L. Zhu, P.P. Liu, M. Zhang, W. Zhang, and Z. Wen. 2012. Runx1 regulates embryonic myeloid fate choice in zebrafish through a negative feedback loop inhibiting Pu.1 expression. *Blood*. 119:5239-5249.

Kalev-Zylinska, M.L., J.A. Horsfield, M.V. Flores, J.H. Postlethwait, M.R. Vitas, A.M. Baas, P.S. Crosier, and K.E. Crosier. 2002. Runx1 is required for zebrafish blood and vessel development and expression of a human RUNX1-CBF2T1 transgene advances a model for studies of leukemogenesis. *Development*. 129:2015-2030.

Kitaguchi, T., K. Kawakami, and A. Kawahara. 2009. Transcriptional regulation of a myeloid-lineage specific gene lysozyme C during zebrafish myelopoiesis. *Mech Dev*. 126:314-323.

Le Guyader, D., M.J. Redd, E. Colucci-Guyon, E. Murayama, K. Kissa, V. Briolat, E. Mordelet, A. Zapata, H. Shinomiya, and P. Herbomel. 2008. Origins and unconventional behavior of neutrophils in developing zebrafish. *Blood*. 111:132-141.

Liang, D., W. Jia, J. Li, K. Li, and Q. Zhao. 2012. Retinoic acid signaling plays a restrictive role in zebrafish primitive myelopoiesis. *PloS one*. 7:e30865.

Lieschke, G.J., A.C. Oates, B.H. Paw, M.A. Thompson, N.E. Hall, A.C. Ward, R.K. Ho, L.I. Zon, and J.E. Layton. 2002. Zebrafish SPI-1 (PU.1) marks a site of myeloid development independent of primitive erythropoiesis: implications for axial patterning. *Dev Biol*. 246:274-295.

Liu, F., and Z. Wen. 2002. Cloning and expression pattern of the lysozyme C gene in zebrafish. *Mech Dev*. 113:69-72.

Liu, Y., S.E. Elf, Y. Miyata, G. Sashida, G. Huang, S. Di Giandomenico, J.M. Lee, A. Deblasio, S. Menendez, J. Antipin, B. Reva, A. Koff, and S.D. Nimer. 2009. p53 regulates hematopoietic stem cell quiescence. *Cell Stem Cell*. 4:37-48.

Liu, Y., D. Luo, Y. Lei, W. Hu, H. Zhao, and C.H. Cheng. 2014. A highly effective TALEN-mediated approach for targeted gene disruption in Xenopus tropicalis and zebrafish. *Methods*. 69:58-66.

Lyons, S.E., N.D. Lawson, L. Lei, P.E. Bennett, B.M. Weinstein, and P.P. Liu. 2002. A nonsense mutation in zebrafish gata1 causes the bloodless phenotype in vlad tepes. *Proc Natl Acad Sci U S A*. 99:5454-5459.

Ma, A.C., M.I. Chung, R. Liang, and A.Y. Leung. 2010. A DEAB-sensitive aldehyde dehydrogenase regulates hematopoietic stem and progenitor cells development during primitive hematopoiesis in zebrafish embryos. *Leukemia*. 24:2090-2099.

Ma, A.C., H.B. Lee, K.J. Clark, and S.C. Ekker. 2013. High efficiency In Vivo genome engineering with a simplified 15-RVD GoldyTALEN design. *PloS one*. 8:e65259.

Meng, X., M.B. Noyes, L.J. Zhu, N.D. Lawson, and S.A. Wolfe. 2008. Targeted gene inactivation in zebrafish using engineered zinc-finger nucleases. *Nat Biotechnol*. 26:695-701.

Nerlov, C., E. Querfurth, H. Kulessa, and T. Graf. 2000. GATA-1 interacts with the myeloid PU.1 transcription factor and represses PU.1-dependent transcription. *Blood*. 95:2543-2551.

Okuda, T., J. van Deursen, S.W. Hiebert, G. Grosveld, and J.R. Downing. 1996. AML1, the target of multiple chromosomal translocations in human leukemia, is essential for normal fetal liver hematopoiesis. *Cell*. 84:321-330.

Pevny, L., M.C. Simon, E. Robertson, W.H. Klein, S.F. Tsai, V. D'Agati, S.H. Orkin, and F. Costantini. 1991. Erythroid differentiation in chimaeric mice blocked by a targeted mutation in the gene for transcription factor GATA-1. *Nature*. 349:257-260.

Rekhtman, N., F. Radparvar, T. Evans, and A.I. Skoultchi. 1999. Direct interaction of hematopoietic transcription factors PU.1 and GATA-1: functional antagonism in erythroid cells. *Genes Dev*. 13:1398-1411.

Rhodes, J., A. Hagen, K. Hsu, M. Deng, T.X. Liu, A.T. Look, and J.P. Kanki. 2005. Interplay of pu.1 and gata1 determines myelo-erythroid progenitor cell fate in zebrafish. *Dev Cell*. 8:97-108.

Robu, M.E., J.D. Larson, A. Nasevicius, S. Beiraghi, C. Brenner, S.A. Farber, and S.C. Ekker. 2007. p53 activation by knockdown technologies. *PLoS Genet*. 3:e78.

Shivdasani, R.A., Y. Fujiwara, M.A. McDevitt, and S.H. Orkin. 1997. A lineage-selective knockout establishes the critical role of transcription factor GATA-1 in megakaryocyte growth and platelet development. *EMBO J*. 16:3965-3973.

Sive, H.L., and P.F. Cheng. 1991. Retinoic acid perturbs the expression of Xhox.lab genes and alters mesodermal determination in Xenopus laevis. *Genes Dev*. 5:1321-1332.

Stopka, T., D.F. Amanatullah, M. Papetti, and A.I. Skoultchi. 2005. PU.1 inhibits the erythroid program by binding to GATA-1 on DNA and creating a repressive chromatin structure. *EMBO J*. 24:3712-3723.

Su, F., M.A. Juarez, C.L. Cooke, L. Lapointe, J.A. Shavit, J.S. Yamaoka, and S.E. Lyons. 2007. Differential regulation of primitive myelopoiesis in the zebrafish by Spi-1/Pu.1 and C/ebp1. *Zebrafish*. 4:187-199.

Thompson, M.A., D.G. Ransom, S.J. Pratt, H. MacLennan, M.W. Kieran, H.W. Detrich, 3rd, B. Vail, T.L. Huber, B. Paw, A.J. Brownlie, A.C. Oates, A. Fritz, M.A. Gates, A. Amores, N. Bahary, W.S. Talbot, H. Her, D.R. Beier, J.H. Postlethwait, and L.I. Zon. 1998. The cloche and spadetail genes differentially affect hematopoiesis and vasculogenesis. *Dev Biol*. 197:248-269.

Ward, A.C., D.O. McPhee, M.M. Condron, S. Varma, S.H. Cody, S.M. Onnebo, B.H. Paw, L.I. Zon, and G.J. Lieschke. 2003. The zebrafish spi1 promoter drives myeloid-specific expression in stable transgenic fish. *Blood*. 102:3238-3240.

White, R.J., and T.F. Schilling. 2008. How degrading: Cyp26s in hindbrain development. *Dev Dyn*. 237:2775-2790.

Wilkinson, R.N., M.J. Koudijs, R.K. Patient, P.W. Ingham, S. Schulte-Merker, and F.J. van Eeden. 2012. Hedgehog signaling via a calcitonin receptor-like receptor can induce arterial differentiation independently of VEGF signaling in zebrafish. *Blood*. 120:477-488.

Williams, C., S.H. Kim, T.T. Ni, L. Mitchell, H. Ro, J.S. Penn, S.H. Baldwin, L. Solnica-Krezel, and T.P. Zhong. 2010. Hedgehog signaling induces arterial endothelial cell formation by repressing venous cell fate. *Dev Biol*. 341:196-204.

Xiao, A., Z. Wang, Y. Hu, Y. Wu, Z. Luo, Z. Yang, Y. Zu, W. Li, P. Huang, X. Tong, Z. Zhu, S. Lin, and B. Zhang. 2013. Chromosomal deletions and inversions mediated by TALENs and CRISPR/Cas in zebrafish. *Nucleic Acids Res*. 41:e141.

Xu, J., L. Du, and Z. Wen. 2012. Myelopoiesis during zebrafish early development. *Journal of genetics and genomics = Yi chuan xue bao*. 39:435-442.

Yoshiura, K., N.J. Leysens, R.S. Reiter, and J.C. Murray. 1998. Cloning, characterization, and mapping of the mouse homeobox gene Hmx1. *Genomics*. 50:61-68.

Zakrzewska, A., C. Cui, O.W. Stockhammer, E.L. Benard, H.P. Spaink, and A.H. Meijer. 2010. Macrophage-specific gene functions in Spi1-directed innate immunity. *Blood*. 116:e1-11.

Zhang, P., G. Behre, J. Pan, A. Iwama, N. Wara-Aswapati, H.S. Radomska, P.E. Auron, D.G. Tenen, and Z. Sun. 1999. Negative cross-talk between hematopoietic regulators: GATA proteins repress PU.1. *Proc Natl Acad Sci U S A*. 96:8705-8710.

Zhang, P., X. Zhang, A. Iwama, C. Yu, K.A. Smith, B.U. Mueller, S. Narravula, B.E. Torbett, S.H. Orkin, and D.G. Tenen. 2000. PU.1 inhibits GATA-1 function and erythroid differentiation by blocking GATA-1 DNA binding. *Blood*. 96:2641-2648.

Chapter 6

Evaluating the mutagenic activity of targeted endonucleases containing a *Sharkey* FokI cleavage domain variant in zebrafish

A version of this chapter has been published. Laura M. Pillay, Lyndsay G. Selland, Valerie C. Fleisch, Patricia L. A. Leighton, Caroline S. Cheng, Jakub K. Famulski, R. Gary Ritzel, Lindsey D. March, Hao Wang, W. Ted Allison, and Andrew J. Waskiewicz (2013). Evaluating the mutagenic activity of targeted endonucleases containing a *Sharkey* FokI cleavage domain variant in zebrafish. *Zebrafish*, 10(3): 353-364.

6.1 Introduction

6.1.1 Zinc finger nucleases

Zinc finger nucleases (ZFNs) selectively target and cleave specific gene sequences, making them a powerful tool for genome manipulation. These synthetic restriction endonucleases are composed of chimeric fusions tandemly linking three or more Cys_2His_2 zinc fingers to the non-specific FokI endonuclease domain (Cathomen and Joung, 2008; Durai et al., 2005; Kim et al., 1996; Porteus and Carroll, 2005). Each zinc finger recognizes and binds to a specific DNA sequence. When two independent ZFNs bind DNA in a tail-to-tail orientation, with proper spacing (Figure 6.1A), their FokI endonuclease domains dimerize and generate double-strand DNA breaks (Bibikova et al., 2001; Gupta et al., 2011; Mani et al., 2005). These breaks are subsequently repaired through homologous recombination (Bibikova et al., 2003; Bibikova et al., 2001; Kandavelou et al., 2005; Porteus and Baltimore, 2003; Urnov et al., 2005) or non-homologous end joining (NHEJ) (Beumer et al., 2006; Bibikova et al., 2002). NHEJ is an error-prone process that generates point mutations, insertions and deletions (Brennan and Schiestl, 1998; Hagmann et al., 1998; Hefferin and Tomkinson, 2005; Kovalchuk et al., 2004; Roth and Wilson, 1986). Repair of ZFN-induced lesions produces frameshift, nonsense or missense mutations, thereby abrogating gene function. ZFNs are especially useful for performing targeted mutagenesis in organisms that are not amenable to the generation of embryonic stem cell lines. To date, ZFNs have been successfully used to mutagenize mammalian cell lines (Lee et al., 2010; Lombardo et al., 2007; Maeder et al., 2008; Miller et al., 2007; Moehle et al., 2007; Perez et al., 2008; Porteus, 2006; Urnov et al., 2005; Zou et al., 2011), plants (Lloyd et al., 2005; Sander et al., 2011b; Shukla et al., 2009; Townsend et al., 2009; Wright et al., 2005; Zhang et al., 2010), *Drosophila melanogaster* (Beumer et al., 2006; Bibikova et al., 2002; Bozas et al., 2009), *Caenorhabditis elegans* (Morton et al., 2006), silkworm (Takasu et al., 2010), sea urchin (Ochiai et al., 2010), *Xenopus laevis* (Bibikova et al., 2001), mice (Carbery et al., 2010), rats (Geurts et al., 2009; Moreno et al., 2011), swine (Whyte and Prather, 2012; Yang et al., 2011), catfish (Dong et al., 2011), and zebrafish (Ben et al., 2011; Doyon et al., 2008; Foley et al., 2009a; Foley et al., 2009b; Meng et al., 2008; Sander et al., 2011b; Sander et al., 2011c).

Individual zinc fingers use a seven-amino acid motif to recognize and bind a specific DNA triplet sequence, with possible additional contact to the fourth base on the opposite strand (Figure 6.1B) (Kim and Berg, 1996; Pavletich and Pabo, 1991). This motif can be modified to generate custom zinc finger domains with novel DNA sequence specificities (Beerli and Barbas, 2002). Precise recognition of ZFN target sequences is achieved by arranging zinc fingers with desirable DNA-binding specificities in tandem arrays. The mutagenesis activity of a ZFN is primarily dependent on the DNA-binding affinity and specificity of its zinc finger array (Cornu et al., 2008; Urnov et al., 2005). Consequently, multiple approaches have been used to generate custom zinc finger arrays. The modular assembly approach makes use of individual, pre-selected zinc finger domains that are assembled into arrays (Bae et al., 2003; Beerli and Barbas, 2002; Gonzalez et al.; Kim et al.; Liu et al., 1997; Mandell and Barbas, 2006; Segal et al., 2003). Although rapid and facile, this strategy does not take context-dependent effects between neighboring zinc fingers into consideration (Isalan et al., 1997; Isalan et al., 1998), and exhibits a high rate of failure in mutagenesis applications (Kim et al., 2009; Ramirez et al., 2008; Sander et al., 2011b). Cell-based library screening methods have successfully been used to construct and identify zinc finger arrays with desirable sequence specificities (Cornu et al., 2008; Foley et al., 2009a; Greisman and Pabo, 1997; Hurt et al., 2003; Isalan and Choo, 2001; Maeder et al., 2008; Meng et al., 2008; Pruett-Miller et al., 2008). However, library construction and validation is time- and labor-intensive. Furthermore, the success rate for obtaining mutations using arrays identified through cell-based screening methods is still somewhat low (~50-67%) (Foley et al., 2009b; Maeder et al., 2008; Townsend et al., 2009; Zhang et al., 2010; Zou et al., 2009).

6.1.2 Transcription activator-like effector nucleases

Transcription activator-like effector nucleases (TALENs) are a second technology used for targeted mutagenesis applications. To date, TALENs have been successfully used to mutagenize mammalian cell lines (Cermak et al., 2011; Ding et al., 2013; Hockemeyer et al., 2011; Mussolino et al., 2011; Sakuma et al., 2013; Sanjana et al., 2012; Stroud et al., 2013; Sun et al., 2012), plants (Cermak et al., 2011; Li et al., 2012; Mahfouz et al., 2011; Zhang et al., 2013), yeast (Li et al., 2011b), *Drosophila melanogaster* (Liu et al., 2012; Sakuma et al., 2013),

nematodes (Wood et al., 2011), silkworm (Ma et al., 2012; Sajwan et al., 2013), *Xenopus laevis* (Ishibashi et al., 2012; Lei et al., 2012; Sakuma et al., 2013), mice (Menoret et al., 2013; Sung et al., 2013; Wefers et al., 2013), rats (Mashimo et al., 2013; Menoret et al., 2013; Tesson et al., 2011), swine (Carlson et al., 2012), medaka (Ansai et al., 2013), and zebrafish (Bedell et al., 2012; Cade et al., 2012; Dahlem et al., 2012; Gupta et al., 2013; Huang et al., 2011; Moore et al., 2012; Sakuma et al., 2013; Sander et al., 2011a). Like ZFNs, TALENs also induce double-strand breaks that are repaired through homologous recombination, or NHEJ to generate insertions and deletions that alter gene function. A TALEN consists of a TAL effector array fused to the FokI endonuclease domain (Christian et al., 2010; Li et al., 2011a). TAL effectors recognize and bind to specific DNA sequences through series of repeated modules (Boch and Bonas, 2010; Bogdanove and Voytas, 2011; Deng et al., 2012; Mak et al., 2012). Each module contains a repeat variable di-residue that preferentially recognizes and binds to a specific nucleotide (C, T, A, or G/A) (Boch and Bonas, 2010; Deng et al., 2012; Mak et al., 2012). Consequently, TALENs can be engineered to recognize nearly any DNA sequence, without the requirement for selection assays. Notably, TALENs have been shown to elicit a greater mutation rate than ZFNs in zebrafish (Chen et al., 2013). However, the somatic mutation rate obtained by using TALENs is still quite variable (<1% to 100%), and depends upon the selected TALEN scaffold, as well as the targeted locus (Bedell et al., 2012).

6.1.3 Summary

We sought to improve the efficiency of ZFN and TALEN synthetic targeted endonucleases for use in zebrafish mutagenesis. Towards this aim, we examined the activity of both ZFNs and TALENs containing a FokI nuclease variant termed *Sharkey* (Guo et al., 2010). We demonstrate that all tested *Sharkey* ZFNs exhibit greater *in vitro* cleavage of target-site DNA than controls. However, only one of three *Sharkey* ZFNs displays significantly greater activity *in vivo* in zebrafish, producing a higher frequency of insertion/deletion mutations than control ZFNs. As with ZFNs, we demonstrate that *Sharkey* TALENs exhibit greater *in vitro* cleavage of target-site DNA than controls. However, all *Sharkey* TALENs examined fail to produce any insertion/deletion mutations in zebrafish, displaying absent or significantly reduced *in vivo* mutagenic activity in comparison to control TALENs. Notably,

embryos injected with *Sharkey* ZFNs and TALENs do not exhibit an increase in toxicity-related defects or mortality.

6.2 Results

6.2.1 Rapid *in vitro* verification of ZFN target-sequence cleavage

We used a previously described bacterial one-hybrid system to screen a diverse library of zinc finger domains for their ability to bind target-sequences within three chosen zebrafish genes: *prion protein 2* (*prp2*/*prnprs3*), *H6 family homeobox 4* (*hmx4*), and *cone-rod homeobox* (*crx*). All zinc finger arrays were cloned into pCS2-FokI ZFN (DD and RR) expression vectors to generate zinc finger nucleases (ZFNs) (Meng et al., 2008). The DD and RR cleavage domain mutations prevent homodimeric cleavage activity, thereby reducing ZFN off-target activity and toxicity (Miller et al., 2007; Pruett-Miller et al., 2008; Szczepek et al., 2007).

Previous studies used restriction, PCR, or sequencing-based genotyping assays to analyze somatic mutations in ZFN-injected zebrafish embryos (Foley et al., 2009b; Meng et al., 2008; Sander et al. 2011b). Such studies demonstrate that mutagenesis success rates are variable, and are highly dependent on target-site sequence and ZFN array construction methodology. Our bacterial one-hybrid screens for *prp2*, *hmx4*, and *crx* yielded a large variety of prospective 5' and 3' ZFN arrays. However, the laborious nature of identifying *in vivo* somatic mutations precludes the analysis of multiple potential ZFN arrays. Consequently, before testing individual pairs of ZFNs *in vivo*, we assayed their ability to cleave their respective gene's target sequence *in vitro*. To do this, we used a modified *in vitro* transcription-translation assay. We synthesized 5' and 3' ZFN crude protein lysates by coupled *in vitro* transcription/translation, and incubated them along with plasmid containing the ZFN target-sequence, buffer, and plasmid-linearizing restriction enzyme. Analysis of purified, digested plasmid DNA by gel electrophoresis demonstrates whether or not ZFN arrays possess appropriate DNA cleavage activity. We selected those ZFNs with the greatest *in vitro* cleavage activity for subsequent analyses.

6.2.2 Increased efficiency of *Sharkey* FokI nuclease-containing ZFNs *in vitro*

ZFN efficiency is dependent on the affinity and specificity of individual ZFN arrays (Cornu et al., 2008; Urnov et al., 2005), length and identity of the spacer region between ZFN recognition sites (Bibikova et al., 2001; Handel et al., 2009), interaction between FokI

nuclease domains (Miller et al., 2007; Szczepek et al., 2007), and catalytic activity of the FokI nuclease domain (Guo et al., 2010). In an attempt to improve the efficiency of our ZFN arrays, we made use of a FokI nuclease variant termed *Sharkey*. This variant was initially developed and identified through a directed-evolution strategy, and demonstrates greater than fifteen-fold more catalytic activity than wild type FokI nuclease (Guo et al., 2010).

We first wanted to determine if incorporating the *Sharkey* FokI nuclease into our ZFN arrays enhanced their function *in vitro*. To do this, we used our *in vitro* DNA cleavage assay to evaluate the abilities of control versus *Sharkey* FokI nuclease-containing ZFNs to cleave target-site-containing plasmid DNA (Figure 6.2). To compare ZFN cleavage activities, we diluted protein lysates (0.5X or 0.1X). As shown for *prp2* ZFN pairs (Figure 6.2A), samples containing *Sharkey prp2* ZFN protein lysate demonstrate more cleavage of *prp2* ZFN target-site-containing plasmid DNA than samples containing control *prp2* ZFN protein lysate. We observe similar results for *hmx4* (Figure 6.2B), and *crx* ZFNs (Figure 6.2C). Western analysis confirmed that comparable amounts of control and *Sharkey* 5' and 3' ZFN proteins were present in the lysates used for these analyses (Figure 6.2D). Our results demonstrate that *Sharkey* ZFNs exhibit increased *in vitro* cutting efficiency over control ZFNs. Combined, these data suggest that *Sharkey* FokI nuclease-containing ZFNs cleave DNA more efficiently than control FokI-nuclease containing ZFNs *in vitro*.

6.2.3 *In vivo* mutagenesis by *Sharkey* FokI nuclease-containing ZFNs

Given that *Sharkey* ZFNs function more efficiently than control ZFNs to cleave target-site DNA *in vitro*, we next wanted to determine if *Sharkey* ZFNs possess more *in vivo* mutagenic activity than control ZFNs. To do this, we injected single-cell zebrafish embryos with mRNAs encoding control or *Sharkey* ZFNs, and determined the sequence of target-site genomic DNA. Sequencing results from control versus *Sharkey* ZFN mRNA-injected embryos are summarized in Table 6.1. For *crx*, embryos injected with *Sharkey* ZFN mRNA exhibit a twenty-six times greater frequency of target-site specific insertion and deletion (indel) mutations than embryos injected with control ZFN mRNA (*Sharkey*, 31.2%, control, 1.2%). This difference in *crx* indel frequency is statistically significant ($P < 0.0001$). For *prp2* and *hmx4*, the difference in indel frequency between embryos injected with *Sharkey* ZFN

mRNA and embryos injected with control ZFN mRNA is not statistically significant (*P*-values: *prp2*, 0.738; *hmx4*, 0.669). Combined, these data suggest that *Sharkey* FokI nuclease-containing ZFNs have the capacity to exhibit greater *in vivo* mutagenic activity than control FokI nuclease-containing ZFNs.

6.2.4 Toxicity of *Sharkey* FokI nuclease-containing ZFNs

One concern with using *Sharkey* ZFNs is that increased activity of the FokI nuclease might result in additional off-target effects, thereby increasing the morbidity, and decreasing the survival of injected embryos. We therefore quantified the proportion of embryos that exhibit non-specific developmental defects (referred to as 'monster'-like), and the mortality rates of embryos injected with mRNAs encoding control or *Sharkey* ZFNs (Figure 6.3). In all cases examined, we failed to observe a significant difference (corrected $P = 1.000$ for each) in the mortality rates of embryos injected with control versus *Sharkey* ZFN mRNAs (Figure 6.3). Furthermore, we note that embryos injected with control and *Sharkey* ZFN mRNAs exhibit a comparable proportion of monster-like phenotypes (Figure 6.3; corrected *P*-values: *prp2,* 0.202; *hmx4,* 1.000*; crx,* 1.000). Combined, these data suggest that, in comparison to control ZFNs, *Sharkey* ZFNs do not significantly alter the morbidity and survival of zebrafish embryos.

6.2.5 Decreased *in vivo* mutagenesis by *Sharkey* FokI nuclease-containing TALENs

Given that some *Sharkey* ZFNs may exhibit increased *in vivo* mutagenesis activity in zebrafish when compared to control ZFNs, we next wanted to determine if applying the *Sharkey* FokI nuclease variant to our *WW domain containing transcription regulator* 1 (*wwtr1/taz*) and *homeobox B1b* (*hoxb1b*) TALENs would also increase their activity. To do this, we injected single-cell zebrafish embryos with mRNAs encoding control or *Sharkey* TALENs, and determined the frequency of indel mutations present in target-site genomic DNA using a combination of high-resolution melt curve analysis and sequencing. Results from control versus *Sharkey* TALEN mRNA-injected embryos are summarized in Table 6.2. Embryos injected with control TALENs demonstrate a modest target-site specific indel frequency (*wwtr1*, 17.2%; *hoxb1b*, 5.9%). Conversely, in each case examined, embryos

injected with *Sharkey* TALENs fail to exhibit any target-site specific indel mutations (*wwtr1*, 0.0%; *hoxb1b*, 0.0%). The difference in *wwtr1* indel formation is statistically significant ($P < 0.0001$). Notably, we fail to observe a significant difference in the mortality rates or monster-like phenotypes of embryos injected with control versus *Sharkey* TALEN mRNAs (Figure 6.4A, corrected *P*-value = 1.000 for each).

We next wanted to determine if incorporating the *Sharkey* FokI nuclease into our TALENs somehow reduced or destroyed their capacity to cleave target-site DNA. We therefore used our *in vitro* DNA cleavage assay to evaluate the abilities of control versus *Sharkey* FokI nuclease-containing TALENs to cleave target-site-containing plasmid DNA (Figure 6.4B). Notably, protein lysate samples containing *Sharkey wwtr1* TALENs demonstrate more cleavage of *wwtr1* TALEN target-site-containing plasmid DNA than samples containing control *wwtr1* TALENs (Figure 6.4B). Western analysis confirmed that comparable amounts of control and *Sharkey* 5' and 3' TALEN proteins were synthesized and present in the lysates used for these analyses (Figure 6.4C). Combined, these results suggest that *Sharkey* FokI nuclease-containing TALENs cleave DNA more efficiently than control FokI-nuclease containing TALENs *in vitro*, but possess absent or reduced *in vivo* mutagenic activity in zebrafish.

6.3 Discussion

Zinc finger nucleases (ZFNs) have been used to generate mutations in organisms that are not amenable to homologous recombination-based genetic modifications (Ben et al., 2011; Doyon et al., 2008; Foley et al., 2009b; Geurts et al., 2009; Meng et al., 2008; Moreno et al., 2011; Sander et al., 2011b), and are being evaluated for usage in gene therapies (Alper, 2009; Cannon and June, 2011; Perez et al., 2008). Improving these molecular tools is therefore relevant to both biological and clinical applications. In this study, we have described techniques that may enhance the efficiency and success of constructing ZFNs for use in mutagenesis applications.

The practical application of ZFNs relies on their ability to generate double-strand breaks in specific DNA sequences. Previous research suggests that both target-site affinity/specificity, and cleavage activity are critical determinants of ZFN function (Bibikova et al., 2003; Bibikova et al., 2002; Porteus and Baltimore, 2003; Urnov et al., 2005). Without DNA-binding specificity, engineered ZFNs demonstrate low or off-target cleavage activity (Alwin et al., 2005; Miller et al., 2007; Porteus, 2006; Porteus and Baltimore, 2003; Szczepek et al., 2007). Off-target ZFN activity results in increased cytotoxicity and non-specific morphological defects (Cornu et al., 2008). Context-dependent array selection strategies account for cooperativity among zinc finger domains, and permit recognition of the fourth base on the opposite strand of the ZFN target-sequence (Desjarlais and Berg, 1993; Dreier et al., 2000; Elrod-Erickson et al., 1996; Isalan et al., 1998; Kim and Berg, 1996; Pavletich and Pabo, 1991). These features allow for the selection of ZFNs with greater target-site affinity and specificity than those obtained through modular assembly approaches (Kim et al., 2009; Ramirez et al., 2008). Multiple context-dependent array construction methods have been used with varying degrees of success to construct ZFN arrays for use in mutagenesis applications.

We successfully constructed ZFNs with desirable target-site specificities using a method that was initially used to generate the Wolfe and Lawson *kdrl* ZFNs. This method uses a two-phase bacterial one-hybrid assay to construct suitable ZFN arrays (Meng et al., 2008). We used this bacterial one-hybrid approach to construct ZFN arrays for *prp2*, *hmx4*, and *crx*. For

prp2 and *crx*, we performed target-site selections and constructed ZFN arrays essentially as previously described (Meng et al., 2008). For *hmx4*, however, we increased context-dependent selection of individual zinc finger domains by modifying the initial screening phase to account for recognition of the fourth base on the opposite strand. We also altered the *hmx4* libraries to include OPEN-method zinc finger domain motifs that were previously shown to recognize triplets in the *hmx4* target-site (Maeder et al., 2008). Our *prp2*, *hmx4*, and *crx* ZFNs each function effectively *in vivo* in zebrafish, generating insertion/deletion (indel) mutations at a detectable frequency in injected embryos (*prp2*: 4.6%; *hmx4*: 1.2%; *crx*: 1.2%).

Not all ZFNs constructed through context-dependent selection strategies function effectively to generate somatic mutations. Testing ZFNs *in vivo* can be time-consuming and expensive, especially in instances where mutation frequencies are quite low. We therefore elaborated on published work (Mani et al., 2005) and established a system to rapidly gauge the target-site-specific cleavage activity of ZFNs *in vitro*. We demonstrate that this system can be used to evaluate the target-site-specific cleavage activity of ZFN pairs. In all cases examined, those ZFNs that functioned to cleave target-site DNA in our *in vitro* assay also generated somatic mutations *in vivo* in zebrafish. Our results therefore establish our *in vitro* cleavage assay as a good predictor of ZFN fitness in *in vivo* mutagenesis applications. Notably, in addition to evaluating ZFN function, we demonstrate that our *in vitro* cleavage assay can also be used to evaluate the target-site-specific cleavage activity of other synthetic restriction endonucleases, such as transcription activator-like effector nucleases (TALENs).

The mutagenesis efficiency of a ZFN is partially dependent on the catalytic activity of its endonuclease domain (Guo et al., 2010). We enhanced the catalytic activity of our ZFNs using the *Sharkey* FokI endonuclease domain variant. We demonstrate that *Sharkey* ZFNs exhibit increased *in vitro* cleavage of target-site DNA over control ZFNs. Our results also suggest that less *Sharkey* ZFN protein is required to elicit site-specific DNA cleavage *in vitro*. More importantly, we demonstrate that, in limited instances, *Sharkey* ZFNs have the capacity to exhibit greater *in vivo* mutagenic activity than control ZFNs, producing up to a twenty-six-fold increase in the indel mutation frequency of injected zebrafish embryos (Table 6.1). This expands upon previous research in cell culture, which has shown that *Sharkey* ZFNs demonstrate three- to six-fold more mutagenic activity in HEK 293 cells when compared to

wild type ZFNs (Guo et al., 2010). Notably, ours is the first study to assess the relative mutagenic activity of control and *Sharkey* ZFNs *in vivo* in embryos. We did not systematically evaluate the off-target cleavage activity of *Sharkey* ZFNs in zebrafish. However, in comparison to control ZFNs, we find that *Sharkey* ZFNs do not increase the frequency of morphological defects, or the mortality of injected embryos. Our overall results suggest that incorporating the *Sharkey* FokI endonuclease domain into ZFNs may be a simple method of enhancing their mutagenic activity *in vivo*. Notably, introducing double-strand DNA breaks near a desired recombination site can dramatically increase the frequency of homologous recombination in mammalian cells (Choulika et al., 1995; Smith et al., 1995). ZFNs have previously been used in this capacity (Bibikova et al., 2003; Porteus and Baltimore, 2003). Consequently, the enhanced catalytic activity of *Sharkey* ZFNs may also be extremely beneficial for homologous recombination-mediated genome engineering applications.

TALENs have recently been shown to be up to ten times more mutagenic than ZFNs in zebrafish (Chen et al., 2013). Furthermore, TALENs can be targeted to nearly any DNA sequence, and their modular nature makes them easy to design and assemble. For these reasons, TALENs are quickly becoming the technology of choice for targeted mutagenesis in animal models. Notably, TALENs have recently been used to elicit genome modification by homologous recombination, albeit at low frequency (Bedell et al., 2012; Zu et al., 2013). Given the partial success that we achieved in increasing the mutagenic activity of our ZFNs using the *Sharkey* FokI endonuclease variant, we sought to determine if this variant could also be applied to TALENs to enhance their catalytic activity. We demonstrate that *Sharkey* TALENs exhibit increased *in vitro* cleavage of target-site specific DNA over control TALENs. However, unlike with ZFNs, we demonstrate that *Sharkey* TALENs exhibit significantly reduced *in vivo* mutagenic activity in injected zebrafish embryos when compared to control TALENs (Table 6.2). Our overall results suggest that incorporating the *Sharkey* FokI endonuclease domain into TALENs may severely abrogate their *in vivo* mutagenesis function in zebrafish.

6.4 Figures

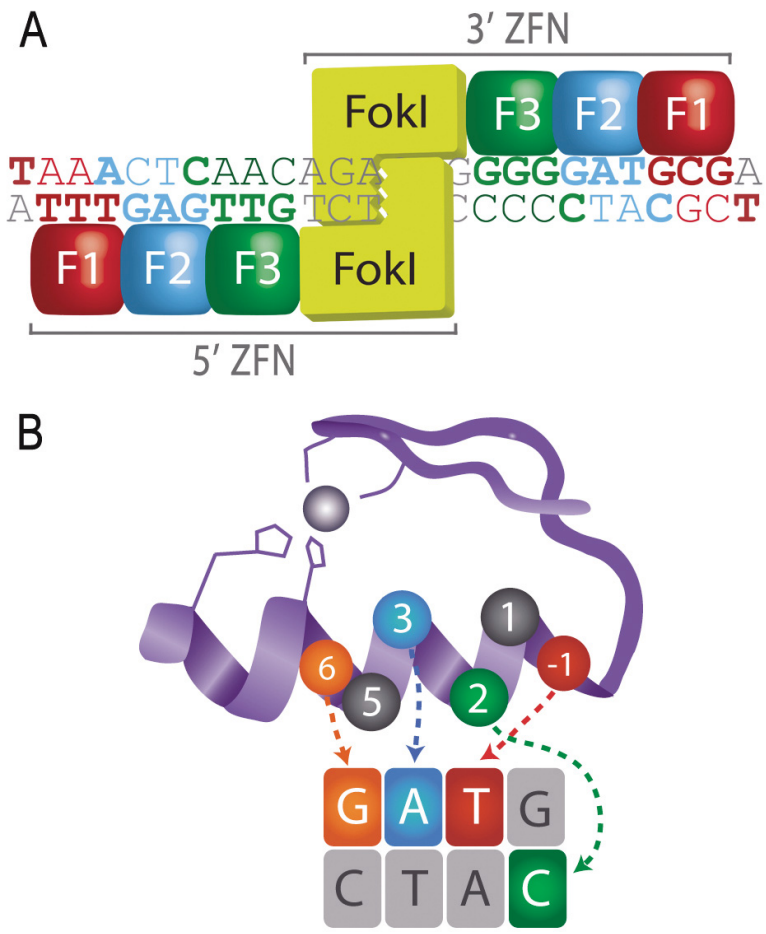

Figure 6.1. Zinc finger nuclease (ZFN) structure and target-site recognition. (A) Schematic diagram of two ZFN arrays bound to *hmx4* ZFN target-site DNA. Each ZFN consists of three zinc finger domains (F1, F2, F3) fused to the non-specific FokI endonuclease domain (FokI). Individual zinc finger recognition of DNA sequence is indicated by matched colors. Upon sequence-specific binding of two ZFNs, dimerized FokI endonuclease domains generate double-strand DNA breaks. (B) Schematic diagram of an individual zinc finger motif bound to target-site DNA. DNA-binding affinity and specificity is achieved by a seven amino-acid recognition motif. The amino acid side chains -1, 3, and 6 contact a triplet of DNA on the top strand, while the amino acid side chain at position 2 contacts a fourth base on the bottom strand.

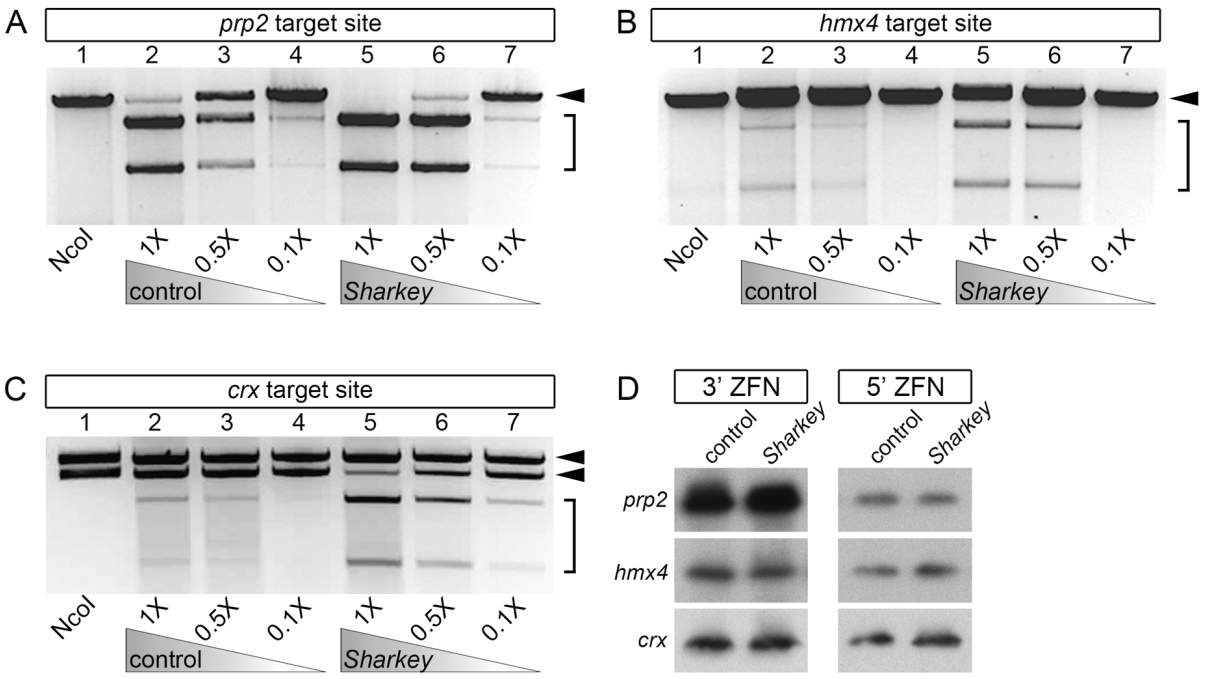

Figure 6.2. *In vitro* comparison of target-site specific DNA cleavage activity between control and *Sharkey* ZFNs. (A-C) ZFN crude protein lysates were used at normal concentration (1X), or were diluted to one-half (0.5X) or one-tenth (0.1X) the amount. Gel-electrophoretic analyses of *prp2* (A), *hmx4* (B), and *crx* (C) target-site cleavage products. Incubation with NcoI alone produces a specific cleavage profile (lane 1; arrowheads). Incubation with NcoI and ZFN crude protein lysates produces two additional cleavage products (brackets), indicating ZFN-mediated cleavage of target-site plasmid. In all cases, *Sharkey* ZFN crude protein lysates (lanes 5-7) exhibit more cleavage of target-site plasmid than control ZFN crude protein lysates (lanes 2-4). (D) Western immunoblot analyses of control and *Sharkey* 5' and 3' ZFN crude protein lysates used in *in vitro* target-site cleavage assay. 3' ZFNs are detected with anti-Flag antibody, while 5' ZFNs are detected with anti-HA antibody.

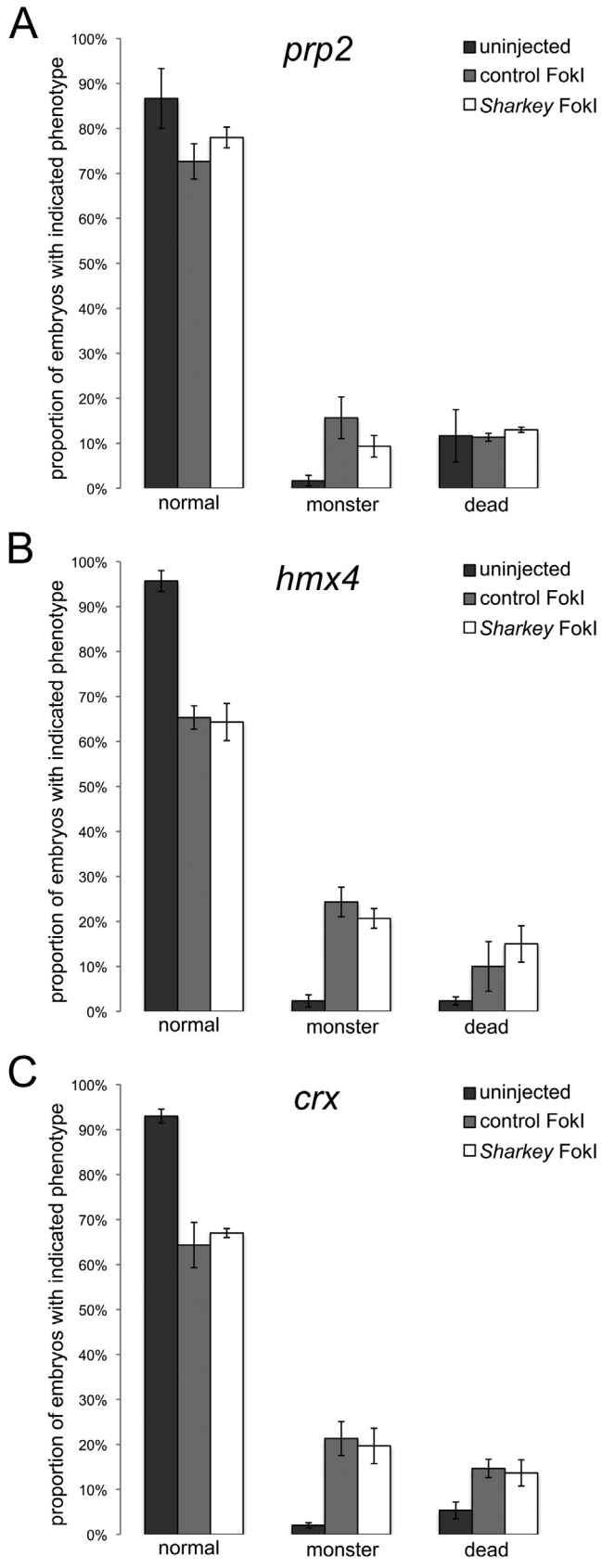

Figure 6.3. Effects of injecting control and *Sharkey* zinc finger nuclease (ZFN) mRNAs on embryonic morphology and mortality. Graphs demonstrating the mean proportion of embryos with indicated phenotype at ~ 24 hours post fertilization, following injection of mRNAs encoding control FokI or *Sharkey* FokI *prp2* (A), *hmx4* (B), or *crx* (C) ZFNs. Mean proportion of uninjected embryos with indicated phenotype are also given. Error bars represent standard error. In no category are proportions of control FokI and *Sharkey* FokI mRNA-injected embryos statistically different from each other (corrected *P*-values > 0.05 for each).

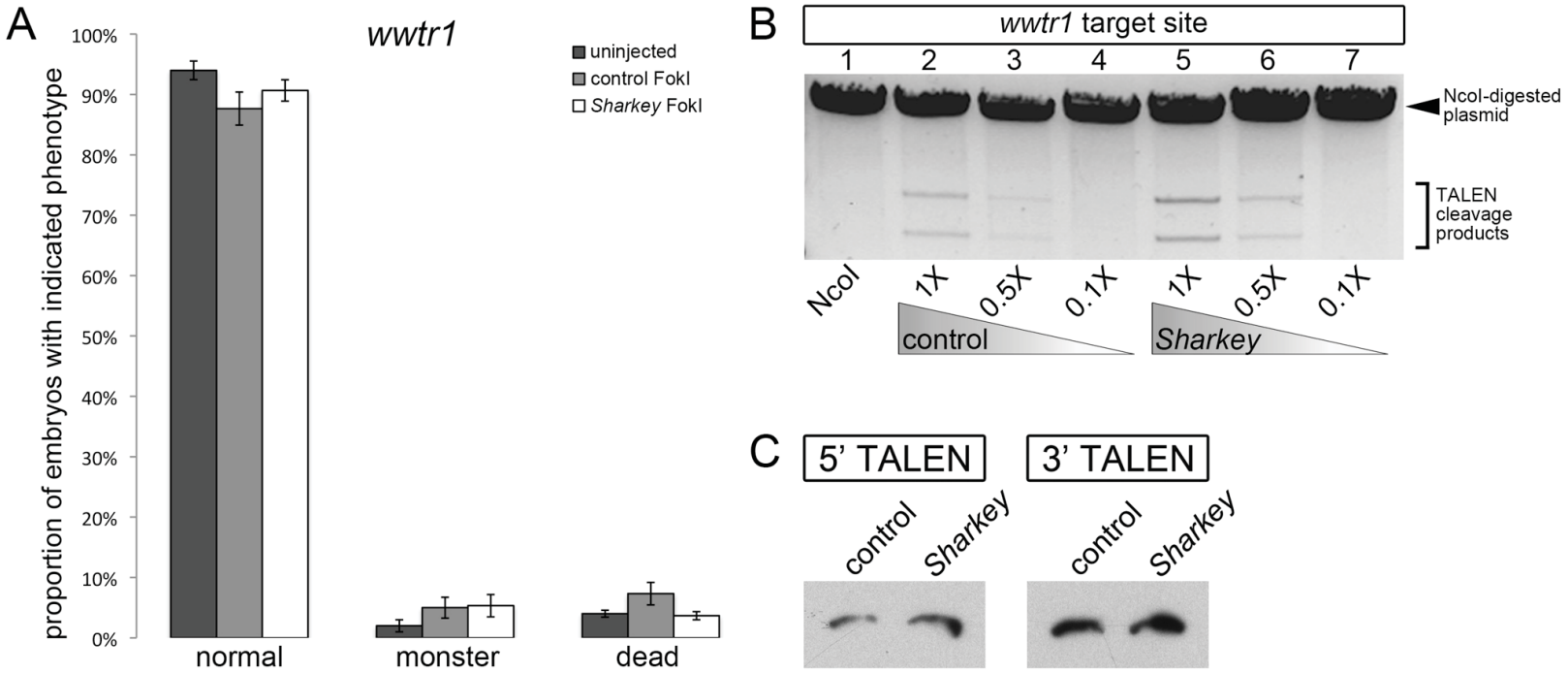
A
wwtr1
uninjected
control FokI
Sharkey FokI
proportion of embryos with indicated phenotype
100%
90%
80%
70%
60%
50%
40%
30%
20%
10%
0%
normal
monster
dead
B
wwtr1 target site
1
2
3
4
5
6
7
NcoI-digested plasmid
TALEN cleavage products
NcoI
1X
0.5X
0.1X
control
1X
0.5X
0.1X
Sharkey
C
5' TALEN
3' TALEN
control
Sharkey
control
Sharkey

Figure 6.4. Comparison of control and *Sharkey wwtr1* transcription activator-like effector nuclease (TALEN)s. (A) Graph demonstrating the mean proportion of embryos with indicated phenotype at ~ 24 hours post fertilization, following injection of mRNAs encoding control FokI or *Sharkey* FokI *wwtr1* TALENs. Mean proportion of uninjected embryos with indicated phenotype are also given. Error bars represent standard error. In no category are proportions of control FokI and *Sharkey* FokI mRNA-injected embryos statistically different from each other (corrected *P*-value > 0.05 for each). See text for statistical tests. (B) *In vitro* comparison of target-site specific DNA cleavage activity between control and *Sharkey wwtr1* TALENs. TALEN crude protein lysates were used at normal concentration (1X), or were diluted to one-half (0.5X) or one-tenth (0.1X) the amount. Gel-electrophoretic analyses of target-site cleavage products. Incubation with NcoI alone produces a specific cleavage profile (lane 1; arrowhead). Incubation with NcoI and TALEN crude protein lysates produces two additional cleavage products (brackets), indicating TALEN-mediated cleavage of target-site plasmid. *Sharkey* TALEN crude protein lysates (lanes 5-7) exhibit more cleavage of target-site plasmid than control TALEN crude protein lysates (lanes 2-4). (C) Western immunoblot analyses of control and *Sharkey* 5' and 3' TALEN crude protein lysates used in *in vitro* target-site cleavage assay. 5' ZFNs are detected with anti-Flag antibody, while 3' ZFNs are detected with anti-HA antibody.

6.5 Tables

Table 6.1: Analyses of target-site specific mutations present in zebrafish embryos injected with control or *Sharkey* zinc finger nuclease (ZFN) mRNAs.

ZFN	Number of Clones Screened	Number of Indel Mutations	Indel Frequency (%)
prp2	130	6	4.6
prp2 (*Sharkey*)	93	3	3.2
hmx4	82	1	1.2
hmx4 (*Sharkey*)	182	5	2.7
prp1	87	1	1.1
prp1 (*Sharkey*)	90	3	3.3
crx	83	1	1.2
crx (*Sharkey*)	157	49	31.2*

PCR fragments containing the ZFN target-site were amplified, cloned, and sequenced. Data indicates combined frequency of insertions and deletions (indel frequency).

*Indicates significant difference in indel mutation frequency between embryos injected with *Sharkey* and control ZFNs, as determined by two-tailed Fisher's exact test ($P < 0.0001$).

Table 6.2: Analyses of target-site specific mutations present in zebrafish embryos injected with control or *Sharkey* transcription activator-like effector nuclease (TALEN) mRNAs.

ZFN	Number of Clones Screened	Number of Indel Mutations	Indel Frequency (%)
wwtr1	81	14	17.2
wwtr1 (*Sharkey*)	82	0	0.0*
hoxb1b	85	5	5.9
hoxb1b (*Sharkey*)	44	0	0.0*

PCR fragments containing the TALEN target-site were amplified, cloned, and analyzed through high-resolution melt curve analysis followed by sequencing. Data indicates combined frequency of insertions and deletions (indel frequency).

*Indicates significant difference in indel mutation frequency between embryos injected with *Sharkey* and control TALENs, as determined by two-tailed Fisher's exact test ($P < 0.0001$).

6.6 References

Alper, J. 2009. One-off therapy for HIV. *Nat Biotechnol*. 27:300.

Alwin, S., M.B. Gere, E. Guhl, K. Effertz, C.F. Barbas, 3rd, D.J. Segal, M.D. Weitzman, and T. Cathomen. 2005. Custom zinc-finger nucleases for use in human cells. *Mol Ther*. 12:610-617.

Ansai, S., T. Sakuma, T. Yamamoto, H. Ariga, N. Uemura, R. Takahashi, and M. Kinoshita. 2013. Efficient targeted mutagenesis in medaka using custom-designed transcription activator-like effector nucleases. *Genetics*. 193:739-749.

Bae, K.H., Y.D. Kwon, H.C. Shin, M.S. Hwang, E.H. Ryu, K.S. Park, H.Y. Yang, D.K. Lee, Y. Lee, J. Park, H.S. Kwon, H.W. Kim, B.I. Yeh, H.W. Lee, S.H. Sohn, J. Yoon, W. Seol, and J.S. Kim. 2003. Human zinc fingers as building blocks in the construction of artificial transcription factors. *Nat Biotechnol*. 21:275-280.

Bedell, V.M., Y. Wang, J.M. Campbell, T.L. Poshusta, C.G. Starker, R.G. Krug, 2nd, W. Tan, S.G. Penheiter, A.C. Ma, A.Y. Leung, S.C. Fahrenkrug, D.F. Carlson, D.F. Voytas, K.J. Clark, J.J. Essner, and S.C. Ekker. 2012. In vivo genome editing using a high-efficiency TALEN system. *Nature*. 491:114-118.

Beerli, R.R., and C.F. Barbas, 3rd. 2002. Engineering polydactyl zinc-finger transcription factors. *Nat Biotechnol*. 20:135-141.

Ben, J., S. Elworthy, A.S. Ng, F. van Eeden, and P.W. Ingham. 2011. Targeted mutation of the talpid3 gene in zebrafish reveals its conserved requirement for ciliogenesis and Hedgehog signalling across the vertebrates. *Development*. 138:4969-4978.

Beumer, K., G. Bhattacharyya, M. Bibikova, J.K. Trautman, and D. Carroll. 2006. Efficient gene targeting in Drosophila with zinc-finger nucleases. *Genetics*. 172:2391-2403.

Bibikova, M., K. Beumer, J.K. Trautman, and D. Carroll. 2003. Enhancing gene targeting with designed zinc finger nucleases. *Science*. 300:764.

Bibikova, M., D. Carroll, D.J. Segal, J.K. Trautman, J. Smith, Y.G. Kim, and S. Chandrasegaran. 2001. Stimulation of homologous recombination through targeted cleavage by chimeric nucleases. *Mol Cell Biol*. 21:289-297.

Bibikova, M., M. Golic, K.G. Golic, and D. Carroll. 2002. Targeted chromosomal cleavage and mutagenesis in Drosophila using zinc-finger nucleases. *Genetics*. 161:1169-1175.

Boch, J., and U. Bonas. 2010. Xanthomonas AvrBs3 family-type III effectors: discovery and function. *Annu Rev Phytopathol*. 48:419-436.

Bogdanove, A.J., and D.F. Voytas. 2011. TAL effectors: customizable proteins for DNA targeting. *Science*. 333:1843-1846.

Bozas, A., K.J. Beumer, J.K. Trautman, and D. Carroll. 2009. Genetic analysis of zinc-finger nuclease-induced gene targeting in Drosophila. *Genetics*. 182:641-651.

Brennan, R.J., and R.H. Schiestl. 1998. Free radicals generated in yeast by the Salmonella test-negative carcinogens benzene, urethane, thiourea and auramine O. *Mutat Res*. 403:65-73.

Cade, L., D. Reyon, W.Y. Hwang, S.Q. Tsai, S. Patel, C. Khayter, J.K. Joung, J.D. Sander, R.T. Peterson, and J.R. Yeh. 2012. Highly efficient generation of heritable zebrafish gene mutations using homo- and heterodimeric TALENs. *Nucleic Acids Res*. 40:8001-8010.

Cannon, P., and C. June. 2011. Chemokine receptor 5 knockout strategies. *Curr Opin HIV AIDS*. 6:74-79.

Carbery, I.D., D. Ji, A. Harrington, V. Brown, E.J. Weinstein, L. Liaw, and X. Cui. 2010. Targeted genome modification in mice using zinc-finger nucleases. *Genetics*. 186:451-459.

Carlson, D.F., W. Tan, S.G. Lillico, D. Stverakova, C. Proudfoot, M. Christian, D.F. Voytas, C.R. Long, C.B. Whitelaw, and S.C. Fahrenkrug. 2012. Efficient TALEN-mediated gene knockout in livestock. *Proc Natl Acad Sci U S A*. 109:17382-17387.

Cathomen, T., and J.K. Joung. 2008. Zinc-finger nucleases: the next generation emerges. *Mol Ther*. 16:1200-1207.

Cermak, T., E.L. Doyle, M. Christian, L. Wang, Y. Zhang, C. Schmidt, J.A. Baller, N.V. Somia, A.J. Bogdanove, and D.F. Voytas. 2011. Efficient design and assembly of custom TALEN and other TAL effector-based constructs for DNA targeting. *Nucleic Acids Res*. 39:e82.

Chen, S., G. Oikonomou, C.N. Chiu, B.J. Niles, J. Liu, D.A. Lee, I. Antoshechkin, and D.A. Prober. 2013. A large-scale in vivo analysis reveals that TALENs are significantly more mutagenic than ZFNs generated using context-dependent assembly. *Nucleic Acids Res*. 41:2769-2778.

Choulika, A., A. Perrin, B. Dujon, and J.F. Nicolas. 1995. Induction of homologous recombination in mammalian chromosomes by using the I-SceI system of Saccharomyces cerevisiae. *Mol Cell Biol*. 15:1968-1973.

Christian, M., T. Cermak, E.L. Doyle, C. Schmidt, F. Zhang, A. Hummel, A.J. Bogdanove, and D.F. Voytas. 2010. Targeting DNA double-strand breaks with TAL effector nucleases. *Genetics*. 186:757-761.

Cornu, T.I., S. Thibodeau-Beganny, E. Guhl, S. Alwin, M. Eichtinger, J.K. Joung, and T. Cathomen. 2008. DNA-binding specificity is a major determinant of the activity and toxicity of zinc-finger nucleases. *Mol Ther*. 16:352-358.

Dahlem, T.J., K. Hoshijima, M.J. Jurynec, D. Gunther, C.G. Starker, A.S. Locke, A.M. Weis, D.F. Voytas, and D.J. Grunwald. 2012. Simple methods for generating and detecting locus-specific mutations induced with TALENs in the zebrafish genome. *PLoS Genet*. 8:e1002861.

Deng, D., C. Yan, X. Pan, M. Mahfouz, J. Wang, J.K. Zhu, Y. Shi, and N. Yan. 2012. Structural basis for sequence-specific recognition of DNA by TAL effectors. *Science*. 335:720-723.

Desjarlais, J.R., and J.M. Berg. 1993. Use of a zinc-finger consensus sequence framework and specificity rules to design specific DNA binding proteins. *Proc Natl Acad Sci U S A*. 90:2256-2260.

Ding, Q., Y.K. Lee, E.A. Schaefer, D.T. Peters, A. Veres, K. Kim, N. Kuperwasser, D.L. Motola, T.B. Meissner, W.T. Hendriks, M. Trevisan, R.M. Gupta, A. Moisan, E. Banks, M. Friesen, R.T. Schinzel, F. Xia, A. Tang, Y. Xia, E. Figueroa, A. Wann, T. Ahfeldt, L. Daheron, F. Zhang, L.L. Rubin, L.F. Peng, R.T. Chung, K. Musunuru, and C.A. Cowan. 2013. A TALEN Genome-Editing System for Generating Human Stem Cell-Based Disease Models. *Cell Stem Cell*. 12:238-251.

Dong, Z., J. Ge, K. Li, Z. Xu, D. Liang, J. Li, W. Jia, Y. Li, X. Dong, S. Cao, X. Wang, J. Pan, and Q. Zhao. 2011. Heritable targeted inactivation of myostatin gene in yellow catfish (Pelteobagrus fulvidraco) using engineered zinc finger nucleases. *PloS one*. 6:e28897.

Doyon, Y., J.M. McCammon, J.C. Miller, F. Faraji, C. Ngo, G.E. Katibah, R. Amora, T.D. Hocking, L. Zhang, E.J. Rebar, P.D. Gregory, F.D. Urnov, and S.L. Amacher. 2008. Heritable targeted gene disruption in zebrafish using designed zinc-finger nucleases. *Nat Biotechnol*. 26:702-708.

Dreier, B., D.J. Segal, and C.F. Barbas, 3rd. 2000. Insights into the molecular recognition of the 5'-GNN-3' family of DNA sequences by zinc finger domains. *Journal of molecular biology*. 303:489-502.

Durai, S., M. Mani, K. Kandavelou, J. Wu, M.H. Porteus, and S. Chandrasegaran. 2005. Zinc finger nucleases: custom-designed molecular scissors for genome engineering of plant and mammalian cells. *Nucleic Acids Res*. 33:5978-5990.

Elrod-Erickson, M., M.A. Rould, L. Nekludova, and C.O. Pabo. 1996. Zif268 protein-DNA complex refined at 1.6 A: a model system for understanding zinc finger-DNA interactions. *Structure*. 4:1171-1180.

Foley, J.E., M.L. Maeder, J. Pearlberg, J.K. Joung, R.T. Peterson, and J.R. Yeh. 2009a. Targeted mutagenesis in zebrafish using customized zinc-finger nucleases. *Nature protocols*. 4:1855-1867.

Foley, J.E., J.R. Yeh, M.L. Maeder, D. Reyon, J.D. Sander, R.T. Peterson, and J.K. Joung. 2009b. Rapid mutation of endogenous zebrafish genes using zinc finger nucleases made by Oligomerized Pool ENgineering (OPEN). *PLoS One*. 4:e4348.

Geurts, A.M., G.J. Cost, Y. Freyvert, B. Zeitler, J.C. Miller, V.M. Choi, S.S. Jenkins, A. Wood, X. Cui, X. Meng, A. Vincent, S. Lam, M. Michalkiewicz, R. Schilling, J. Foeckler, S. Kalloway, H. Weiler, S. Menoret, I. Anegon, G.D. Davis, L. Zhang, E.J. Rebar, P.D. Gregory, F.D. Urnov, H.J. Jacob, and R. Buelow. 2009. Knockout rats via embryo microinjection of zinc-finger nucleases. *Science*. 325:433.

Gonzalez, B., L.J. Schwimmer, R.P. Fuller, Y. Ye, L. Asawapornmongkol, and C.F. Barbas, 3rd. 2010. Modular system for the construction of zinc-finger libraries and proteins. *Nature protocols*. 5:791-810.

Greisman, H.A., and C.O. Pabo. 1997. A general strategy for selecting high-affinity zinc finger proteins for diverse DNA target sites. *Science*. 275:657-661.

Guo, J., T. Gaj, and C.F. Barbas, 3rd. 2010. Directed evolution of an enhanced and highly efficient FokI cleavage domain for zinc finger nucleases. *Journal of molecular biology*. 400:96-107.

Gupta, A., V.L. Hall, F.O. Kok, M. Shin, J.C. McNulty, N.D. Lawson, and S.A. Wolfe. 2013. Targeted Chromosomal Deletions and Inversions in Zebrafish. *Genome research*.

Gupta, A., X. Meng, L.J. Zhu, N.D. Lawson, and S.A. Wolfe. 2011. Zinc finger protein-dependent and -independent contributions to the in vivo off-target activity of zinc finger nucleases. *Nucleic Acids Res*. 39:381-392.

Hagmann, M., R. Bruggmann, L. Xue, O. Georgiev, W. Schaffner, D. Rungger, P. Spaniol, and T. Gerster. 1998. Homologous recombination and DNA-end joining reactions in zygotes and early embryos of zebrafish (Danio rerio) and Drosophila melanogaster. *Biological chemistry*. 379:673-681.

Handel, E.M., S. Alwin, and T. Cathomen. 2009. Expanding or restricting the target site repertoire of zinc-finger nucleases: the inter-domain linker as a major determinant of target site selectivity. *Mol Ther*. 17:104-111.

Hefferin, M.L., and A.E. Tomkinson. 2005. Mechanism of DNA double-strand break repair by non-homologous end joining. *DNA Repair (Amst)*. 4:639-648.

Hockemeyer, D., H. Wang, S. Kiani, C.S. Lai, Q. Gao, J.P. Cassady, G.J. Cost, L. Zhang, Y. Santiago, J.C. Miller, B. Zeitler, J.M. Cherone, X. Meng, S.J. Hinkley, E.J. Rebar, P.D. Gregory, F.D. Urnov, and R. Jaenisch. 2011. Genetic engineering of human pluripotent cells using TALE nucleases. *Nat Biotechnol*. 29:731-734.

Huang, P., A. Xiao, M. Zhou, Z. Zhu, S. Lin, and B. Zhang. 2011. Heritable gene targeting in zebrafish using customized TALENs. *Nat Biotechnol*. 29:699-700.

Hurt, J.A., S.A. Thibodeau, A.S. Hirsh, C.O. Pabo, and J.K. Joung. 2003. Highly specific zinc finger proteins obtained by directed domain shuffling and cell-based selection. *Proc Natl Acad Sci U S A*. 100:12271-12276.

Isalan, M., and Y. Choo. 2001. Rapid, high-throughput engineering of sequence-specific zinc finger DNA-binding proteins. *Methods Enzymol*. 340:593-609.

Isalan, M., Y. Choo, and A. Klug. 1997. Synergy between adjacent zinc fingers in sequence-specific DNA recognition. *Proc Natl Acad Sci U S A*. 94:5617-5621.

Isalan, M., A. Klug, and Y. Choo. 1998. Comprehensive DNA recognition through concerted interactions from adjacent zinc fingers. *Biochemistry*. 37:12026-12033.

Ishibashi, S., R. Cliffe, and E. Amaya. 2012. Highly efficient bi-allelic mutation rates using TALENs in Xenopus tropicalis. *Biol Open*. 1:1273-1276.

Kandavelou, K., M. Mani, S. Durai, and S. Chandrasegaran. 2005. "Magic" scissors for genome surgery. *Nat Biotechnol*. 23:686-687.

Kim, C.A., and J.M. Berg. 1996. A 2.2 A resolution crystal structure of a designed zinc finger protein bound to DNA. *Nature structural biology*. 3:940-945.

Kim, H.J., H.J. Lee, H. Kim, S.W. Cho, and J.S. Kim. 2009. Targeted genome editing in human cells with zinc finger nucleases constructed via modular assembly. *Genome research*. 19:1279-1288.

Kim, S., E.J. Kim, and J.S. Kim. 2010. Construction of combinatorial libraries that encode zinc finger-based transcription factors. *Methods Mol Biol*. 649:133-147.

Kim, Y.G., J. Cha, and S. Chandrasegaran. 1996. Hybrid restriction enzymes: zinc finger fusions to Fok I cleavage domain. *Proc Natl Acad Sci U S A*. 93:1156-1160.

Kovalchuk, I., P. Pelczar, and O. Kovalchuk. 2004. High frequency of nucleotide misincorporations upon the processing of double-strand breaks. *DNA Repair (Amst)*. 3:217-223.

Lee, H.J., E. Kim, and J.S. Kim. 2010. Targeted chromosomal deletions in human cells using zinc finger nucleases. *Genome research*. 20:81-89.

Lei, Y., X. Guo, Y. Liu, Y. Cao, Y. Deng, X. Chen, C.H. Cheng, I.B. Dawid, Y. Chen, and H. Zhao. 2012. Efficient targeted gene disruption in Xenopus embryos using engineered transcription activator-like effector nucleases (TALENs). *Proc Natl Acad Sci U S A*. 109:17484-17489.

Li, L., M.J. Piatek, A. Atef, A. Piatek, A. Wibowo, X. Fang, J.S. Sabir, J.K. Zhu, and M.M. Mahfouz. 2012. Rapid and highly efficient construction of TALE-based

transcriptional regulators and nucleases for genome modification. *Plant Mol Biol*. 78:407-416.

Li, T., S. Huang, W.Z. Jiang, D. Wright, M.H. Spalding, D.P. Weeks, and B. Yang. 2011a. TAL nucleases (TALNs): hybrid proteins composed of TAL effectors and FokI DNA-cleavage domain. *Nucleic Acids Res*. 39:359-372.

Li, T., S. Huang, X. Zhao, D.A. Wright, S. Carpenter, M.H. Spalding, D.P. Weeks, and B. Yang. 2011b. Modularly assembled designer TAL effector nucleases for targeted gene knockout and gene replacement in eukaryotes. *Nucleic Acids Res*. 39:6315-6325.

Liu, J., C. Li, Z. Yu, P. Huang, H. Wu, C. Wei, N. Zhu, Y. Shen, Y. Chen, B. Zhang, W.M. Deng, and R. Jiao. 2012. Efficient and specific modifications of the Drosophila genome by means of an easy TALEN strategy. *Journal of genetics and genomics = Yi chuan xue bao*. 39:209-215.

Liu, Q., D.J. Segal, J.B. Ghiara, and C.F. Barbas, 3rd. 1997. Design of polydactyl zinc-finger proteins for unique addressing within complex genomes. *Proc Natl Acad Sci U S A*. 94:5525-5530.

Lloyd, A., C.L. Plaisier, D. Carroll, and G.N. Drews. 2005. Targeted mutagenesis using zinc-finger nucleases in Arabidopsis. *Proc Natl Acad Sci U S A*. 102:2232-2237.

Lombardo, A., P. Genovese, C.M. Beausejour, S. Colleoni, Y.L. Lee, K.A. Kim, D. Ando, F.D. Urnov, C. Galli, P.D. Gregory, M.C. Holmes, and L. Naldini. 2007. Gene editing in human stem cells using zinc finger nucleases and integrase-defective lentiviral vector delivery. *Nat Biotechnol*. 25:1298-1306.

Ma, S., S. Zhang, F. Wang, Y. Liu, H. Xu, C. Liu, Y. Lin, P. Zhao, and Q. Xia. 2012. Highly efficient and specific genome editing in silkworm using custom TALENs. *PloS one*. 7:e45035.

Maeder, M.L., S. Thibodeau-Beganny, A. Osiak, D.A. Wright, R.M. Anthony, M. Eichtinger, T. Jiang, J.E. Foley, R.J. Winfrey, J.A. Townsend, E. Unger-Wallace, J.D. Sander, F. Muller-Lerch, F. Fu, J. Pearlberg, C. Gobel, J.P. Dassie, S.M. Pruett-Miller, M.H. Porteus, D.C. Sgroi, A.J. Iafrate, D. Dobbs, P.B. McCray, Jr., T. Cathomen, D.F. Voytas, and J.K. Joung. 2008. Rapid "open-source" engineering of customized zinc-finger nucleases for highly efficient gene modification. *Mol Cell*. 31:294-301.

Mahfouz, M.M., L. Li, M. Shamimuzzaman, A. Wibowo, X. Fang, and J.K. Zhu. 2011. De novo-engineered transcription activator-like effector (TALE) hybrid nuclease with novel DNA binding specificity creates double-strand breaks. *Proc Natl Acad Sci U S A*. 108:2623-2628.

Mak, A.N., P. Bradley, A.J. Bogdanove, and B.L. Stoddard. 2012. TAL effectors: function, structure, engineering and applications. *Curr Opin Struct Biol*. 23:93-99.

Mandell, J.G., and C.F. Barbas, 3rd. 2006. Zinc Finger Tools: custom DNA-binding domains for transcription factors and nucleases. *Nucleic Acids Res*. 34:W516-523.

Mani, M., K. Kandavelou, F.J. Dy, S. Durai, and S. Chandrasegaran. 2005. Design, engineering, and characterization of zinc finger nucleases. *Biochem Biophys Res Commun*. 335:447-457.

Mashimo, T., T. Kaneko, T. Sakuma, J. Kobayashi, Y. Kunihiro, B. Voigt, T. Yamamoto, and T. Serikawa. 2013. Efficient gene targeting by TAL effector nucleases coinjected with exonucleases in zygotes. *Sci Rep*. 3:1253.

Meng, X., M.B. Noyes, L.J. Zhu, N.D. Lawson, and S.A. Wolfe. 2008. Targeted gene inactivation in zebrafish using engineered zinc-finger nucleases. *Nat Biotechnol*. 26:695-701.

Menoret, S., S. Fontaniere, D. Jantz, L. Tesson, R. Thinard, S. Remy, C. Usal, L.H. Ouisse, A. Fraichard, and I. Anegon. 2013. Generation of Rag1-knockout immunodeficient rats and mice using engineered meganucleases. *FASEB journal : official publication of the Federation of American Societies for Experimental Biology*. 27:703-711.

Miller, J.C., M.C. Holmes, J. Wang, D.Y. Guschin, Y.L. Lee, I. Rupniewski, C.M. Beausejour, A.J. Waite, N.S. Wang, K.A. Kim, P.D. Gregory, C.O. Pabo, and E.J. Rebar. 2007. An improved zinc-finger nuclease architecture for highly specific genome editing. *Nat Biotechnol*. 25:778-785.

Moehle, E.A., J.M. Rock, Y.L. Lee, Y. Jouvenot, R.C. DeKelver, P.D. Gregory, F.D. Urnov, and M.C. Holmes. 2007. Targeted gene addition into a specified location in the human genome using designed zinc finger nucleases. *Proc Natl Acad Sci U S A*. 104:3055-3060.

Moore, F.E., D. Reyon, J.D. Sander, S.A. Martinez, J.S. Blackburn, C. Khayter, C.L. Ramirez, J.K. Joung, and D.M. Langenau. 2012. Improved somatic mutagenesis in zebrafish using transcription activator-like effector nucleases (TALENs). *PloS one*. 7:e37877.

Moreno, C., M. Hoffman, T.J. Stodola, D.N. Didier, J. Lazar, A.M. Geurts, P.E. North, H.J. Jacob, and A.S. Greene. 2011. Creation and characterization of a renin knockout rat. *Hypertension*. 57:614-619.

Morton, J., M.W. Davis, E.M. Jorgensen, and D. Carroll. 2006. Induction and repair of zinc-finger nuclease-targeted double-strand breaks in Caenorhabditis elegans somatic cells. *Proc Natl Acad Sci U S A*. 103:16370-16375.

Mussolino, C., R. Morbitzer, F. Lutge, N. Dannemann, T. Lahaye, and T. Cathomen. 2011. A novel TALE nuclease scaffold enables high genome editing activity in combination with low toxicity. *Nucleic Acids Res*. 39:9283-9293.

Ochiai, H., K. Fujita, K. Suzuki, M. Nishikawa, T. Shibata, N. Sakamoto, and T. Yamamoto. 2010. Targeted mutagenesis in the sea urchin embryo using zinc-finger nucleases. *Genes Cells*. 15:875-885.

Pavletich, N.P., and C.O. Pabo. 1991. Zinc finger-DNA recognition: crystal structure of a Zif268-DNA complex at 2.1 A. *Science*. 252:809-817.

Perez, E.E., J. Wang, J.C. Miller, Y. Jouvenot, K.A. Kim, O. Liu, N. Wang, G. Lee, V.V. Bartsevich, Y.L. Lee, D.Y. Guschin, I. Rupniewski, A.J. Waite, C. Carpenito, R.G. Carroll, J.S. Orange, F.D. Urnov, E.J. Rebar, D. Ando, P.D. Gregory, J.L. Riley, M.C. Holmes, and C.H. June. 2008. Establishment of HIV-1 resistance in CD4+ T cells by genome editing using zinc-finger nucleases. *Nat Biotechnol*. 26:808-816.

Porteus, M.H. 2006. Mammalian gene targeting with designed zinc finger nucleases. *Mol Ther*. 13:438-446.

Porteus, M.H., and D. Baltimore. 2003. Chimeric nucleases stimulate gene targeting in human cells. *Science*. 300:763.

Porteus, M.H., and D. Carroll. 2005. Gene targeting using zinc finger nucleases. *Nat Biotechnol*. 23:967-973.

Pruett-Miller, S.M., J.P. Connelly, M.L. Maeder, J.K. Joung, and M.H. Porteus. 2008. Comparison of zinc finger nucleases for use in gene targeting in mammalian cells. *Mol Ther*. 16:707-717.

Ramirez, C.L., J.E. Foley, D.A. Wright, F. Muller-Lerch, S.H. Rahman, T.I. Cornu, R.J. Winfrey, J.D. Sander, F. Fu, J.A. Townsend, T. Cathomen, D.F. Voytas, and J.K. Joung. 2008. Unexpected failure rates for modular assembly of engineered zinc fingers. *Nature methods*. 5:374-375.

Roth, D.B., and J.H. Wilson. 1986. Nonhomologous recombination in mammalian cells: role for short sequence homologies in the joining reaction. *Mol Cell Biol*. 6:4295-4304.

Sajwan, S., Y. Takasu, T. Tamura, K. Uchino, H. Sezutsu, and M. Zurovec. 2013. Efficient disruption of endogenous Bombyx gene by TAL effector nucleases. *Insect Biochem Mol Biol*. 43:17-23.

Sakuma, T., S. Hosoi, K. Woltjen, K.I. Suzuki, K. Kashiwagi, H. Wada, H. Ochiai, T. Miyamoto, N. Kawai, Y. Sasakura, S. Matsuura, Y. Okada, A. Kawahara, S. Hayashi, and T. Yamamoto. 2013. Efficient TALEN construction and evaluation methods for human cell and animal applications. *Genes Cells*.

Sander, J.D., L. Cade, C. Khayter, D. Reyon, R.T. Peterson, J.K. Joung, and J.R. Yeh. 2011a. Targeted gene disruption in somatic zebrafish cells using engineered TALENs. *Nat Biotechnol*. 29:697-698.

Sander, J.D., E.J. Dahlborg, M.J. Goodwin, L. Cade, F. Zhang, D. Cifuentes, S.J. Curtin, J.S. Blackburn, S. Thibodeau-Beganny, Y. Qi, C.J. Pierick, E. Hoffman, M.L. Maeder, C. Khayter, D. Reyon, D. Dobbs, D.M. Langenau, R.M. Stupar, A.J. Giraldez, D.F. Voytas, R.T. Peterson, J.R. Yeh, and J.K. Joung. 2011b. Selection-free zinc-finger-nuclease engineering by context-dependent assembly (CoDA). *Nature methods*. 8:67-69.

Sander, J.D., J.R. Yeh, R.T. Peterson, and J.K. Joung. 2011c. Engineering zinc finger nucleases for targeted mutagenesis of zebrafish. *Methods in cell biology*. 104:51-58.

Sanjana, N.E., L. Cong, Y. Zhou, M.M. Cunniff, G. Feng, and F. Zhang. 2012. A transcription activator-like effector toolbox for genome engineering. *Nature protocols*. 7:171-192.

Segal, D.J., R.R. Beerli, P. Blancafort, B. Dreier, K. Effertz, A. Huber, B. Koksch, C.V. Lund, L. Magnenat, D. Valente, and C.F. Barbas, 3rd. 2003. Evaluation of a modular strategy for the construction of novel polydactyl zinc finger DNA-binding proteins. *Biochemistry*. 42:2137-2148.

Shukla, V.K., Y. Doyon, J.C. Miller, R.C. DeKelver, E.A. Moehle, S.E. Worden, J.C. Mitchell, N.L. Arnold, S. Gopalan, X. Meng, V.M. Choi, J.M. Rock, Y.Y. Wu, G.E. Katibah, G. Zhifang, D. McCaskill, M.A. Simpson, B. Blakeslee, S.A. Greenwalt, H.J. Butler, S.J. Hinkley, L. Zhang, E.J. Rebar, P.D. Gregory, and F.D. Urnov. 2009. Precise genome modification in the crop species Zea mays using zinc-finger nucleases. *Nature*. 459:437-441.

Smith, G.R., S.K. Amundsen, P. Dabert, and A.F. Taylor. 1995. The initiation and control of homologous recombination in Escherichia coli. *Philos Trans R Soc Lond B Biol Sci*. 347:13-20.

Stroud, D.A., L.E. Formosa, X.W. Wijeyeratne, T.N. Nguyen, and M.T. Ryan. 2013. Gene knockout using transcription activator-like effector nucleases (TALENs) reveals that

human NDUFA9 protein is essential for stabilizing the junction between membrane and matrix arms of complex I. *J Biol Chem*. 288:1685-1690.

Sun, N., J. Liang, Z. Abil, and H. Zhao. 2012. Optimized TAL effector nucleases (TALENs) for use in treatment of sickle cell disease. *Mol Biosyst*. 8:1255-1263.

Sung, Y.H., I.J. Baek, D.H. Kim, J. Jeon, J. Lee, K. Lee, D. Jeong, J.S. Kim, and H.W. Lee. 2013. Knockout mice created by TALEN-mediated gene targeting. *Nat Biotechnol*. 31:23-24.

Szczepek, M., V. Brondani, J. Buchel, L. Serrano, D.J. Segal, and T. Cathomen. 2007. Structure-based redesign of the dimerization interface reduces the toxicity of zinc-finger nucleases. *Nat Biotechnol*. 25:786-793.

Takasu, Y., I. Kobayashi, K. Beumer, K. Uchino, H. Sezutsu, S. Sajwan, D. Carroll, T. Tamura, and M. Zurovec. 2010. Targeted mutagenesis in the silkworm Bombyx mori using zinc finger nuclease mRNA injection. *Insect Biochem Mol Biol*. 40:759-765.

Tesson, L., C. Usal, S. Menoret, E. Leung, B.J. Niles, S. Remy, Y. Santiago, A.I. Vincent, X. Meng, L. Zhang, P.D. Gregory, I. Anegon, and G.J. Cost. 2011. Knockout rats generated by embryo microinjection of TALENs. *Nat Biotechnol*. 29:695-696.

Townsend, J.A., D.A. Wright, R.J. Winfrey, F. Fu, M.L. Maeder, J.K. Joung, and D.F. Voytas. 2009. High-frequency modification of plant genes using engineered zinc-finger nucleases. *Nature*. 459:442-445.

Urnov, F.D., J.C. Miller, Y.L. Lee, C.M. Beausejour, J.M. Rock, S. Augustus, A.C. Jamieson, M.H. Porteus, P.D. Gregory, and M.C. Holmes. 2005. Highly efficient endogenous human gene correction using designed zinc-finger nucleases. *Nature*. 435:646-651.

Wefers, B., M. Meyer, O. Ortiz, M. Hrabe de Angelis, J. Hansen, W. Wurst, and R. Kuhn. 2013. Direct production of mouse disease models by embryo microinjection of TALENs and oligodeoxynucleotides. *Proc Natl Acad Sci U S A*. 110:3782-3787.

Whyte, J.J., and R.S. Prather. 2012. CELL BIOLOGY SYMPOSIUM: Zinc finger nucleases to create custom-designed modifications in the swine (Sus scrofa) genome. *J Anim Sci*. 90:1111-1117.

Wood, A.J., T.W. Lo, B. Zeitler, C.S. Pickle, E.J. Ralston, A.H. Lee, R. Amora, J.C. Miller, E. Leung, X. Meng, L. Zhang, E.J. Rebar, P.D. Gregory, F.D. Urnov, and B.J. Meyer. 2011. Targeted genome editing across species using ZFNs and TALENs. *Science*. 333:307.

Wright, D.A., J.A. Townsend, R.J. Winfrey, Jr., P.A. Irwin, J. Rajagopal, P.M. Lonosky, B.D. Hall, M.D. Jondle, and D.F. Voytas. 2005. High-frequency homologous recombination in plants mediated by zinc-finger nucleases. *Plant J*. 44:693-705.

Yang, D., H. Yang, W. Li, B. Zhao, Z. Ouyang, Z. Liu, Y. Zhao, N. Fan, J. Song, J. Tian, F. Li, J. Zhang, L. Chang, D. Pei, Y.E. Chen, and L. Lai. 2011. Generation of PPARgamma mono-allelic knockout pigs via zinc-finger nucleases and nuclear transfer cloning. *Cell Res*. 21:979-982.

Zhang, F., M.L. Maeder, E. Unger-Wallace, J.P. Hoshaw, D. Reyon, M. Christian, X. Li, C.J. Pierick, D. Dobbs, T. Peterson, J.K. Joung, and D.F. Voytas. 2010. High frequency targeted mutagenesis in Arabidopsis thaliana using zinc finger nucleases. *Proc Natl Acad Sci U S A*. 107:12028-12033.

Zhang, Y., F. Zhang, X. Li, J.A. Baller, Y. Qi, C.G. Starker, A.J. Bogdanove, and D.F. Voytas. 2013. Transcription activator-like effector nucleases enable efficient plant genome engineering. *Plant Physiol*. 161:20-27.

Zou, J., M.L. Maeder, P. Mali, S.M. Pruett-Miller, S. Thibodeau-Beganny, B.K. Chou, G. Chen, Z. Ye, I.H. Park, G.Q. Daley, M.H. Porteus, J.K. Joung, and L. Cheng. 2009. Gene targeting of a disease-related gene in human induced pluripotent stem and embryonic stem cells. *Cell Stem Cell*. 5:97-110.

Zou, J., C.L. Sweeney, B.K. Chou, U. Choi, J. Pan, H. Wang, S.N. Dowey, L. Cheng, and H.L. Malech. 2011. Oxidase-deficient neutrophils from X-linked chronic granulomatous disease iPS cells: functional correction by zinc finger nuclease-mediated safe harbor targeting. *Blood*. 117:5561-5572.

Zu, Y., X. Tong, Z. Wang, D. Liu, R. Pan, Z. Li, Y. Hu, Z. Luo, P. Huang, Q. Wu, Z. Zhu, B. Zhang, and S. Lin. 2013. TALEN-mediated precise genome modification by homologous recombination in zebrafish. *Nature methods*.

Chapter 7

Conclusions and Future Directions

Previous analyses using vertebrate models have identified molecular pathways that govern both primitive and definitive hematopoiesis. These pathways are conserved among vertebrates, and the critical mammalian hematopoietic genes have clear orthologues in zebrafish (reviewed by Davidson and Zon, 2004). Using zebrafish as a model organism, we have identified essential regulators of both primitive and definitive hematopoiesis (Figure 7.1). We have defined a critical role for the homeodomain transcription factors Meis1 and Pbx in regulating primitive erythropoiesis. We have also elucidated a novel role for retinoic acid (RA) signaling in hematopoietic stem cell formation. Finally, we have identified putative RA-independent and dependent roles for the homeodomain transcription factor Hmx4 in regulating primitive and definitive hematopoiesis, respectively.

7.1 Meis1 and Pbx in primitive hematopoiesis

Previous studies implicated the Hox cofactors Meis1 and Pbx in hematopoiesis; *Pbx1*-knockout and *Meis1*-deficient mice exhibit profound embryonic anemia (Azcoitia et al., 2005; DiMartino et al., 2001; Hisa et al., 2004). However, prior to this work, the precise molecular function of Meis1 and Pbx in regulating primitive hematopoiesis was not known. Through targeted ablation of Meis1 and Pbx2/4 proteins, we demonstrate that Meis1 and Pbx are required for the transcriptional activation of *gata1*, a gene that has an evolutionarily conserved role in specifying erythroid cell fate (Galloway et al., 2005; Pevny et al., 1991; Rhodes et al., 2005; Shivdasani et al., 1997). Consequently, in the absence of Meis1 and Pbx, embryos exhibit severe defects in primitive erythropoiesis, and are unable to produce visible circulating blood cells. Concomitant with a loss of *gata1*, Meis1 and Pbx-depleted embryos also exhibit increased numbers of myelocytes, and fail to maintain wild type levels of *scl*, a broad marker of hematopoietic cell fate. We further demonstrate that the nuclear localization and stability of Pbx is dependent on Meis1, and that Meis-Pbx complexes are required for proper expression of *gata1*, but are not required to initiate *scl* expression. In zebrafish, Caudal homeobox (Cdx) depletion results in diminished posterior lateral-plate mesoderm *hox* gene expression, and a concomitant loss of erythroid gene expression (Davidson et al., 2003; Davidson and Zon, 2006). Overexpressing *hoxb6b*, *hoxb7a*, and *hoxa9a* partially rescues erythroid gene expression in *cdx1a/cdx4*-depleted embryos (Davidson et al., 2003; Davidson

and Zon, 2006), placing Hox downstream of Cdx in the hematopoietic transcription factor hierarchy. Pbx/Meis1-depletion produces a phenotype that is strikingly different from that of a *cdx1a/cdx4*-depleted zebrafish embryo, which completely lacks early *scl* expression. Consequently, although we demonstrate that Pbx4 and Cdx4 proteins have the capacity to interact both *in vitro* and *in vivo,* we propose a model placing Meis1 and Hox downstream of Cdx, and upstream of *gata1* in the molecular hierarchy of primitive hematopoiesis.

All Hox proteins possess similar biochemical properties, binding a core 5'-TAAT-3' recognition element in the regulatory region of target genes (reviewed in Affolter et al., 2008; Berger et al., 2008; Noyes et al., 2008). The specificity of Hox proteins is therefore achieved through their interaction with other DNA-binding cofactors such as Pbx and Meis (Mann, 1995; Mann and Affolter, 1998; Mann and Chan, 1996; Mann et al., 2009). However, *pbx2* and *pbx4* are ubiquitously expressed within the developing embryo (Waskiewicz et al., 2002), and *meis1* is broadly expressed across numerous tissue types. Consequently, it is difficult to understand how each member of the Hox family regulates unique developmental programs that lead to the generation of distinct segmental identities. This question is confounded by the fact that very few direct transcriptional targets of Hox, Pbx, or Meis have been identified within the literature. It is therefore unclear how exactly these transcription factors are regulating *gata1* expression, or what their other hematopoietic transcriptional targets may be.

Previous research has shown that Hoxa10 has the capacity to bind directly to the *gata1* promoter (Magnusson et al., 2007). Meis1 and Pbx1 form a heterotrimeric complex with Hoxa10 (Shanmugam et al., 1999). Consequently, the transcriptional activation of *gata1* by Pbx and Meis1 may occur in a direct fashion. The identification of direct transcriptional targets of Pbx and/or Meis1 using chromatin immunoprecipitation and massively parallel sequencing (ChIP-seq) could serve to test this hypothesis. This technique would also potentially identify direct regulatory targets of Pbx/Meis/Hox in a variety of tissues, and may give us insight into the genetic pathways governing a variety of integral developmental processes that these proteins serve to regulate. Such processes include anterior-posterior patterning, hindbrain patterning, limb development, and (of course) hematopoiesis. As *hox, pbx,* and *meis* are also implicated as proto-oncogenes in hematological malignancies (Kroon et al., 2001; Nakamura et al., 1996a; Nakamura et al., 1996b; Pineault et al., 2003; Slape and

Aplan, 2004), identifying their direct targets may give us invaluable information about their role in leukemia.

Pbx binds Hox paralogue groups 1-4 through both its TALE motif and a tryptophan-containing hexapeptide motif termed the Pbx-Interaction Domain (PID). Cdx proteins possess a putative PID. We demonstrate that Pbx4 and Cdx4 proteins have the capacity to interact both *in vitro* and *in vivo*. This interaction requires an intact Cdx4 PID. As previously mentioned, the hematopoietic and *hox* gene expression defects of Cdx-depleted embryos differ from those of Pbx-depleted embryos. Our data therefore support a model whereby Pbx/Meis1 and Cdx function at disparate points in the hematopoietic transcription factor hierarchy. Consequently, the biological significance of a Pbx-Cdx interaction currently remains unclear and requires further analyses. It would therefore be of interest to identify common, direct transcriptional targets of Pbx4 and Cdx4 using ChIP-seq.

7.2 RA in definitive hematopoiesis

Loss and gain of function analyses in mouse have implicated the retinoic acid (RA) signaling pathway in vertebrate HSC formation. Aldh1a2 is the predominant RA-synthesis enzyme in the vertebrate embryo (Niederreither et al., 1999; Niederreither et al., 2000). Analyses of *Aldh1a2*-mutant mice (Goldie et al., 2008), and mice with a conditional deletion of *Aldh1a2* in VE-cadherin-positive endothelial cells (Chanda et al., 2013) have demonstrated a role for RA-signaling in hemogenic endothelial cell specification. However, *Aldh1a2*-mutant mice die of severe vascular defects prior to HSC emergence (Niederreither et al., 1999), precluding global analyses of *Aldh1a2*-function in murine definitive hematopoiesis. Consequently, previous studies have failed to elucidate other potential molecular functions of RA signaling in specifying HSCs *in vivo*.

By impairing RA synthesis in the developing zebrafish embryo, we provide evidence that RA is an essential regulator of zebrafish HSC formation. RA-depleted embryos demonstrate nearly abolished *cmyb* HSC gene expression, and a concomitant loss of *rag1* and *ikaros* thymic lymphoid progenitor gene expression. We demonstrate that RA is required between 4 hpf and 19 hpf for HSC formation, prior to hemogenic endothelial cell formation, at a time when *aldh1a2* is expressed in the paraxial mesoderm and somites. We therefore

propose a model whereby RA signaling acts outside of pre-hemogenic endothelium to regulate zebrafish HSC formation.

Previous research in both mouse and zebrafish has established a model whereby Notch1-expressing cells within the dorsal aorta are instructed by adjacent cells to form HSCs (Gering and Patient, 2010; Hadland et al., 2004; Kumano et al., 2003; Robert-Moreno et al., 2005; Robert-Moreno et al., 2008). We, however, demonstrate that both *notch1a/b* and *gata2* expression are unaffected by loss of RA in zebrafish. We further demonstrate that RA is required for HSC formation prior to the formation of dorsal aorta hemogenic endothelium. Our combined results therefore suggest that, unlike in mice, zebrafish RA does not regulate Notch1-signaling. RA is therefore functioning independently of the Notch1 signaling pathway to regulate zebrafish definitive hematopoiesis.

Recently, Clements et al., (2011) demonstrated a requirement for somitic Wnt16 in zebrafish hematopoiesis. Both RA and Wnt16 function outside of dorsal aorta pre-hemogenic endothelium to regulate zebrafish HSC formation prior to 19 hpf (Clements et al., 2011). We demonstrate that RA-deficient embryos possess wild type expression levels of *wnt16* and its transcriptional targets *dlc* and *dld*. Our data therefore indicate that, despite their similar localization, and their common temporal requirement in definitive hematopoiesis, RA does not regulate *wnt16* or its downstream targets *dlc* and *dld*. Notch3 is required by Wnt16-induced Dlc/Dld to regulate HSC formation (Kim et al., 2014). RA-deficient embryos also exhibit wild type levels of *notch3* expression. Our combined results therefore suggest that RA and Wnt16/Notch3 participate in convergent pathways to regulate HSC formation, or that RA is functioning downstream of the Wnt16-Notch pathway in zebrafish definitive hematopoiesis. Our results do not exclude the possibility that RA is acting in a Notch-independent fashion to regulate HSC formation. It would therefore be of interest to determine if activating the heat-shock induction of the Notch signaling pathway in 19 hpf RA-deficient embryos rescues their definitive hematopoietic defects.

The dorsal aorta forms from angioblasts that arise from bilateral stripes of posterior lateral-plate mesoderm. These angioblasts migrate towards the midline and aggregate (Ellertsdottir et al., 2010). Angioblast migration occurs between 14 and 18 hpf, in close proximity to the somites, which express *aldh1a2*. We demonstrate that RA is required

between 4 hpf and 19 hpf for HSC formation. RA is a diffusible morphogen. It is therefore plausible that RA signaling within angioblats may render them competent to form hemogenic endothelium and or HSCs. Consequently, to gain a better understanding of how RA regulates HSC formation, it would also be useful to identify downstream transcriptional targets of the RA signaling pathway. This could be accomplished using RNA-sequencing (RNA-seq) to compare the mRNA expression profiles of 17 hpf wild type versus DEAB-treated or *aldh1a2*-morphant embryos.

7.3 Hmx4 in primitive and definitive hematopoiesis

Morpholino-based analyses have shown that the homeodomain transcription factor H6 homeobox 4 (*hmx4*) participates in eye and forebrain development (K. Berry-Wynne, unpublished; Boisset and Schorderet, 2012; Gongal et al., 2011). *hmx4*-morphant zebrafish display a host of defects, which include micropthalmia, narrowed eye-field, loss of pectoral fins, open neural tube, small ear, and reduced numbers of vagal motor neurons (Gongal et al., 2011). RA treatment rescues the forebrain patterning defects of *hmx4*-morphants (Gongal et al., 2011), implicating *hmx4* as a regulator of the RA signaling pathway. Given that RA is an essential regulator of both primitive and definitive hematopoiesis, we sought to determine the contribution of *hmx4* to embryonic hematopoiesis.

We provide evidence that *hmx4* is required for proper RA synthesis in the developing embryo, as *hmx4*-morphants demonstrate reduced *aldh1a2* expression, and an expansion in the domain of *cyp26a1* expression. Consistent with defects in RA signaling, *hmx4*-morphant embryos also exhibit defects that are consistent with reduced hematopoietic stem cell (HSC) formation. These include severely downregulated *runx1* expression, and concomitant loss of *rag1* and *ikaros* thymic lymphoid progenitor gene expression. Supplementation of *hmx4*-morphants with a biologically relevant dose of RA rescues their *runx1* HSC gene expression defects, placing Hmx4 upstream of the RA signaling pathway in zebrafish definitive hematopoiesis.

hmx4-morphants also exhibit defects in primitive hematopoiesis. These embryos exhibit increased numbers of *pu.1*-expressing myeloid progenitors, but reduced numbers of more mature *lyz*-expressing myeloid cells. This gene expression profile may indicate that the

myeloid progenitors of *hmx4*-morphants are specified correctly, but fail to mature properly. The myelopoietic defects of *hmx4*-morphants are consistent with a loss of RA signaling, as zebrafish treated with an RA-synthesis inhibitor exhibit upregulated *pu.1* gene expression (Ma et al., 2010). The myelopoietic defects of *hmx4*-morphants are also consistent with a decrease in *runx1* gene expression, as Runx1 negatively regulates *pu.1* expression, and activates *lyz* expression, promoting neutrophil over macrophage fate (Jin et al., 2012).

hmx4-morphants also exhibit reduced *gata1* primitive erythropoietic gene expression, and reduced levels of differentiated erythrocytes, as evidenced by nearly abolished o-dianisidine staining. While the primitive myeloid phenotype of *hmx4*-morphants is consistent with reduced RA levels, their erythropoietic gene expression defects cannot be rescued with RA treatment, and lie in direct opposition to phenotypes obtained by loss of RA signaling (Ma et al., 2010). Our analyses of *hmx4*-morphants therefore indicate that Hmx4 regulates primitive erythropoiesis in an RA-independent fashion.

To date, no direct transcriptional targets of any Hmx family member have been identified in the literature. The identification of direct transcriptional targets of Hmx4 using chromatin immunoprecipitation and massively parallel sequencing (ChIP-seq) could help determine how this transcription factor regulates both retinoic acid signaling, and primitive erythropoiesis. Analyses of *hmx4*-morphants suggest that Hmx4 is also required for proper eye, ear, pectoral fin, and forebrain development, as well neural tube closure (Gongal et al., 2011). Consequently, identifying direct transcriptional targets of Hmx4 may provide valuable insights into the genetic pathways that govern a variety of developmental processes.

We generated *hmx4*-mutant zebrafish embryos using zinc finger nucleases (ZFNs) containing a *Sharkey* FokI cleavage domain variant. These embryos possess a nonsense mutation that generates a premature stop codon immediately upstream of the Hmx4 homeodomain. Overexpression of wild type, but not mutant *hmx4* mRNAs generates severe morphological defects. Our results therefore indicate that our embryos possess loss-of-function mutations in *hmx4*. Surprisingly, *hmx4*-mutants fail to exhibit any overt morphological or hematopoietic defects, confounding our understanding of the role of Hmx4 in RA signaling and embryonic hematopoiesis.

Several possibilities exist to explain the discrepancy between *hmx4*-morphant and *hmx4*-mutant phenotypes. For example, it is possible that our morpholinos may bind to, and inhibit the function of unintended target genes. We speculate that our *hmx4*-morphants retain some level of Hmx4 protein function. If this is the case, some compensatory mechanism may exist to differentially upregulate *hmx4* and/or *hmx4*-target RNA levels in *hmx4*-morphants versus mutants. It is also possible that our *hmx4*-mutant embryos retain homeodomain-independent Hmx4 functions that are revealed by our analyses of *hmx4*-morphants. To test this hypothesis, we could ascertain if overexpressing our mutant *hmx4* mRNAs in *hmx4*-morphants rescues their morphological defects.

Both transcription activator-like effector nucleases (TALENs) and the clustered regularly interspaced short palindromic repeats (CRISPR)/Cas9 systems have successfully been used to delete whole loci from the zebrafish genome (reviewed by Auer and Del Bene, 2014; Gupta et al., 2013; Liu et al., 2014; Ma et al., 2013; Xiao et al., 2013). These targeted endonuclease technologies could potentially be used to generate *hmx4*-null zebrafish. These mutants could then be used to more confidently assess Hmx4 function in zebrafish hematopoiesis.

7.4 Analyses of targeted endonucleases containing *Sharkey* FokI

ZFNs and transcription activator-like effector nucleases (TALENs) have been used to generate mutations in organisms that are not amenable to homologous recombination-based genetic modifications. Both ZFNs and TALENs consist of DNA-binding arrays fused to the non-specific FokI nuclease domain. In an effort to improve targeted endonuclease mutagenesis efficiency, we enhanced their catalytic activity using the *Sharkey* FokI nuclease domain variant. All constructs tested display increased DNA cleavage activity *in vitro*. We demonstrate that ZFN arrays containing the *Sharkey* FokI variant may exhibit a dramatic increase in mutagenesis frequency *in vivo* in zebrafish. Conversely, we demonstrate that TALENs containing the *Sharkey* FokI variant exhibit absent or severely reduced *in vivo* mutagenic activity in zebrafish. Our overall results suggest that incorporating the *Sharkey* FokI endonuclease domain into TALENs may severely abrogate their *in vivo* mutagenesis function in zebrafish. Notably, *Sharkey* ZFNs and TALENs do not generate increased

toxicity-related defects or mortality. These data suggest that *Sharkey* ZFNs are an effective alternative to conventional ZFNs, but advise against the use of *Sharkey* TALENs.

7.5 Figures

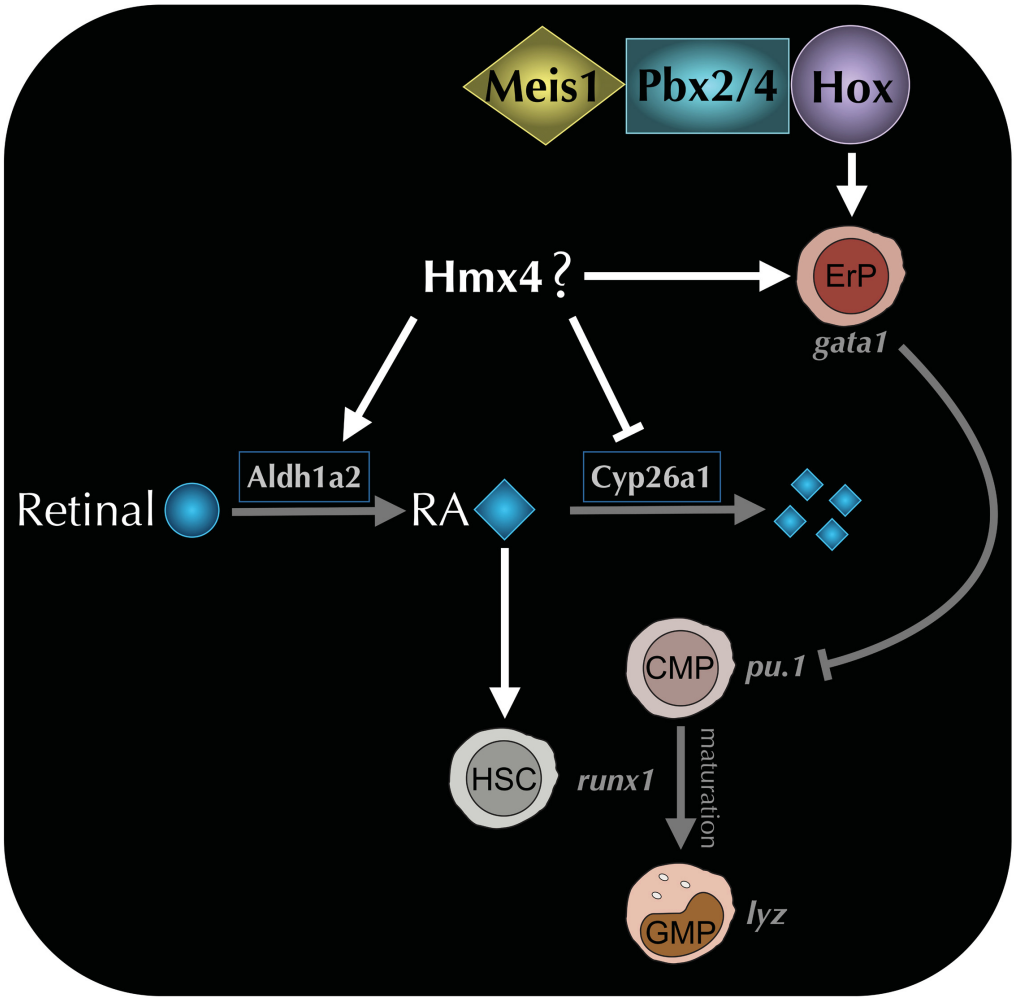

Figure 7.1. Summary detailing regulation of embryonic hematopoiesis by factors described in this thesis. Chapter 3 describes the role that Meis1 and Pbx play in association with posterior Hox proteins to regulate primitive erythropoiesis and repress myeloid cell fate. Chapter 4 describes a novel role for retinoic acid (RA) signaling in hematopoietic stem cell (HSC) formation. Chapter 5 describes the possible involvement of Hmx4 in modulating RA levels by positively regulating *aldh1a2* RA-synthesis gene expression, and by repressing *cyp26a1* RA metabolism gene expression. Chapter 5 also describes a potential RA-dependent role for Hmx4 in regulating HSC formation and primitive myelopoiesis, as well as an RA-independent role for Hmx4 in regulating primitive erythropoiesis. ErP, erythroid progenitor; CMP, common myeloid progenitor; GMP, granulocyte monocyte progenitor.

7.6 References

Affolter, M., M. Slattery, and R.S. Mann. 2008. A lexicon for homeodomain-DNA recognition. *Cell*. 133:1133-1135.

Auer, T.O., and F. Del Bene. 2014. CRISPR/Cas9 and TALEN-mediated knock-in approaches in zebrafish. *Methods*. 69:142-150.

Azcoitia, V., M. Aracil, A.C. Martinez, and M. Torres. 2005. The homeodomain protein Meis1 is essential for definitive hematopoiesis and vascular patterning in the mouse embryo. *Dev Biol*. 280:307-320.

Berger, M.F., G. Badis, A.R. Gehrke, S. Talukder, A.A. Philippakis, L. Pena-Castillo, T.M. Alleyne, S. Mnaimneh, O.B. Botvinnik, E.T. Chan, F. Khalid, W. Zhang, D. Newburger, S.A. Jaeger, Q.D. Morris, M.L. Bulyk, and T.R. Hughes. 2008. Variation in homeodomain DNA binding revealed by high-resolution analysis of sequence preferences. *Cell*. 133:1266-1276.

Boisset, G., and D.F. Schorderet. 2012. Zebrafish hmx1 promotes retinogenesis. *Experimental eye research*. 105:34-42.

Chanda, B., A. Ditadi, N.N. Iscove, and G. Keller. 2013. Retinoic acid signaling is essential for embryonic hematopoietic stem cell development. *Cell*. 155:215-227.

Clements, W.K., A.D. Kim, K.G. Ong, J.C. Moore, N.D. Lawson, and D. Traver. 2011. A somitic Wnt16/Notch pathway specifies haematopoietic stem cells. *Nature*. 474:220-224.

Davidson, A.J., P. Ernst, Y. Wang, M.P. Dekens, P.D. Kingsley, J. Palis, S.J. Korsmeyer, G.Q. Daley, and L.I. Zon. 2003. cdx4 mutants fail to specify blood progenitors and can be rescued by multiple hox genes. *Nature*. 425:300-306.

Davidson, A.J., and L.I. Zon. 2004. The 'definitive' (and 'primitive') guide to zebrafish hematopoiesis. *Oncogene*. 23:7233-7246.

Davidson, A.J., and L.I. Zon. 2006. The caudal-related homeobox genes cdx1a and cdx4 act redundantly to regulate hox gene expression and the formation of putative hematopoietic stem cells during zebrafish embryogenesis. *Dev Biol*. 292:506-518.

DiMartino, J.F., L. Selleri, D. Traver, M.T. Firpo, J. Rhee, R. Warnke, S. O'Gorman, I.L. Weissman, and M.L. Cleary. 2001. The Hox cofactor and proto-oncogene Pbx1 is required for maintenance of definitive hematopoiesis in the fetal liver. *Blood*. 98:618-626.

Ellertsdottir, E., A. Lenard, Y. Blum, A. Krudewig, L. Herwig, M. Affolter, and H.G. Belting. 2010. Vascular morphogenesis in the zebrafish embryo. *Dev Biol*. 341:56-65.

Galloway, J.L., R.A. Wingert, C. Thisse, B. Thisse, and L.I. Zon. 2005. Loss of gata1 but not gata2 converts erythropoiesis to myelopoiesis in zebrafish embryos. *Dev Cell*. 8:109-116.

Gering, M., and R. Patient. 2010. Notch signalling and haematopoietic stem cell formation during embryogenesis. *Journal of cellular physiology*. 222:11-16.

Goldie, L.C., J.L. Lucitti, M.E. Dickinson, and K.K. Hirschi. 2008. Cell signaling directing the formation and function of hemogenic endothelium during murine embryogenesis. *Blood*. 112:3194-3204.

Gongal, P.A., L.D. March, V.L. Holly, L.M. Pillay, K.M. Berry-Wynne, H. Kagechika, and A.J. Waskiewicz. 2011. Hmx4 regulates Sonic hedgehog signaling through control of retinoic acid synthesis during forebrain patterning. *Dev Biol*. 355:55-64.

Gupta, A., V.L. Hall, F.O. Kok, M. Shin, J.C. McNulty, N.D. Lawson, and S.A. Wolfe. 2013. Targeted chromosomal deletions and inversions in zebrafish. *Genome research*. 23:1008-1017.

Hadland, B.K., S.S. Huppert, J. Kanungo, Y. Xue, R. Jiang, T. Gridley, R.A. Conlon, A.M. Cheng, R. Kopan, and G.D. Longmore. 2004. A requirement for Notch1 distinguishes 2 phases of definitive hematopoiesis during development. *Blood*. 104:3097-3105.

Hisa, T., S.E. Spence, R.A. Rachel, M. Fujita, T. Nakamura, J.M. Ward, D.E. Devor-Henneman, Y. Saiki, H. Kutsuna, L. Tessarollo, N.A. Jenkins, and N.G. Copeland. 2004. Hematopoietic, angiogenic and eye defects in Meis1 mutant animals. *EMBO J*. 23:450-459.

Jin, H., L. Li, J. Xu, F. Zhen, L. Zhu, P.P. Liu, M. Zhang, W. Zhang, and Z. Wen. 2012. Runx1 regulates embryonic myeloid fate choice in zebrafish through a negative feedback loop inhibiting Pu.1 expression. *Blood*. 119:5239-5249.

Kim, A.D., C.H. Melick, W.K. Clements, D.L. Stachura, M. Distel, D. Panakova, C. MacRae, L.A. Mork, J.G. Crump, and D. Traver. 2014. Discrete Notch signaling requirements in the specification of hematopoietic stem cells. *EMBO J*. 33:2363-2373.

Kroon, E., U. Thorsteinsdottir, N. Mayotte, T. Nakamura, and G. Sauvageau. 2001. NUP98-HOXA9 expression in hemopoietic stem cells induces chronic and acute myeloid leukemias in mice. *EMBO J*. 20:350-361.

Kumano, K., S. Chiba, A. Kunisato, M. Sata, T. Saito, E. Nakagami-Yamaguchi, T. Yamaguchi, S. Masuda, K. Shimizu, T. Takahashi, S. Ogawa, Y. Hamada, and H. Hirai. 2003. Notch1 but not Notch2 is essential for generating hematopoietic stem cells from endothelial cells. *Immunity*. 18:699-711.

Liu, Y., D. Luo, Y. Lei, W. Hu, H. Zhao, and C.H. Cheng. 2014. A highly effective TALEN-mediated approach for targeted gene disruption in Xenopus tropicalis and zebrafish. *Methods*. 69:58-66.

Ma, A.C., M.I. Chung, R. Liang, and A.Y. Leung. 2010. A DEAB-sensitive aldehyde dehydrogenase regulates hematopoietic stem and progenitor cells development during primitive hematopoiesis in zebrafish embryos. *Leukemia*. 24:2090-2099.

Ma, A.C., H.B. Lee, K.J. Clark, and S.C. Ekker. 2013. High efficiency In Vivo genome engineering with a simplified 15-RVD GoldyTALEN design. *PloS one*. 8:e65259.

Magnusson, M., A.C. Brun, N. Miyake, J. Larsson, M. Ehinger, J.M. Bjornsson, A. Wutz, M. Sigvardsson, and S. Karlsson. 2007. HOXA10 is a critical regulator for hematopoietic stem cells and erythroid/megakaryocyte development. *Blood*. 109:3687-3696.

Mann, R.S. 1995. The specificity of homeotic gene function. *Bioessays*. 17:855-863.

Mann, R.S., and M. Affolter. 1998. Hox proteins meet more partners. *Curr Opin Genet Dev*. 8:423-429.

Mann, R.S., and S.K. Chan. 1996. Extra specificity from extradenticle: the partnership between HOX and PBX/EXD homeodomain proteins. *Trends Genet*. 12:258-262.

Mann, R.S., K.M. Lelli, and R. Joshi. 2009. Hox specificity unique roles for cofactors and collaborators. *Current topics in developmental biology*. 88:63-101.

Nakamura, T., D.A. Largaespada, M.P. Lee, L.A. Johnson, K. Ohyashiki, K. Toyama, S.J. Chen, C.L. Willman, I.M. Chen, A.P. Feinberg, N.A. Jenkins, N.G. Copeland, and J.D. Shaughnessy, Jr. 1996a. Fusion of the nucleoporin gene NUP98 to HOXA9 by the chromosome translocation t(7;11)(p15;p15) in human myeloid leukaemia. *Nat Genet*. 12:154-158.

Nakamura, T., D.A. Largaespada, J.D. Shaughnessy, Jr., N.A. Jenkins, and N.G. Copeland. 1996b. Cooperative activation of Hoxa and Pbx1-related genes in murine myeloid leukaemias. *Nat Genet*. 12:149-153.

Niederreither, K., V. Subbarayan, P. Dolle, and P. Chambon. 1999. Embryonic retinoic acid synthesis is essential for early mouse post-implantation development. *Nat Genet*. 21:444-448.

Niederreither, K., J. Vermot, B. Schuhbaur, P. Chambon, and P. Dolle. 2000. Retinoic acid synthesis and hindbrain patterning in the mouse embryo. *Development*. 127:75-85.

Noyes, M.B., R.G. Christensen, A. Wakabayashi, G.D. Stormo, M.H. Brodsky, and S.A. Wolfe. 2008. Analysis of homeodomain specificities allows the family-wide prediction of preferred recognition sites. *Cell*. 133:1277-1289.

Pevny, L., M.C. Simon, E. Robertson, W.H. Klein, S.F. Tsai, V. D'Agati, S.H. Orkin, and F. Costantini. 1991. Erythroid differentiation in chimaeric mice blocked by a targeted mutation in the gene for transcription factor GATA-1. *Nature*. 349:257-260.

Pineault, N., C. Buske, M. Feuring-Buske, C. Abramovich, P. Rosten, D.E. Hogge, P.D. Aplan, and R.K. Humphries. 2003. Induction of acute myeloid leukemia in mice by the human leukemia-specific fusion gene NUP98-HOXD13 in concert with Meis1. *Blood*. 101:4529-4538.

Rhodes, J., A. Hagen, K. Hsu, M. Deng, T.X. Liu, A.T. Look, and J.P. Kanki. 2005. Interplay of pu.1 and gata1 determines myelo-erythroid progenitor cell fate in zebrafish. *Dev Cell*. 8:97-108.

Robert-Moreno, A., L. Espinosa, J.L. de la Pompa, and A. Bigas. 2005. RBPjkappa-dependent Notch function regulates Gata2 and is essential for the formation of intra-embryonic hematopoietic cells. *Development*. 132:1117-1126.

Robert-Moreno, A., J. Guiu, C. Ruiz-Herguido, M.E. Lopez, J. Ingles-Esteve, L. Riera, A. Tipping, T. Enver, E. Dzierzak, T. Gridley, L. Espinosa, and A. Bigas. 2008. Impaired embryonic haematopoiesis yet normal arterial development in the absence of the Notch ligand Jagged1. *EMBO J*. 27:1886-1895.

Shanmugam, K., N.C. Green, I. Rambaldi, H.U. Saragovi, and M.S. Featherstone. 1999. PBX and MEIS as non-DNA-binding partners in trimeric complexes with HOX proteins. *Mol Cell Biol*. 19:7577-7588.

Shivdasani, R.A., Y. Fujiwara, M.A. McDevitt, and S.H. Orkin. 1997. A lineage-selective knockout establishes the critical role of transcription factor GATA-1 in megakaryocyte growth and platelet development. *EMBO J*. 16:3965-3973.

Slape, C., and P.D. Aplan. 2004. The role of NUP98 gene fusions in hematologic malignancy. *Leuk Lymphoma*. 45:1341-1350.

Waskiewicz, A.J., H.A. Rikhof, and C.B. Moens. 2002. Eliminating zebrafish pbx proteins reveals a hindbrain ground state. *Dev Cell*. 3:723-733.

Xiao, A., Z. Wang, Y. Hu, Y. Wu, Z. Luo, Z. Yang, Y. Zu, W. Li, P. Huang, X. Tong, Z. Zhu, S. Lin, and B. Zhang. 2013. Chromosomal deletions and inversions mediated by TALENs and CRISPR/Cas in zebrafish. *Nucleic Acids Res*. 41:e141.

Appendix A

Bacterial-one-hybrid zinc finger nuclease array selection protocol

A version of this appendix has been published. Laura M. Pillay, Lyndsay G. Selland, Valerie C. Fleisch, Patricia L. A. Leighton, Caroline S. Cheng, Jakub K. Famulski, R. Gary Ritzel, Lindsey D. March, Hao Wang, W. Ted Allison, and Andrew J. Waskiewicz (2013). Evaluating the mutagenic activity of targeted endonucleases containing a *Sharkey* FokI cleavage domain variant in zebrafish. *Zebrafish*, 10(3): 353-364.

A.1 Electrocompetent Cell Preparation

Bacterial Strain	Addgene No.	Full Title	Resistance
USO	18049	USO HisB$^-$ pyrF$^-$ rpoZ$^-$	Tet

Reagents

2X YT + 10mM MgSO4 Recipe (Makes 1L)

16g Bacto Tryptone

10g Bacto Yeast Extract

5g NaCl

10mL 1M MgSO4

- Adjust pH to 7.0 with 10N NaOH.
- Top up to 1L with distilled water.
- Autoclave.

You will also need 2L of 10% glycerol (autoclaved).

Pre-chill: (4°C)

Sterile 1.7mL tubes

Autoclaved 250mL centrifuge bottles

Autoclaved repeat pipette tips

Autoclaved 10% glycerol

Protocol

Day 1:

- Streak LB + Tet plate with USO strain glycerol stock to obtain single colony isolates.
- Grow overnight at 37°C.

Day 2:

- Inoculate 5mL of LB + 10μg/mL Tet culture with single USO colony.
- Grow overnight at 37°C with shaking.

Day 3:

- Inoculate 100mL 2X YT + 10mM MgSO4 + 50μg/mL Tet culture with yesterday's USO culture.
- Grow overnight at 37°C with shaking.

Day 4:

From 100mL culture prepared and grown overnight:

- Inoculate 1L 2X YT + 10mM MgSO4 culture with 10mL of yesterday's USO culture.

Note: It is easy to make double the amount of cells (start with 2 x 1L culture).

- Grow at 37°C with shaking to an OD600 of 0.6-0.8 (approximately 5 hours).
- Ice culture for 30 min.

Note: Everything should be kept cold (<4°C) from this point onward.

- In 250mL bottles (chilled), spin down cells at 3700 rpm for 15 min at 4°C.
- Poor off supernatant.
- Resuspend cells in 50mL of 10% glycerol (chilled).
- Merge bottles so there is only one left.
- Fill each bottle to 200mL with 10% glycerol and resuspend cells.

Note: Resuspend cells with gentle swirling on ice.

- Spin 15 min at 3700 rpm at 4°C.
- Poor off supernatant.
- Resuspend cells in 200mL 10% glycerol.
- Spin 15 min at 3700 rpm at 4°C.

- Poor off supernatant.
- Resuspend cells in 5mL 10% glycerol.
- Aliquot 200µL cells to pre-chilled 1.7mL tubes, and flash-freeze in dry ice.
- Store electrocompetent cells at -80°C.

Test Electrocompetent Cells:

- Transform 200µL cells with 1µL of 0.1ng/µL high-copy AmpR plasmid (Ex. pBSK+).

Electroporation:

Cuvette: 2mm = 2.45

Capacitance: 001

R: 25kV

RS: 129

Aim for ~5.4ms

Following Electroporation:

Add 800µL SOC

Incubate at 37°C for 1 hr.

Make serial dilutions of culture, including a no-plasmid control (10^{-4} – 10^{-8}).

Plate each dilution on an LB + Amp plate.

Grow overnight at 37°C.

Determine approximate number of transformants per µg DNA:

Ex. If 59 colonies grow on the 10^{-6} plate, then:

$59/(1 \times 10^{-6}$ ng) x 1000ng/µg = 5.9×10^{10} transformants per µg DNA

Expect 10^9 to 10^{10} transformants per µg DNA.

****Note: To control for contamination, plate untransformed cells on LB + Carb and LB+ Kan. Expect no growth.***

A.2 Maxiprep Bacterial-One-Hybrid Plasmids

Required Plasmids:

Library Plasmid	Addgene No.	Full Title	Resistance	Copy No.
F1bbs	18753	1352ωUV2F1bbs	Amp/Kan	High
F2bbs	18752	1352ωUV2F2bbs	Amp/Kan	High
F3bbs	18756	1352ωUV2F3bbs	Amp/Kan	High
pKBStop	20704	1352ωUV2-KpnIBamHI-Stop	Amp	High
Target Plasmid	**Addgene No.**	**Full Title**	**Resistance**	**Copy No.**
pH3U3	12609	pH3U3-mcs	Kan	Low
ZFN Plasmid	**Addgene No.**	**Full Title**	**Resistance**	**Copy No.**
pCS2-HA-Fok1-RR	18754	pCS2-HA-GAAZFP-Fok1-RR	Amp	High
pCS2-FLAG-Fok1-DD	18755	pCS2-FLAG-TTGZP-Fok1-DD	Amp	High
pCS2-HA-*Sharkey*Fok1-RR	N/A	pCS2-HA-GAAZFP-ShFok1-RR	Amp	High
pCS2-FLAG-*Sharkey*Fok1-DD	N/A	pCS2-FLAG-TTGZP-ShFok1-DD	Amp	High

Optional Plasmids:

Control Plasmid	Addgene No.	Full Title	Resistance	Copy No.
pH3U3-Zif268	18046	pH3U3-Zif268 Ω	Kan	Low
pB1H2ω2-Zif268	18045	pB1H2ω2-Zif268	Amp	High
pB1H2ω2-mutOdd	18044	pB1H2ω2-mutOdd	Amp	High
Wolfe kdrl ZFN	**Addgene No.**	**Full Title**	**Resistance**	**Copy No.**
Pmd26 kdr	N/A	Pmd26 kdrl (pCS2-Fok1)	Amp	High
Pmd27 kdr	N/A	Pmd27 kdrl (pCS2-Fok1)	Amp	High
Bacterial Strain	**Addgene No.**	**Full Title**	**Resistance**	**Copy No.**
USO	18049	USO HisB$^-$ pyrF$^-$ rpoZ$^-$	Tet	N/A

Medium Copy No. Plasmids

- Inoculate 2 x 250mL LB + antibiotic culture with glycerol stock.
- Grow overnight at 37°C with shaking.
- Maxiprep.
- Resuspend DNA in 50µL MQ water.

Expect ~1µg/µl concentration.

Low Copy No. Plasmids

- Inoculate 2 x 250mL LB + antibiotic culture with glycerol stock.
- Grow at 37°C with shaking to an OD600 of 0.7-0.9 (approximately 5 hours).
- Add Chloramphenicol to a final concentration of 170µg/mL.

- Grow overnight at 37°C with shaking.
- Maxiprep.
- Resuspend DNA in 20µL MQ water.

Expect ~0.15µg/µl concentration.

A.3 Prepare pH3U3 Target Site Constructs

Digest pH3U3 Plasmid

In 1.7mL tube:

- 2.5µL 10X Buffer H (Promega)
- 1µL EcoRI
- 1µL NotI
- 0.5µg DNA
- + MQ water = 25µL total.

Digest overnight at 37°C.

Gel-extract digested plasmid.

Anneal Complementary Target Site Oligos (8 pairs total)

In PCR tube:

- 0.5µL (100µM) F (Top) Oligo
- 0.5µL (100µM) R (Bottom) Oligo
- 0.3µL 10X T4 DNA Ligase Buffer
- 2.7µL MQ water

= 4µL total.

PCR Program:

95°C 5 min (initial denaturation)

70X: (slow anneal)

- 95°C 1 min
- -1°C per cycle

Hold at 4°C.

Store annealed oligos at 4°C.

Ligate Annealed Target Site Oligos to Digested, Gel-Purified pH3U3

In PCR tube:

- 4µL oligo insert (or MQ water control)
- 5µL pH3U3 vector (or MQ water control)
- 2µL 10X T4 DNA Ligase Buffer
- 1µL T4 DNA Ligase
- + 8µL MQ water = 20µL total.

Ligate overnight at 16°C.

Transform TOP10 Cells (Invitrogen) with Ligations

- Mix entire ligation with 10µL TOP10 Cells (30µL total).
- Ice 20 min.
- Heat shock 45 sec at 42°C.
- Ice 2 min.
- Add 250µL LB.
- Incubate at 37°C for 30 min.
- Plate on LB + Kan.
- Grow overnight at 37°C.

Miniprep pH3U3 Target Site Plasmid

- Inoculate 2 x 5mL LB + 10µg/mL Kan culture with single colony (16 cultures total).
- Grow overnight at 37°C with shaking.
- Miniprep 10mL culture for each.

Expect ~0.05µg/µl concentration.

Sequence pH3U3 Target Site Plasmid Minipreps (8 total)

In PCR tube:

- 5.5µL miniprep DNA
- 0.5µL (10µM) pH3U3 Sequencing Primer

- 4μL ET Sequencing Mix

= 10μL total

A.4 Prepare Individual Zinc Finger Libraries

Digest Fxbbs Library Plasmid

In 1.7mL tube:

- 4μL 10X Buffer
- 2.5μL BbsI
- 4μg DNA (F1bbs, F2bbs, or F3bbs)
- + MQ water = 40μL total.

Digest at 37°C for ≥ 2hrs.

Note: Aliquot BbsI buffer, and store along with enzyme at -80°C. It goes off!

Dephosphorylate to prevent re-annealing:

- Add 1μL SAP to digest.
- Incubate at 37°C for 1 hr.
- Incubate at 70°C for 15 min to inactivate SAP.

Gel-extract digested, dephosphorylated plasmid.

Kinase Library and Complementary Oligos

Note: 12 reactions total:

6 library oligos

2 complementary oligos per 3 finger types (F1, F2, F3)

In PCR tube:

- 1.25μL 10X T4 DNA Ligase Buffer
- 0.25μL PNK
- 0.5μL (100μM) oligo
- 10.5μL MQ water

= 12.5μL total.

Heat at 37°C for 45 min.

Anneal Library and Complementary Oligos

In PCR tube:

Mix 1:1:1 ratio (4µL each or 50µM per 12µL ÷3 = 1.39µM):

Library oligo with correct complementary oligos.

Ex. 3P1 with CF1 3' and CF1 5'

PCR Program:

95°C 5 min (initial denaturation)

70X: (slow anneal)

- 95°C 1 min
- -1°C per cycle

Hold at 4°C.

Store annealed oligos at 4°C.

Ligate Digested, Dephosphorylated, Gel-Purified Fxbbs and Kinased Library Insert

In PCR tube:

- 10µL (~400ng) Fxbbs vector (or MQ water control)
- 2µL library insert (or MQ water control)
- 2µL 10X T4 DNA ligase buffer
- 1µL T4 DNA ligase
- + 5µL MQ water = 20µL total.

Ligate overnight at 16°C.

****Note: F1bbs vector is used for 3P1 or 5P1 library insert.***

****Note: F2bbs vector is used for 3P2 or 5P2 library insert.***

****Note: F3bbs vector is used for 3P3 or 5P3 library insert.***

Desalt and Purify Ligations using MinElute PCR Purification Kit (QIAGEN)

Follow manufacturer specifications.

Elute DNA with 10µL of a 1/10 dilution of EB/MQ water.

Transform USO Electrocompetent Cells with Desalted Library Ligation Product

Day1:

In 1.7mL tube:

- Mix 200µL cells with 10µL desalted ligation product.
- Electroporate.
- Add 800µL SOC.
- Incubate 1hr at 37°C.

Determine transformation efficiency:

- Generate 5µL into 50µL LB serial dilutions (10^{-1}-10^{-5}).
- Spot 5µL of each dilution onto an LB + Carb plate.
- Let dry.
- Grow up overnight at 37°C.

Control for Fxbbs vector re-closure:

- Spot 5µL dilutions of Fxbbs digested vector only onto an LB + Carb plate.
- Grow up overnight at 37°C.

Plate Library:

- Plate remaining (~1mL) culture on 2X YT + Carb plate (150mm).
- Grow up overnight at 37°C.

Day2:

Calculate approximate transformation efficiency:

Ex. If 3 colonies grow on the 10^{-2} spot, then:

$[3/(1 \times 10^{-2}) \div 5\mu L] \times 1000\mu L = 6 \times 10^{4}$ transformants in original 1mL culture.

Note: Efficiency should not be above 10^{7}, or colonies on plate will be too dense.

Note: For each individual library, the final transformation efficiency should represent 3X the library diversity. Consequently, it may be necessary to conduct multiple transformations to generate a single library. 1X the library diversity may be sufficient for libraries with extremely high diversity.

Sequence Individual Library Colonies to Verify Presence of Correct Insert

Inoculate LB + Carb culture.

Miniprep.

In PCR tube:

- 5.5µL miniprep DNA
- 0.5µL (10µM) Universal F1 Primer
- 4µL ET Sequencing Mix

= 10µL total

Follow normal lab sequencing protocol.

Note: If you are sequencing the 3P1 or 5P1 library, a dye blot will run right above the sequence of interest. To solve this problem, purify the sequencing reaction using a MinElute column before the DNA precipitation step.

Prepare Library for Screening

- Scrape library colonies into 2 x 250mL LB + Carb cultures.
- Grow 2 hours at 37°C with shaking.
- Maxiprep.

A.5 Screen Individual Zinc Finger Libraries

Reagents:

33.3X Amino Acid Mixture (150mL)

Prepare the following 6 solutions (200X each):

25mL total volume each, in autoclaved milliQ water.

Solution I	Solution II
0.25g Phe	0.05g Gly
0.275g Lys	0.175g Val
0.625g Arg	0.21g Ala
	0.103g Trp

Solution III	Solution IV
0.1775g Thr	Prepare 0.83 mL concentrated HCl in 21.4mL MQ water.
2.1g Ser	To this add:
1.15g Pro	0.26g Asp
0.24g Asn	3.65g Gln

Solution V	Solution VI
1g NaOH pellets	0.1975g Ile
4.675g K-Glu	0.1925g Leu
0.09g Tyr	

Pool solutions I – VI (150mL total) and filter sterilize.

Store at 4°C.

20mM Adenine HCl (200mL)

0.68g Adenine HCl

+ MQ water = 200mL total

Filter sterilize.

Store at 4°C.

10% L-Histidine Mono-HCl (50mL)

5g L-Histidine Mono-HCl

+MQ water = 50mL total

Filter sterilize.

Store at 4°C.

20mM Uracil (150mL)

0.34g Uracil

+MQ water = 150mL total

Filter sterilize.

Store at 4°C.

10mg/mL Thiamine (50mL)

0.5g Thiamine

+MQ water = 50mL total

Filter sterilize.

Store at RT.

20mM ZnSO4 (50mL)

0.161g ZnSO4

+MQ water = 50mL total

Filter sterilize.

Store at RT

20X M9 Salts (500mL)

74g Na2HPO4

30g KH2PO4

5g NaCl

10g NH4Cl

+ MQ water = 500mL total.

Autoclave.

Store at RT.

	NM Media	**3AT Plates**
20X M9 Salts	25 ml	25 ml
40% Glucose (f.s.)	5 ml	5 ml
20mM Adenine HCl	5 ml	5 ml
20mM Uracil	5 ml	5 ml (+/-)
10% Histidine Mono-HCl	5 ml (+/-)	-
0.1M CaCl2	0.5 ml	0.5 ml
1M MgSO4	0.5 ml	0.5 ml
10mg/ml Thiamine	0.5 ml	0.5 ml
20mM ZnSO4	0.25 ml	0.25 ml
33.3X Amino Acids	15 ml	15 ml
1M 3AT	-	0-80 mM
IPTG (100mM)	-	0.5 ml (+/-)

NM Media (500mL)

Combine above ingredients.

Make with and without Histidine Mono-HCl.

Filter Sterilize.

Store at 4°C.

3AT Plates (500mL = ~5x150mm Plates)

Combine:

- 448mL distilled water
- 7.5g bacto-agar
- A stir bar

Autoclave.

While autoclaving, combine above ingredients, ***without*** CaCl2, 3AT, and IPTG. Filter sterilize.

When autoclaved agar has cooled to 65°C, add filter sterilized mixture, CaCl2, 3AT, and IPTG.

Pour plates.

Note: 3AT Plates only last 2-3 weeks. Make right before use.

Note: For individual finger screens:

Low Stringency Plates: 0-5mM 3AT + 100μM IPTG.

High Stringency Plates: 10-20mM 3AT, without IPTG.

Protocol:

Co-Transform Library and Target Plasmids

In 1.7mL tube:

- 0.5μg-1μg Fxbbs Library DNA
- 0.5 μg pH3U3 Target Site DNA

Desalt using MinElute Kit (QIAGEN), according to manufacturer specifications.

*Elute DNA with 10μL of a 1/10 dilution of EB/MQ water.

Electroporate.

Following Electroporation:

- Incubate 1 hr in 1mL SOC at 37°C.
- Pellet cells (centrifuge 5 min at 4000 rpm).
- Poor off supernatant.
- Resuspend in 1mL NM + 0.1% L-Histidine Mono-HCl + 0.2mM Uracil + Kan + Carb.
- Incubate 2 hrs at 37°C.
- Pellet cells.
- Poor off supernatant.
- Resuspend in 1mL NM without L-Histidine Mono-HCl.
- Pellet cells.
- Poor off supernatant.
- Wash 2 more times in NM without L-Histidine Mono-HCl (3 total).

Determine co-transformation efficiency:

- Generate 5μL into 50μL LB serial dilutions (10^{-1}-10^{-4}).
- Spot 5μL of each dilution onto an LB + Kan + Carb plate.
- Let dry.

- Grow up overnight at 37°C.

Note: Fxbbs library plasmid is now only Amp resistant.

Note: pH3U3 target site plasmid is Kan resistant.

Plate Library:

- Plate remaining culture (~500µL each) on high and low stringency 3AT plates.
- Grow **up to 5 days** at 37°C.

Note: Check plates for growth beginning at 3 days.

Note: 3AT may precipitate out of media. Do not worry about this.

Determine if Selection Occurred

Inoculate LB + Carb culture with colonies from high and low stringency 3AT plates.

Note: Number of colonies selected depends on amount of growth obtained.

Miniprep.

Sequence:

In PCR tube:

- 5.5µL miniprep DNA
- 0.5µL (10µM) Universal F1 Primer
- 4µL ET Sequencing Mix

= 10µL total

Follow normal lab sequencing protocol.

Note: If you are sequencing the 3P1 or 5P1 library, a dye blot will run right above the sequence of interest. To solve this problem, purify the sequencing reaction using a MinElute column before the DNA precipitation step.

A.6 Prepare Combined Zinc Finger Libraries

Select Colonies for Final Library Construction

- Inoculate 100mL LB + Carb with ~100 colonies from high stringency 3AT plate(s).

  Note: Pick individual colonies (do not scrape plate).
- Incubate 2-3 hrs at 37°C with shaking.
- Maxiprep.

Amplify Individual Finger Pools

In PCR tube:

- 10µL 5X HF Buffer
- 1µL 10mM dNTPs (2.5mM each)
- 5µL Fx Universal Forward Primer (5µM)
- 5µL Fx Universal Reverse Primer (5µM)
- 100ng DNA
- 0.5µL Phusion
- + MQ water = 50µL total.

PCR Program:

98°C 1 min (initial denaturation)

40X:

- 98°C 20 sec (denaturation)
- 56°C 15 sec (annealing)
- 72°C 15 sec (extension)

72°C 10 min (final extension)

Hold at 20°C.

Run out PCR products on a 2% gel. (Product size is 100-116 bp.)

Gel extract.

Overlapping PCR to Assemble Combined Finger Arrays

a) Primary Reaction (in PCR tube):

- 10µL 5X HF Buffer
- 1µL 10mM dNTPs (2.5mM each)
- 2µL 5P1 or 3P1 gel-purified, amplified finger DNA.
- 2µL 5P2 or 3P2 gel-purified, amplified finger DNA.
- 2µL 5P3 or 3P3 gel-purified, amplified finger DNA.
- 0.5µL Phusion
- 32.5µL MQ water

= 50µL total.

3 Cycles of "Phusion" PCR Program:

- Annealing temperature 58°C.
- Extension time 40 sec.

Secondary Reaction (in PCR tube):

- 10µL 5X HF Buffer
- 1µL 10mM dNTPs (2.5mM each)
- 5µL of Primary Reaction PCR Product
- 5µL F1 Universal Forward Primer (5µM)
- 5µL F3 Universal Reverse Primer (5µM)
- 0.5µL Phusion
- 23.5µL MQ water

= 50µL total.

PCR Program:

- Annealing temperature 58°C.
- Extension time 20 sec.

Run out PCR products on a 1.5% gel. (Product size is 278 bp.)

Gel extract.

Digest Gel-Purified, Assembled Library PCR Product

In 1.7mL tube:

- 5µL 10X Multicore Buffer
- 2.5µL BamHI
- 2.5µL KpnI
- 30µL Gel-Extracted PCR Product
- 10µL MQ water

= 50µL total.

Digest at 37°C for ≥ 2hrs.

Run out on a 1.5% gel.

Gel extract.

Digest pKBStop Combined Library Plasmid

In 1.7mL tube:

- 5µL 10X Multicore Buffer
- 2.5µL BamHI
- 2.5µL KpnI
- 1µg pKBStop Plasmid DNA
- + MQ water = 50µL total.

Digest at 37°C for ≥ 2hrs.

Run out on a 1.5% gel.

Gel extract.

Ligate Assembled Library Inserts into pKBStop

In PCR tube:

- 4µL 10X T4 DNA Ligase Buffer
- 2µL T4 DNA Ligase
- 24µL Gel-Extracted, Digested pKBStop (or MQ water control)
- 10µL Gel-Extracted, Digested Library Insert (or MQ water control)

  = 40µL total.

Incubate overnight at 16°C.

Desalt and Purify Ligation using MinElute PCR Purification Kit (QIAGEN)

Follow manufacturer specifications.

Elute DNA with 10µL of a 1/10 dilution of EB/MQ water.

Transform USO Electrocompetent Cells with Desalted Library Ligation Product

Day1:

In 1.7mL tube:

- Mix 200µL cells with 10µL desalted ligation product.
- Electroporate.
- Add 800µL SOC.
- Incubate 1hr at 37°C.

Determine transformation efficiency:

- Generate 5µL into 50µL LB serial dilutions (10^{-1}-10^{-5}).
- Spot 5µL of each dilution onto an LB + Carb plate.
- Let dry.
- Grow up overnight at 37°C.

Control for pKBStop vector re-closure:

- Spot 5µL dilutions of pKBStop only onto an LB + Carb plate.
- Grow up overnight at 37°C.

Plate Library:

- Plate remaining (~1mL) culture on 2X YT + Carb plate (150mm).

- Grow up overnight at 37°C.

Day2:

Calculate approximate transformation efficiency:

Ex. If 3 colonies grow on the 10^{-2} spot, then:

$[3/(1 \times 10^{-2}) \div 5\mu L] \times 1000\mu L = 6 \times 10^4$ transformants in original 1mL culture.

Sequence a Few Library Colonies

Inoculate LB + Carb culture.

Miniprep.

In PCR tube:

- 5.5µL miniprep DNA
- 0.5µL (10µM) Universal F1 Primer
- 4µL ET Sequencing Mix

= 10µL total

Follow normal lab sequencing protocol.

Note: A dye blot will run above part of the sequence of interest. To solve this problem, purify the sequencing reaction using a MinElute column before the DNA precipitation step.

Prepare Combined Zinc Finger Library for Screening

- Scrape library colonies into 2 x 250mL LB + Carb cultures.
- Grow 2 hours at 37°C with shaking.
- Maxiprep.

A.7 Screen Combined Zinc Finger Libraries

Co-Transform Library and Target Plasmids

Follow basic *"Individual Zinc Finger Library Screening Protocol"* (page 11).

Note: For combined finger screens:

Low Stringency Plates: 10-20mM 3AT, without IPTG.

High Stringency Plates: 30-80mM 3AT, without IPTG.

Determine if Selection Occurred

Inoculate LB + Carb culture with colonies from high and low stringency 3AT plates.

Note: Number of colonies selected depends on amount of growth obtained.

Miniprep.

Amplify Zinc Finger Array (in PCR tube):

- 10µL 5X HF Buffer
- 1µL 10mM dNTPs (2.5mM each)
- 5µL F1 Universal Forward Primer (5µM)
- 5µL F3 Universal Reverse Primer (5µM)
- 5µL DNA
- 0.5µL Phusion
- 23.5µL MQ water

= 50µL total.

PCR Program:

98°C 1 min (initial denaturation)

40X:

- 98°C 20 sec (denaturation)
- 58°C 15 sec (annealing)
- 72°C 20 sec (extension)

72°C 10 min (final extension)

Hold at 20°C.

Run out PCR products on a 1.5% gel. (Product size is 278 bp).

Gel extract.

Clone into pCR4-TOPO using normal (El Cheapo) lab protocol.

Transform TOP10 Cells (Invitrogen).

Miniprep.

Sequence:

In PCR tube:

- 5.5µL miniprep DNA

- 0.5µL (10µM) Universal F1 Primer
- 4µL ET Sequencing Mix

= 10µL total

Follow normal lab sequencing protocol.

Note: A dye blot will run above the sequence. To solve this problem, purify the sequencing reaction using a MinElute column before the DNA precipitation step.

A.8 Assemble ZFN Arrays

Digest Selected ZFN Array (in pCR4-TOPO)

In 1.7mL tube:

- 2.5µL 10X Multicore Buffer
- 1µL BamHI
- 1µL KpnI
- 10µL miniprep DNA
- 10.5µL MQ water

= 25µL total.

Digest at 37°C for ≥ 2hrs.

Run out on a 1.5% gel.

Gel extract.

Digest pCS2-FokI Plasmids (HA-RR, and FLAG-DD, *Sharkey* or wild type)

In 1.7mL tube:

- 5µL 10X Multicore Buffer
- 2.5µL BamHI
- 2.5µL KpnI
- 0.5µg pCS2-FokI Plasmid DNA
- + MQ water = 50µL total.

Digest at 37°C for ≥ 2hrs.

Run out on a 1.5% gel.

Gel extract.

Ligate ZFN Arrays into pCS2-FokI

Note: Ligate 3P arrays into pCS2-FLAG-FokI-DD.

Note: Ligate 5P arrays into pCS2-HA-FokI-RR.

In PCR tube:

- 2μL 10X T4 DNA Ligase Buffer
- 1μL T4 DNA Ligase
- 5μL Gel-Extracted, Digested pCS2-FokI (or MQ water control)
- 10μL Gel-Extracted, Digested ZFN Array (or MQ water control)
- 2μL MQ water

= 20μL total.

Incubate overnight at 16°C.

Transform TOP10 Cells (Invitrogen) with ligations.

Plate on LB + Carb.

Miniprep ZFN Constructs.

Sequence using Universal F1 primer.

Note: A dye blot will run above the sequence. To solve this problem, purify the sequencing reaction using a MinElute column before the DNA precipitation step.

Maxiprep.

A.9 In Vitro Cutting Assay to Test ZFN Arrays

Adapted from Mani et al. (2005).

ZFN Protein Synthesis Using TNT SP6 Coupled Reticulocyte Lysate (Promega)

In 1.7mL tube (quarter reactions):

- 6.25µl Rabbit Reticulocyte Lysate
- 0.5µl TNT Reaction Buffer
- 0.25µl SP6 RNA Polymerase
- 0.25µl Amino Acid Mixture Minus Leucine
- 0.25µl Amino Acid Mixture Minus Methionine
- 0.25µl RNase Inhibitor
- 100-500ng Circular Plasmid (5P or 3P Array in pCS2-FokI)
- + DEPC water = 12.5µl total.

Incubate 90 min at 30°C.

- Add 1µl of RNase H

Incubate 15 min at 37°C.

Note: Use filter tips. Wear Gloves.

Note: Thaw all kit components on ice. Do not thaw lysate more than twice.

In Vitro Cutting Assay Digest

In 1.7mL tube:

- 300ng - 1µg Plasmid (Containing Target Site)
- 1µl ZFN 5P Array Lysate (From Step 1)
- 1µl ZFN 3P Array Lysate (From Step1)
- 2µl 10x NEB Buffer 4
- 0.5µl RE (Linearizes Target Site Plasmid)
- + MQ water =20µl total.

Digest at 37°C for ≥ 2 hrs.

Purify Digests Using Gel Extraction Kit (QIAGEN):

- Add 20µl Isopropanol and 3X Volume QG to sample.
- Load onto column.
- Wash with 500µl QG.
- Wash twice with 300µl PE.
- Spin column twice to dry membrane.
- Elute in 20µl EB

Run Samples Out on Agarose Gel

Negative Control: Run out linearized plasmid containing target site.

Positive Control: Digest *prp2* target site plasmid with *prp2* ZFNs.

A.10 ZFN mRNA Synthesis

To make ZFN mRNA:

Linearize with NotI.

Use mMessage mMachine SP6 Kit (Ambion).

A.11 References

Mani, M., K. Kandavelou, F.J. Dy, S. Durai, and S. Chandrasegaran. 2005. Design, engineering, and characterization of zinc finger nucleases. *Biochem Biophys Res Commun*. 335:447-457.